



# BRNO UNIVERSITY OF TECHNOLOGY

VYSOKÉ UČENÍ TECHNICKÉ V BRNĚ

## FACULTY OF MECHANICAL ENGINEERING

FAKULTA STROJNÍHO INŽENÝRSTVÍ

## INSTITUTE OF SOLID MECHANICS, MECHATRONICS AND BIOMECHANICS

ÚSTAV MECHANIKY TĚLES, MECHATRONIKY A BIOMECHANIKY

# VÝPOČTOVÁ SIMULACE MECHANICKÝCH ZKOUŠEK IZOLOVANÝCH ŽIVOČIŠNÝCH BUNĚK

COMPUTATIONAL SIMULATION OF MECHANICAL TESTS OF ISOLATED ANIMAL CELLS

### DOCTORAL THESIS

DIZERTAČNÍ PRÁCE

### AUTHOR

AUTOR PRÁCE

Yogesh Deepak Bansod, M.Sc.

### SUPERVISOR

ŠKOLITEL

prof. Ing. Jiří Burša, Ph.D.

BRNO 2016

## Abstrakt

Buňka tvoří složitý biologický systém vystavený mnoha mimobuněčným mechanickým podnětům. Hlubší pochopení jejího mechanického chování je důležité pro charakterizaci její odezvy v podmínkách zdraví i nemoci. Výpočtové modelování může rozšířit pochopení mechaniky buňky, která může přispívat k vytvoření vztahů mezi strukturou a funkcí různých typů buněk v různých stavech.

Za tímto účelem byly pomocí metody konečných prvků (MKP) vytvořeny dva bendotensegritní modely buňky v různých stavech: model vznášející se buňky pro analýzu její globální mechanické odezvy, jako je protažení nebo stlačení, a model buňky přilnuté k podložce, který vysvětluje odezvu buňky na lokální mechanické zatížení, jako třeba vtlačování hrotu při mikroskopii atomárních sil (AFM). Oba zachovávají základní principy tensegritních struktur jako je jejich předpětí a vzájemné ovlivnění mezi komponentami, ale prvky se mohou nezávisle pohybovat. Zahrnutí nedávno navržené bendotensegritní koncepce umožňuje těmto modelům brát v úvahu jak tahové, tak i ohybové namáhání mikrotubulů (MTs) a také zahrnout vlnitost intermediálních filament (IFs). Modely předpokládají, že jednotlivé složky cytoskeletu mohou měnit svůj tvar a uspořádání, aniž by při jejich odstranění došlo ke kolapsu celé buněčné struktury, a tak umožňují hodnotit mechanický příspěvek jednotlivých složek cytoskeletu k mechanice buňky.

Model vznášející se buňky napodobuje realisticky odezvu síla-deformace během protahování a stlačování buňky a obě odezvy ilustrují nelineární nárůst tuhosti s růstem mechanického zatížení. Výsledky simulací ukazují, že aktinová filamenta i mikrotubuly hrají klíčovou úlohu při určování tahové odezvy buňky, zatímco k její tlakové odezvě přispívají podstatně jen aktinová filamenta. Model buňky přilnuté k podložce dává odezvu síla-hloubka vtlačení ve dvou různých místech odpovídající nelineární odezvě zjištěné

experimentálně při AFM. Výsledky simulací ukazují, že pro chování buňky je rozhodující místo vtlačení a její tuhost určují aktinová povrchová vrstva, mikrotubuly a cytoplazma.

Navržené modely umožňují cenný vhled do vzájemných souvislostí mechanických vlastností buněk, do mechanické úlohy komponent cytoskeletu jak individuálně, tak i ve vzájemné synergii a do deformace jádra buňky za různých podmínek mechanického zatížení. Tudiž tato práce přispívá k lepšímu pochopení mechaniky cytoskeletu zodpovědné za chování buňky, což naopak může napomáhat ve zkoumání různých patologických podmínek jako je rakovina a cévní choroby.

Klíčová slova: Cytoskelet, bendo-tensegritní struktura, modelování, metoda konečných prvků, biomechanika buňky, mechanotransdukce, tahová zkouška, tlaková zkouška, AFM (mikroskopie atomárních sil)

## **Abstract**

A cell is complex biological system subjected to the myriad of extracellular mechanical stimuli. A deeper understanding of its mechanical behavior is important for the characterization of response in health and diseased conditions. Computational modeling can enhance the understanding of cell mechanics, which may contribute to establish structure-function relationships of different cell types in different states.

To achieve this, two finite element (FE) bendo-tensegrity models of a cell in different states are proposed: a suspended cell model elucidating the cell's response to global mechanical loads, such as elongation and compression and an adherent cell model explicating the cell's response to local mechanical load, such as indentation using atomic force microscopy (AFM). They keep the central principles of tensegrity such as prestress and interplay between components, but the elements are free to move independently of each other. Implementing the recently proposed bendo-tensegrity concept, these models take into account flexural (buckling) as well as tensional behavior of microtubules (MTs) and also incorporate the waviness of intermediate filaments (IFs). The models assume that individual cytoskeletal components can change form and organization without collapsing the entire cell structure when they are removed and thus, can evaluate the mechanical contribution of individual cytoskeletal components to the cell mechanics.

The suspended cell model mimics realistically the force-elongation response during cell stretching and the force-deformation response during cell compression, and both responses illustrate a non-linear increase in stiffness with mechanical loads. The simulation results demonstrate that actin filaments (AFs) and MTs both play a crucial role in defining the tensile response of cell, whereas AFs contribute substantially to the compressive response of cell. For adherent cell model, the force-indentation responses at two distinct locations

are in accordance with the non-linear behavior of AFM experimental data. The simulation results exhibit that the indentation site dominates the cell behavior and for cell rigidity actin cortex (AC), MTs, and cytoplasm are essential.

The proposed models provide valuable insights into the interdependence of cellular mechanical properties, the mechanical role of cytoskeletal components individually and synergistically, and the nucleus deformation under different mechanical loading conditions. Therefore, this thesis contributes to the better understanding of the cytoskeletal mechanics, responsible for cell behavior, which in turn may aid in investigation of various pathological conditions like cancer and vascular diseases.

**Keywords:** Cytoskeleton, Bendo-tensegrity, Finite element modelling, Cell biomechanics, mechanotransduction, tensile test, compression test, AFM (atomic force microscopy)

## **Declaration**

Prohlašuji, že tuto disertační práci jsem vypracoval samostatně s použitím odborné literatury a dalších informačních zdrojů, které jsou všechny citovány. V disertační práci jsem také použil texty a informace z článků, kterých jsem autor nebo spoluautor.

I herewith declare that I have personally penned this doctoral thesis. I have only used the mentioned sources and utilities and have marked parts copied from elsewhere, either literally or by content as such. I have also used texts and information from my own co-authored publications.

Yogesh Deepak Bansod

# Acknowledgments

First and foremost, I would like to take this opportunity to express my sincere gratitude towards my supervisor Prof. Ing. Jiří Burša, Ph.D. for his valuable guidance and continuous motivation in performing this research work. I would like to thank him for being a pillar of support and for his patience in corroborating with me through the course of this research. His innovative ideas and continuous encouragement to participate in multiple conferences, collaborations, internships and networking round the globe made my PhD program the best experiences one can have.

I would also like to express my sincere gratitude towards Ing. Stanislav Polzer, Ph.D. and Ing. Dr. Pavel Skácel, Ph.D. for co-supervising my work and giving me valuable scientific advice in many situations. I would also like to thank all my committee members for taking time out from their busy schedules and reviewing my work.

Additionally, I am also grateful to the Faculty of Mechanical Engineering at the Brno University of Technology and its staff for their support in all possible ways. I sincerely acknowledge the financial support from the Brno University of Technology and South Moravian Centre for International Mobility (JCMM) for this research project which helped me to stay focused.

I am deeply grateful to Prof. Takeo Matsumoto and Prof. Kazuaki Nagayama for sharing their experimental data, valuable guidance, and discussion. I would also like to extend my gratitude towards Prof. Kozaburo Hayashi for his timely expert advice and valuable suggestions.

I sincerely appreciate and thank all my lab mates Vojtěch Man, Kamil Novák, Svetlana Fedorova, and Martin Slažanský for their time to time helpful tips.

The encouragement which I have received from my parents and my brother Vikram is an everlasting source of inspiration for me. I will always be indebted to them for showing the way and for providing me the means to achieve my dreams. It would be impossible for me to thank them for their innumerable sacrifices, on which I am standing today.

I would like to thank my wife Abhidnya. Her never-ending support, encouragement, quiet patience is a testament in itself of her unyielding devotion and love for me.

Finally, I am very grateful to the Almighty God for His grace and blessings, without which this work would not have been possible.

## List of Figures

Fig. 2.1: Structure of an eukaryotic cell [ <a href="#">Alberts et al. (2002)</a> ].	7
Fig. 2.2: Microscopic view of major cytoskeletal components and single filament diagrammatic representations: (a) AFs, (b) MTs, (c) IFs, and (d) ABs modified from [ <a href="#">different sources</a> ].	9
Fig. 2.3: Experimental techniques and associated biological events for different force and length scales [ <a href="#">Sunyer (2008)</a> , <a href="#">Barreto (2013)</a> ].	13
Fig. 2.4: Experimental techniques to probe cell mechanics modified from [ <a href="#">Vaziri et al. (2008)</a> ].	14
Fig. 2.5: The stiffness of adherent endothelial cell before (CONTROL) and after disruption of individual cytoskeletal components measured using MTC [ <a href="#">Wang (1998)</a> ].	19
Fig. 2.6: The schematic representation of computational approaches for cell mechanics modified from [ <a href="#">Bansod and Bursa (2015)</a> ].	21
Fig. 2.7: (a) A simple octahedron tensegrity cited from <a href="#">Intension Designs</a> and (b) the cellular tensegrity model modified from [ <a href="#">Stamenović et al. (2009)</a> ].	22
Fig. 2.8: Tensegrity FE model of suspended cell by <a href="#">Bursa et al. (2006, 2012)</a> , including (a) solid elements representing nucleus (purple), cytoplasm (blue) and (b) discrete elements representing cytoskeleton structure, where AFs (purple), MTs (light blue), and IFs (green) connected to the nucleoskeleton (red) and shell for CM (dark blue).	23
Fig. 2.9: (a) The granular cell model in non-adherent state by <a href="#">Maurin et al. (2008)</a> . The grains represent the nucleus (biggest central sphere), some CSK cross-linking proteins (internal spheres), the centrosome within the cytoplasm and the plasma membrane (peripheral spheres) with anchoring protein (integrins) outside. (b) The scenario of cytoskeleton structuration in cell adhesion process where the MTs grow from the centrosome and push integrins towards the substrate until adhesion is achieved.	24
Fig. 2.10: The self-stabilizing tensegrity based computational cell model by <a href="#">Kardas et al. (2013)</a> , illustrating different cellular components that includes MTs (blue), IFs (green), actin cytoskeleton (orange), centrosome and nucleus (red), and integrins in the outside.	26
Fig. 2.11: FE adherent cell model by <a href="#">McGarry et al. (2004)</a> , including discrete elements for MTs (red) and MFs (blue), solid elements for the nucleus (green), cytoplasm, and CM (light blue).	27
Fig. 2.12: FE adherent cell model by <a href="#">Bursa et al. (2006, 2012)</a> , including discrete	



cytoskeletal elements representing MTs (light blue), microfilaments (purple), IFs (green), and nucleoskeleton (red) and shell representing CM (blue). Although not shown here, the nucleus and cytoplasm were modeled using solid elements. ....28

Fig. 2.13: Non-regular tensegrity models for an epithelial cell by [Baudriller et al. \(2006\)](#). ....28

Fig. 2.14: A multi-structural model by [Barreto \(2013\)](#), including discrete elements for ABs (yellow) and MTs (pink), solid elements for the nucleus (blue) and cytoplasm, and shell for AC (green). ....29

Fig. 3.1: For suspended cell model: (a) sections of continuous (volume) elements and (b) structural arrangement of cytoskeletal components with respect to the nucleus. ....37

Fig. 3.2: (a) Microscopic fluorescence images of MTs distributions (in green), cited from [Wyss Institute at Harvard University](#) and (b) their corresponding architecture in the proposed computational model. ....38

Fig. 3.3: (a) Microscopic fluorescence images of IFs distributions, cited from [Wyss Institute at Harvard University](#) and (b) their corresponding architecture in the proposed computational model. ....39

Fig. 3.4: Stress-strain relationship defining the mechanical behavior of (a) IFs with applied positive strain and (b) AFs with applied negative strain (pre-strain) in the undeformed configuration. ....40

Fig. 3.5: (a) Microscopic fluorescence images of AFs distributions [[Ananthakrishnan et al. \(2006\)](#)] and (b) their corresponding architecture in the proposed computational model....41

Fig. 3.6: Sectional views of the suspended cell model during consecutive steps in simulation of tensile test: (a) spherical cell and micropipettes, (b) compressing the cell against fixed micropipette, and (c) stretching the cell with movable micropipette. (d) Snapshots of a cell during tensile test experiment [[Nagayama et al. \(2006\)](#)]. ....43

Fig. 3.7: Sectional views of the suspended cell model during consecutive steps in simulation of compression test: (a) spherical cell and microplates, compressing the cell with the movable microplate to (b) 30% and (c) 50% deformation against the fixed microplate. (d) Snapshots of a cell during compression test experiment [[Ujihara et al. \(2012\)](#)]. ....45

Fig. 3.8: Comparison of simulated force-elongation curve with the experimental curves taken from a study by [Nagayama et al. \(2006\)](#), measuring the tensile properties of cultured aortic SMCs of diameter ( $D$ ) using a cell tensile tester. ....47

Fig. 3.9: Simulation results of 6.3  $\mu\text{m}$  cell elongation: (a) deformed shape of the

cytoskeletal components and nucleus; distribution of axial stress in the discrete elements representing (b) MTs and (c) AFs; (d) distribution of axial strain in the discrete elements representing IFs; (e) distribution of first principal strain in the continuous elements representing nucleus.....	49
Fig. 3.10: Contribution of the cytoskeletal components individually and in mutual combination to response of cell model during stretching, highlighting their synergistic effect. The reaction force of different cell models is normalized with respect to that from the control model.....	50
Fig. 3.11: The effect of varying elastic modulus of individual cell components from the control values ( <a href="#">Table 3.2</a> and <a href="#">Table 3.3</a> ) on the overall cell reaction force during stretching. ....	51
Fig. 3.12: Effect of increase in the density of cytoskeletal components (a) AFs, (b) MTs, and (c) IFs on the overall cell reaction force; (d) effect of varying the thickness of CM on the cell response to stretching. ....	53
Fig. 3.13: Comparison of simulated force-deformation curve with the experimental curves taken from a study by <a href="#">Nguyen et al. (2009)</a> , investigating the biomechanical properties of a single chondrocyte using a micromanipulation technique. ....	54
Fig. 3.14: Simulation results of 50% cell compression: (a) deformed shape of the cytoskeletal components and nucleus; distribution of axial stress in the discrete elements representing (b) MTs and (c) AFs; (d) distribution of axial strain in the discrete elements representing IFs; (e) distribution of first principal strain in the continuous elements representing nucleus.....	55
Fig. 3.15: Contribution of the cytoskeletal components individually and in mutual combination to response of cell model during compression, highlighting their synergistic effect. The reaction force of different cell models is normalized with respect to that from the control model.....	57
Fig. 3.16: The effect of varying elastic modulus of individual cell components from the control values ( <a href="#">Table 3.2</a> and <a href="#">Table 3.3</a> ) on the overall cell reaction force under compression. ....	58
Fig. 3.17: Effect of increase in the density of cytoskeletal components (a) AFs, (b) MTs, and (c) IFs on the overall cell reaction force; (d) effect of variation of CM thickness on the global cell response to compression.....	59
Fig. 4.1: Typical images of: (a) an adherent cell on a rigid microplate [ <a href="#">Thoumine et al. (1999)</a> ] and (b) corresponding proposed FE adherent cell model.....	63

Fig. 4.2: For adherent cell model: (a) sections of continuous (volume) elements and (b) structural arrangement of cytoskeletal components with respect to the nucleus. ....	64
Fig. 4.3: (a) Microscopic fluorescence image of the architecture of ABs cited from <a href="#">Cytoskeleton, Inc</a> and (b) their corresponding architecture in the proposed computational model.....	65
Fig. 4.4: (a) <i>FE</i> model of an adherent cell in the indentation test, with constraints and displacement load applied at the tip acting on the top of the cell. (b) Snapshot of a cell during AFM indentation experiment (top view) [ <a href="#">Hemmer (2008)</a> ].....	67
Fig. 4.5: Sectional views comparing the contour plots of von Misses stress in cytoplasm during AFM simulation for indentation depth of 1 $\mu\text{m}$ at (a) the apex and (b) a receptor; (c) comparison of simulated force-indentation curves with the experimental curves taken from a study by <a href="#">Pillarisetti et al. (2011)</a> , measuring the stiffness of ESCs using AFM indentation.....	69
Fig. 4.6: Simulation results for indentation depth of 2.5 $\mu\text{m}$ at a receptor: (a) deformed shape of cell; distribution of axial stress in the discrete elements representing (b) MTs and (c) ABs; (d) distribution of axial strain in the discrete elements representing IFs. ....	70
Fig. 4.7: Distribution of first principal strain in the elements representing nucleus when indenting cell at (a) the apex and (b) a receptor.....	71
Fig. 4.8: Contribution of the cytoskeletal components individually and in mutual combination to cell's response to indentation (at a receptor), highlighting their synergistic effect. The reaction force of different cell models is normalized with respect to that from the control model.....	72
Fig. 4.9: The effect of varying elastic modulus of individual cell components from the control values ( <a href="#">Tables 4.2 and 4.3</a> ) on the overall cell reaction force during indentation..	73
Fig. 4.10: (a) Additional ABs created in the model with new orientation for parametric studies and (b) their effect on the overall cell reaction force during indentation. ....	74
Fig. 4.11: Effect of increase in the density of cytoskeletal components (a) MTs and (b) IFs on the overall cell reaction force; (c) effect of varying the thickness of AC on the cell's response to indentation.....	75

## List of Tables

Table 2.1: Major cell components and their functions [Mofrad et al. (2006)] .....	8
Table 2.2: Properties of the cytoskeletal filaments [Mofrad et al. (2006), Boal (2005), Rodriguez et al. (2013)] .....	11
Table 3.1: Mesh properties of the suspended cell model in ANSYS.....	41
Table 3.2: Elastic properties of discrete components of suspended cell model.....	42
Table 3.3: Hyperelastic properties of continuous components of suspended cell model ...	42
Table 4.1: Mesh properties of the adherent cell model in ANSYS.....	65
Table 4.2: Elastic properties of discrete components of adherent cell model.....	66
Table 4.3: Hyperelastic properties of continuous components of adherent cell model .....	66

# Nomenclature

<i>1D</i>	one-dimensional
<i>3D</i>	three-dimensional
<i>a</i>	cross-sectional area of cell, $\mu\text{m}^2$
<i>ABPs</i>	actin-binding proteins
<i>ABs</i>	actin bundles
<i>AC</i>	actin cortex
<i>AFM</i>	atomic force microscopy
<i>AFs</i>	actin filaments
<i>CM</i>	cell membrane
<i>D</i>	diameter of suspended cell, $\mu\text{m}$
<i>DOFs</i>	degrees of freedom
<i>ECM</i>	extracellular matrix
<i>ESCs</i>	embryonic stem cells
<i>f</i>	reaction force at stretched edge, $\mu\text{N}$
<i>FAs</i>	focal adhesions
<i>FE</i>	finite element
<i>ID</i>	inner diameter, $\mu\text{m}$
<i>IFs</i>	intermediate filaments
<i>l</i>	elongated length of cell, $\mu\text{m}$
<i>l<sub>o</sub></i>	length of cell at zero reaction force, $\mu\text{m}$
<i>MA</i>	micropipette aspiration
<i>MTC</i>	magnetic twisting cytometry
<i>MTs</i>	microtubules
<i>OD</i>	outer diameter, $\mu\text{m}$
<i>OS</i>	optical stretcher
<i>OT</i>	optical tweezers
<i>SD</i>	substrate deformation
<i>SFs</i>	stress fibers
<i>SMCs</i>	smooth muscle cells
$\varepsilon$	conventional strain
$\sigma$	conventional stress, $\text{N}/\text{m}^2$

# Contents

<b>List of Figures</b> .....	<b>i</b>
<b>List of Tables</b> .....	<b>v</b>
<b>Nomenclature</b> .....	<b>vi</b>
<b>Introduction</b> .....	<b>1</b>
1.1. General background .....	1
1.2. Motivation .....	2
1.3. Objective .....	4
<b>Literature review</b> .....	<b>7</b>
2.1. Outline .....	7
2.2. The cell and cytoskeletal components .....	8
2.3. Cell mechanical behavior .....	13
2.3.1. Experimental methods for measuring cell mechanics .....	13
2.3.2. Power-law rheology .....	17
2.3.3. Cytoskeleton disruption .....	18
2.4. Cell mechanics modeling approaches .....	19
2.4.1. Continuum approaches .....	22
2.4.2. Microstructural approaches .....	22
2.4.3. Active approaches.....	30
2.5. Summary .....	34
<b>Finite element bendo-tensegrity model of a suspended cell</b> .....	<b>35</b>
3.1. Hypothesis .....	35
3.2. FE model formulation .....	36
3.3. Material properties .....	42
3.4. Loads and boundary conditions.....	43
3.4.1. For tension test.....	43
3.4.2. For compression test.....	44
3.5. Parametric studies.....	46
3.6. Results of simulated tension test .....	46
3.6.1. Validation of the proposed model.....	46

3.6.2. Predictions of deformations inside the cell.....	48
3.6.3. Mechanical contribution of the cytoskeletal components .....	50
3.6.4. Parametric variations of material properties.....	51
3.6.5. Effect of increase in the density of cytoskeletal components.....	52
3.7. Results of simulated compression test.....	53
3.7.1. Validation of the proposed model.....	53
3.7.2. Predictions of deformations inside the cell.....	54
3.7.3. Mechanical contribution of the cytoskeletal components .....	56
3.7.4. Parametric variations of material properties.....	58
3.7.5. Effect of increase in the density of cytoskeletal components.....	59
3.8. Summary of suspended cell model.....	60
<b>Finite element modified bendo-tensegrity model of adherent cell.....</b>	<b>62</b>
4.1. Hypothesis .....	62
4.2. FE model formulation .....	63
4.3. Material properties .....	66
4.4. Loads and boundary conditions.....	67
4.5. Parametric Studies .....	68
4.6. Results of simulated AFM indentation test .....	68
4.6.1. Validation of the proposed model.....	68
4.6.2. Predictions of deformations inside the cell.....	70
4.6.3. Mechanical contribution of the cytoskeletal components .....	72
4.6.4. Parametric variations of material properties.....	73
4.6.5. Effect of increase in the density of cytoskeletal components.....	74
4.7. Summary of adherent cell model.....	75
<b>Discussion.....</b>	<b>77</b>
<b>Conclusions .....</b>	<b>82</b>
6.1. Concluding remarks .....	82
6.2. Future works.....	84
<b>References .....</b>	<b>87</b>
<b>Author's Publications .....</b>	<b>100</b>

Appendix A. A finite element bendo-tensegrity model of eukaryotic cell .....	100
Appendix B. Continuum-based modelling approaches to cell mechanics .....	127
Appendix C. Overview of tensegrity-II: high frequency spheres .....	141
Appendix D. Overview of tensegrity-I: basic structures.....	157
Appendix E. A concise review of soft glassy rheological model of cytoskeleton.....	173
<b>List of author's publications .....</b>	<b>183</b>
<b>Curriculum vitae .....</b>	<b>185</b>



### INTRODUCTION

---

#### **1.1. General background**

Living cell is a universe unto itself and can be considered as one of the most complex form of matter. Study of mechanical behavior of living cells and their mechanical interactions with the extracellular space was the first step to understand their response to applied forces. Within living organisms, cells are constantly exposed to different mechanical stimuli such as compression while moving through tissues; tension through deformed extracellular matrix (ECM); or shear stress, due to air or blood flow. Cells respond to these forces by altering their morphology, function, and behavior. With the technological advancement, the concept of cellular mechanics, physical forces existing within them, and specifically its relations to cell physiology grew speedily.

Cell was initially considered as small compartments containing homogenous gels, elastic, or viscoelastic fluids. Later, the development of microscopic techniques, such as dark field illumination, optical microscopy, etc. and advancements in sample preparations, contributed to the observation of other cellular components such as nucleus, membrane filamentous networks, cytoskeletal filamentous structure, etc. This self-sufficient system of compartmentalized structural physiology enables cells to interact with each other as well as with external surrounding, that requires coordination of complex biochemical and various biomechanical environments. Since then, it is of high interest to know how the cytoskeletal filamentous network and cell as a whole respond to distinct mechanical forces from the environment.

Since the forces acting on cells are sometimes local and temporal, where as other time they are global and sustained [[Fletcher et al. \(2010\)](#)], understanding their active nature in

different domains such as spatial and temporal is still a challenge for the researchers. In the recent decades, with the development of modern experimental techniques such as cell optical stretchers (OS), AFM, microplates, magnetic twisting cytometry (MTC), and laser tweezers it became feasible to measure mechanical properties of a single cell precisely. Many of the theoretical models that have been proposed for mechanical behavior of cells describe the cellular mechanics as either elastic or viscoelastic continuum, dense meshwork of discrete elements or a combination of both [Ingber et al. (2000), Huang et al. (2004), Bao et al. (2003)]. Employing novel theoretical models and experimental techniques it is now possible to measure the mechanical properties of cells and their components and predict their response to specific type of force.

Therefore, novel experimental techniques that complement the robust computational approaches capable of modeling cell mechanical response at varying temporal and spatial scales provide new pathways to understand cell mechanics and mechanobiology. Studying cellular mechanics is of great importance for two main reasons: first, cells are continuously exposed to physical stresses and strains arising from external physical forces or physiological environment that determine health and function of human body [Lim et al. (2006)] and second, biomechanical investigations can provide quantitative information on the changes in cell mechanical properties through the progression of certain diseases. It has been evident that the mechanical properties of cells as well as their ability to sense and respond to mechanical signals, are associated to a myriad of biological functions [Hoffman et al. (2009)].

## 1.2. Motivation

Cells convert different forms of energy and signals, maintain and modify their internal structure and respond to extracellular stimuli. They possess structural and physical properties attributed to the intracellular components that enable them to withstand the

physiological environment and mechanical stimuli within the body. The coupling between the mechanical forces and biological processes is referred to as mechanobiology. Over last few decades, the importance of mechanical load was confirmed not only for the functional development of various tissues but also at cellular level. Many *in vivo* and *in vitro* studies have proved the significance of mechanical load on different cellular processes such as cell growth, contractility, and apoptosis [Janmey et al. (1998), Mayr et al. (2000)].

The mechanism by which cells transduce mechanical signals into biochemical responses is known as mechanotransduction, which is divided into two parts: the first is the mechanical response, where the loads are transmitted from the extracellular to intracellular space via integrin-cytoskeleton-nucleus causing the cell's load bearing structure to deform [Gardel et al. (2006), Janmey et al. (2004)] and the second is the biochemical response, which leads to force-induced phenotypic changes controlled by the cell nucleus. Therefore, study of both intracellular load transfer mechanism and mechanotransduction is of high interest for better understanding of cell's physiology.

The cytoskeleton network is composed of three major types of filamentous proteins namely AFs, MTs, and IFs. This highly complex network of proteins provides a structural stability and dynamic organization to the cell. It also governs many cellular processes such as cell growth, differentiation, motility, and apoptosis, etc. [Ingber (1993), Maniotis et al. (1997)]. The cell structure is controlled by the dynamic balance of mechanical forces generated from intrinsic molecular components together with actively generated forces from cell-cell interaction and cell-substrate adhesion, which are ultimately transmitted to the nucleus via cytoskeleton [Wang et al. (1994)]. Loss of tissue homeostasis is an indication of various mechanobiological diseases and can be attributed to loss of force transmission between the ECM, the cytoskeleton, and the interior of the nucleus [Wang et al. (2009), Tapley et al. (2013)].

It has been demonstrated that application of mechanical forces on cell induced chemo-mechanical responses associated to alteration of gene expression and differentiation pathways [Charras et al. (2002a), Huang et al. (2004), Hoey et al. (2012)]. To date, a major challenge is to investigate how mechanical signal results in biochemical signal. Even though a particular pathway for biochemical signaling may be dominant under given circumstances depending on the cell type and mechanical loading conditions, experimental findings suggest that cells use multiple pathways [Huang et al. (2004)]. For better understanding of changes in cell function, it is necessary to fully understand the fundamentals of cell mechanics.

The mechano-computational studies are of paramount interest for evaluating the cell mechanical properties such as stiffness (rigidity), which initiates the understanding of cellular processes involving mechanical changes. Further, for better understanding of whole-cell mechanics, it is important to understand how cytoskeletal components behave individually and in synergy. The cell forces, intracellular structures, and cell function are coupled phenomenon and their quantification using computational models will provide better understanding of their relationship.

### **1.3. Objective**

*In vitro* studies have demonstrated that cytoskeletal components play a vital role in cell mechanobiology, but the relationship between their properties and cell mechanics is still ambiguous. Also, the experiments in different time scales reported a large variation in cell responses to mechanical loading. The broad objective of this thesis is to investigate and model the mechanisms that determine the intracellular force propagation and the mechanical behavior of a cell and its structural components. More specifically formulated as follows:

- Investigate the cell response to distinct mechanical stimuli with global cell

deformation by simulating mechanical tests such as tension and compression

- Investigate the cell response to local cell deformation by simulating AFM indentation test at distinct locations
- Investigate the mechanical contribution of cytoskeletal components to cell mechanics, individually and synergistically by simulating cytoskeleton disruption
- Investigate the effect of material properties of cellular components on cell's response by performing their parametric studies in all the three mechanical tests; for cytoskeletal components also investigate the effect of increase in their density

The computational modeling approach employed here investigates the architecture and mechanics of cells focusing on the mechanical analysis of different cytoskeletal components. The simulation results obtained can contribute to the better understanding of cell biophysics and biology, which in turn outlines the potential future advancement in mechanobiology for physiology and diseases.

The objectives of this thesis are investigated throughout the chapters and are organized as follows:

- In chapter 2, a literature review of fundamental concepts of cell mechanics is presented. This includes the description of biological cell concepts, a brief review on common experimental techniques, and single cell modeling approaches both computational and theoretical to elucidate the cell mechanics.
- In chapter 3, a novel FE bendo-tensegrity model of cell in suspended state is presented to investigate the response of cytoskeletal components and a whole-cell to two distinct mechanical tests with global cell deformation, elongation and compression. These tests are also simulated with cytoskeleton disruption studies to investigate the mechanical contribution of individual cytoskeletal components. The

sensitivity studies with change in material properties and increase in the density of cytoskeletal components are also performed to investigate the variability in cell mechanics.

- In chapter 4, another novel FE bendo-tensegrity model of cell in adherent state is presented to investigate the response of cytoskeletal components and a whole-cell to local cell deformation, AFM indentation. To explore the significance of cell structural inhomogeneity, this test is simulated at two distinct locations on the cell, at the apex and at a receptor. The parametric studies that are simulated with suspended cell model, the same are simulated with adherent cell model.
- Chapter 5 is dedicated to the generalized discussion and limitations of the proposed computational cell models. Finally, this thesis ends with conclusions in chapter 6, where the main results and contributions of this thesis to cell mechanics along with future works are summarized.

LITERATURE REVIEW

---

## 2.1. Outline

In the last few decades, a wide range of experimental techniques along with the computational approaches have been developed to unravel the cell responses to distinct mechanical stimuli. Comparing the experimental measurements of living cells is challenging due to the plethora of experimental techniques, the structural variability among different cell types, the cytoskeletal dynamics, irregular cell geometries, and complex mechanical properties [Lim et al. (2006)]. The computational models that can define cell responses to distinct mechanical stimuli corresponding to experimental findings serve as a tool to investigate the mechanics of cell. This literature review covers general description of cell biological concepts, fundamentals of cell mechanics, a brief review on common experimental techniques, and an overview of theoretical and computational modeling approaches. Finally, it concludes with technical challenges that need to be overcome in the development of more realistic computational models.

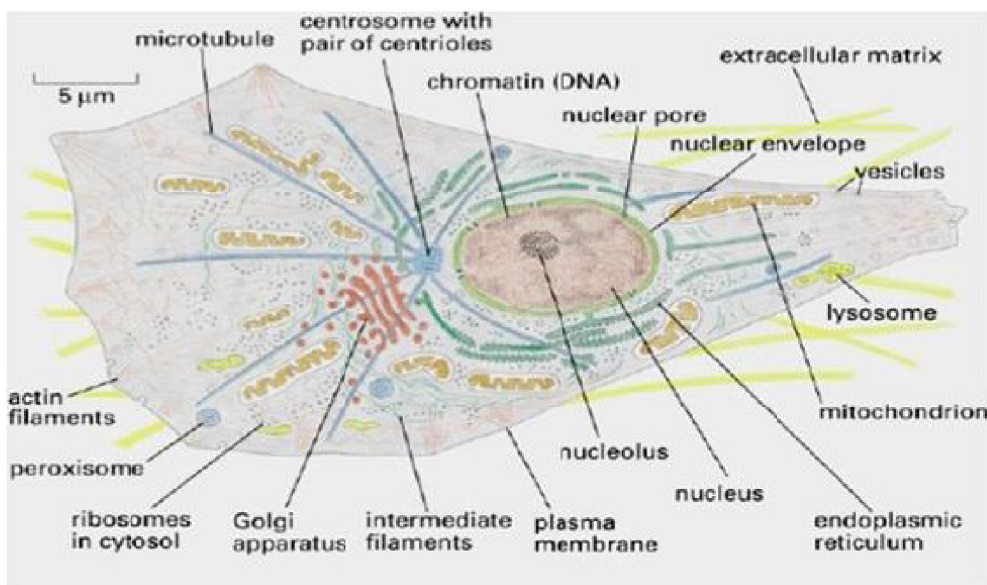


Fig. 2.1: Structure of an eukaryotic cell [Alberts et al. (2002)].

## 2.2. The cell and cytoskeletal components

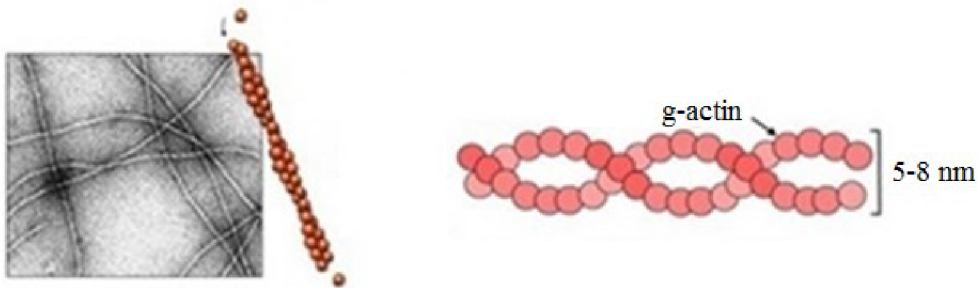
Living cells are highly complex structures consisting of large number of distinct components as depicted in Fig. 2.1. Among these components some gain attraction in the field of cell mechanics as they have been found to dominate the cell mechanical behavior and are summarized in Table 2.1.

Table 2.1: Major cell components and their functions [Mofrad et al. (2006)]

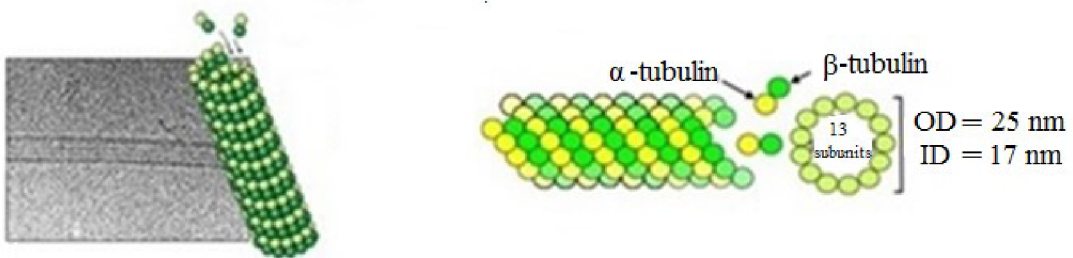
Cell components	Composition	Functions
Cell membrane (CM)	Thin lipid bilayer with thickness of 5-10 nm	Protects cell interior from extracellular environment and enable signal transduction
Nucleus	DNA and proteins enclosed by nuclear envelope of lipid bilayer	Regulate gene expression and plays a vital role in mechanotransduction
Cytoplasm	Protein complexes and organelles	Govern rheological properties of cells
Cytoskeleton	Dynamic network of filaments that interact with multifarious cross-linking proteins	Resist, transmit, and generate cellular forces
Cross-linkers	Comprises large number of cytoskeletal proteins like myosin, spectrin, titin, etc.	Their geometry and binding kinetics affect the structural organization of cytoskeleton
Extracellular matrix (ECM)	A network of macromolecules with distinctive physical, biochemical, and biomechanical properties	Provide adhesion and support to the cell. Also, Contribute to cell growth and wound healing processes
Focal adhesions (FAs)	Large protein complexes formed by binding of integrins	Couple and transmit forces between ECM and cytoskeleton



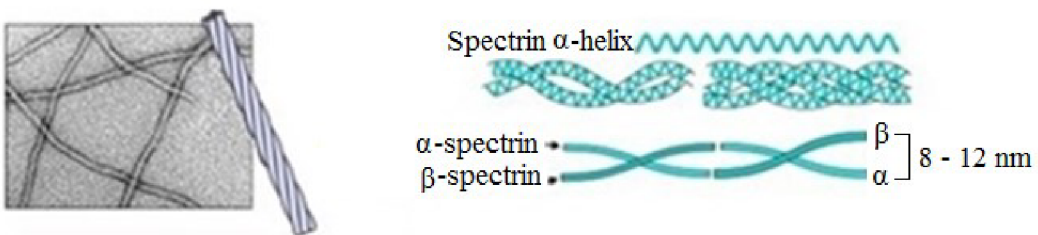
(a) Actin filaments (AFs)



(b) Microtubules (MTs)



(c) Intermediate filaments (IFs)



(d) Actin bundles (ABs)

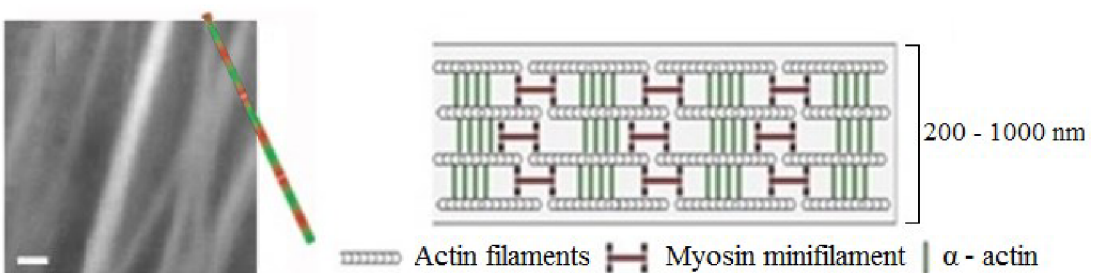


Fig. 2.2: Microscopic view of major cytoskeletal components and single filament diagrammatic representations: (a) AFs, (b) MTs, (c) IFs, and (d) ABs modified from [different sources].

The cytoskeleton is an interconnected structure of various cross-linked and interlinked

filamentous biopolymers that extend from the nucleus to the cell surface [[Stamenovic et al. \(2002\)](#)]. The cell functioning is mainly attributed to the structural stiffness and rheology of the cytoskeleton and its mechanical interaction with extracellular environment. The cytoskeleton undergoes dynamic polymerisation and depolymerisation of its components, which allows the cell to move, contract, and divide or merge. The cytoskeleton is thus considered to be an important mechanoreceptor responsible for structural integrity and stiffness of the cell.

The cytoskeletal network is composed of three types of filaments: AFs, MTs, and IFs as illustrated in [Fig. 2.2](#), which are spread throughout the cytoplasm. For cell in suspended state, a dense network of thin AFs ([Fig. 2.2a](#)) is observed at cell periphery, whereas for cell in adherent state, thick actin bundles (ABs) ([Fig. 2.2b](#)) are observed at the cell periphery running almost uniformly in the longitudinal direction [[Nagayama et al. \(2006\)](#), [Li et al. \(2006\)](#)].

The cytoskeletal components are physically interlinked that enables transmission of mechanical signals within them. Even though highly distinct, these components determine the structural integrity of cell to maintain a particular shape to accomplish a specific function. Thus, the cytoskeleton determines the mechanical characteristics of cell deformation needed for regulating different cellular processes. The properties that differentiate the cytoskeletal filaments from each other are tabulated in [Table 2.2](#).

Depending on the type and concentration of actin binding proteins (ABPs), mechanically different but functionally important actin appears in different cell states: linear ABs as stress fibers (SFs) in adherent cell state and three-dimensional (3D) lattice network of actin as the cell cortex in suspended cell state [[Nagayama et al. \(2006\)](#), [Li et al. \(2006\)](#)]. The actin-myosin contractility leads to the development of isometric tension or prestress in the cell, which is partly balanced by MTs and partly by the ECM to which the

cell is tethered [[Stamenovic et al. \(2002\)](#), [Wang et al. \(2002\)](#), [Ingber \(1993\)](#)].

Table 2.2: Properties of the cytoskeletal filaments [[Mofrad et al. \(2006\)](#), [Boal \(2005\)](#),  
[Rodriguez et al. \(2013\)](#)]

Properties	Cytoskeletal filaments			
	Actin filaments (AFs)	Microtubules (MTs)	Intermediate filaments (IFs)	Actin bundles (ABs)
<b>Composition</b>	Two helically twisted strands of actin sub-units	Hollow tubes with walls consisting of thirteen columns of tubulin molecules	Eight parallel proto-filaments held together by lateral hydrophobic interactions	Bundles of actin and myosin cross-linked by other proteins
<b>Protein sub-units</b>	G-actin and F-actin	$\alpha$ -tubulin and $\beta$ -tubulin	keratin family	$\alpha$ -actinin and myosin-II
<b>Polymerization and depolymerisation</b>	Rapid cycles	Constant	Stable	Graded polarity
<b>Persistent length, <math>l_p</math> (<math>\mu\text{m}</math>)</b>	3 – 17	6000	0.3 – 1	0.2 – 1
<b>Bending stiffness (<math>\text{Nm}^2</math>)</b>	$7 \times 10^{-26}$	$2.6 \times 10^{-23}$	$4 \times 10^{-27}$	–
<b>Governed by energy type</b>	Enthalpic elasticity ( $l_p \sim l_c$ )	Elastic (bending) energy ( $l_p > l_c$ )	Entropic elasticity ( $l_p < l_c$ )	Enthalpic elasticity
<b>Appearance of isolated filament under microscope</b>	More or less straight, thus referred to as semi-flexible polymers	Straight, thus referred to as stiff polymers	Highly wavy or convolute, thus referred to as flexible polymers	More or less straight

<b>Properties</b>	<b>Properties of the cytoskeletal filaments</b>			
	<b>Actin filaments (AFs)</b>	<b>Microtubules (MTs)</b>	<b>Intermediate filaments (IFs)</b>	<b>Actin bundles (ABs)</b>
<b>Diameter (nm)</b>	5 - 8	25 (OD) 17 (ID)	8 - 12	200-1000
<b>Young's modulus (MPa)</b>	2600	1200	7.6	0.34
<b>Structural arrangement</b>	Dense filamentous network beneath the CM	Radiating outwards from the centrosome near the nucleus, forming a star-like shape	Dense filamentous network extending from the perinuclear region to the CM	They are outlined based on their location in the cell, morphology and function at FAs
<b>Main functions</b>	<ul style="list-style-type: none"> <li>- Regulate cell shape</li> <li>- Play a vital role in cell motility</li> <li>- Contract muscles</li> </ul>	<ul style="list-style-type: none"> <li>- Maintain cell shape by undergoing compression</li> <li>- Manage chromosome movements in cell division process</li> <li>- Serve as transportation highway for motor proteins</li> </ul>	<ul style="list-style-type: none"> <li>- Act as passive reinforcement to the cell and can withstand high elastic stresses</li> <li>- Serve as anchorage to the nucleus and certain other organelles</li> <li>- Contribute to formation of nuclear lamina</li> </ul>	<ul style="list-style-type: none"> <li>- Play a vital role in cell's morphological stability, adhesion, and motility</li> <li>- Contribute significantly to mechanosensing</li> <li>- Contract muscles</li> </ul>

Although distinct in properties, these cytoskeletal filaments are interlinked to each other, to the nucleus, and the CM. Their structural arrangement is decisive for the cytoskeletal response to both, external or internal mechanical stimuli. To investigate their

individual contribution to cytoskeletal mechanics, several *in vitro* studies have been performed to isolate them from cells [Hawkins et al. (2010), Brangwynne et al. (2006), Deguchi et al. (2006)].

## 2.3. Cell mechanical behavior

### 2.3.1. Experimental methods for measuring cell mechanics

For observation of static and dynamic responses of the cell, a variety of experimental techniques have been developed that involves mechanical perturbation to the cells in the form of imposed force or deformation. In the recent decade, the precise quantitative mechanical measurements of single living cells became feasible with the development of microrheological techniques such as AFM, MTC, optical tweezers (OT), substrate deformation (SD), etc. (Fig. 2.3).

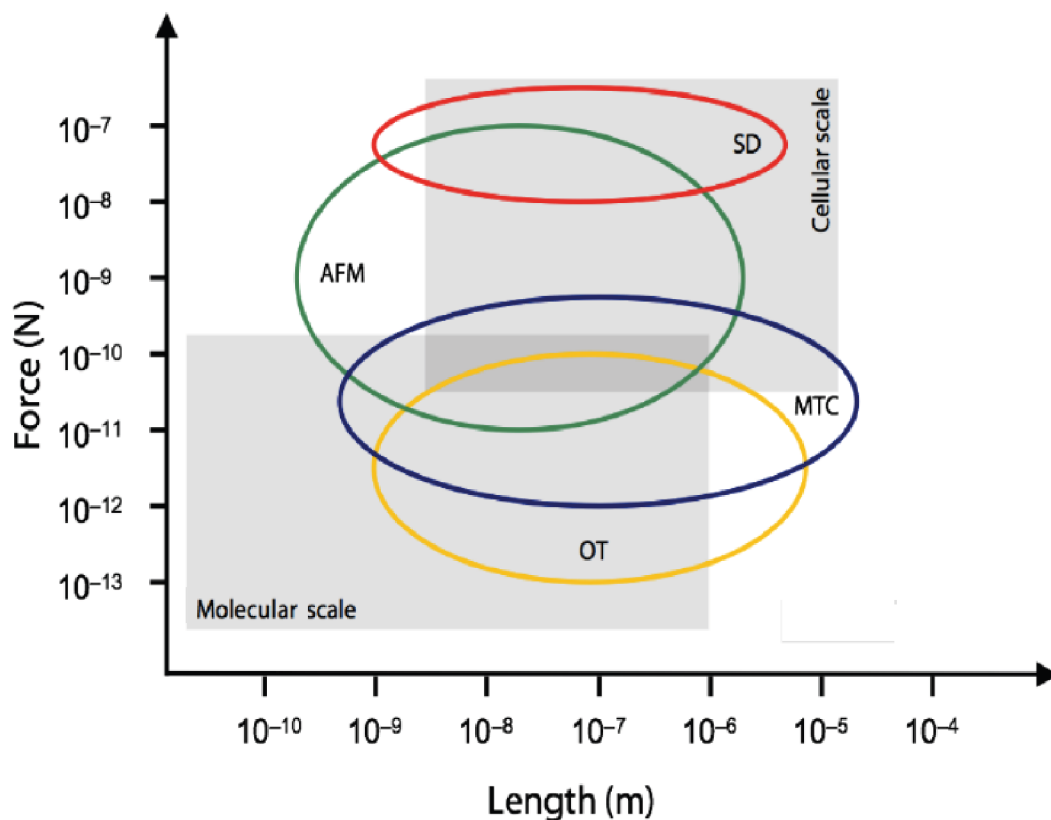


Fig. 2.3: Experimental techniques and associated biological events for different force and length scales [Sunyer (2008), Barreto (2013)].

The reported values of Young's modulus, stiffness, force, and deformation measured using distinct experimental techniques vary by more than one order of magnitude and this scattering increases for different cell types. It is of high interest to describe the cell behavior in different time scales including its immediate response to forces as well as its propagation over different time scales, since in physiological environment cells are subjected to static and dynamic forces. To probe the mechanical response of the entire cell, the microrheological techniques imposed forces in the range of  $10^{-14}$  to  $10^{-5}$  N and displacements from  $10^{-8}$  to  $10^{-4}$  m. Although complementary to each other, each experimental technique is suited for a different force and length scales (Fig. 2.3).

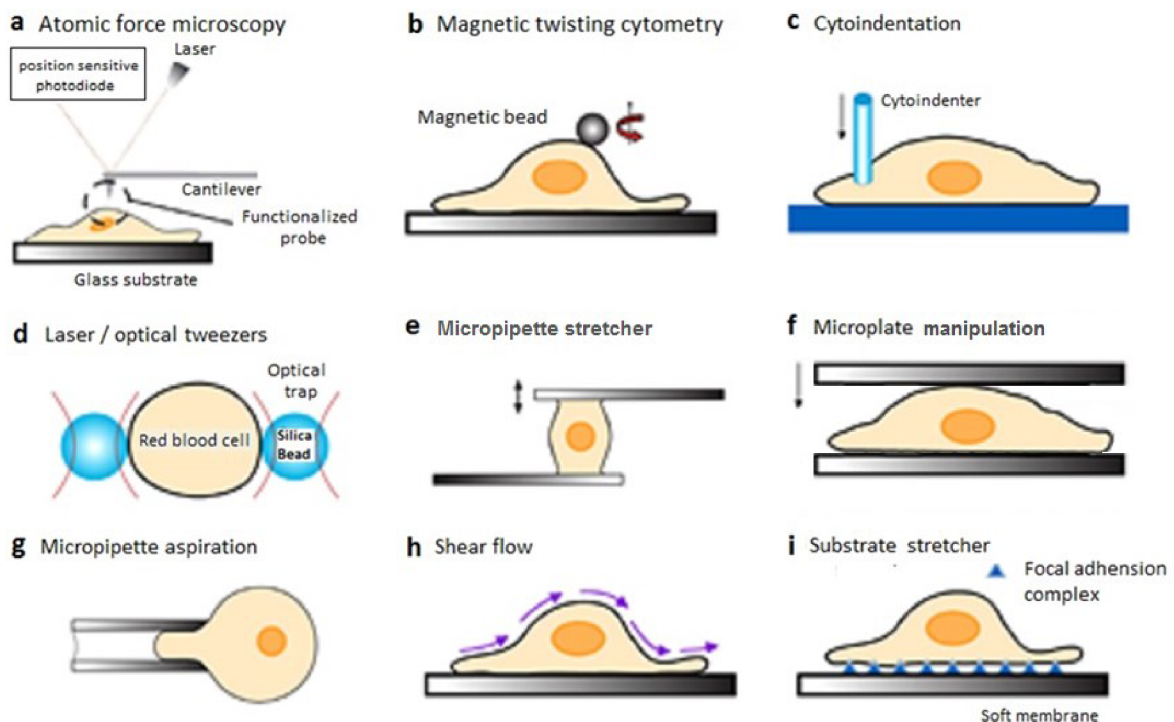


Fig. 2.4: Experimental techniques to probe cell mechanics modified from [Vaziri et al. (2008)]

The microrheological techniques are broadly classified into two different classes: the passive measurement methods and the active measurement methods. The former examines the motion of particles introduced into the cell due to thermal fluctuations, while the latter involves direct application of forces to cell. The active methods are further divided in two

categories of experiments: those that apply mechanical stimulus to localized portion of the cell such as AFM, MTC, cytoindentation (Fig. 2.4a-c) and those where a mechanical stimulus is applied to the entire cell such as OT, microplate stretcher, microplate manipulation, micropipette aspiration (MA), shear flow, and substrate stretcher (Fig. 2.4d-i). Forces can be applied to the cells either in suspended state or in adherent state. In particular three experimental techniques will be discussed in this literature review: tensile test, compression test, and AFM, since they will be used to corroborate the computational models developed in this thesis.

The micropipette stretcher technique is used to perform the tensile test that measures the global mechanical response of whole-cell to uniaxial stretching (Fig. 2.4e). Generally, this test is performed by attaching the cell to pair of micro-tools such as glass micropipettes or glass microplates. One of the micro-tools (fixed) is flexible and acts as a transducer, while the other (movable) is displaced to stretch the cell. Forces are typically within the range of 10 nN – 10  $\mu$ N and tool deflection can be measured with an accuracy of about 50 nm [Pullarkat et al. (2007)]. Initially, this test was performed using gripping technique for binding of cells to the micro-tools, thus it was only possible for relatively long cells [Glerum et al. (1990)]. However, nowadays these micro-tools can be functionalized via adhesion promoting proteins. This test has been used to measure the tensile properties of the smooth muscle cells (SMCs) [Nagayama et al. (2006), Nagayama et al. (2008)] and fibroblasts [Miyazaki et al (2000), Ujihara et al. (2010)]. It has been employed to investigate the non-linear behavior and creep responses of cell over long times [Fernández et al. (2006), Desprat et al. (2005)].

The microplate manipulation technique is used to perform the compressive test that measures the global mechanical responses of whole-cell to uniaxial compression (Fig. 2.4f). Typically, this test is performed by growing a cell on a fixed plate (bottom) and then

allowing the movable plate (top) to come into contact with this cell. There are two modes of force application in this test: gravitational force and mechanical force. In former the movable plate is simply allowed to rest on top of the cell, while in the later the movable plate is mechanically driven towards the cell. Alternatively, cells seeded in gel can also be compressed between spacers [Brown et al. (2000), Ujihara et al. (2012)] or can be compressed laterally via compression of their underlying substrate [Cheng et al. (2009)]. Recently, this technique has been used to determine the material properties of chondrocyte and chondron [Nyguyen et al. (2009)], properties of individual cellular components [Caille et al. (2002)], and compressive properties of fibroblast [Ujihara et al. (2012)]. Advantages of this method include its versatility to perform simulation with different cell profiles and with single cell or cell populations in two or three dimensions [Rodriguez et al. (2013)].

AFM (Fig. 2.4a) is used to perform indentation test that measures the cell local mechanical response with high precision. It was primarily developed to characterize the atomic and surface properties of materials for electronic devices [Binnig et al. (1986)]. Later, it was modified with environmental control chambers for microscopy to investigate the biological samples. This technique falls under cantilever manipulation techniques that uses flexible cantilever with a tip at its free end to probe the cell and its components. The tip is directed downward by a cantilever (piezoelectric motor driven) and used to probe a cell by measuring its displacement in vertical direction using a laser with high precision. AFM can investigate the cell mechanical properties in nanoscale and forces in piconewtons.

Typically, this technique has been used to examine the mechanics of intracellular components such as nucleus [Hirano et al. (2008)], cytoskeletal structures [Pesen et al. (2005)], and whole-cell [Pillarsetti et al. (2011), Pelling et al. (2008), Hiratsuka et al. (2009), Maloney et al. (2010), Sen et al. (2009)]. They have also been used to measure the



cell's mechanotransductive response to mechanical stimulus [Charras et al. (2002a)]. Recently, AFMs with modified setups have been employed to resolve point forces exerted on the cell surface by attaching the tip to CM, and then measuring the deflections of the cantilever arm induced due to cellular events such as contraction and migration. With this new configuration, AFMs have been employed to measure tugging forces at cell-cell interface [Puech et al. (2006)], cell contractile forces [Liu et al. (2012)], and forces at cell-ECM interface [Chaudhuri et al. (2009)].

Although it provides data with high precision for single-indentation point at a time, it is limited with multiple-indentation point with high temporal resolution. Furthermore, scanning with high force may damage the cell; also, CM deformation without application of any force can overestimate the force-indentation curve and consequently, the stiffness of whole-cell using Hertz theory. Moreover, shape of indentation tip and its location of contact affect the force-deformation curve behavior and may bias the test results [Rodriguez et al. (2013)].

The passive microrheological techniques observe the microbeads embedded into the cytoskeleton either employing video recordings and particle tracking or laser beam interferometry [Mofrad (2009)]. The beads embedded inside the cell are either stimulated via the cellular matrix or engulfed by the phagocytic cells. However, this may damage the cell and affect its interior by inducing changes in the cytoskeletal architecture. Also, these techniques have a risk of being erroneous due to any non-Brownian motion such as cell crawling or intracellular trafficking [Barreto (2013)]. Due to this, techniques with application of localized external force, active methods are preferred over the passive methods.

### **2.3.2. Power-law rheology**

Most of the *in vitro* studies measure the dependence of cell deformation over time or

frequency, considering the cytoskeleton rheology. Cells deform showing both solid-like elastic and fluid-like viscous properties, when subjected to external physical forces thus can be better described as viscoelastic materials [Hoffman et al. (2009)]. The dynamic responses of the cytoskeleton to mechanical perturbation was investigated using MTC [Fabry et al. (2001), Hoffman et al. (2006)] and AFM [Alcaraz et al. (2003)] on different cell types have demonstrated that the viscoelastic properties of the adherent cell (creep and stress relaxation) were believed to be governed by power-law. More details on cell rheological behavior are provided in [Appendices B and E](#).

### **2.3.3. Cytoskeleton disruption**

One of the ways to investigate the mechanical role of cytoskeletal components, individually and synergistically is by performing the disruption study using cytoskeleton-disruptor chemical drugs. Some of the most commonly used drugs to selectively disrupt the individual cytoskeletal components are: cytochalasin-D (CytD) to destabilize the actin networks, nocodazole (Noc) to destabilize the MTs, Taxol to stabilize the MTs, and acrylamide (Acry) that disrupts the IFs.

For various cell types, disruption of all cytoskeletal components showed decrease in the cell reaction force when measured using different experimental techniques such as MTC [Wang (1998)] as depicted in [Fig. 2.5](#) and AFM [Charras et al. (2002a), Kasas et al. (2005)]. However, the mechanical role of each cytoskeletal components in cell force balance is still ambiguous. For instance, after disruption of MTs, increase in traction force was observed for SMCs [Stamenović et al. (2002), Wang et al. (2001b, 2002)], whereas it showed no effect on the elastic modulus of osteoblast [Takai et al. (2005)] using AFM. Furthermore, on disruption of MTs, 20% decrease in the stiffness of endothelial cells was reported when measured using MTC [Wang (1998)], and 30% decrease in the stiffness of SMCs was reported when measured during tensile test [Nagayama et al. (2008)].

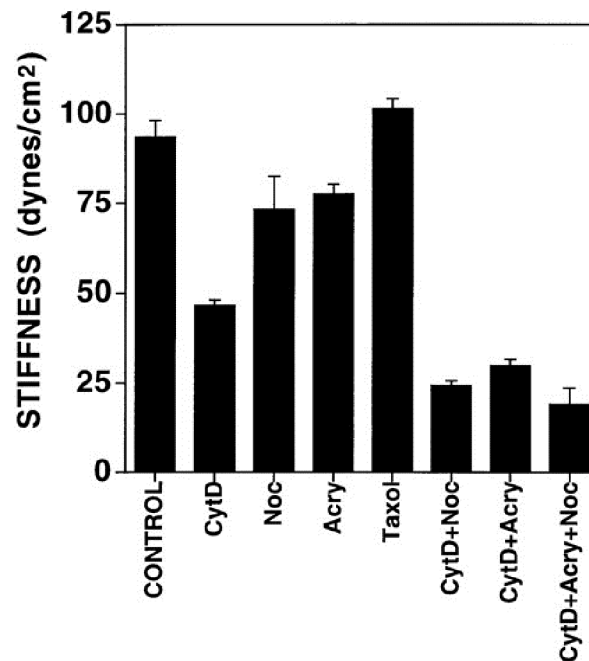


Fig. 2.5: The stiffness of adherent endothelial cell before (CONTROL) and after disruption of individual cytoskeletal components measured using MTC [Wang (1998)].

Moreover, 15% decrease in cell stiffness was measured using MTC on inhibition of IFs [Wang (1998)]. For disruption of actin structure, the cell stiffness was reported to decrease by 50% [Wang (1998)], 90% [Wakatsuki et al. (2001)], and 42% [Nagayama et al. (2008)]. However, it was not possible to identify the mechanical role of AC individually from other actin network to study its contribution to cell integrity.

## 2.4. Cell mechanics modeling approaches

Living cells are constantly exposed to a variety of extracellular and intracellular mechanical forces. It has been well established that cell's mechanical interactions with its environment influence cell morphology, cell fate, and gene expression [Janmey et al. (1991)]. The cytoskeleton transmits mechanical stimuli to intracellular region and facilitates changes in cell morphology through cytoskeletal remodeling. The cytoskeletal architecture modulates cell stiffness and its individual components may have distinct mechanical roles in the cell [Ingber (1993)]. During mechanotransduction, the extent of

the changes evoked in cell behavior due to applied mechanical loads partially depends on the distribution of forces within the cell components. Although pioneering studies have provided the basic framework for understanding mechanotransduction [Huang et al. (2004)], the fundamental mechanical processes for sensation and transduction of mechanical stimuli into biochemical signals are still ambiguous.

The novel experimental techniques mentioned in above section 2.3.1 provide substantial information regarding the mechanical properties of the cell along with their responses to diverse mechanical and chemical stimuli. This leads to the development of new theories and mechanical models of living cells that can characterize the cell responses to distinct loading types. The cell type, the experimental conditions, and the time scales are decisive factors for a model to describe the experimental observation [Zhu et al. (2000)]. The ideal cell mechanics model should consider the stress-dependent stiffening, the cell heterogeneity, the power-law behavior, and the non-equilibrium features of the cytoskeleton [Sunyer (2008)].

Computational modeling provides better control over the form and organization of individual cytoskeletal components, thus it can be used to unravel the potential mechanism of cell responses to distinct mechanical stimuli [Yao et al. (2016), Ghaffari et al. (2016), Xue et al. (2015), Dowling et al. (2014), Reynolds et al. (2014), Ronan et al.(2014), Barreto et al. (2013), Karadas et al. (2013), Bursa et al. (2012, 2006), Ujihara et al. (2012, 2010), Kiyomarsioskouei et al. (2012), De Santis et al. (2011), Nguyen et al. (2010), Slomka et al. (2010), Ofek et al. (2009), Maurin et al. (2008), Vaziri et al. (2008), Unnikrishnan et al. (2007), Cañadas et al. (2002, 2003, 2006), Ananthakrishnan et al. (2006), Prendergast et al. (2007), Jean et al. (2005), McGarry et al. (2005a, 2004)]. These computational models at distinct temporal and spatial scales have been developed to capture and simulate the cell responses corresponding to the experimental observations.

Although experimental force measurements have shown discrete propagation of force in cells, these were highly dependent on the simulation technique used [Hu et al. (2003)]. The existing computational modeling approaches for cell mechanics are broadly classified into two categories: the continuum approaches and the microstructural approaches, outlined in Fig. 2.6 from Appendix B.

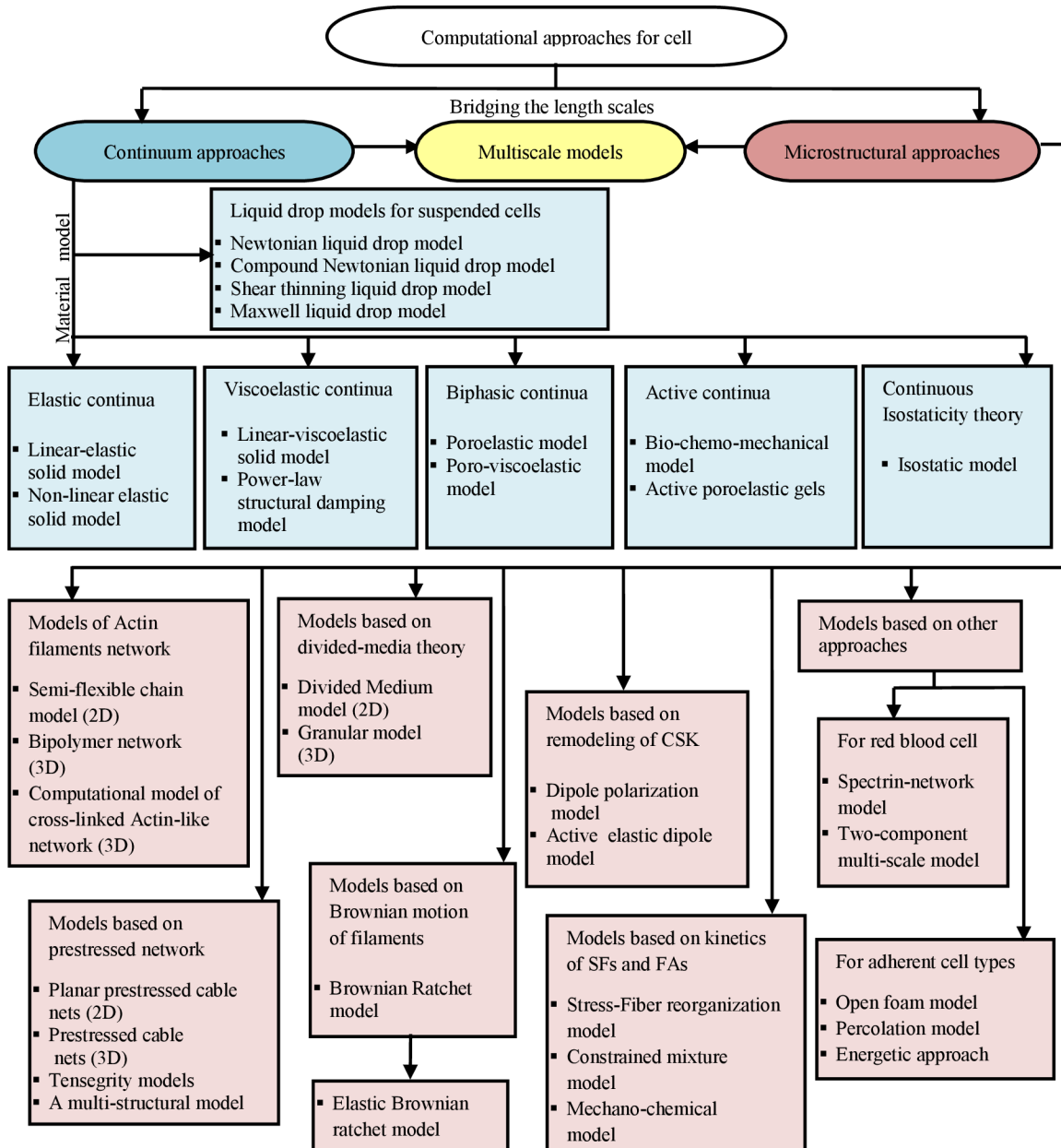


Fig. 2.6: The schematic representation of computational approaches for cell mechanics modified from [Bansod and Bursa (2015)].

### 2.4.1. Continuum approaches

Earlier, cell mechanics studies considered cell as a homogeneous continuum structure and are employed when the smallest length scale of interest is much larger than the space over which the structures and properties of the cell vary significantly. An overview of previously proposed continuum cell models is presented in [Appendix B](#).

### 2.4.2. Microstructural approaches

The microstructural approaches also known as discrete approaches describe the cytoskeleton as a system of discrete elements critical for cell mechanics. The earlier proposed simple spring-dashpot models and worm-like chain models do not explicate how the observed cell behavior can be related to the composition and structure of cytoskeleton. This was overcome by presenting a structural model of cell by drawing analogy to the tensegrity structures by [Ingber \(1993\)](#). An overview of tensegrity structures is presented in [Appendices C and D](#). One of the most frequently used models in the microstructural class is the cellular tensegrity model that envisioned cytoskeleton as an interconnected network of cables and struts ([Fig. 2.7a](#)), where the cables in tension represent AFs and the struts in compression represent MTs [[Ingber \(1993\)](#)] ([Fig. 2.7b](#)).

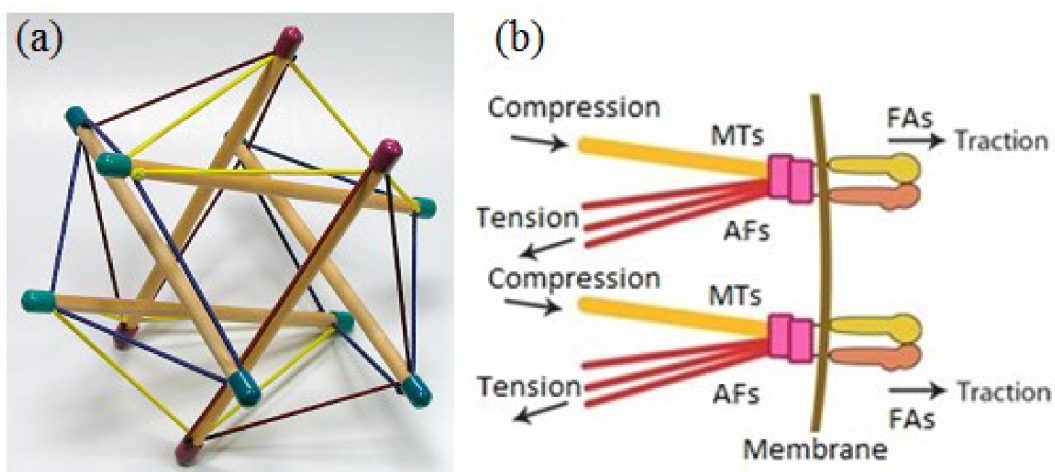


Fig. 2.7: (a) A simple octahedron tensegrity cited from [Intension Designs](#) and (b) the cellular tensegrity model modified from [[Stamenović et al. \(2009\)](#)].

The tensegrity model revealed that prestress in AFs and interplay of the cytoskeletal

components affect the cell stiffness [Stamenović et al. (1996)]. This model has successfully predicted viscosity modules of the cytoskeleton [Cañadas et al. (2002, 2003, 2006)], as well as many experimentally observed features of cell mechanical behavior such as prestress-induced stiffening [Wang et al. (2001b), Hu et al. (2003), Stamenović et al. (1999), Lebiš (2007)] and strain hardening [Stamenović et al. (1996)]. It has been observed that MTs balanced substantial portion of cytoskeletal prestress by undergoing compression and IFs transfer the loads between the cell surface and the nucleus only at large strains [Wang et al. (2001b)]. However, tensegrity model does not take into consideration other cellular components such as nucleus, cytoplasm and CM. Also, this model was not able to explain the cytoskeleton remodeling and the frequency dependence response following a power-law behavior.

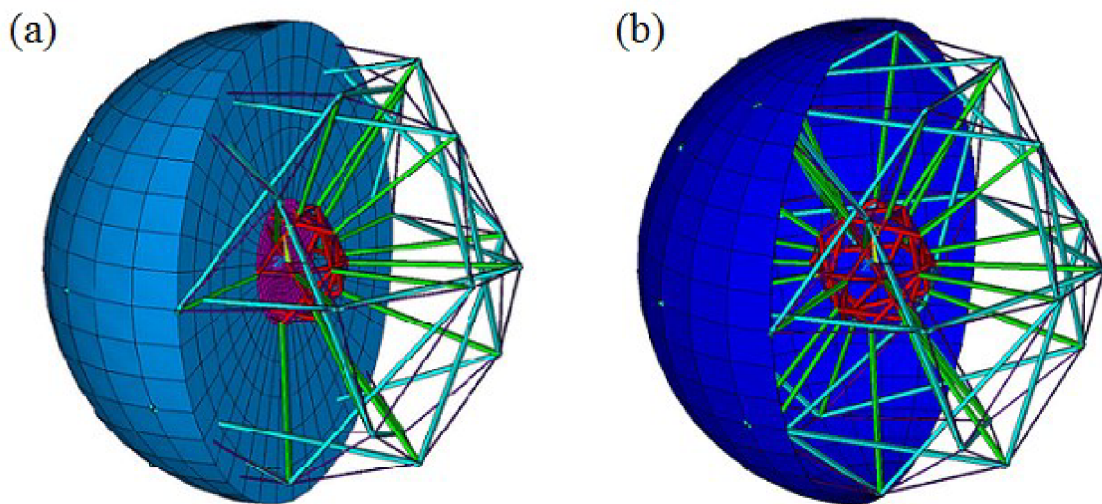
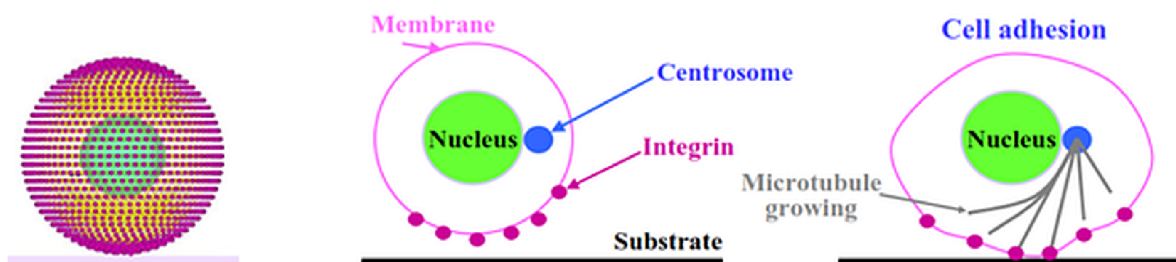


Fig. 2.8: Tensegrity FE model of suspended cell by Bursa et al. (2006, 2012), including (a) solid elements representing nucleus (purple), cytoplasm (blue) and (b) discrete elements representing cytoskeleton structure, where AFs (purple), MTs (light blue), and IFs (green) connected to the nucleoskeleton (red) and shell for CM (dark blue).

For more reliable formulation of cell mechanical behavior using FE analysis, the hybrid modeling approach was put forward by McGarry et al. (2004). Following the same approach, a more complex cell model of 210-members tensegrity structure has been

proposed by [Bursa et al. \(2006, 2012\)](#), simulating the tensile and AFM indentation tests. The suspended cell model depicted in [Fig. 2.8](#) is based on realistic shape and includes all cytoskeletal components. The tension test was simulated with this model and the results obtained were in good accordance with the experimental findings. Further, to simulate AFM indentation, the same model was modified to adherent cell model and details of its creation are described in [[Lebiš \(2007\)](#)].

The granular model has been developed by [Maurin et al. \(2008\)](#), to simulate the cell adhesion and the cell spreading process. This model is different from others in the sense that it assumed the dynamic microtubule-based polymerization for the cell spreading process. It employs the divided-media theory in combination with the tensegrity concept and generating the prestressed structure of CSK formed during the cell adhesion process.



[Fig. 2.9](#): (a) The granular cell model in non-adherent state by [Maurin et al. \(2008\)](#). The grains represent the nucleus (biggest central sphere), some CSK cross-linking proteins (internal spheres), the centrosome within the cytoplasm and the plasma membrane (peripheral spheres) with anchoring protein (integrins) outside. (b) The scenario of cytoskeleton structuration in cell adhesion process where the MTs grow from the centrosome and push integrins towards the substrate until adhesion is achieved.

The granular cell model of spherical shape is composed of three types of grains ([Fig. 2.9](#)). The nucleus is modeled as the biggest grain located at center of the cell. The cytoplasm circumscribing the nucleus is modeled using identical small grains and the two specific grains located next to the nucleus are assigned to represent the centrosome that



originates the MTs. The cross-linking proteins that connect the MTs to the AFs are represented by internal grains arranged in multilayer. The plasma membrane is modeled as the peripheral grains and some of them are randomly assigned to represent the adhesion receptors (integrins) [Maurin et al. (2008)].

To achieve the tensegrity analogy, each grain in the model except the biggest one is connected to the neighboring ones through distant interactions. The biggest central grain corresponding to nucleus has been kept unattached to avoid any interpenetration and to preserve its integrity. The connection between the two neighboring grains is assumed to behave either as a linear-elastic spring that corresponds to an actin filament or as a linear-elastic rod corresponding to a microtubule. At initial stage, there were no internal forces but, as the distance between grains changes with change in geometry of the cell during adhesion, traction or compression forces are evoked.

To simulate the cell spreading process a detection method has been developed, in which the shortest path of the grains from the centrosome to the integrin that lies closest to the ECM was defined in every time step of the simulation. The microtubule-based polymerization was then implemented through gradual lengthening of elastic rods growing from the centrosome pushing the integrins outward. Following this stepwise approach, the cell model gradually deformed to spread on the ECM. It has been observed that the granular model of total spreading of the cell has force distribution and topologies similar to those of living cells where the tensile force distribution corresponds to the actin filament network and the compressive force distribution corresponds to the microtubule network [Maurin et al. (2008)]. The granular model under the assumption of dynamic microtubule-based polymerization shows distinct feature to mimic the forced distribution in the cytoskeletal network; however, this model does not demonstrate the cell mechanical properties [Chen et al. (2012)].

The FE model based on self-stabilizing tensegrity structures was developed by [Kardas et al. \(2013\)](#), to study the mechanosensory process of osteocytes that influences remodeling and mineralization of the bone tissue. This process was studied by incorporating direct linkage between the actin cytoskeleton and the nucleus via IFs. This computational model includes major cellular components important from the mechanical point of view: the integrins that connect cell with ECM, among cytoskeleton AFs and IFs as the prestressed elements and MTs as the compression-bearing elements, the nucleus and the centrosome ([Fig. 2.10](#)).

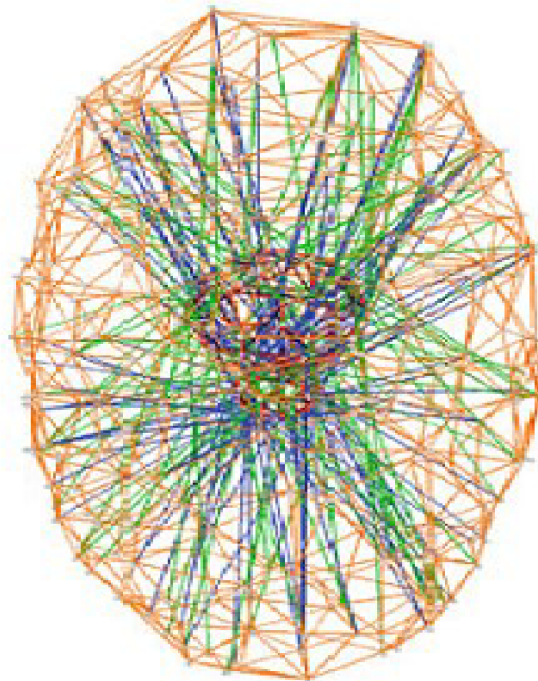


Fig. 2.10: The self-stabilizing tensegrity based computational cell model by [Kardas et al. \(2013\)](#), illustrating different cellular components that includes MTs (blue), IFs (green), actin cytoskeleton (orange), centrosome and nucleus (red), and integrins in the outside.

This model simulated the cell in physiological environment, representing *in vivo* conditions and demonstrated that the deformation of actin cytoskeleton is directly mapped on the nucleus. Later, this gets affected more with random distribution of the force carrying elements of cytoskeletal network. However, this model does not take into account the buckling of MTs and active cell responses [[Kardas et al. \(2013\)](#)].

Since cells are structurally and mechanically inhomogeneous, cell global properties do not represent their local properties [Miyazaki et al. (2002)]. The previous models are better to describe the mechanics of cell in suspended state, whereas the following ones describe cell in adherent state. Presenting the hybrid modeling approach, McGarry et al. (2004) proposed an adherent cell model that combines continuum modeling with tensegrity approach. This model was based on the idealized geometry, incorporating the cytoskeleton, and other structurally significant cellular components such as the cytoplasm, nucleus, and CM (Fig. 2.11).

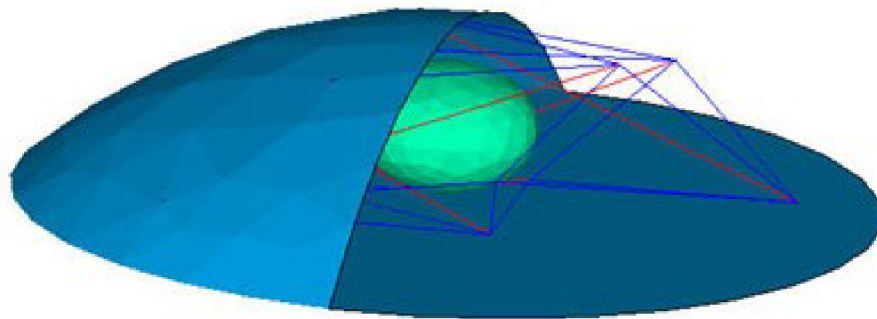


Fig. 2.11: FE adherent cell model by McGarry et al. (2004), including discrete elements for MTs (red) and MFs (blue), solid elements for the nucleus (green), cytoplasm, and CM (light blue).

By applying external forces, it has been shown that the cytoskeleton determines the cellular stiffness. This model is complex enough to capture the non-linear structural behavior of cell such as prestress-induced stiffening and variable compliance along the cell surface. Parametric studies demonstrated that the elasticity and compressibility of cytoplasm has a substantial influence on cellular stiffness. Later, this model was modified to predict quantitative information on the differences in cellular deformation caused by substrate strain and fluid shear stress [McGarry et al. (2005a)].

Modifying the suspended cell model, Bursa et al. (2006, 2012) proposed more complex adherent cell model as depicted in Fig. 2.12 simulating AFM indentation. Comparing to

the model by [McGarry et al. \(2004\)](#), this model includes all cytoskeletal components with AC being connected to the nucleoskeleton via IFs.

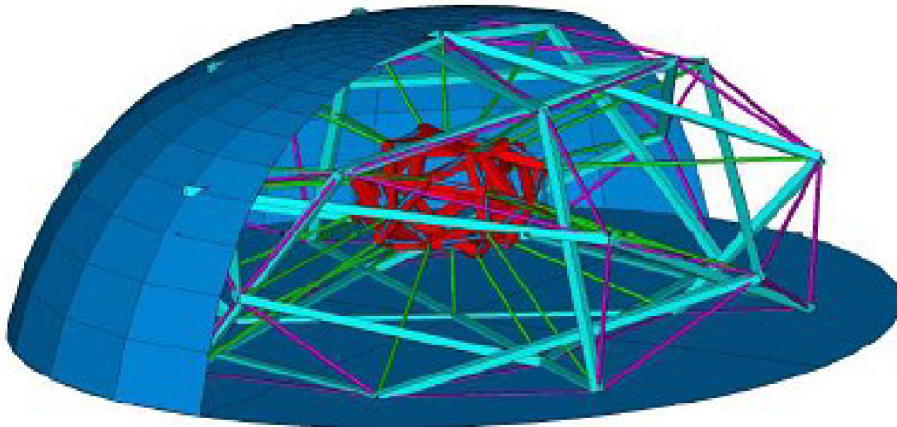


Fig. 2.12: FE adherent cell model by [Bursa et al. \(2006, 2012\)](#), including discrete cytoskeletal elements representing MTs (light blue), microfilaments (purple), IFs (green), and nucleoskeleton (red) and shell representing CM (blue). Although not shown here, the nucleus and cytoplasm were modeled using solid elements.

This model successfully explained the dispersion of AFM indentation experimental results. It was also able to stimulate the transmission of mechanical signals from membrane receptors to deep intracellular region (the nucleus), where the cell biochemical responses are initiated [[Bursa et al. \(2006, 2012\)](#)].

A non-regular self-stressed tensegrity models with high diversity and complexity were developed using novel form-finding technique by [Baudriller et al. \(2006\)](#).

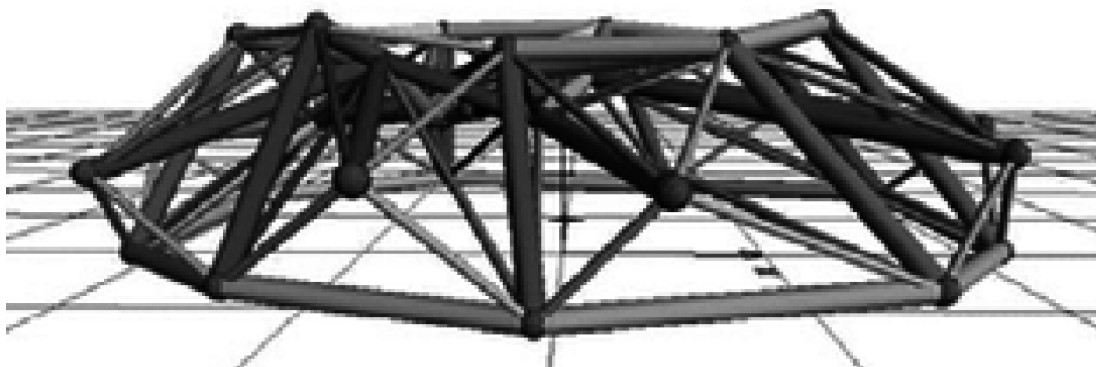


Fig. 2.13: Non-regular tensegrity models for an epithelial cell by [Baudriller et al. \(2006\)](#).

Using this technique, an epithelial cell was modeled by assembling two complex tensegrities: one representing the star-shaped MTs originating from the centrosome and other representing the actin filament network distributed both in the interior and at the periphery of cell (Fig. 2.13). This model does not provide better results compared to the regular tensegrity model.

Recently, a multi-structural FE model of single adherent cell was proposed by Barreto et al. 2013, investigating the biophysical and biochemical differences of the mechanical role of individual cytoskeletal components under loading. This model improves the tensegrity concept with no restriction on the spatial distribution of fibers but keeping its fundamental principles (prestress and interplay of the discrete components) and thus put forward the more realistic structural arrangement of the cytoskeletal components. It was based on the idealized cell geometry with semi-ellipsoidal form and incorporated the prestressed ABs and MTs within cytoplasm and nucleus enclosed by AC as depicted in Fig. 2.14.

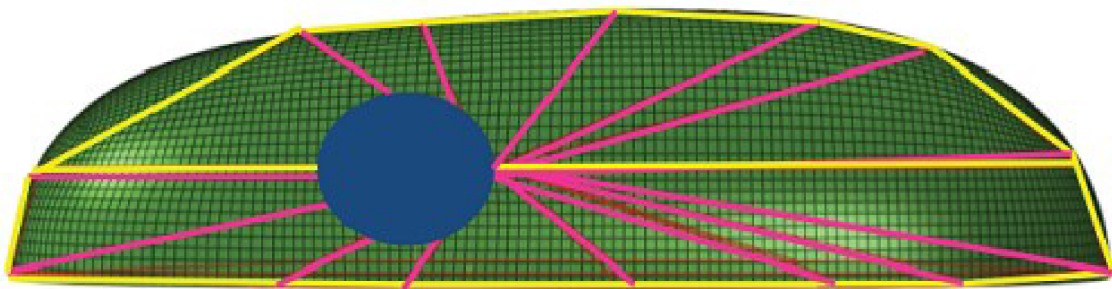


Fig. 2.14: A multi-structural model by Barreto (2013), including discrete elements for ABs (yellow) and MTs (pink), solid elements for the nucleus (blue) and cytoplasm, and shell for AC (green).

The stiffness calculated by the model for fibroblasts and osteosarcoma cells is in good accordance with AFM force-indentation measurements. This model quantified the changes in the overall cell reaction force during cytoskeleton disruption studies and demonstrated that MTs along with AC are essential to maintain the cell rigidity during indentation. It not

only explains the mechanical contribution of each cytoskeletal component, but also enables to differentiate the specific role of ABs from AC, during indentation. Although being the most sophisticated model to date, it is not able to predict the role of nucleus in signal transmission since the nucleoskeleton structure and IFs connecting the AC with the nucleus were not considered. Additionally, this model also does not take into account the active cell responses, where the cytoskeletal fibers undergo polymerization and depolymerization during loading.

### **2.4.3. Active approaches**

This thesis aims toward FE modeling of a single cell to investigate the passive response of whole-cell and its cytoskeletal components to distinct mechanical stimuli. The cell contractility is incorporated in the proposed models by assigning the prestrain to AFs/ABs at the beginning of simulations. However, it is important to note that the tension generation is a complex process and is associated with the cytoskeleton remodeling. The active cell models discussed here take into account the inherent active nature of cells and measure their respective material characteristics.

A bio-chemo-mechanical model has been proposed by [Deshpande et al. \(2006\)](#), to simulate the force dependent assembly and disassembly of SFs and FAs by incorporating the dynamic reorganization of the cytoskeleton. This model is discussed in greater detail in [Appendix B](#).

The active elastic dipole model is a theoretical model also known as the dynamic stochastic model was proposed to predict the changes in orientation of the cells in response to cyclic stresses [[De et al. \(2007\)](#)]. In a coarse-grained approximation, this model characterizes the needle-like cells (for instance, Fibroblasts) as an elastic force dipole that changes its contractility (i.e. magnitude of deformation) and orientation (i.e. direction of contraction) in response to external applied forces. The dipole description

lumps many molecular processes into coarse-grained variables. Each cell is modeled as an anisotropic force dipole tensor,  $P_{ij} = l_i f_i$ , where  $l_i$  is a measure of the distance between two equal and oppositely directed contraction forces  $f_i$  due to actin-myosin contractility [De et al. (2007, 2008)].

This model is established on the principle of “tensional homeostasis” assuming that the cells can actively manipulate their contractility by reorganizing their FAs and SFs to maintain an optimal set-point stress or strain in the adjacent matrix [De et al. (2007, 2008), Safran et al. (2009)] and any deviation from this state results in the development of intracellular forces which re-establish this optimal stress and strain [Safran et al. (2009)]. These forces are derived from the generalized gradients of an effective free energy,  $F_e$  which is function of the two degrees of freedom (DOFs) of the problem: the dipole magnitude and its direction [De et al. (2010)]. For the cell which shows bipolar morphology in response to an external applied uniaxial load,  $\sigma_a$  applied at an angle,  $\theta$  with its middle axis, an effective free energy is expressed as:

$$F_e = \frac{1}{2} \chi (P^*)^2 [-p + p_a(t)(\phi - \phi_1) - 1]^2 \quad (2.1)$$

where,  $\chi$  is a measure of cell activity that establishes its optimal set-point stress or strain. Both the cell dipole represented by  $p = P/P^*$  and the applied external stress given by  $p_a(t) = P_a(t)/(\alpha_0 P^*)$ , are dimensionless quantities and related to the optimal set-point stress or strain,  $P^*$  (where,  $\alpha_0$  is a function of Poisson’s ratio of the matrix,  $\nu$ ). The cellular dipole is given by  $\phi_1 = \cos^2 \theta_0 = \nu/(1+\nu)$  (where,  $\theta_0$  is the zero strain direction [De et al. (2010)]). The free energy of the matrix,  $F_m$  is defined as the product of the force dipole,  $P_{ij}$  and the external strain field,  $u_{ij}^a$  and is written as:

$$F_m = P_{ij} u_{ij}^a \quad (2.2)$$

The free energy,  $F$  that has been utilized by the cell contractile dipole in deforming the matrix in response to an applied external stress can be evaluated by summation of the

effective free energy of the cell,  $F_e$  and the free energy of the matrix,  $F_m$ . The dynamic equations of the dipole magnitude,  $P$  and its orientation,  $\theta$  are related in a linear manner to the generalized forces that are derived from the variation of the free energy,  $F$  and are expressed as:

$$\frac{dP}{dt} = \frac{1}{\tau_p} \left( \frac{\partial F}{\partial P} \right) \quad (2.3)$$

$$\frac{d\theta}{dt} = \frac{1}{\tau_\theta} \left( \frac{\partial F}{\partial \theta} \right) \quad (2.4)$$

where,  $\tau_p$  and  $\tau_\theta$  are the times taken for the readjustment of the magnitude and orientation of the force dipole, respectively. It has been assumed that  $\tau_p \ll \tau_\theta$ : the time taken for the changes in magnitude of the force dipole,  $\tau_p$  is much faster than the time taken for the dynamics of its highly correlated reorientation,  $\tau_\theta$  [De et al. (2010)].

The dipole theory predicts the orientation of the cells, in response to an externally applied cyclic stress over a wide range of frequencies and in presence of random forces originated due to intracellular activities. At high frequencies and low effective temperatures, the cell does not attain its optimal set-point due to swift variation in the stress and aligns perpendicular to the direction of the applied dynamic stress. At very low frequencies and in absence of effective temperature, the cell gets sufficient time to attain its optimal set-point and align nearly parallel to the direction of the applied dynamic stress on the other hand, at the same frequency but in presence of effective temperature, the orientation of the cell is random. These predictions about cellular orientations are in accordance with the experimental findings [De et al. (2007, 2008), Safran et al. (2009), Jungbauer et al. (2008)]. It has been observed that the cell orientation can be changed from perpendicular to nearly parallel by modifying the response time of CSK [Hoffman et al. (2011)].

The dynamical theory has also been employed to evaluate the characteristic time



required for the cell to attain its steady-state orientation in response to an externally applied stress. It predicts that at high frequencies, the characteristic time is frequency independent, whereas at low frequencies, it increases as the frequency decreases; but in both frequency regimes the characteristic time depends on the amplitude of an externally applied stress [Safran et al. (2009), De et al. (2010), Schwarz et al. (2013)]. The theoretical predictions of frequency and amplitude dependence on an externally applied stress are in line with the experimental findings [Safran et al. (2009), De et al. (2010), Jungbauer et al. (2008)].

This model suggests that measurements of the cell orientation are expressed as a function of Poisson's ratio of the matrix and can identify whether the controlling factor of the cellular activity is strain or stress [De et al. (2008, 2008a, 2010)]. However, in this coarse-grained description of the cell mechanical response, the origin and theoretical nature of the effective temperature are ambiguous and many molecular details involved in the mechanosensitivity are not addressed [De et al. (2010)].

To model SF dynamics, a kinematic model was proposed by Kaunas et al. (2009) based on constrained mixture theory assuming that SFs dissociation occurs when a fiber has been stretched more than its critical length. This model predicted that in response to a step change in matrix stretch, the SFs are initially stretched together with the matrix, but these overly stretched fibers are then gradually replaced by the new ones assembled with the homeostatic level of stretch in the new configuration of matrix. The model was able to elucidate experimentally measured time courses of SFs orientation perpendicular to the direction of cyclic uniaxial stretch, as well as the lack of their alignment in response to equibiaxial stretch, as observed experimentally with endothelial cells [Kaunas et al. (2006)]. Moreover, it predicted that the SFs tend to orient toward the direction of minimum matrix stretch and the rate of stretch-induced SF disassembly evaluates the rate

of alignment [Kaunas et al. (2009)]. Later, a simple quantitative sarcomeric model of SF was developed by Kaunas et al. (2011) predicting the role of acto-myosin cross bridge cycling in SFs tension regulation and reorientation, in response to cyclic stretching.

Although recent active cell models are equipped with the formulations to explain the passive responses of cells, they do not elucidate the contribution of other cytoskeletal components such as MTs, IFs, etc. and lack in differentiating the mechanical role of actin networks focusing mainly on SFs behavior.

## **2.5. Summary**

The lack of consensus on the observed biophysical and biomechanical cellular responses from diverse single-cell simulation techniques thus calls for a new structural model. This model should aim at describing the cell mechanical structure-function relationship to predict the non-linear behavior of cell and its stiffness more precisely. It should be compatible with intracellular mechanical signaling pathways that may contribute towards better understanding of mechanotransduction. Therefore, the objective of this thesis is to develop more generic FE cell model to predict the cell mechanical properties during different experimental techniques for various cell types and at the same time, describe the passive response of intracellular components.

---

**FINITE ELEMENT BENDO-TENSEGRITY MODEL  
OF A SUSPENDED CELL**

---

**3.1. Hypothesis**

The cytoskeletal tensegrity models presented in literature do not take into account the flexural behavior of MTs and are not able to elucidate the contribution of individual cytoskeletal components to the overall cell response. Recently, the concept of “bendo-tensegrity” was proposed by [Mehrbood et al. \(2011\)](#) as a modification to these models that takes into account the flexural response of MTs. Thus implementing this concept with hybrid modeling approach, a FE bendo-tensegrity model of suspended cell incorporating MTs, AFs, IFs, nucleus, cytoplasm, and CM is proposed in the current study. The unique features of this structural model keep fundamental principles governing cell behavior, including cellular prestress and interaction between the cytoskeletal components with their more realistic morphological representation for suspended cell.

The hypothesis of this work is that the proposed bendo-tensegrity model of suspended cell can describe the cellular structural behavior and determine cell’s global response to distinct mechanical stimuli. The proposed model can predict the relation between cellular mechanical response and stress/strain distributions within the specific cytoskeletal components. It is not only important to study the cell response to global deformation of extracellular environment but also if it responds differently depending on the stimulus. For this, two mechanical tests are simulated with the proposed suspended cell model: tensile test with micropipettes measuring the cell tensile response and compression test with microplates characterizing the cell compressive response. These experimental techniques aid to establish a link between the biochemical and mechanical environment of suspended

cells. The goal of this study is to extend the knowledge of how mechanical signals in the form of forces propagate within cells due to global cell deformation. More specifically, aiming towards the study of mechanical role of individual cytoskeletal components in intracellular force propagation and the quantitative characterization of nucleus deformation hypothetically decisive for mechanotransduction, which in turn helps in better understanding of how cellular processes are mechanically controlled.

### 3.2. FE model formulation

In this study, simulations of two mechanical tests with the proposed FE suspended cell model were performed and the results obtained were compared with corresponding experimental results. Tensile test with micropipettes and compression test with microplates were simulated by means of the proposed model created in ANSYS (ANSYS Inc. PA, US).

*In situ* microscopic observations of cell shape in suspended state as well as images of distributions of cytoskeletal proteins were referred to create the 3D suspended cell model and the architecture of its cytoskeletal components. The suspended cell model encompasses the nucleus and cytoplasm surrounded by the CM (Fig. 3.1a) and cytoskeletal components like AFs, MTs, and IFs (Fig. 3.1b). For the proposed model implementing the hybrid modeling approach, the continuum parts (nucleus, cytoplasm) were modeled using continuous (volume) elements circumscribed by a thin layer of shell elements (representing CM) and the cytoskeletal components were modeled using discrete (beam or truss) elements.

The shape of this cell model was defined as spherical with diameter ( $D$ ) of 32.264  $\mu\text{m}$ , taken from one of the experimental measurements by Nagayama et al. (2006). The nucleus was also modeled as spherical and positioned at the center of the cell (Fig. 3.1a). Both cytoplasm and nucleus were modeled with eight-node hexahedral isoparametric elements.

A thin flexible layer circumscribing the cytoplasm referred to as the CM was modeled with four-node quadrilateral shell elements on the outer surface of the cytoplasm, with thickness of  $0.01 \mu\text{m}$  [Rand (1964)] and no bending stiffness.

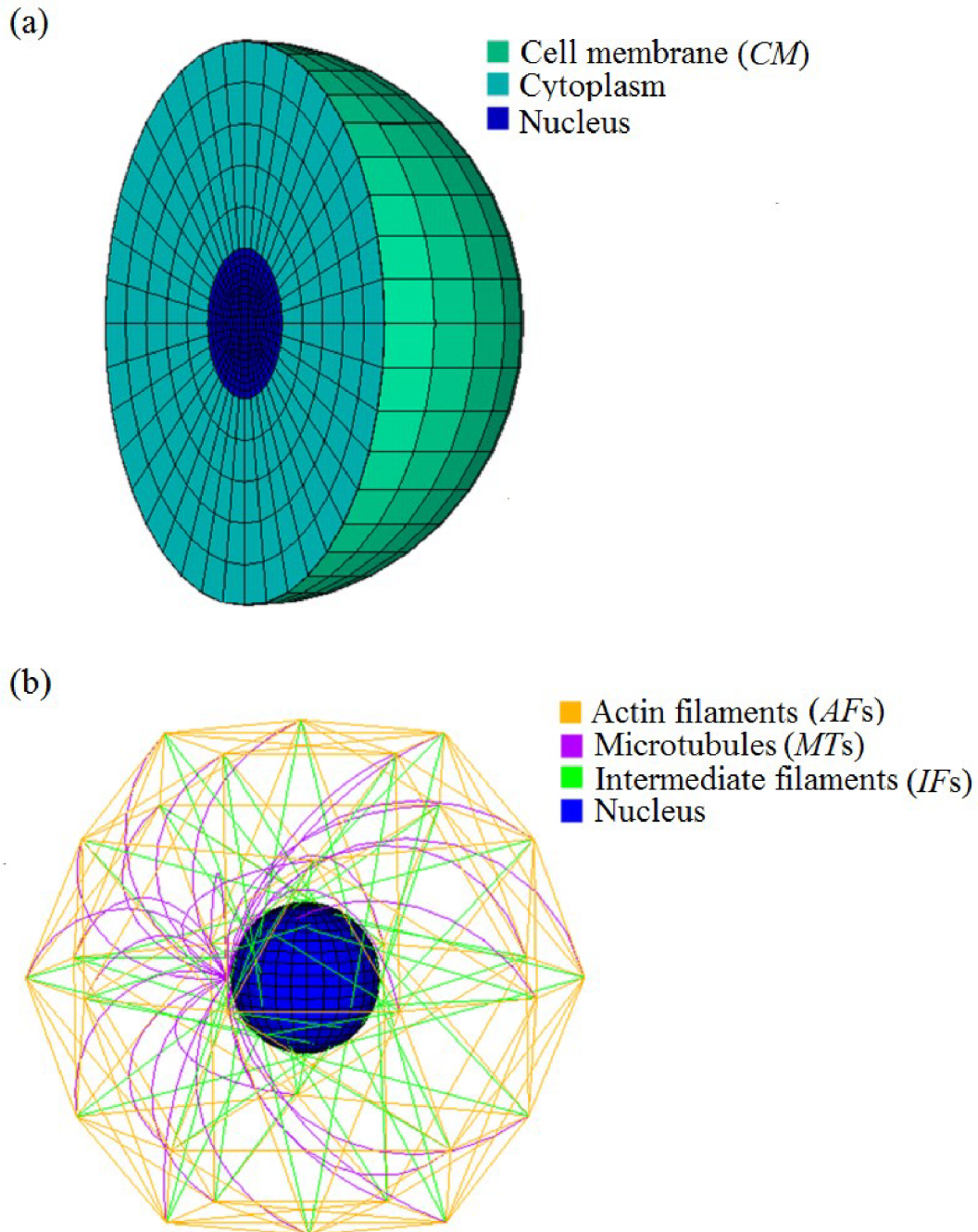


Fig. 3.1: For suspended cell model: (a) sections of continuous (volume) elements and (b) structural arrangement of cytoskeletal components with respect to the nucleus.

In a real cell, MTs of unequal lengths originate from the centrosome located near the

nucleus and emanate outward through the cytoplasm till the cortex where they interact with other cytoskeletal filaments at FAs (Fig. 3.2a). It is now evident that MTs do not have compression-only behavior but they appear highly curved (buckled) in living cells under no external load. This indicates that compressive forces in MTs induce substantial bending solely by the action of prestressed AFs; this is referred to as the “bendo-tensegrity” concept [Mehrbood et al. (2011)]. Implementing this concept, the MTs of varying curvature were modeled using beam elements, originating from a single node near the nucleus (representing the centrosome) and further extending till the FAs to form a star-like shape (Fig. 3.2b) [Kaverina et al. (1998), Maurin et al.(2008), Barreto (2013)].

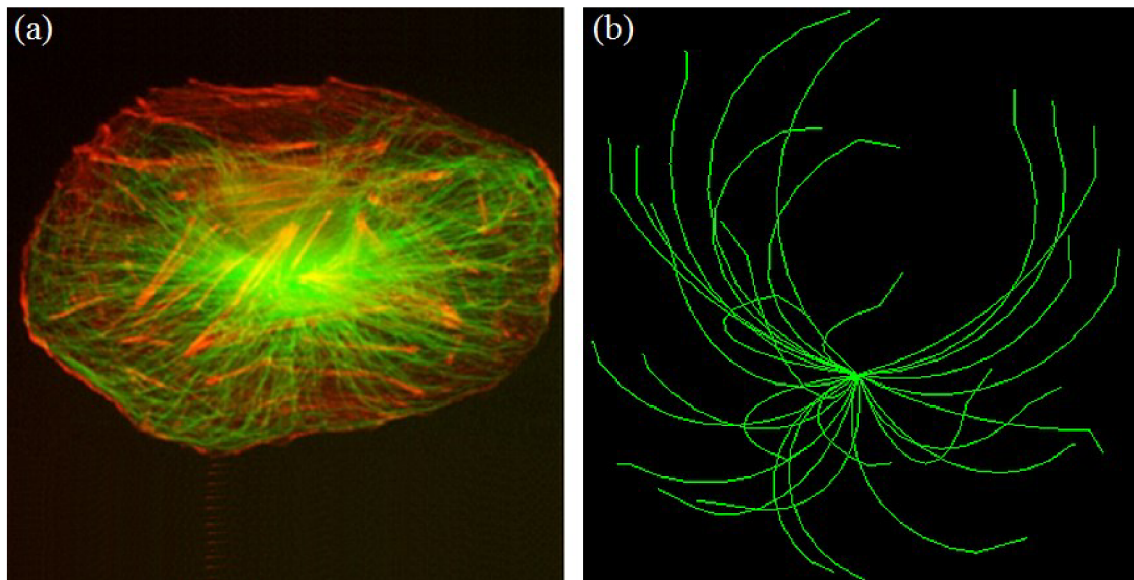


Fig. 3.2: (a) Microscopic fluorescence images of MT distributions (in green), cited from [Wyss Institute at Harvard University](#) and (b) their corresponding architecture in the proposed computational model.

Beam elements are one-dimensional line elements that have three nodes (two end nodes define element geometry and 3<sup>rd</sup> node defines the cross sectional orientation) and 6-DOFs (both translational and rotational) at each end node. These elements offer additional flexibility associated with transverse shear deformation between the axis of beam and its cross-sectional directions. Thus, the MTs are able to resist tensional as well as compressive

forces with their flexural (buckling) behavior taken into consideration. Every FA was connected to the centrosome with only one MT and it was ensured that they do not penetrate the nucleus.

IFs are scattered throughout the intracellular space, connecting the FAs to the nucleus and creating a dense network in perinuclear region that stabilizes the nucleus at the center of cell (Fig. 3.3a) [Wang et al. (2000)].

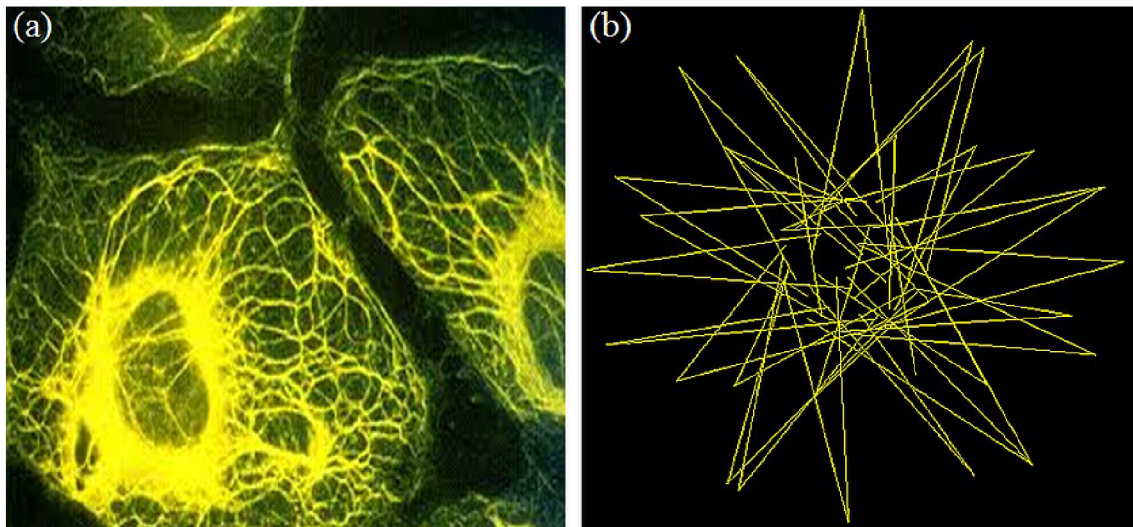


Fig. 3.3: (a) Microscopic fluorescence images of IF distributions, cited from [Wyss Institute at Harvard University](#) and (b) their corresponding architecture in the proposed computational model.

On stretching these filaments become straight and behave stiffer, thus contributing to the cell mechanics only at large strains (above 20%) [Janmey et al. (1991), Wang et al. (2000)]. To incorporate their waviness, the IFs were modeled as truss elements (Fig. 3.3b) resisting only tensile loads under elongations higher than 20% (Fig. 3.4a) and all the IFs were equally strained for simplification. In this way, these truss elements behave like wavy fibers although they are modeled straight in contrast to real IFs as depicted in Fig. 3.3a. For better transmission of mechanical stimuli to the nucleus and its stabilization at the center of the cell, each FA was connected to the nucleus via at least two IFs. To mimic their real structural arrangement, they were modeled tangentially to the nucleus thus

mimicking a dense network in perinuclear region.

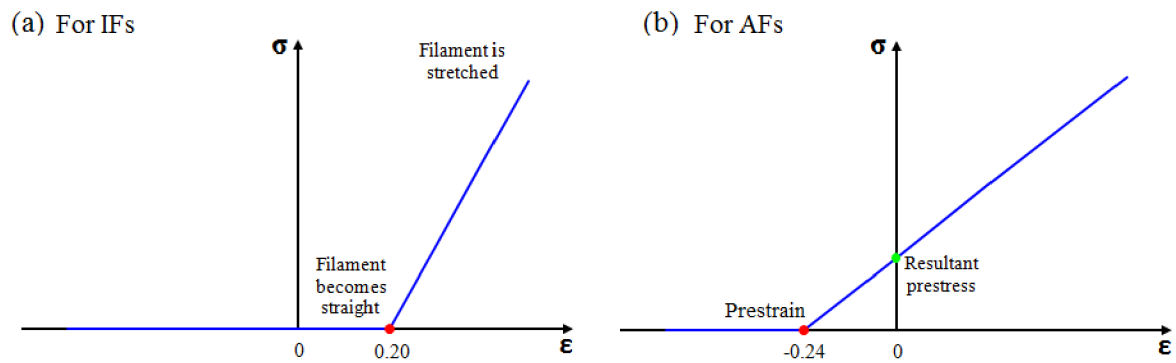


Fig. 3.4: Stress-strain relationship defining the mechanical behavior of (a) IFs with applied positive strain and (b) AFs with applied negative strain (pre-strain) in the undeformed configuration.

For cell in suspended state, a dense network of thin AFs (Fig. 3.5a) localized beneath the CM [Nagayama et al. (2006)] plays a vital role in maintaining the cell shape. This framework was created by employing the geometrical shape of icosidodecahedron with its vertices representing FAs. Thin AFs filaments were modeled as truss elements (Fig. 3.5b) that resist only tensile loads. Truss elements are one-dimensional (1D) line elements that have 2 nodes, axial stiffness, and only 3-DOFs (translational) in each node. Thus, they were selected to represent the mechanical behavior of AFs and IFs that behave in similar way as ropes.

AFs are internally prestressed (i.e. stressed even without application of an external load); to achieve this in the proposed models, experimentally measured prestrain of 24% [Deguchi et al. (2005), Kojima et al. (1994)] was assigned to them generating the initial force (prestress) essential for cell shape stability (Fig. 3.4b). For simplification, this prestrain was equal in all AFs of the model. To achieve the synergistic effect of cytoskeletal components, the elements representing AFs, MTs, and IFs were connected by sharing the same end nodes at the CM representing FAs.



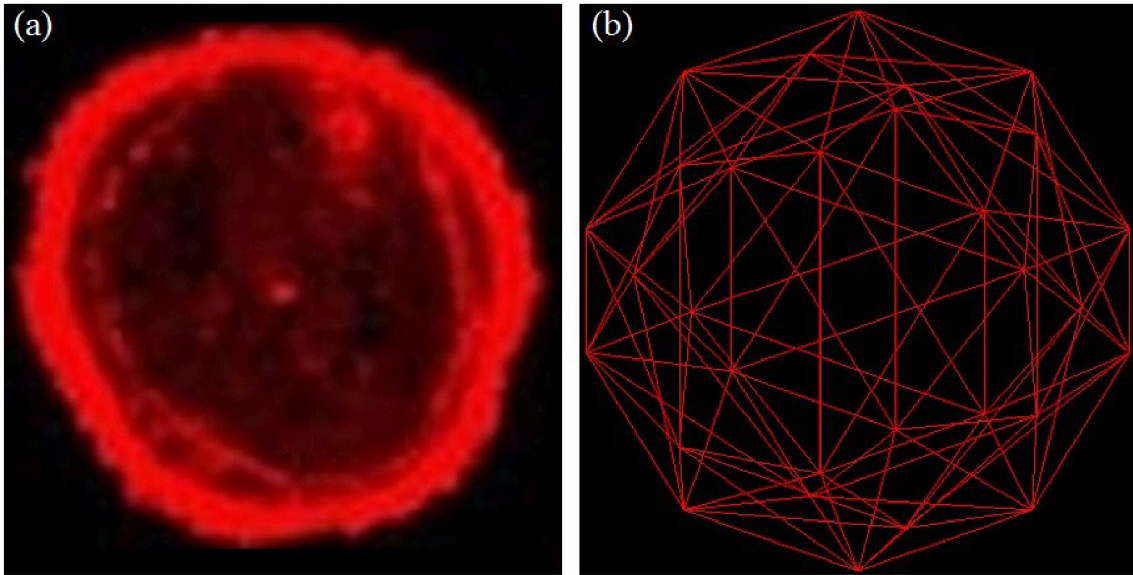


Fig. 3.5: (a) Microscopic fluorescence images of AF distributions [Ananthkrishnan et al. (2006)] and (b) their corresponding architecture in the proposed computational model.

In this way, the element types used for modeling cytoskeletal components were chosen to represent their idealized structural role in a realistic manner and are summarized in Table 3.1. It is decisive for mechanical response of the model because the mechanical behavior of living cells is mainly determined by the cytoskeletal filaments [Ingber (1993, 2003)].

Table 3.1: Mesh properties of the suspended cell model in ANSYS

Cell component	Element type	Element definition
Microtubules (MTs)	Beam	Beam188
Actin filaments (AFs)	Truss	Link180
Intermediate filaments (IFs)	Truss	Link180
Cell membrane (CM)	Shell	Shell181
Cytoplasm	Continuous (volume)	Solid185
Nucleus	Continuous (volume)	Solid185

### 3.3. Material properties

Homogenous, isotropic, and linear elastic material properties were considered for all the cytoskeletal components; their elastic parameters taken from the literature are summarized in [Table 3.2](#).

Table 3.2: Elastic properties of discrete components of suspended cell model

Cell component	Elastic modulus, E (Pa)	Poisson's ratio, $\nu$	Diameter (nm)
Microtubules (MTs) [ <a href="#">Gittes et al. (1993)</a> ]	$1.2 \times 10^9$	0.3	(outer/inner) 25/17
Actin filaments (AFs) [ <a href="#">Gittes et al. (1993)</a> ]	$2.6 \times 10^9$	0.3	7
Intermediate filaments (IFs) [ <a href="#">Xue et al. (2015)</a> ; <a href="#">Bertaud et al. (2010)</a> ]	$7.6 \times 10^6$	0.3	10

For the elasticity of cell components modeled using continuous elements, however, a Neo-Hookean hyperelastic incompressible description was used with shear modulus being the only material parameter ([Table 3.3](#)).

Table 3.3: Hyperelastic properties of continuous components of suspended cell model

Cell component	Elastic modulus, E (Pa)	Calculated shear modulus, G (Pa)
Cytoplasm [ <a href="#">Caille et al. (2002)</a> ]	$0.5 \times 10^3$	$0.17 \times 10^3$
Nucleus [ <a href="#">Caille et al. (2002)</a> ]	$5 \times 10^3$	$1.7 \times 10^3$
Cell membrane (CM) [ <a href="#">Rand (1964)</a> ]	$1 \times 10^6$	$0.33 \times 10^6$

Due to the difficulty of measuring the mechanical properties of cellular components from a single cell type, those employed in the current study were acquired from literature for distinct cell types measured using various experimental techniques.

### 3.4. Loads and boundary conditions

#### 3.4.1. For tension test

The tensile test of a suspended cell with rigid micropipettes (Fig. 3.6) was simulated to investigate the cell response to stretching.

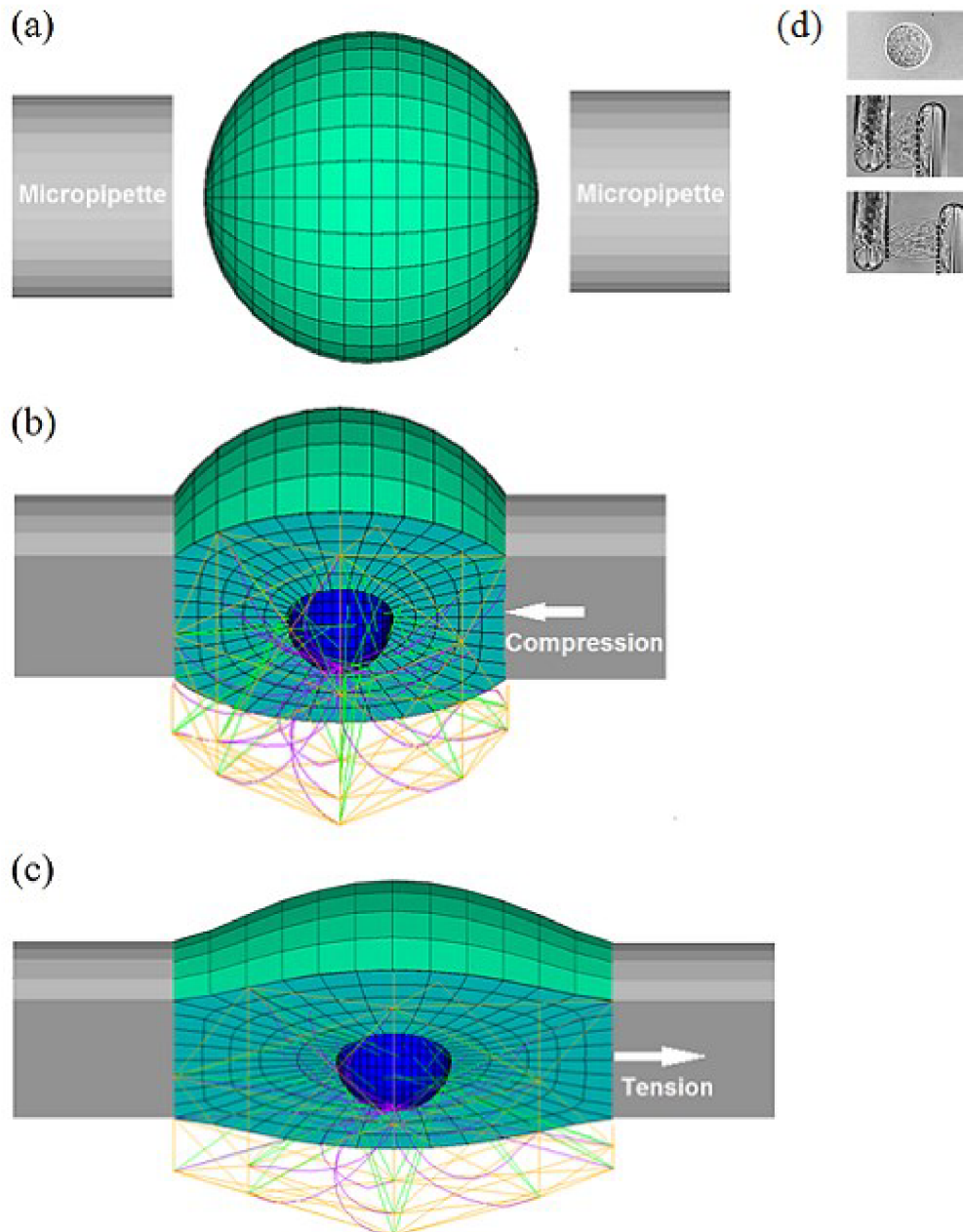


Fig. 3.6: Sectional views of the suspended cell model during consecutive steps in simulation of tensile test: (a) spherical cell and micropipettes, (b) compressing the cell against fixed micropipette, and (c) stretching the cell with movable micropipette. (d) Snapshots of a cell during tensile test experiment [Nagayama et al. (2006)].

The simulation was performed in several steps, mimicking the experiment [Nagayama et al. (2006)]. In the first step, contact between the spherical cell and both micropipettes was established by compressing the cell (with the left micropipette being fixed). The contact was set as bonded in the program to enable transmission of tensile forces in the following steps of the simulation. In the next step, the cell was elongated to achieve zero reaction forces in the micropipettes; this shape serves then as the initial (unloaded) state of the cell. In the final step, the displacement that corresponds to cell stretching in the tensile test was applied to the nodes of the movable micropipette. The reaction force was assessed as the sum of forces at the nodes of the contact surface between the cell and the movable micropipette. The distance between micropipettes in the state with zero reaction force was taken as the unloaded length of cell and therefore, it differs from the cell diameter.

### **3.4.2. For compression test**

The compression test of a suspended cell model with rigid microplates (Fig. 3.7) was simulated to investigate the cell response to compression. The simulation was performed in several successive steps, mimicking the experiment [Nguyen et al. (2009)]. The spherical shape of the cell serves as the initial state. First, the contact was established between the cell and both microplates without cell deformation. The contact setting as bonded was kept in the program from the tensile test simulation. The cell was then compressed against the fixed microplate (bottom) by applying vertical displacements to the nodes of the movable microplate to achieve successively 10%, 30%, and 50% deformation of the cell. The reaction force was evaluated as the sum of forces at nodes of the contact surfaces between the cell and the movable microplate.

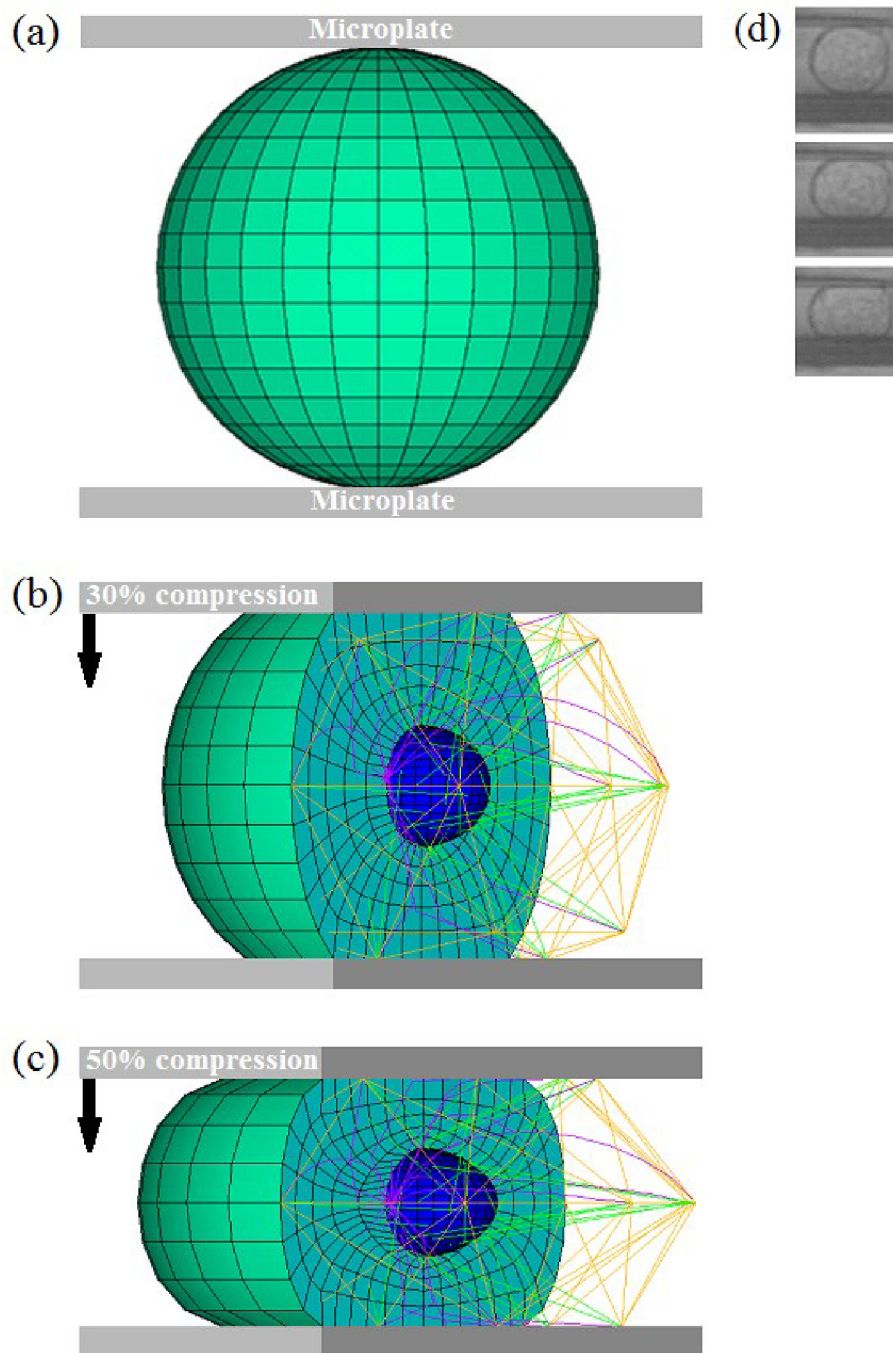


Fig. 3.7: Sectional views of the suspended cell model during consecutive steps in simulation of compression test: (a) spherical cell and microplates, compressing the cell with the movable microplate to (b) 30% and (c) 50% deformation against the fixed microplate. (d) Snapshots of a cell during compression test experiment [Ujihara et al. (2012)].

### **3.5. Parametric studies**

For the proposed model, parametric studies were performed considering the material properties of different cell components as parameters. The cell model incorporating all discrete and continuous elements with the material properties specified in [Tables 3.2](#) and [3.3](#) are referred to as the control model. To illustrate the influence of the material parameters on cell mechanical response, their values were increased and decreased by 50% of the values used for the control model. In addition, eight different cell models were created by totally removing one or more of the cytoskeletal components to investigate their contribution to cell mechanical response. In simulation of tensile test, the reaction force of altered cell models was compared with that from the control model for 6.3  $\mu\text{m}$  elongation and in simulation of compression test similarly, the reaction force of the altered cell models was compared with that from the control model for 50% deformation.

In the current study, effect of increase in the density of cytoskeletal filaments included in the model was analyzed in terms of overall cell reaction force by varying their number. Additional AFs and IFs were created in the cell interior with different orientation than earlier. More MTs were created originating from the centrosome with their end nodes being chosen randomly at the CM. To investigate a similar effect of CM thickness on the overall cell reaction force its value was increased and decreased with respect to the control value. Also, mesh sensitivity studies were performed and increase in mesh densities for continuum parts showed negligible change in the results.

### **3.6. Results of simulated tension test**

#### **3.6.1. Validation of the proposed model**

The force-elongation curve calculated from tensile test simulation is in good agreement with the non-linear responses of the experimental curves obtained from the tensile test of cultured aortic SMCs [[Nagayama et al. \(2006\)](#)], as depicted in [Fig. 3.8](#), and thus validates

the proposed bendo-tensegrity model of a suspended cell.

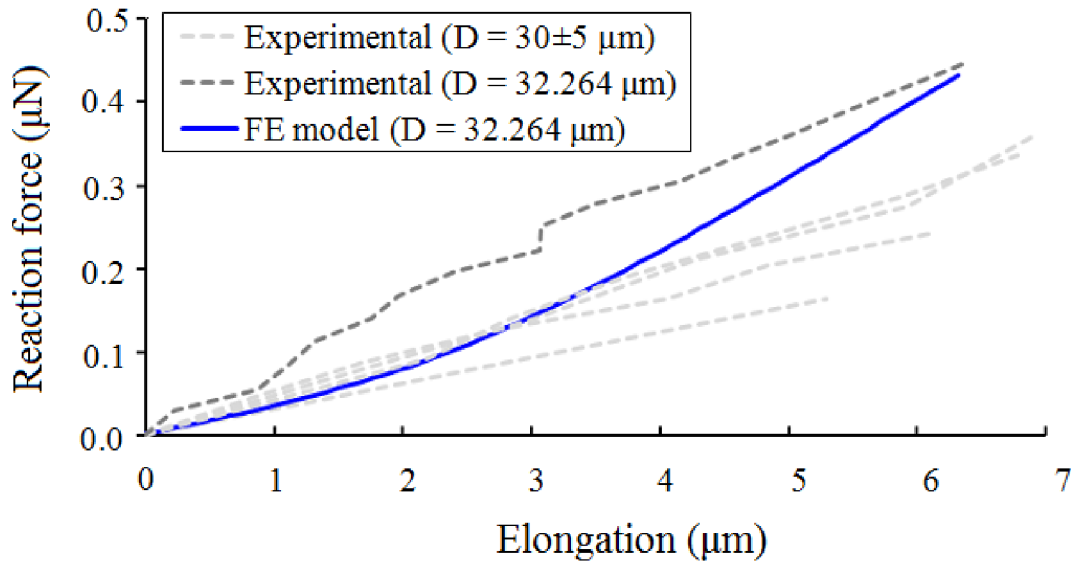


Fig. 3.8: Comparison of simulated force-elongation curve with the experimental curves taken from a study by Nagayama et al. (2006), measuring the tensile properties of cultured aortic SMCs of diameter ( $D$ ) using a cell tensile tester.

The stiffness of the control model of suspended cell in tension was evaluated as the ratio of conventional stress ( $\sigma$ ) to conventional strain ( $\varepsilon$ ) being proportional to the slope of the resulting force-elongation curve. The conventional stress is given as:

$$\sigma = \frac{f}{a} \quad (3.1)$$

where,  $f = 0.433 \mu\text{N}$  was the reaction force of cell at the stretched edge and  $a = 817.15 \mu\text{m}^2$  was the (maximal undeformed) cross-sectional area of cell. The conventional strain is expressed as:

$$\varepsilon = \frac{l - l_0}{l_0} \quad (3.2)$$

where,  $l = 33.264 \mu\text{m}$  was the elongated length of cell and  $l_0 = 26.942 \mu\text{m}$  was the length of cell at zero reaction force after having created bonded contact with the faces of

micropipettes. With reference to [Fig. 3.8](#), the stiffness of 2.3 kPa calculated for the FE model ( $D=32.264 \mu\text{m}$ ) using [Eqs. \(3.1\)](#) and [\(3.2\)](#), is in good accordance with the stiffness of 2.5 kPa calculated for the experimental ( $D=32.264 \mu\text{m}$ ) cell sample.

### 3.6.2. Predictions of deformations inside the cell

This model enables visualization of the mechanics of individual cytoskeletal components during tensile test. [Figure 3.9a](#) exhibits the deformed shape of cytoskeletal components and nucleus during simulation of tensile test where the nucleus appears elongated in the direction of stretch concomitant of cell elongation, as observed experimentally by [Nagayama et al. \(2006\)](#), [Ujihara et al. \(2010\)](#). During cell stretching, the randomly oriented AFs were likely to be aligned in the direction of stretch. This passive realignment gradually increased the overall reaction force of the cell, causing the force-elongation curve to be non-linear [[Ujihara et al. \(2010\)](#), [Miyazaki et al. \(2002\)](#)]. During cell stretching some of the MTs were straightened out, while others remain bended ([Fig. 3.9b](#)), similar to that observed in experiments [[Nagayama et al. \(2008\)](#)].

The proposed model can predict the relation between cellular mechanical response to stretching and stress/strain distributions within the specific cytoskeletal components. MTs that were straightened and aligned in the direction of stretch resist tensile forces and generate high stresses, while the ones that were bended due to compressive forces generate low negative stresses ([Fig. 3.9b](#)); this effect highlights the influence of the shape of this component on cell deformation. High stresses in straightened MTs can be attributed to the large difference between their flexural and tensional stiffness, which may significantly contribute to the non-linearity of cell responses. High stresses were observed also in AFs ([Fig. 3.9c](#)) that were aligned in the direction of stretch and resist tensile forces. IFs aligned in the direction of stretch were linearized from their assumed initial waviness and exhibited high strains, while low strains were observed in the ones localized in the central



region indicating that they remain wavy (Fig. 3.9d).

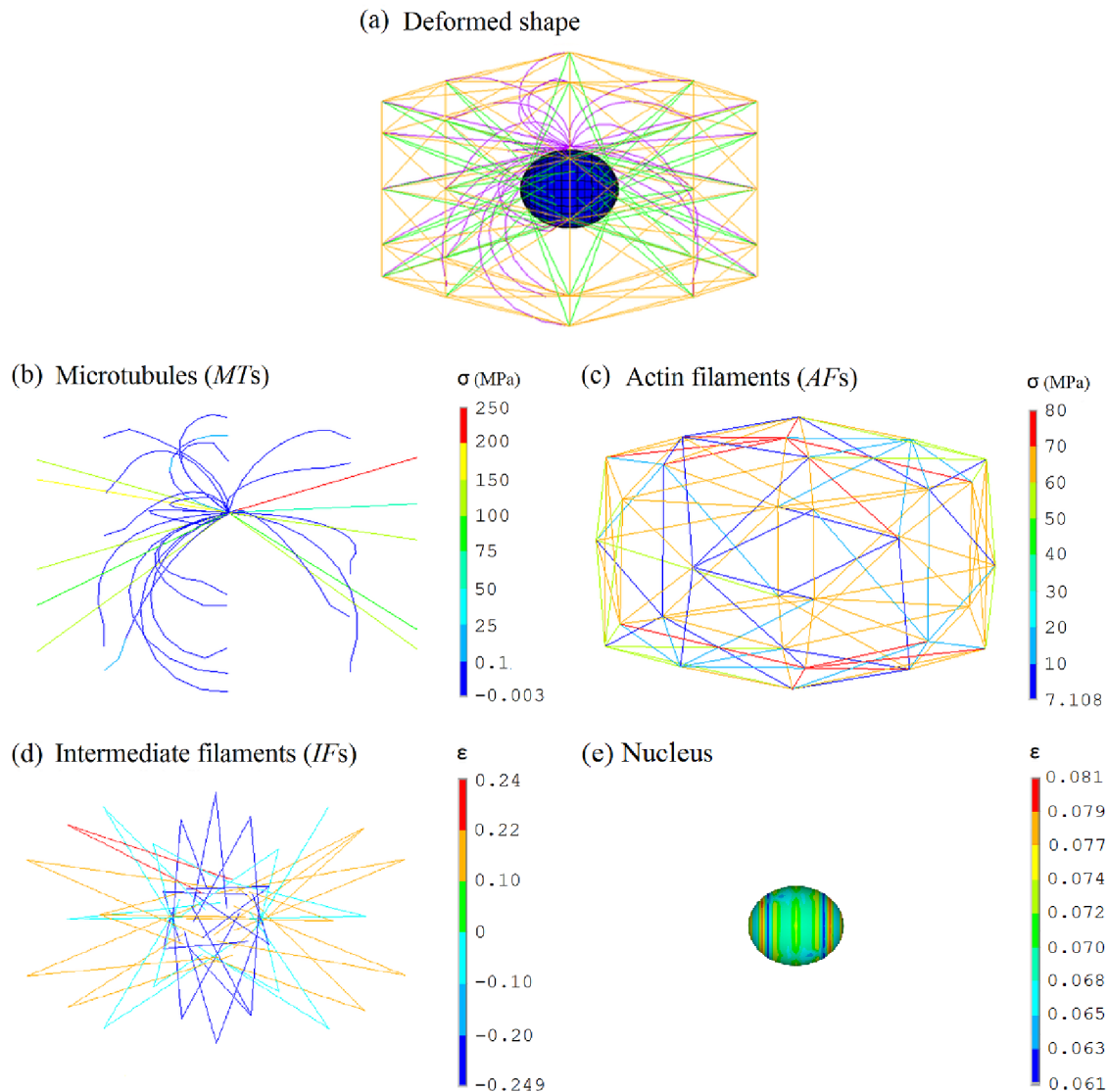


Fig. 3.9: Simulation results of 6.3  $\mu\text{m}$  cell elongation: (a) deformed shape of the cytoskeletal components and nucleus; distribution of axial stress in the discrete elements representing (b) MTs and (c) AFs; (d) distribution of axial strain in the discrete elements representing IFs; (e) distribution of first principal strain in the continuous elements representing nucleus.

A symmetrical and uniform strain distribution pattern was observed in the nucleus (Fig. 3.9e) with a maximum deformation of 8% (first principal strain). This quantitative characterization of nucleus deformation could be hypothetically decisive for transducing mechanical signals into changes in gene expression for cell stretching of 6.3  $\mu\text{m}$

(approximately 20% global deformation).

### 3.6.3. Mechanical contribution of the cytoskeletal components

Figure 3.10 illustrates the results of parametric studies investigating the mechanical contribution of individual cytoskeletal components to the overall cell reaction force during stretching. When the cytoskeletal components were incorporated in the continuum parts, the cell reaction forces were higher and concentrated in the nodes where cytoskeletal components interact with each other (FAs). The role of each cytoskeletal component in resisting tensile forces on cell was investigated via removal of each cytoskeletal component from the control model.

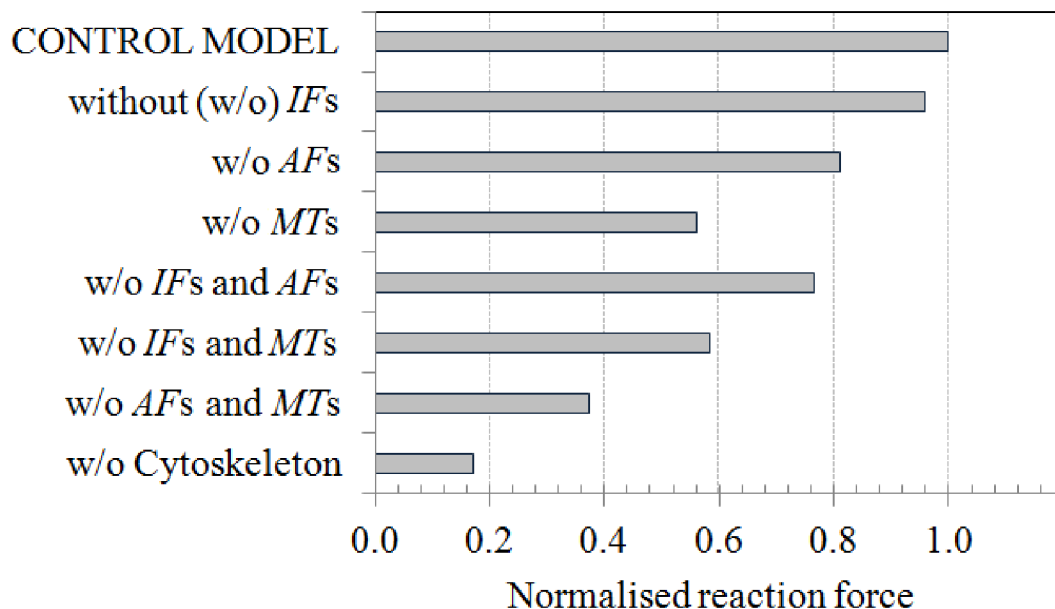


Fig. 3.10: Contribution of the cytoskeletal components individually and in mutual combination to response of cell model during stretching, highlighting their synergistic effect. The reaction force of different cell models is normalized with respect to that from the control model.

The maximum reaction force of the cell model (under elongation of 6.3  $\mu\text{m}$ ) without cytoskeleton was 5.82 times lower than the control model, emphasizing their pivotal role in characterizing the tensile properties of cell. The reaction force of the cell model without

IFs was slightly less than the reaction force of the control model indicating their minimal contribution to cell stiffness at low strains (below 20%). Compared to the reaction force of the control model, removal of AFs reduced the reaction force of cell model by one fifth, whereas removal of MTs reduced it to approximately half, suggesting that MTs resist intracellular tension generated by AFs. Moreover, removal of both AFs and MTs drastically reduced the reaction force of cell model making it more compliant and highlighting thus their synergistic effect. Therefore, AFs and MTs play crucial roles in maintaining cell stiffness during stretching, similar to that observed in experiment by [Nagayama et al. \(2008\)](#).

### 3.6.4. Parametric variations of material properties

[Figure 3.11](#) depicts the results of parametric studies investigating the effect of varying modulus of elasticity of individual cellular components on the cell response to stretching.

During these studies, the prestress in AFs was retained constant.

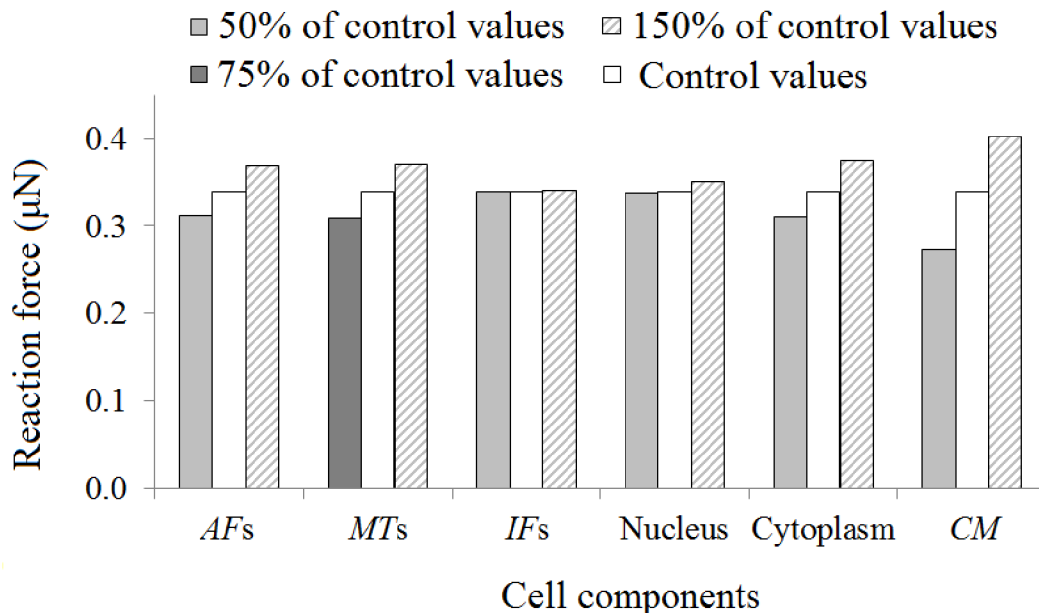


Fig. 3.11: The effect of varying elastic modulus of individual cell components from the control values ([Table 3.2](#) and [Table 3.3](#)) on the overall cell reaction force during stretching.

It was observed that the reaction force of the model was highly sensitive to the variation of Young's modulus of certain cellular components. The variation of Young's modulus of both AFs and MTs substantially affected the cell reaction force. A 50% decrease in Young's modulus of MTs was not realized due to problems with convergence and thus, only 25% decrease in the same was considered. Among continuum elements, regardless of small thickness the change in Young's modulus of CM had significant influence on the overall cell reaction force followed by cytoplasm. The parametric studies revealed that during stretching the overall cell reaction force was relatively insensitive to the changes in elastic modulus of IFs and nucleus. Although not presented in Fig. 3.11, simulations have demonstrated that inclusion of the compressibility for both nucleus and cytoplasm, did not much affect the overall cell reaction force.

### **3.6.5. Effect of increase in the density of cytoskeletal components**

Measuring the number of the cytoskeletal components experimentally is one of the most difficult parameters however, effect of increase in the density of these components can be determined computationally. The structural arrangement of cytoskeletal components in the proposed model is a simplified representation of their complexity in real cell. The number of nodes that define interconnectivity between the cytoskeletal components (FAs) affects the cell response to stretching.

An increase in overall cell reaction force was observed for increased number of AFs and MTs as depicted in Figs. 3.12a and 3.12b. During cell stretching, additional AFs created in the cell interior got aligned in the direction of stretch and increased the cell stiffness. In the same way, additional MTs orientated in the loading direction were straightened to resist tensile forces and thus substantially increased the overall cell reaction force. Increase in the density of elements representing IFs did not show much variation in cell reaction force (Fig. 3.12c), suggesting low impact of these filaments on the cell

stiffness due to their waviness.

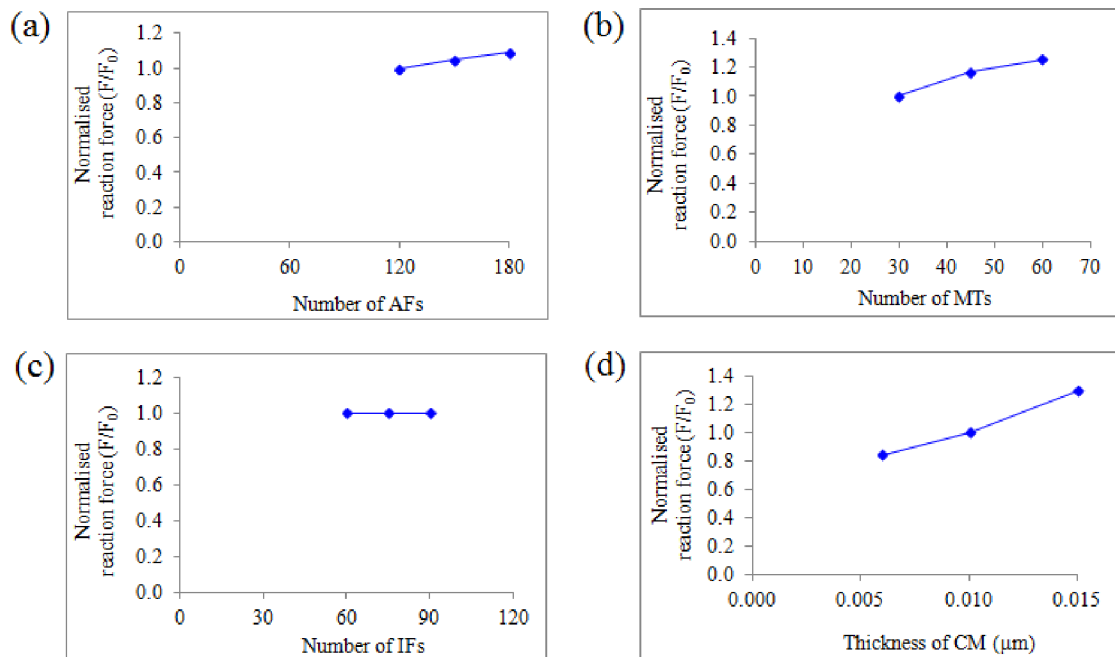


Fig. 3.12: Effect of increase in the density of cytoskeletal components (a) AFs, (b) MTs, and (c) IFs on the overall cell reaction force; (d) effect of varying the thickness of CM on the cell response to stretching.

Variation of the thickness of CM affected the overall cell reaction force substantially (Fig. 3.12d).

## 3.7. Results of simulated compression test

### 3.7.1. Validation of the proposed model

The force-deformation curve calculated from compression test simulation is in good agreement with the non-linear response of the experimental curve obtained from the compressive test of a single chondrocyte [Nguyen et al. (2009)], as depicted in Fig. 3.13 and thus validates the proposed bendo-tensegrity model of a suspended cell. The slope of the simulated force-deformation curve increased with increase in cell compression, similar to that observed in the experiments [Nguyen et al. (2009), Ujihara et al. (2012)].

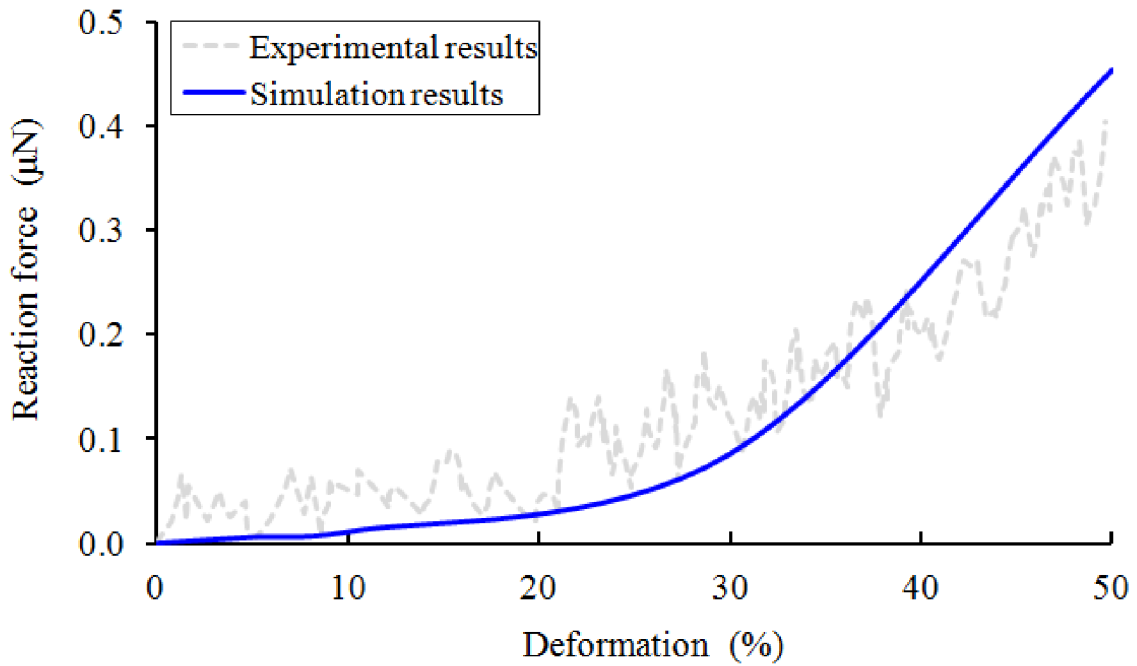


Fig. 3.13: Comparison of simulated force-deformation curve with the experimental curves taken from a study by [Nguyen et al. \(2009\)](#), investigating the biomechanical properties of a single chondrocyte using a micromanipulation technique.

Similar to tension test, the stiffness of the control model of suspended cell in compression was calculated as the ratio of conventional stress ( $\sigma$ ) to conventional strain ( $\epsilon$ ) using [Eqs. \(3.1\)](#) and [\(3.2\)](#). Here,  $f = 0.4537 \mu\text{N}$  was the reaction force of cell at the compressed edge,  $l = 16.132 \mu\text{m}$  was the deformed length of cell, both for 50% compression,  $a = 817.15 \mu\text{m}^2$  was the (maximal undeformed) cross-sectional area of cell, and  $l_0 = 32.264 \mu\text{m}$  the undeformed length of cell at zero reaction force. Thus the stiffness of 1.109 kPa was calculated for the model.

### 3.7.2. Predictions of deformations inside the cell

This model also enables visualization of the mechanics of individual cytoskeletal components during compression test. The cell was initially spherical ([Fig. 3.7a](#)), but with compression, it elongated perpendicularly to the direction of loading. [Figure 3.14a](#) exhibits the deformed shape of cytoskeletal components and nucleus during compression test

simulation, where the nucleus appears elongated perpendicularly to the loading direction concomitant of cell compression, analogous to that observed in experiments [Ujihara et al. (2012), Caille et al. (2002)]. During cell compression, the randomly oriented AFs and IFs were likely to be aligned passively in the direction perpendicular to loading. The filaments aligned in the loading direction were compressed, whereas the perpendicular ones were stretched.

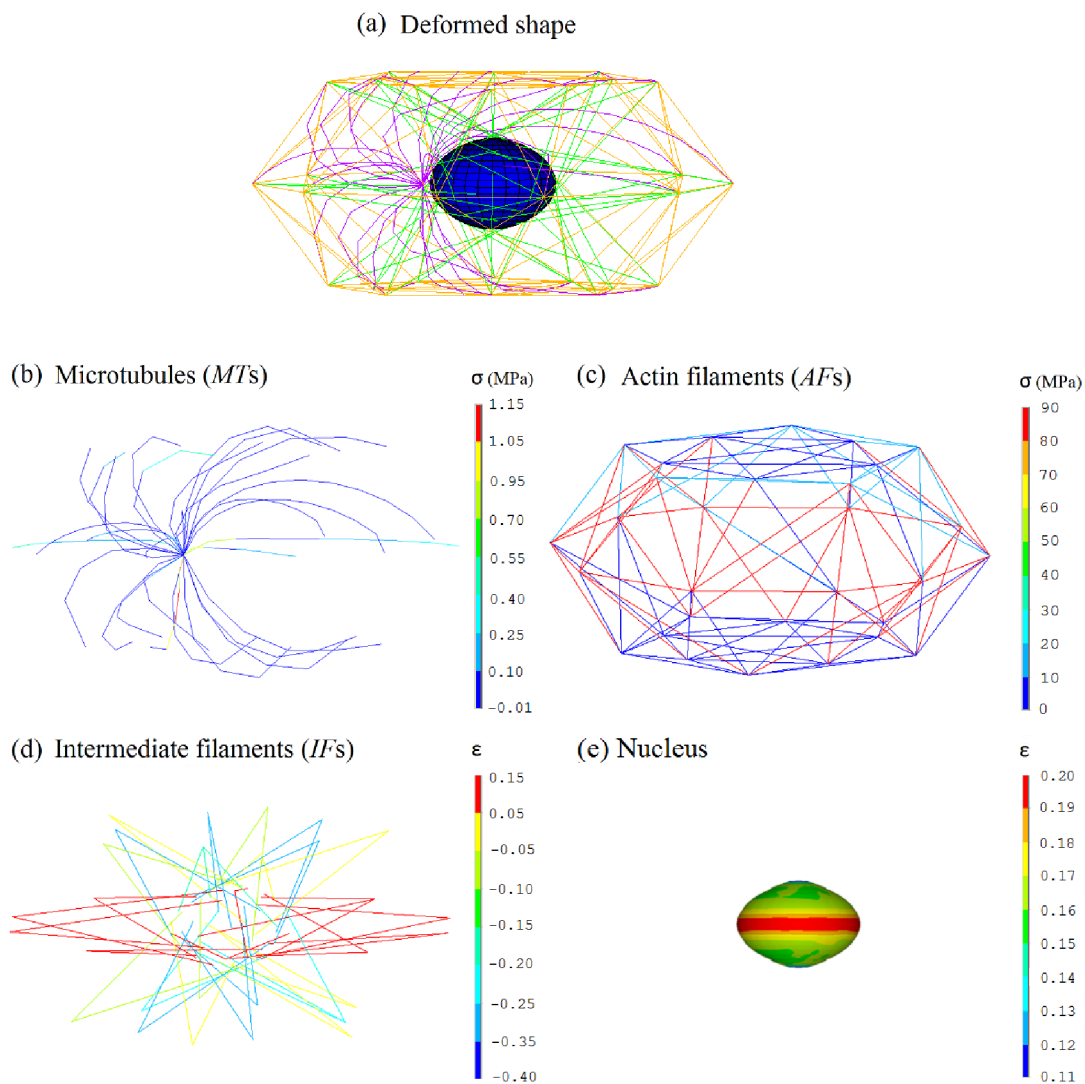


Fig. 3.14: Simulation results of 50% cell compression: (a) deformed shape of the cytoskeletal components and nucleus; distribution of axial stress in the discrete elements representing (b) MTs and (c) AFs; (d) distribution of axial strain in the discrete elements representing IFs; (e) distribution of first principal strain in the continuous elements representing nucleus.

MTs localized in the central region perpendicular to the direction of loading were straightened, while the others remain bended (Fig. 3.14b). The number of stretched filaments increased as the cell was compressed more. The proposed model can predict correlation of cellular mechanical properties and stress/strain distribution within the specific cytoskeletal components during compression. MTs that were straightened and aligned in the direction perpendicular to compression resist tensile forces and generate low positive stresses, while those ones that were bended due to compressive forces generate low negative stresses (Fig. 3.14b); this effect highlights the influence of the shape of MTs on cell deformation. AFs reoriented perpendicularly to the loading direction resist tensile forces and generate high stresses (Fig. 3.14c) consequently increasing stiffness of the entire cell. The number of these reoriented filaments increased with cell compression that in turn increased the cell stiffness gradually as observed experimentally by Ujihara et al. (2012).

IFs reoriented perpendicularly to the direction of compression were slightly uncoiled from their assumed initial waviness and exhibited positive strains with no stresses induced, while negative strains were observed in those ones aligned in the compression direction indicating that they remained wavy (Fig. 3.14d). A symmetrical and non-uniform strain distribution pattern concentrated at equatorial region was observed in the nucleus (Fig. 3.14e) with a maximum deformation of 20% (first principal strain). This quantitative characterization of nucleus deformation could be hypothetically decisive for transducing mechanical signals into changes in gene expression for 50% cell compression (global deformation) [Leipzig et al. (2008), Shieh et al. (2007)].

### 3.7.3. Mechanical contribution of the cytoskeletal components

Figure 3.15 illustrates the results of parametric studies investigating the mechanical contribution of individual cytoskeletal components to the overall cell reaction force under



compression of 50%. The role of each cytoskeletal component in resisting compressive forces acting on cell was investigated via removal of each cytoskeletal component from the control model.

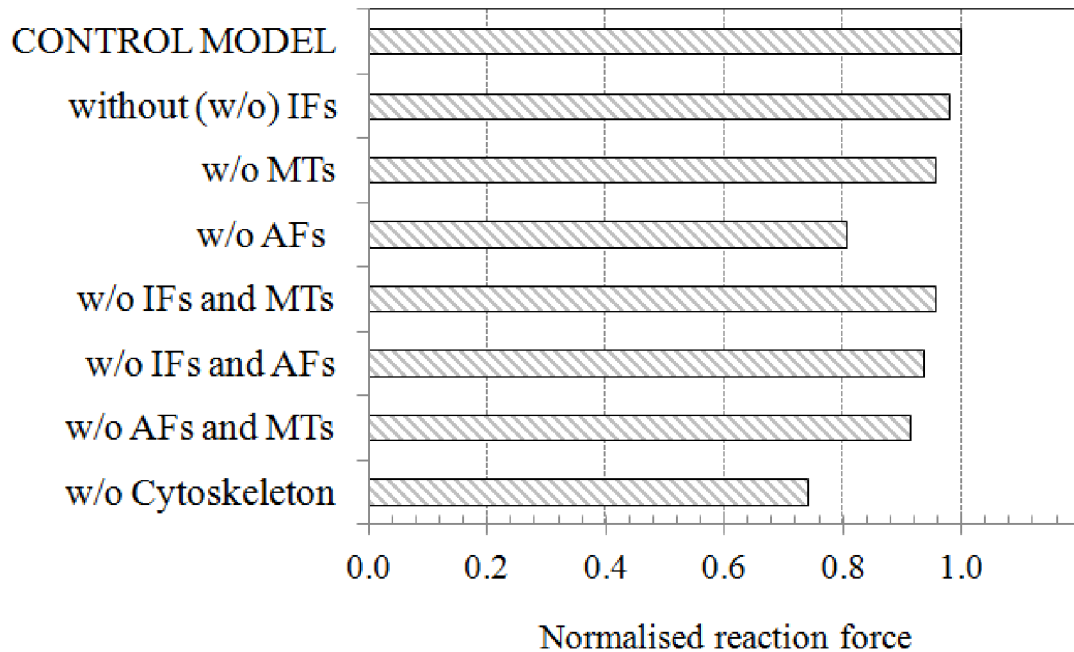


Fig. 3.15: Contribution of the cytoskeletal components individually and in mutual combination to response of cell model during compression, highlighting their synergistic effect. The reaction force of different cell models is normalized with respect to that from the control model.

The maximum reaction force of the cell model without cytoskeleton was 1.35 times lower than the control model, highlighting their role in characterizing the compressive properties of cell. When MTs were removed the model showed an approximately twofold decrease in the cell reaction force compared to the model with IFs being removed. Compared to the reaction force of the control model, removal of AFs reduced the reaction force of the cell model by one fifth. Even though AFs are tension bearing elements, they play a vital role in maintaining the cell stiffness during compression, similar to that observed experimentally by [Ujihara et al. \(2012\)](#). Additionally, the cell models created without one or more cytoskeletal components were also inadequate to withstand the cell

forces, underlining their synergistic effect.

### 3.7.4. Parametric variations of material properties

Figure 3.16 shows the results of parametric studies investigating the effect of varying modulus of elasticity of individual cellular components on the cell response to compression. During these studies, the prestress in AFs was retained constant. It was observed that the reaction force of the model was highly sensitive to the variation of elastic modulus of certain cellular components.

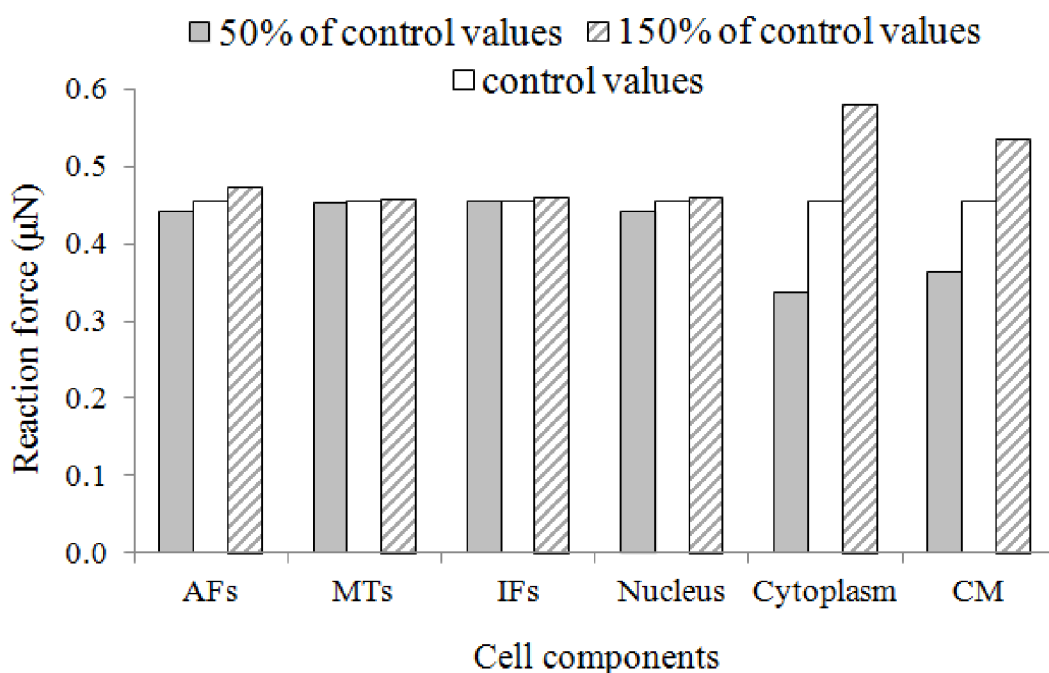


Fig. 3.16: The effect of varying elastic modulus of individual cell components from the control values (Table 3.2 and Table 3.3) on the overall cell reaction force under compression.

The variation of Young's modulus of AFs considerably affected the cell reaction force. Among continuum elements, cytoplasm with its large volume had significant influence on the cell reaction force followed by CM regardless of its small thickness. On the other hand, the cell model sensitivity to elastic modulus of the nucleus was limited that can be associated to its small volume. The parametric study revealed that the cell reaction force

was relatively insensitive to the changes in Young's modulus of both MTs and IFs. Although not presented in Fig. 3.16, simulation results have demonstrated that inclusion of cytoplasm compressibility minimally affected the overall cell reaction force.

### 3.7.5. Effect of increase in the density of cytoskeletal components

The number of nodes that define interconnectivity between the cytoskeletal components (FAs) affects the cell response to compression. Additional AFs created in cell interior increased the overall cell reaction force (Fig. 3.17a), whereas increase in the density of both MTs and IFs did not show much variation (Figs. 3.17b and 3.17c).

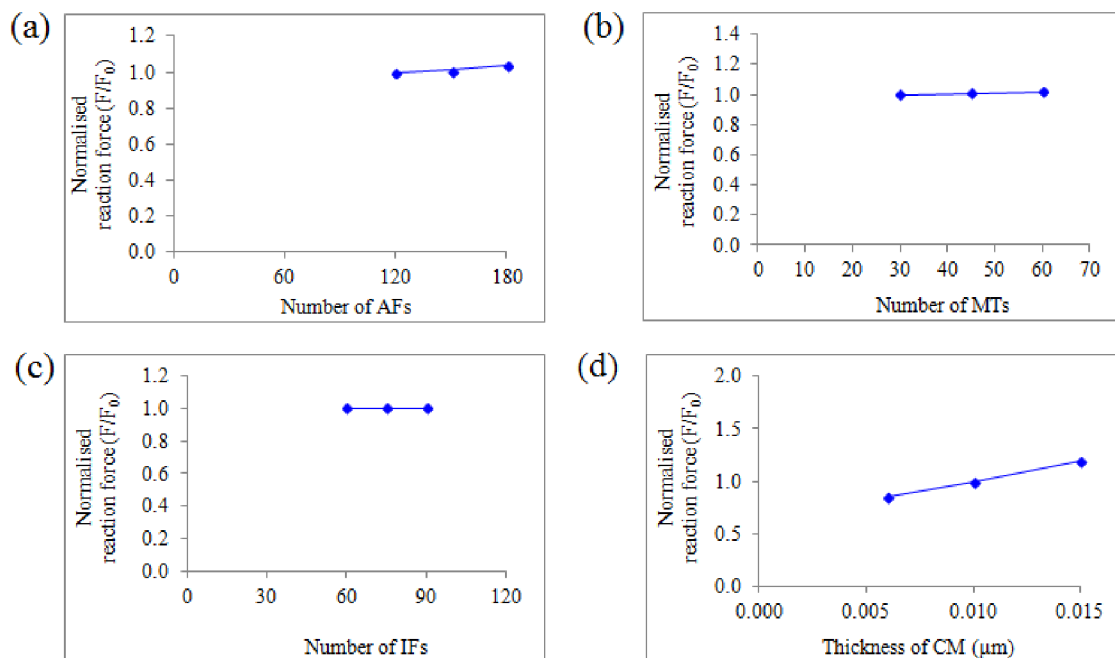


Fig. 3.17: Effect of increase in the density of cytoskeletal components (a) AFs, (b) MTs, and (c) IFs on the overall cell reaction force; (d) effect of variation of CM thickness on the global cell response to compression.

Similar to that observed in tension test simulations, variations of CM thickness substantially affected the overall cell reaction force (Fig. 3.17d) during compression. It has been observed that the influence of increase in the number of cytoskeletal components shows an effect similar to that of increase in their elastic modulus. A similar effect

occurring for CM suggests that its behavior is dominated by tension (membrane stresses) rather than by bending (bending stiffness of a shell is proportional to the 3rd power of its thickness).

### **3.8. Summary of suspended cell model**

The proposed bendo-tensegrity model of suspended cell describes the response of cytoskeletal components and cell as a whole to distinct mechanical stimuli (elongation and compression), thus satisfying the initial hypothesis. The proposed model predicted the relation between cellular mechanical response and stress/strain distributions within the specific cytoskeletal components under different loading conditions. For simulation of both tests, it provides quantitative characterization of nucleus deformation.

The tensile test simulations demonstrated that AFs and MTs play a crucial role in cell stiffness including its increase with stretching, while the compression test simulations revealed that although being tension-bearing elements, AFs contribute significantly to the compressive response of a cell. Thus, the proposed bendo-tensegrity model identifies the cytoskeletal components that influence the global mechanical response of suspended cell depending on the type of mechanical loading.

Parametric studies of material properties of cell components demonstrated that cell response to stretching was highly affected by changes in elastic modulus of AFs, MTs, CM, and cytoplasm. Likewise, cell response to compression was highly affected by variations of elastic modulus of AFs, CM, and cytoplasm. Similar results were obtained from parametric studies of increase in the density of cytoskeletal components: the cell response to both stimuli was sensitive to increase in the density of AFs and variations of the thickness of CM, but only the cell response to stretching was sensitive to increase in the density of MTs.

Thus, the proposed suspended cell model based on the bendo-tensegrity concept

provides new insights into the interdependence of cellular mechanical properties, the mechanical role of components of cytoskeleton, and the nucleus deformation under different mechanical loading conditions.

---

**FINITE ELEMENT MODIFIED BENDO-TENSEGRITY MODEL  
OF ADHERENT CELL**

---

**4.1. Hypothesis**

Implementing the bendo-tensegrity concept [Mehrbood et al. (2011)] with fusion of continuum and discrete approaches, a FE bendo-tensegrity model of adherent cell modified from the suspended cell model (chapter 3) incorporating MTs, ABs, IFs, nucleus, cytoplasm, and AC is proposed in the current study. The unique features of this structural model keep fundamental principles governing cell behavior, including cellular prestress and interaction between the cytoskeletal components with their more realistic morphological representation for cell in adherent state.

The hypothesis of this study is that the proposed modified bendo-tensegrity model of adherent cell can describe the cellular structural behavior and determine cell's local response to extracellular deformation. The proposed model can not only study the cell's response to local surface deformation initiated by some extracellular body but also if it responds differently depending on the deformation location. For this, indentation using AFM is simulated with the proposed model indenting at two distinct locations at the apex (between the FAs above the nucleus) and at a receptor (at FA away from the nucleus), providing local mechanical response of cell. This experimental technique helps to establish a link between the biochemical and mechanical environment of adherent cells. The aim of this study is to extend the knowledge of how mechanical signals in the form of forces due to indentation propagate within cells. More specifically, focusing on the mechanical role of each cytoskeletal component in the intracellular force propagation and the quantitative characterization of the deformation of nucleus hypothetically decisive for

mechanotransduction, which in turn aids in better understanding of how cellular processes are mechanically controlled.

## 4.2. FE model formulation

In this study, the simulation of AFM indentation test with the proposed FE adherent cell model was performed and the results obtained were compared with corresponding experimental results. *In situ* microscopic observations of cell shape in adherent state (Fig. 4.1) as well as images of distributions of cytoskeletal proteins (Figs. 3.2a and 3.3a) were referred to create a 3D adherent cell model and the architecture of its cytoskeletal components.

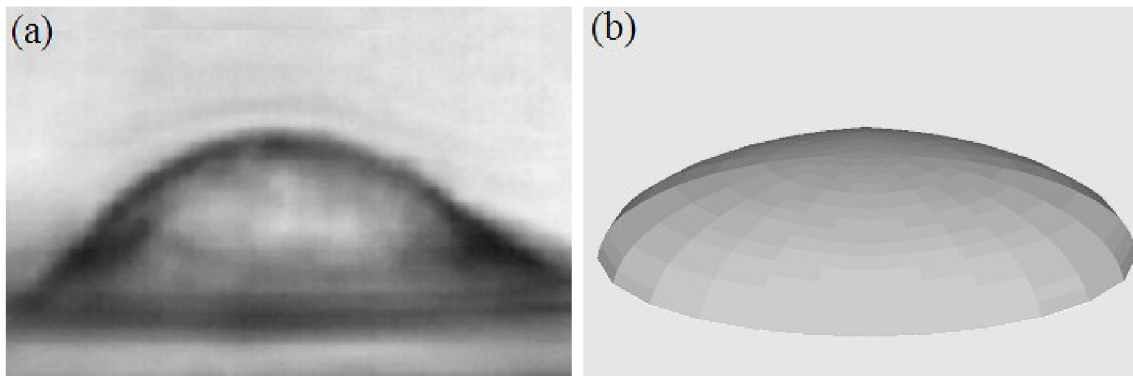


Fig. 4.1: Typical images of: (a) an adherent cell on a rigid microplate [Thoumine et al. (1999)] and (b) corresponding proposed FE adherent cell model.

The adherent cell model is slightly different from the suspended cell model (section 3.2), it encompasses the nucleus and cytoplasm enclosed by the AC (Fig. 4.2a) and cytoskeletal components like ABs, MTs, and IFs (Fig. 4.2b).

For this model, the size and approximate geometry was based on the rules described by McGarry et al. (2004). The model geometry was semi-ellipsoidal with the radius of  $19\ \mu\text{m}$  (semi-major axis in both front and top views), height of  $8\ \mu\text{m}$  (semi-minor axis in front view), and half-width of  $12.66\ \mu\text{m}$  (semi-minor axis in top view). Based on the experimental observations [Caille et al. (2002)], nucleus was also modeled ellipsoidal. It is positioned at the center of the top view at the height of  $2\ \mu\text{m}$  from the substrate with radius

of  $2.5\ \mu\text{m}$  (semi-major axis) and height of  $3\ \mu\text{m}$  (semi-minor axis of  $1.5\ \mu\text{m}$ ).

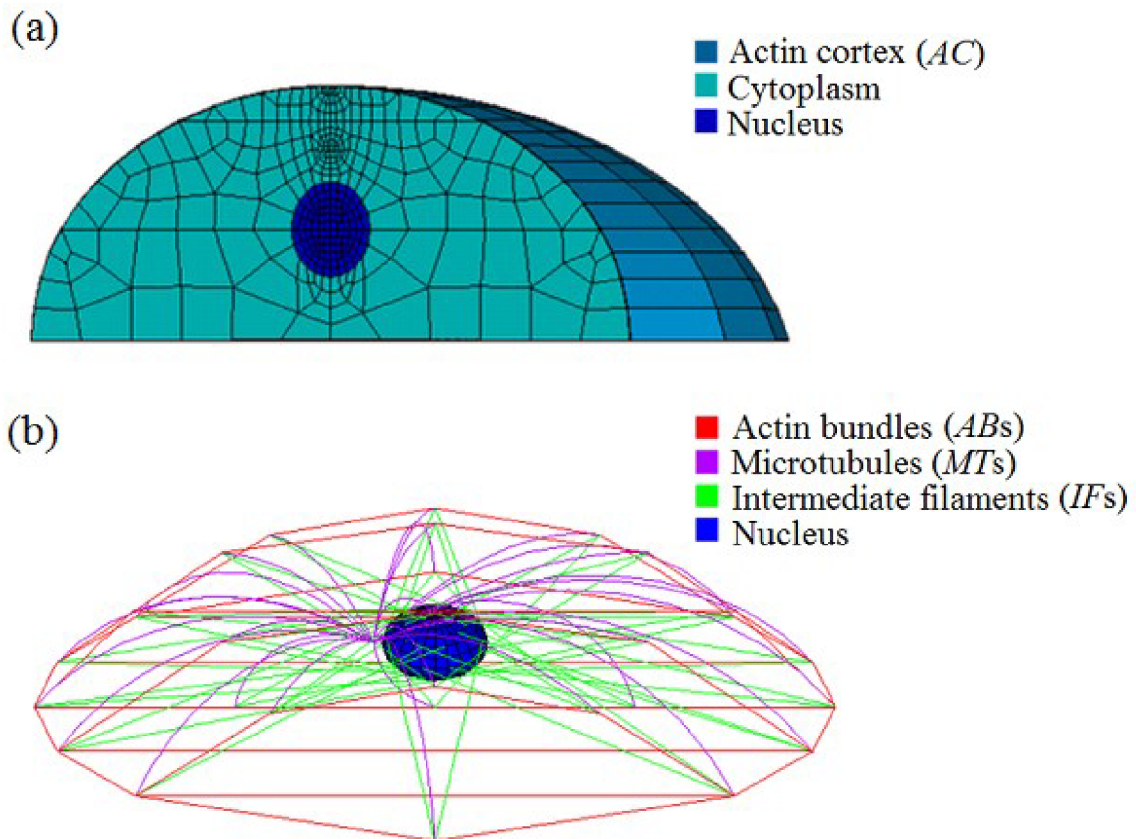


Fig. 4.2: For adherent cell model: (a) sections of continuous (volume) elements and (b) structural arrangement of cytoskeletal components with respect to the nucleus.

Due to the geometric complexity of cell configuration, both cytoplasm and nucleus were meshed with four-node tetrahedral solid elements. Using analogous approach as presented by Barreto et al. (2013), a thin layer of actin-gel at the cell surface referred to as AC was modeled with four-node quadrilateral shell elements of  $0.2\ \mu\text{m}$  thickness [Unnikrishnan et al. (2007), Jean et al. (2005)] and no bending stiffness. Here, the CM was not explicitly considered as it is thinner than the adjacent AC and therefore its minor contribution to resisting local deformation was included in the shell stiffness dominated by AC.

For this model, the morphological representation and spatial distribution of both MTs and IFs were retained analogous to that of the suspended cell model (see section 3.2). In contrast, however, in a cell adhered to a rigid substrate thick ABs were observed localized



at the cell periphery running almost uniformly in the longitudinal direction [Barreto et al. (2013), Deguchi et al. (2005)] as depicted in Fig. 4.3a.

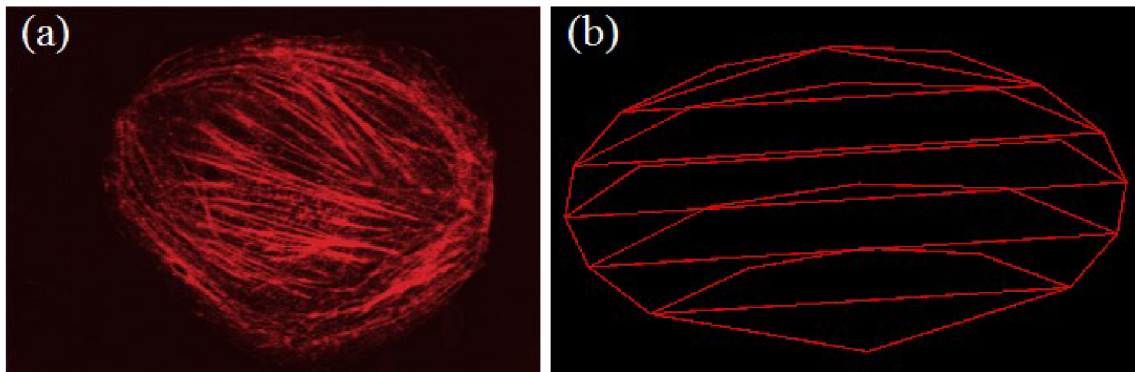


Fig. 4.3: (a) Microscopic fluorescence image of the architecture of ABs cited from Cytoskeleton, Inc and (b) their corresponding architecture in the proposed computational model.

These bundles were modeled using truss elements (Fig. 4.3b) that resist only tensile loads and arranged along the AC with both ends anchored to it at FAs together with elements representing MTs and IFs to achieve their synergistic effect. ABs are internally prestressed (stressed even without application of an external load); to achieve this in the proposed model, the prestress caused by 24% of prestrain [Deguchi et al. (2005), Barreto et al. (2013)] was assigned to them generating the initial force essential for cell shape stability (Fig. 3.4b). For simplification, all ABs in the model were prestressed equally.

Table 4.1: Mesh properties of the adherent cell model in ANSYS

Cell component	Element type	Element definition
Microtubules (MTs)	Beam	Beam188
<b>Actin bundles (ABs)</b>	<b>Truss</b>	<b>Link180</b>
Intermediate filaments (IFs)	Truss	Link180
<b>Actin cortex (AC)</b>	<b>Shell</b>	<b>Shell181</b>
Cytoplasm	Continuous (volume)	Solid185
Nucleus	Continuous (volume)	Solid185

*Note: The cell components in bold differ from the suspended cell model*

The mechanical behavior of living cells is mainly characterized by the cytoskeletal filaments that contribute significantly to the mechanical stiffness of the cell. The element types used for modeling cytoskeletal components were chosen to better represent their idealized structural role and are summarized in [Table 4.1](#).

### 4.3. Material properties

Material properties have been set mostly identical with the suspended cell model presented in [chapter 3](#); differences are highlighted in [Table 4.2](#) and [4.3](#). Due to the difficulty of obtaining elastic parameters of cellular components from a single cell type, those employed in the current study were acquired from literature for distinct cell types measured using various experimental techniques.

Table 4.2: Elastic properties of discrete components of adherent cell model

Cell component	Elastic modulus, E (Pa)	Poisson's ratio, $\nu$	Diameter (nm)
Microtubules (MTs) [ <a href="#">Gittes et al. (1993)</a> ]	$1.2 \times 10^9$	0.3	(outer/inner) 25/17
<b>Actin bundles (ABs)</b> [ <a href="#">Deguchi et al. (2005)</a> ]	<b><math>0.34 \times 10^6</math></b>	<b>0.3</b>	<b>250</b>
Intermediate filaments (IFs) [ <a href="#">Xue et al. (2015)</a> ; <a href="#">Bertaud et al. (2010)</a> ]	$7.6 \times 10^6$	0.3	10

*Note: The cell component in bold differ from the suspended cell model*

Table 4.3: Hyperelastic properties of continuous components of adherent cell model

Cell component	Elastic modulus, E (Pa)	Calculated shear modulus, G (Pa)
Cytoplasm [ <a href="#">Caille et al. (2002)</a> ]	$0.5 \times 10^3$	$0.17 \times 10^3$
Nucleus [ <a href="#">Caille et al. (2002)</a> ]	$5 \times 10^3$	$1.7 \times 10^3$
<b>Actin cortex (AC)</b> [ <a href="#">Stricker et al. (2010)</a> ]	<b><math>2 \times 10^3</math></b>	<b><math>0.67 \times 10^3</math></b>

*Note: The cell component in bold differ from the suspended cell model*

#### 4.4. Loads and boundary conditions

Indentation of a rigid AFM tip into a cell adhered to a rigid substrate (Fig. 4.4) was simulated to investigate the cell's response to indentation (local deformation).

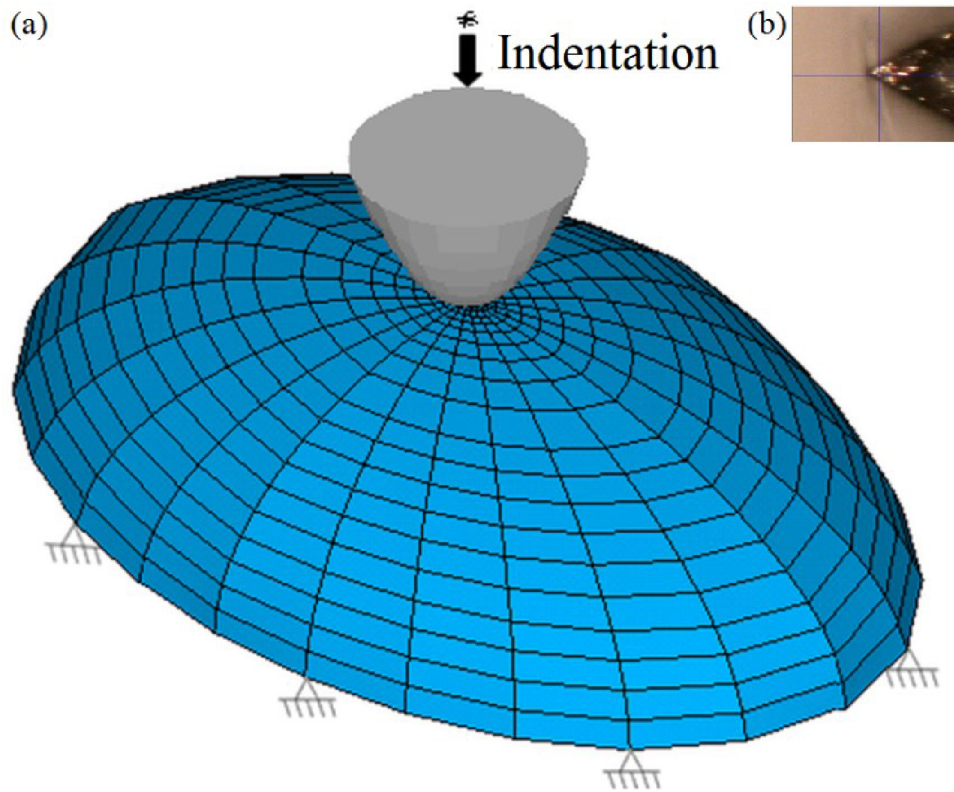


Fig. 4.4: (a) *FE* model of an adherent cell in the indentation test, with constraints and displacement load applied at the tip acting on the top of the cell. (b) Snapshot of a cell during AFM indentation experiment (top view) [Hemmer (2008)].

A rigid paraboloid indenter with the tip curvature radius of 200 nm was modeled above the cell in line with nucleus, to exert a stimulus and obtain the reaction force in the assigned pilot node. By prescribing a vertical shift to the pilot node, the tip was advanced towards the cell to penetrate it after having come into contact. Corresponding to indentation depth in AFM experiments, the vertical displacement of 2.5  $\mu\text{m}$  was applied to the tip. For a non-linear contact problem of tip-cell interaction the augmented Lagrangean algorithm was considered. For all nodes at the bottom of the cell a constrained boundary condition was prescribed, simulating a cell adhered to a rigid substrate.

## 4.5. Parametric Studies

For the proposed model, parametric studies were performed considering the material properties of different cell components as parameters. The cell model incorporating all discrete and continuous elements with the material properties mentioned in [Tables 4.2](#) and [4.3](#) are referred to as the control model. To illustrate the influence of the material parameters on cell mechanical response, their values were increased and decreased by 50% of the values used for the control model. In addition, ten different cell models were created by totally removing one, two, or more of the cytoskeletal components to investigate their mechanical contribution. The reaction force of altered cell models was compared with that from the control model under 1  $\mu\text{m}$  indentation.

In the current study, effect of increase in the density of cytoskeletal filaments present in the model was analyzed in terms of overall cell reaction force by varying their number. Additional ABs were created at the cell periphery as well as in the cell interior with different orientation than earlier. The number of MTs originating from the centrosome was increased with their end nodes being chosen randomly at the AC. The density of IFs was increased by creating more IFs in the cell interior making their network denser in the perinuclear region. To investigate a similar effect of AC thickness on the overall cell reaction force its value was increased and decreased with respect to the control value.

## 4.6. Results of simulated AFM indentation test

### 4.6.1. Validation of the proposed model

The force-indentation curves calculated from simulations of AFM tip indenting the adherent cell model at the apex ([Fig. 4.5a](#)) and at a receptor distant from the apex ([Fig. 4.5b](#)) are depicted in [Fig. 4.5c](#). Both results lie within the variation range of the experimental curves obtained with AFM indentation of embryonic stem cells (ESCs) [[Pillariseti et al. \(2011\)](#)], which thus validates the proposed bendo-tensegrity model of an

adherent cell. The indentation test was simulated at two distinct locations on the cell, to explore the significance of its structural inhomogeneity that could be one of the reasons for scattering of experimental curves [Ohara et al. (2000)].

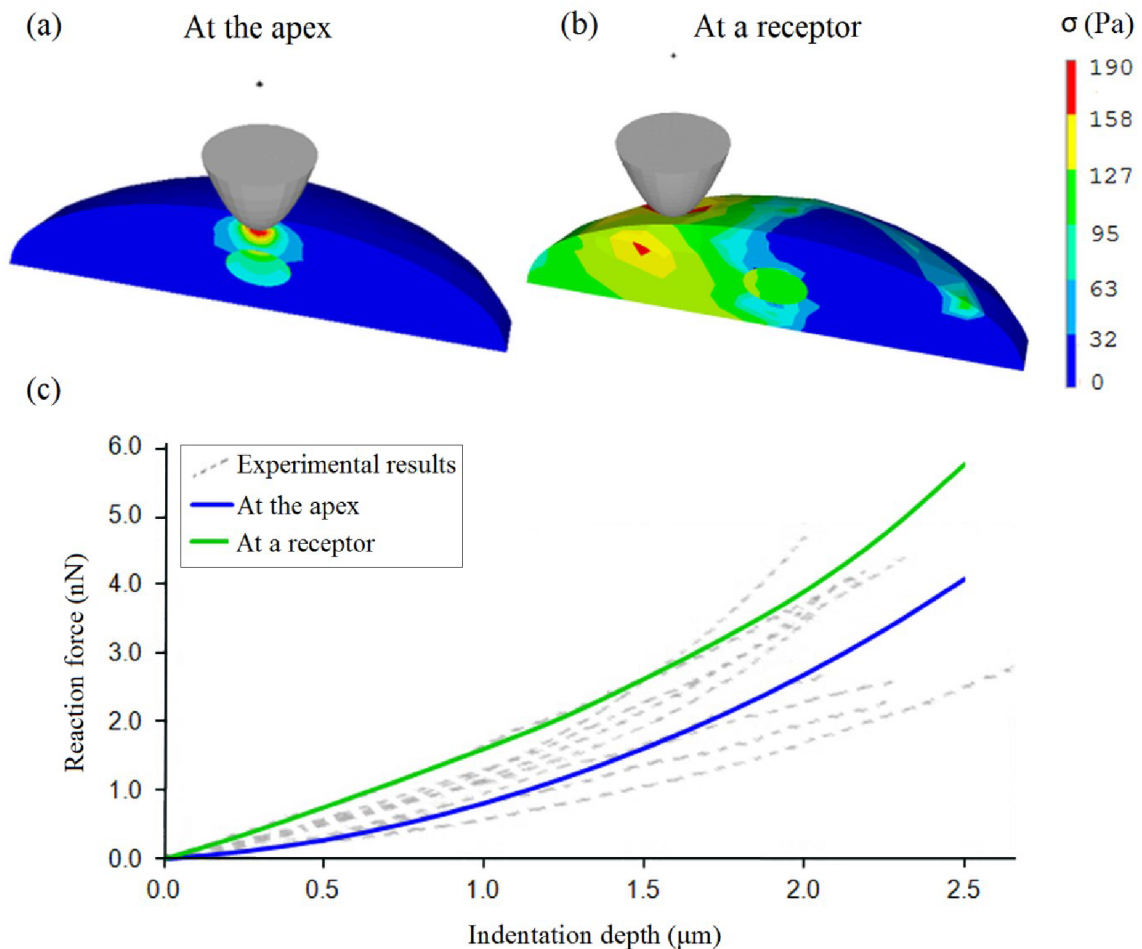


Fig. 4.5: Sectional views comparing the contour plots of von Mises stress in cytoplasm during AFM simulation for indentation depth of 1  $\mu\text{m}$  at (a) the apex and (b) a receptor; (c) comparison of simulated force-indentation curves with the experimental curves taken from a study by Pillarisetti et al. (2011), measuring the stiffness of ESCs using AFM indentation.

For indentation depth of 2.5  $\mu\text{m}$ , the reaction force predicted by the model at the apex was 4.05 nN and at a receptor was 5.72 nN, thus illustrating approximately 40% stiffer response when indenting at a receptor compared to the apex. This can be explained by the direct transmission of indenting force to cytoskeleton that is much stiffer than the

surrounding cytoplasm. Therefore, these results exhibit that the indentation site dominates the force-indentation curve which corresponds to the experimental observations [Ohara et al. (2000), Ohashi et al. (2002), Sato et al. (2000)]. A remarkable difference in stress (von Misses) distribution pattern within the cell was observed when indenting at the apex compared to a receptor, underlining the synergistic effect of cytoskeletal components on localized load transmission to the distant parts of the cell known as action-at-a-distance effect [Wang et al. (2005)]. For both simulations, stiffening of force-indentation curve with increase in indentation depth was observed.

#### 4.6.2. Predictions of deformations inside the cell

A common way to evaluate and characterize cell mechanical properties is measuring the deformation of cell in response to external stimuli. The proposed model can predict the relation between cellular mechanical response to indentation and stress/strain distributions within the specific cytoskeletal components.

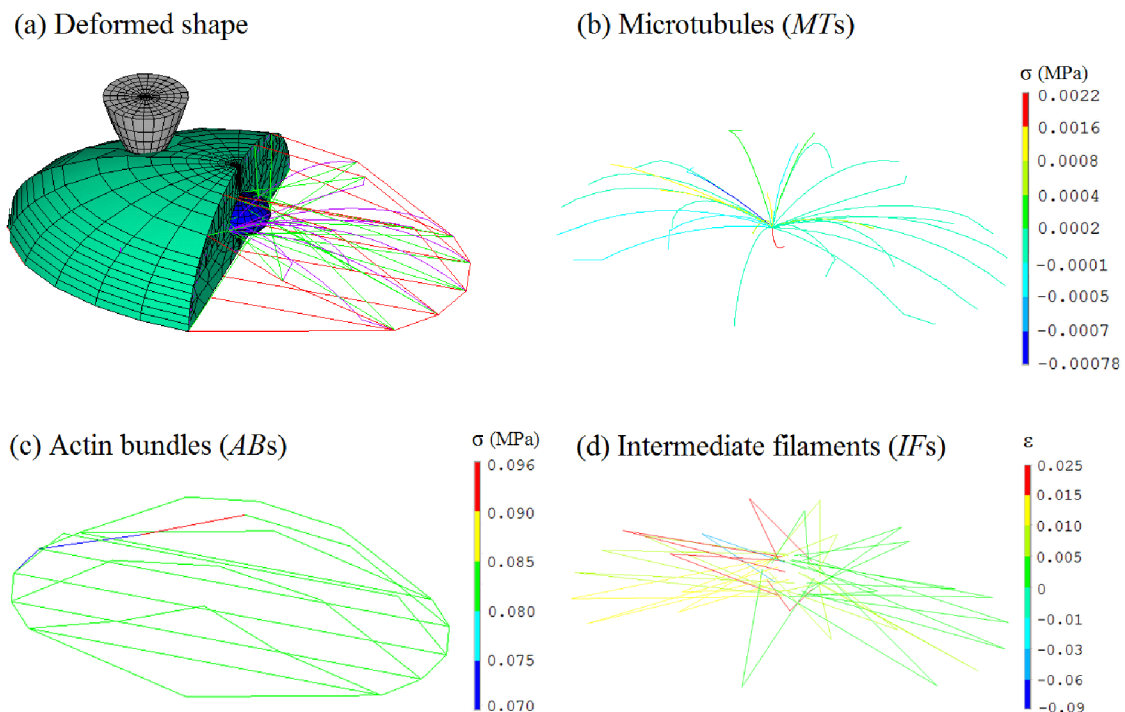


Fig. 4.6: Simulation results for indentation depth of 2.5  $\mu\text{m}$  at a receptor: (a) deformed shape of cell; distribution of axial stress in the discrete elements representing (b) *MTs* and (c) *ABs*; (d) distribution of axial strain in the discrete elements representing *IFs*.

Figure 4.6a exhibits the deformed shape of cell during indentation simulation at a receptor. The model predicted low stresses in MTs, which can be explained by their flexural behavior. MTs that were compressed due to localized load generated low negative stresses (Fig. 4.6b), while those that were stretched resisting intracellular tension generated low positive stresses. Higher stresses were observed in ABs (Fig. 4.6c) compared to MTs, highlighting the effect of this component on the localized cell deformation although they do not propagate compressive forces due to the level of prestress they are subjected to. For IFs strains are shown instead of stresses, because stresses in them are zero due to their high waviness. IFs localized around a receptor were slightly uncoiled from their assumed initial waviness and exhibited high strains, while the remaining ones showed low strains indicating that they continue to remain wavy (Fig. 4.6d).

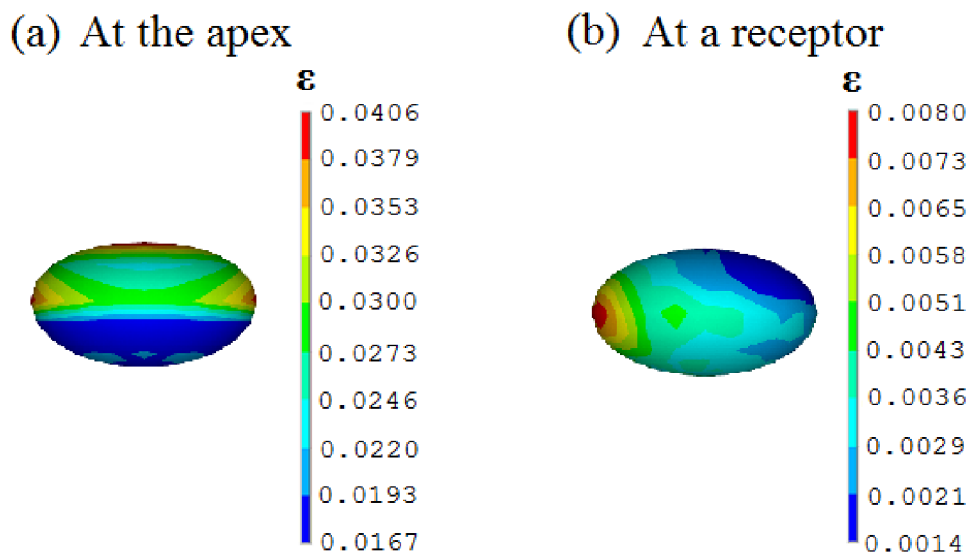


Fig. 4.7: Distribution of first principal strain in the elements representing nucleus when indenting cell at (a) the apex and (b) a receptor.

For the same indentation depth of 2.5  $\mu\text{m}$ , the nucleus deformation was about 4% when indenting cell at the apex in line with the nucleus (Fig. 4.7a), whereas it was about 0.08% when indenting cell at a receptor away from the nucleus (Fig. 4.7b); this highlights the dominance of indentation site on nucleus deformation. This quantitative characterization

of nucleus deformations could be hypothetically decisive for mechanotransduction. In both simulations a non-uniform strain distribution pattern was observed, symmetrical and concentrated at the top center region in the former, whereas non-symmetrical and concentrated at the side region (facing indentation location) in the latter.

### 4.6.3. Mechanical contribution of the cytoskeletal components

Figure 4.8 illustrates the results of parametric studies investigating the mechanical contribution of individual cytoskeletal components to the overall cell reaction force during indentation. When the cytoskeletal components were incorporated in the continuum parts, the cell reaction forces were higher and concentrated in the nodes where cytoskeletal components interact with each other (FAs). The role of each cytoskeletal component in cell's response to indentation was investigated via removal of one or more cytoskeletal components from the control model.

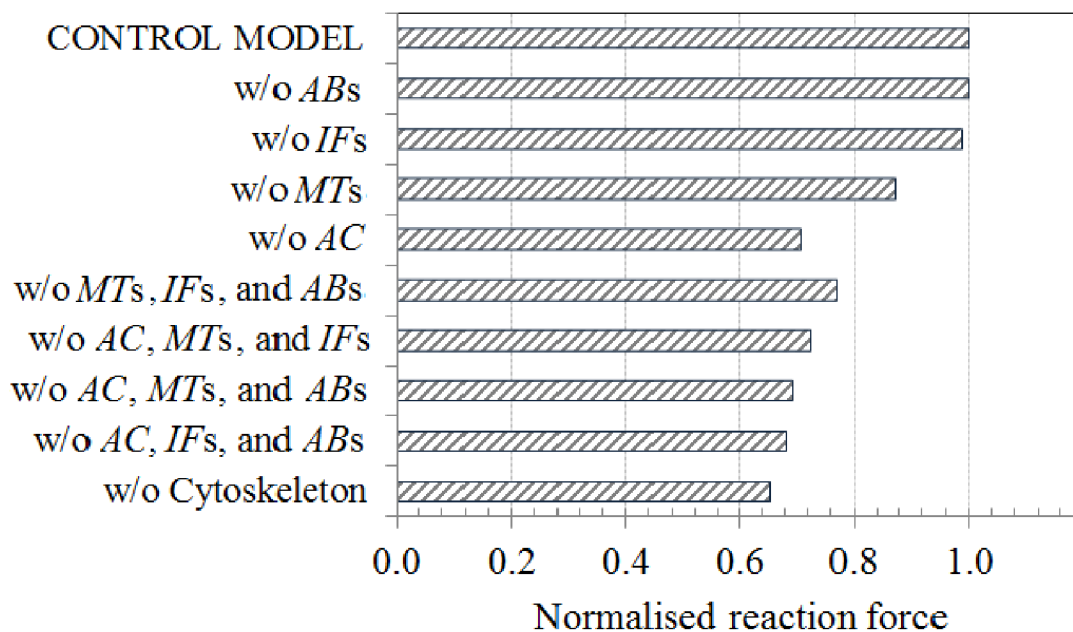


Fig. 4.8: Contribution of the cytoskeletal components individually and in mutual combination to cell's response to indentation (at a receptor), highlighting their synergistic effect. The reaction force of different cell models is normalized with respect to that from the control model.



The maximum reaction force of the cell model without cytoskeletal components was 1.52 times lower than the control model, highlighting their contribution in resisting the mechanical perturbations from exterior. For model without ABs and model without IFs, the reaction force was comparable to that of the control model, indicating their minimal effect on cell rigidity during indentation. When AC was removed the model showed approximately twofold decrease in the reaction force compared to the model with MTs being removed. Thus, AC and MTs play critical role in maintaining cell rigidity during indentation, analogous to that observed experimentally by Barreto et al. (2013). Furthermore, the cell models created without two or more cytoskeletal components were also incompetent to withstand cell forces, emphasizing their mutual interdependence during indentation.

#### 4.6.4. Parametric variations of material properties

Figure 4.9 shows the results of parametric studies investigating the effect of varying modulus of elasticity of individual cellular components on the cell's response to indentation. During these studies, the prestress in ABs was retained constant.

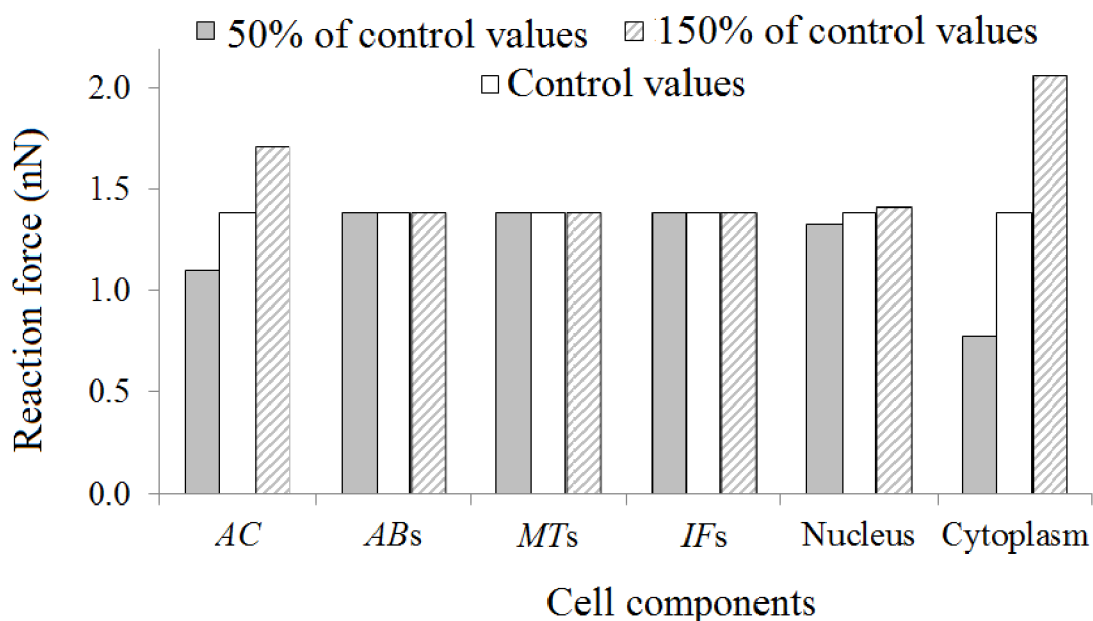


Fig. 4.9: The effect of varying elastic modulus of individual cell components from the control values (Tables 4.2 and 4.3) on the overall cell reaction force during indentation.

It was observed that the reaction force of the model was highly sensitive to the variation of elastic modulus of certain cellular components. The variation of Young's modulus of AC considerably affected the reaction force of adherent cell model, probably due to constraining the volume of cytoplasm. Parametric analysis revealed that the adherent cell model was highly sensitive to the variations in elastic modulus of cytoplasm, whereas its sensitivity to the changes in elastic modulus of nucleus was very limited that can be associated to their different volumes. On the contrary, changing the Young's modulus of ABs, MTs, and IFs to 50% or 150% of their control values did not affect the overall cell reaction force. Although not presented in Fig. 4.9, simulation results have demonstrated that inclusion of cytoplasm compressibility affect the overall cell reaction force approximately by only 2%.

#### 4.6.5. Effect of increase in the density of cytoskeletal components

Measuring the number of cytoskeletal filaments experimentally is one of the most difficult parameters however, effect of increase in the density of these filaments present in the cell model can be determined computationally.

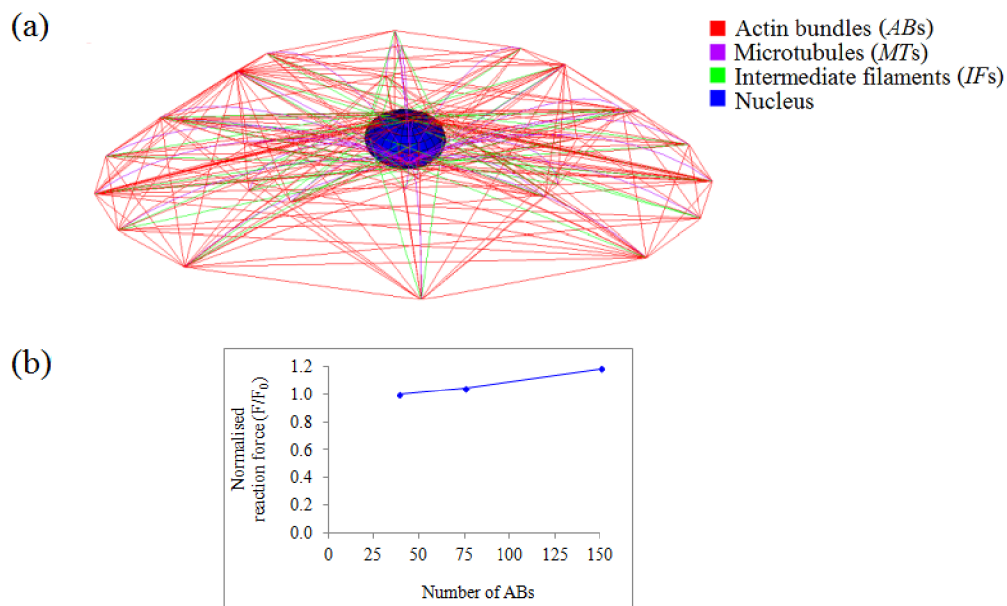


Fig. 4.10: (a) Additional ABs created in the model with new orientation for parametric studies and (b) their effect on the overall cell reaction force during indentation.

The structural arrangement of cytoskeletal components in the proposed model is a simplified representation of their complexity in real cell. Thus, it is of high interest to study effect of increase in their density on the cell's response to indentation (local deformation). Figure 4.10a exhibits additional ABs created at the cell periphery and interior. An increase in overall cell reaction force was observed for increased number of ABs (Fig. 4.10b), which might be attributed to the more number of ABs resisting local mechanical load due to their new configuration.

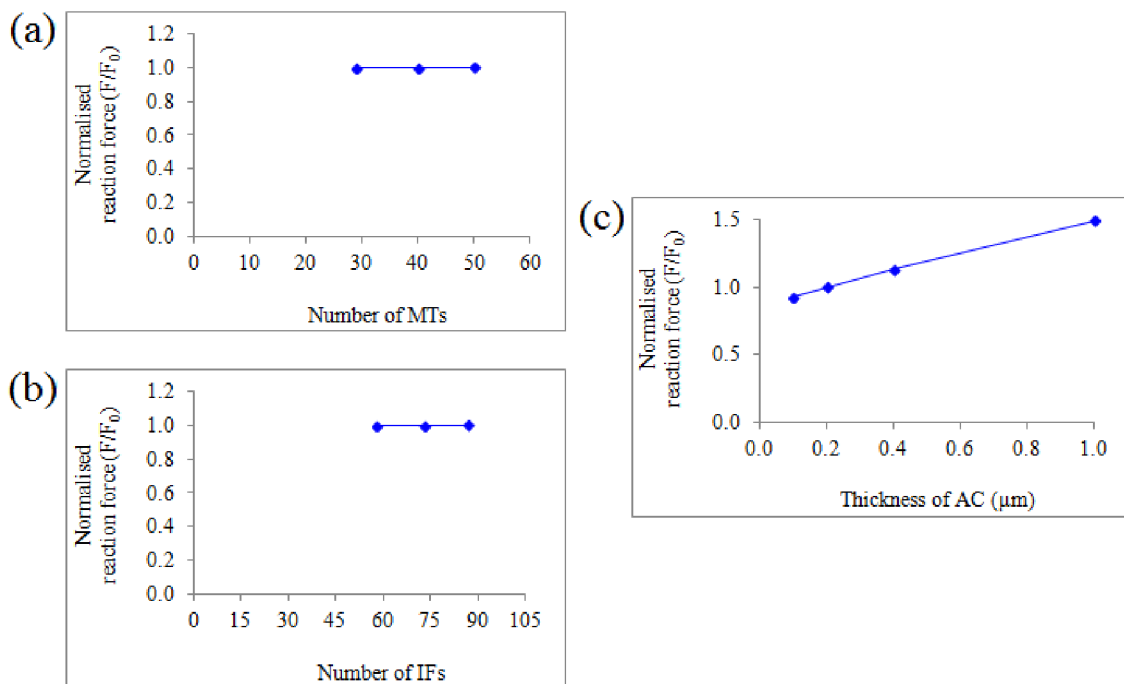


Fig. 4.11: Effect of increase in the density of cytoskeletal components (a) MTs and (b) IFs on the overall cell reaction force; (c) effect of varying the thickness of AC on the cell's response to indentation.

Increase in the density of elements representing MTs and IFs did not show much variation in the cell reaction force (Figs. 4.11a and 4.11b), whereas variation of AC thickness significantly changed the cell's response to indentation (Fig. 4.11c).

## 4.7. Summary of adherent cell model

The proposed bendo-tensegrity model of adherent cell describes the response of

cytoskeletal components and cell as a whole to AFM indentation, thus satisfying the initial hypothesis. This model describes the mechanical role of individual cytoskeletal components including stress/strain distribution within them. It provides quantitative characterization of nucleus deformation for both indenting sites (at the apex and at a receptor).

The indentation simulations exhibited that indentation site dominates the cell behavior where AC and MTs were essential for cell rigidity. Thus, the proposed model identifies the cytoskeletal components that influence the local mechanical response of adherent cell. Parametric studies of material properties exhibited that changes in elastic modulus of AC and cytoplasm highly affected the cell's response to indentation. Further, parametric studies of increase in the density of cytoskeletal components revealed that the same was sensitive to increase in the density of ABs in the cell interior and variations of the thickness of AC.

Thus, the proposed adherent cell model based on the bendo-tensegrity concept opens new perspectives in studying the interdependence of cellular mechanical properties, mechanical contribution of individual cytoskeletal components, and the nucleus deformation.

### DISCUSSION

---

The presented models aim at realistic simulation of the deformation of cell, primarily focusing on mimicking its structure to obtain realistic nucleus deformation. It is well established that cells respond to mechanical stimuli in a variety of ways that range from changes in cell morphology to activation of biochemical responses, which affect the cell's phenotype. The nucleus plays a central role in defining cell responses thus the current study provides an insight into its deformation by means of FE modeling of distinct single cell mechanical tests. The nucleus deformation of 8% (maximum first principal strain) was observed for cell stretching of 6.3  $\mu\text{m}$  (20% global cell deformation), whereas the maximum first principal strain in nucleus was about 20% for cell compression of 16.132  $\mu\text{m}$  (50% global cell deformation). Moreover, the maximum first principal strain in nucleus was approximately 4% under indentation of 2.5  $\mu\text{m}$  at cell apex, suggesting that the nucleus deformation depends on the nature of biophysical stimulus [Prendergast et al. (2007)]. Further, it is observed that the same maximum first principal strain of 4% in nucleus can be induced either by cell indentation of 2.5  $\mu\text{m}$  at the apex or by cell stretching of 2.081  $\mu\text{m}$  or by cell compression of 3.871  $\mu\text{m}$ . This quantitative characterization of nucleus deformation during distinct mechanical tests of single-cell could be hypothetically decisive for initiating the mechanotransduction. It means that, from the point of view of biochemical responses, the indentation of 2.5  $\mu\text{m}$  could be equivalent to stretching by 2.081  $\mu\text{m}$  or to compression by 3.871  $\mu\text{m}$ .

Although it was intended to simulate various mechanical tests using the same model, the distinctness in the form and organization of actin protein for cell in suspended and adherent states served as a motivation for creating two distinct models of cell. In numerous

experimental studies, for cell in suspended state a dense network of thin AFs is observed at cell periphery localized beneath the CM [Casati et al. (2014), Ofek et al. (2010), Li et al. (2006), Nagayama et al. (2006), Guck et al. (2005), Reinhart-King et al. (2005), Sato et al. (1987)], whereas for cell in adherent state a thin layer of actin-gel referred as AC is observed at the cell periphery along with thick ABs running almost uniformly in the longitudinal direction [Barreto et al. (2013), Matsumoto et al. (2012), Roy et al. (2009), Darling et al. (2007), Li et al. (2006), Nagayama et al. (2006), Deguchi et al. (2005), Gardel et al. (2004)].

The tensile test simulation results demonstrated that the bended MTs were highly compliant with stresses below 1 MPa, whereas the straight ones (being in tension only) showed much higher stresses (Fig. 3.9b), highlighting the significant contribution of MTs arranged in loading direction to the cell stiffness during stretching. When stretched by approximately 100 % the suspended cell model gave the reaction force of 1.8  $\mu$ N that evaluated the cell stiffness of 2.4 kPa, which is in good agreement with normalized stiffness of  $2.6 \pm 0.5$  kPa measured for cultured SMC [Nagayama et al. (2006)]. Although the simulated response showed higher non-linearity (strain stiffening) than the experiments (Fig. 3.8), this tendency is in accordance with other experimental results [Miyazaki et al. (2002)]. The contribution studies of the cytoskeletal components in tension test (Fig. 3.10) and compression test (Fig. 3.15) simulations demonstrated that removal of AFs reduced the cell stiffness by approximately 20%, which is less than the value observed experimentally [Nagayama et al. (2006), Ofek et al. (2009), Ujihara et al. (2012)]. This difference in stiffness might be attributed to the treatment with cytochalasin D that resulted in disruption of not only the deep actin fibers but also an actin meshwork beneath the CM [Ujihara et al. (2012)]. As a result, the cell stiffness was reduced substantially during experiments in contrast to the simulations.

The structural arrangement of cytoskeletal components in adherent cell model creates an elastic network that can sense and transmit mechanical stimuli and explains the different published results obtained with local experimental techniques, such as AFM. To the author's best knowledge, this is the first computational model showing the capability to predict stresses/strains within the different cellular components, especially the cytoskeleton and the nucleus. The adherent cell model shows that local application of load is preferably borne by AC and bulk components of the cell while the cytoskeleton is not much active, with the exception of MTs (Fig. 4.8) and this could be attributed to the longitudinal configuration/orientation of the ABs (Fig. 4.3). When these were removed from the model, the overall cell reaction force was about the same as the control model (Fig. 4.8). At the same time, when present in the model they sustain high deformation to resist indentation (Fig. 4.6c), which is related to the fact that these elements were prestressed. Therefore, the prestress in ABs is identified as a requirement for force generation in the model and the AC to maintain its local surface rigidity, supported by MTs at receptors.

The cellular tensegrity models envision AFs as tension supporting cables and MTs as compression supporting struts [Ingber (1993)]. Although these models successfully explain several observations in cell mechanics, the excessive compression stiffness of the struts introduces non-realistic artifacts in tension test simulations as shown by Bursa et al. (2012, 2006). The previous tensegrity-based models neither take into account the influence of flexural behavior of MTs nor predict the mechanics of individual cytoskeletal components during cytoskeleton disruption studies. The proposed bendo-tensegrity models modify this structural concept by taking into account both flexural (buckling) as well as tensional behavior of MTs and having no restriction on the spatial distribution of fibers.

Implementing the hybrid modeling approach, the interaction of discrete and continuous elements is ensured at the nodes representing FAs and thus, the external forces transmitted through FAs are sensed by the entire discrete structure as well as all the continuum parts. These models defined the structural adaptability for cytoskeleton components, where they can move independently of each other and can be completely removed individually or in combination without disintegrating the cell structure, as opposite to the tensegrity theory. In both proposed models, the suggested form and organization of individual cytoskeletal components allow exploration of the force transmission pathways for mechanical stimuli acting on the cell surface to propagate to the nucleus, ultimately resulting in mechanotransduction. The quantitative information on forces transmitted by individual cytoskeletal components in distinct cell types can be obtained by varying the mechanical properties of individual cytoskeletal components in them. The simulation results show capability of the proposed models in describing the response of not only the cell as a whole but also nucleus and individual cytoskeletal components to distinct mechanical stimuli.

The prestress plays a vital role in the mechanical behavior of AFs/ABs [Kumar et al. (2006), Deguchi et al. (2005)]. Many of the earlier tensegrity-based models accounted for small values of prestress considering only 1-2% of AFs prestrain [Xue et al. (2015), De Santis et al. (2011), McGarry et al. (2004)], whereas some of them accounted for the value as high as 90% [Karadas et al. (2013)]. This could be probably due to the model's construction or computational time required. However in this thesis, the measured physiological prestress is incorporated in the proposed models.

Although the proposed models have some advantages over the previous models, they have certain limitations as well. The structural arrangement of cytoskeletal components does not capture their true complexity and dynamic behavior as observed in living cells.



These models also do not take into consideration the viscoelastic nature of cell. Due to their passive nature, they are not able to capture the active responses of cell such as remodeling of AFs and MTs exhibited under mechanical loading.

Taken together, the proposed models describe the short term response of intracellular components and cell as a whole to distinct external mechanical stimuli not only qualitatively but also quantitatively, thus contribute to better understanding of structure-function paradigm of living cells. An attempt is made to develop these models as computational tools that may serve as a novel way to investigate the cell mechanical behavior, which, when combined with *in vitro* observations could be more effective.

---

**CONCLUSIONS**

---

**6.1. Concluding remarks**

The present thesis was aimed towards a realistic computational modeling of cytoskeleton and cell as a whole. Two FE bendo-tensegrity models focusing on cytoskeletal mechanics of cell in different states were proposed to study passive cell behavior: a suspended cell model and an adherent cell model. In this study, three mechanical tests of single cell were simulated and the results obtained were compared with corresponding published experimental results. Tensile test with micropipettes and compression test with microplates were simulated by means of the suspended cell model to elucidate the global cell response, while AFM indentation test was simulated by means of the adherent cell model to explicate the local cell response. The findings of this thesis predict and explain distinct cellular behaviors that emerge from mutual interaction between specific cytoskeletal components observed under different experimental conditions. The main findings of this thesis can be summarized as follows:

- The proposed models provide simulation of the cell mechanical responses during tension, compression, and indentation tests, aid to illustrate the mechanical role of individual cytoskeletal components including stress/strain distribution within them, and offer quantitative information on the nucleus deformation hypothetically decisive for mechanotransduction.
- Analogous to cellular tensegrity concept, the proposed models incorporate the preexisting tensile stress and interaction among cytoskeletal components. Further, this concept is modified by incorporating both flexural (buckling) as well as tensional

behavior of MTs, waviness of IFs, and with no restriction on the spatial distribution of cytoskeletal components, where they can move independently of each other. Therefore, they predict relations among cellular mechanical properties and stress/strain distributions within the specific cytoskeletal components, under different mechanical loading conditions.

- Depending on external mechanical stimuli, the models predict role of specific cytoskeletal components in force transmission through the cell. Parametric studies of the mechanical role of the components of cytoskeleton exhibited that AFs and MTs play a crucial role in cell stiffness including its increase with stretching. It was observed that, even though AFs are tension bearing elements, they contribute significantly to the compressive properties of cell. On the other hand, AC and MTs were essential for cell rigidity during indentation and the indentation site dominated the cell behavior.
- Parametric studies of material properties demonstrated that the dependence of reaction force on deformation of the suspended cell model during both tensile and compression tests was affected by changes in elastic modulus of AFs, CM, and cytoplasm, whereas during tensile test the same was also affected by changes in MTs modulus of elasticity. On the other hand, the reaction force of adherent cell model during indentation test was affected by changes in elastic modulus of AC and cytoplasm. Furthermore, inclusion of cytoplasm compressibility affected the reaction force of suspended cell model during compression only.
- Parametric studies of increase in the density of cytoskeletal components revealed that the suspended cell model during tensile test was sensitive to the increase in the density of both AFs and MTs, whereas the same during compression test was sensitive to the

increase in the density of AFs only. On the other end, the adherent cell model during indentation test was sensitive only to the increase in the density of ABs. The models were sensitive to the changes in thickness of the surface layer, created of shell elements representing CM in the suspended cell model or AC in the adherent cell model.

- These parametric studies identify the biological parameters in cells that influence tissue mechanics the most and provide valuable guidelines about the structure of individual cytoskeletal component for future cell-phenotype modeling.
- The proposed cell models take into account the distinctness in form and organization of actin protein for cell in different states (suspended and adherent) and highlight its influence on the interpretation of force-deformation measurements.

The proposed models may thus contribute to a better understanding of various cellular mechanical processes such as mechanotransduction or cytoskeleton remodeling.

## **6.2. Future works**

Some of the previous limitations of the proposed models serve as a basis for their optimization. The followings are recommended to be incorporated:

- By applying appropriate boundary conditions, multiple other single-cell mechanical tests (MTC, MA, etc.) can be also simulated. Further these models can be incorporated into multi-scale models, which may provide a key link between the responses of tissues and cells to distinct mechanical stimuli, that is, to explain the relations between macroscopic mechanical loads and the mechano-biological response at the molecular level.

- Most of the *in vitro* studies measure the cell deformation over time or frequency. Under external mechanical loads, cells deform exhibiting both solid-like elastic and fluid-like viscous behaviors. Therefore, cells and their components can be better described as viscoelastic materials and the specific mechanical properties measured will depend on the time scale [[Hoffman et al. \(2009\)](#)]. In the proposed models, viscoelastic properties can be defined for the continuous components using a standard linear solid model.
- The inclusion of a nucleoskeleton [[Kardas et al. \(2013\)](#), [Xue et al. \(2015\)](#), [Bursa et al. \(2012, 2006\)](#)] composed of lamina [[Dahl et al. \(2005\)](#)] and chromatin integrated with the cytoskeleton is proposed for better understanding of focal adhesion-cytoskeleton-nucleus mechanotransduction pathway.
- Following the approach put forward by [Maurin et al. \(2008\)](#) using granular media, inclusion of the centrosome in the proposed models might explain the link between nucleus and MTs, however, little is known about the mechanics of centrosome. To achieve this, computational simulations with or without the centrosome should be performed which can help in better understanding of its contribution to cell mechanics under different loading conditions.
- Active cell responses could be incorporated in the proposed models using a cytoskeletal remodeling description proposed by [Deshpande et al. \(2006\)](#) following the approach of [Dowling et al. \(2013\)](#). The remodeling process is based on three coupled phenomena: an activation signal that triggers actin polymerization and myosin phosphorylation, the tension-dependent assembly of the actin and myosin into SFs, and the cross-bridge mechanics between the actin and myosin filaments that generates the tension.

Implementing the bendo-tensegrity concept with hybrid modeling approach, the proposed models present cell geometries in different states with more realistic morphological representations of the cytoskeletal proteins that can predict reliable cell mechanical responses, which aids in research areas of drug development, tissue engineering, investigation of cancer cells, or regenerative medicine therapies.

---

## REFERENCES

---

- Alberts, B., Johnson, A., Lewis, J., Raff, M., Roberts, K., and Walter, P., 2002. *Molecular biology of the cell*. Garland Science, 4th ed, New York.
- Alcaraz, J., Buscemi, L., Grabulosa, M., Trepast, X., Fabry, B., Farre, R., and Navajas, D., 2003. Microrheology of Human lung epithelial cells measured by atomic force microscopy. *Biophys J.*, 84, 2071-2079.
- Ananthakrishnan, R., Guck, J., Wottawah, F., Schinkinger, S., Lincoln, B., Romeyke, M., Moon, T., and Kas, J., 2006. Quantifying the contribution of actin networks to the elastic strength of fibroblasts. *J.Theor.Biol.*, 242, 502-516.
- Bansod, Y. D., Bursa, J., 2015. Continuum-based modeling approaches for cell mechanics. World Academy of Science, Engineering and Technology, *International Journal of Biological, Biomolecular, Agricultural, Food and Biotechnological Engineering*, 9(9), 921-32.
- Bao, G., and Suresh, S., 2003. Cell and molecular mechanics of biological materials. *Nature Mater*, 2, 715-25.
- Barreto, S., 2013. *Biomechanical Study of the Mechanical and Structural Properties of Adherent Cells*. PhD Thesis, The University of Sheffield.
- Barreto, S., Clausen, C., Perrault, C., Fletcher, D., and Lacroix, D., 2013. A multi-structural single cell model of force-induced interactions of cytoskeletal components. *Biomaterials*, 34(26), 6119-26.
- Baudriller, H., Maurin, B., Cañadas, P., Montcourrier, P., Parmeggiani, A., and Bettache, N., 2006. Form-finding of complex tensegrity structures: application to cell cytoskeleton modelling. *Comptes Rendus Mécanique*, 334(11), 662-668.
- Bertaud, J., Qin, Z., and Buehler, M., 2010. Intermediate filament-deficient cells are mechanically softer at large deformation: a multi-scale simulation study. *Acta Biomater*, 6(7), 2457-2466.
- Binnig, G., Quate, C. F., and Gerber, C., 1986. Atomic Force Microscope. *Phys. Rev. Lett.*, 56(9), 930-933.
- Boal, D., 2005. *Mechanics of the cell*. Cambridge University Press, 3rd ed., UK

(Cambridge).

Brangwynne, C.P., Frederick, C., MacKintosh, F. C., Kumar, S., Geisse, N., Talbot, J., Mahadevan, L., Parker, K., Ingber, D., and Weitz, D., 2006. Microtubules can bear enhanced compressive loads in living cells because of lateral reinforcement. *J. Cell Biol.*, 173(5), 733-741.

Brown, T. D., 2000, Techniques for Mechanical Stimulation of Cells in vitro: A Review. *J. Biomech.*, 33(1), 3-14.

Bursa, J., Holata, J., and Lebis, R., 2012 Tensegrity finite element models of mechanical tests of individual cells. *Technol Health Care*, 20(2), 135-150.

Bursa, J., Lebis, R., and Janicek, P., 2006. FE models of stress-strain states in vascular smooth muscle cell. *Technol Health Care*, 14(4,5), 311-20.

Caille, N., Thoumine, O., Tardy, Y., and Meister, J., 2002. Contribution of the nucleus to the mechanical properties of endothelial cells. *J Biomech*, 35, 177-87.

Cañadas, P., Laurent V., Chabrand P., Isabey D., and Wendling-Mansuy S., 2003. Mechanisms governing the visco-elastic responses of living cells assessed by foam and tensegrity models. *Med Biol Eng Comput*, 41(6), 733-9.

Cañadas, P., Laurent, V., Oddou, C., Isabey, D., and Wendling, S., 2002. A cellular tensegrity model to analyse the structural viscoelasticity of the cytoskeleton. *J Theor Biol*, 218, 155-173.

Cañadas, P., Wendling-Mansuy, S., and Isabey, D., 2006. Frequency response of a viscoelastic tensegrity model: Structural rearrangement contribution to cell dynamics. *Journal of Biomechanical Engineering*, 128(4), 487-495.

Casati, L., Celotti, F., Negri-Cesi, P., Sacchi, M. C., Castano, P., and Colciago, A., 2014. Platelet derived growth factor (PDGF) contained in Platelet Rich Plasma (PRP) stimulates migration of osteoblasts by reorganizing actin cytoskeleton. *Cell Adhesion & Migration*, 8(6), 595-602.

Charras, G. T., and Horton, M. A., 2002a. Single cell mechanotransduction and its modulation analyzed by atomic force microscope indentation. *Biophys. J.*, 82(6), 2970-2981.

Chaudhuri, O., Parekh, S., Lam, W., and Fletcher, D., 2009. Combined atomic force



microscopy and side-view optical imaging for mechanical studies of cells. *Nat. Methods*, 6(5), 383-387.

Chen, Ting-Jung, Chia-Ching Wu, and Fong-Chin Su., 2012. Mechanical models of the cellular cytoskeletal network for the analysis of intracellular mechanical properties and force distributions: A review. *Medical Engineering & Physics*, 34(10), 1375-1386.

Cheng, C. M., Steward, R. L., Jr., and Leduc, P. R., 2009. Probing Cell Structure by controlling the mechanical environment with cell–substrate interactions. *J. Biomech.*, 42(2), 187-192.

Cytoskeleton, Inc - The Proteine experts, Denver, USA. Availabe at: [www.cytoskeleton.com](http://www.cytoskeleton.com)

Dahl, K. N., Engler, A. J., Pajerowski, J. D., and Discher, D. E., 2005. Power- law rheology of isolated nuclei with deformation mapping of nuclear sub-structures. *Biophys J*, 89, 2855-64.

Darling, E., Zauscher, S., Block, J., and Guilak, F., 2007. A thin-layer model for viscoelastic, stress-relaxation testing of cells using atomic force microscopy: do cell properties reflect metastatic potential? *Biophys J*, 92(5), 1784-91.

De Santis, G., Lennon, A. B., Boschetti, F., Verheghe, B., Verdonck, P., and Prendergast, P. J., 2011. How can cells sense the elasticity of a substrate?: an analysis using a cell tensegrity model. *European Cells & Materials*, 22, 202-13.

De, R., and Safran, S. A., 2008. Dynamical theory of active cellular response to external stress. *Phys. Rev. E*, 78, 031923.

De, R., Zemel, A., and Safran, S. A., 2008a. Do cells sense stress or strain? Measurement of cellular orientation can provide a clue. *Biophys. J.*, 94, 29.

De, R., Zemel, A., and Safran, S., 2007. Dynamics of cell orientation. *Nat. Phys.*, 3, 655.

De, R., Zemel, A., and Safran, S., 2010. Theoretical concepts and models of cellular mechanosensing. *Methods in Cell Biology*, 98, 143-175.

Deguchi, S., Ohashi, T., and Sato, M., 2005. Evaluation of tension in actin bundle of endothelial cells based on preexisting strain and tensile properties measurements. *Mol Cell Biomech*, 2(3), 125-133.

Deguchi, S., Ohashi, T., and Sato, M., 2006. Tensile properties of single stress fibers

- isolated from cultured vascular smooth muscle cells. *J. Biomech*, 39, 2603-2310.
- Deshpande, V. S., McMeeking, R. M., and Evans, A. G., 2006. A bio-chemo-mechanical model for cell contractility. *Proc. Natl. Acad. Sci. U.S.A.*, 103(38), 14015–14020.
- Desprat, N., Richert, A., Simeon, J., and Asnacios, A., 2005. Creep function of a single living cell. *Biophysical Journal*, 88(3), 2224-33.
- Dowling, E. P., and McGarry, J. P., 2014. Influence of spreading and contractility on cell detachment. *Annals of Biomedical Engineering*, 42(5), 1037-48.
- Dowling, E. P., Ronan, W., and McGarry, J. P., 2013. Computational investigation of in situ chondrocyte deformation and actin cytoskeleton remodelling under physiological loading. *Acta Biomater*, 9, 5943-55.
- Fabry, B., Maksym, G., Butler, J., Glogauer, M., Navajas, D., and Fredberg, J., 2001. Scaling the Microrheology of living cells. *The American Physical Society*, 87(14), 148102.
- Fernández, P., Pullarkat, P. A., and Ott, A., 2006. A master relation defines the nonlinear viscoelasticity of single fibroblasts. *Biophysical Journal*, 90(10), 3796-805.
- Fletcher, D. A., and Mullins, R. D., 2010. Cell mechanics and the cytoskeleton. *Nature*, 463, 485-492.
- Gardel, M. L., Shin, J. H., MacKintosh, F. C., Mahadevan, L., Matsudaira, P., and Weitz, D. A., 2004. Elastic behavior of cross-linked and bundled actin networks. *Science*, 304(5675), 1301-5.
- Gardel, M., Nakamura, F., Hartwig, J., Crocker, J., Stossel, T., and Weitz, D., 2006. Stress-dependent elasticity of composite actin networks as a model for cell behavior. *Physical Rev Lett*, 96, 12-15.
- Ghaffari, H., Saidi, M. S., Firoozabadi, B., 2016. Biomechanical analysis of actin cytoskeleton function based on a spring network cell model. *Proceedings of the Institution of Mechanical Engineers, Part C: Journal of Mechanical Engineering Science*, 0954406216668546.
- Gittes, F., Mickey, B., Nettleton, J., and Howard, J., 1993. Flexural rigidity of microtubules and actin filaments measured from thermal fluctuations in shape. *J Cell Biol*, 120, 923-934.
- Glerum, J. J., Van Mastrigt, R., Van Koeveringe, A. J., 1990. Mechanical properties of

- mammalian single smooth muscle cells. III. Passive properties of pig detrusor and human a terme uterus cells. *J. Muscle Res. Cell Motil.*, 11, 453- 462.
- Guck, J., Schinkinger, S., Lincoln, B., Wottawah, F., Ebert, S., Romeyke, M., Lenz, D., Erickson, H., Ananthakrishnan, R., Mitchell, D., Kas, J., Ulvick, S., and Bilby, C., 2005. Optical deformability as an inherent cell marker for testing malignant transformation and metastatic competence. *Biophys J*, 88(5), 3689-3698.
- Hawkins, T., Mirigian, M., Selcuk Yasar, M., and Ross, J. L., 2010. Mechanics of microtubules. *J Biomech*, 43, 23-30.
- Hemmer, J., 2008. *Characterization of vascular smooth muscle cell mechanical and frictional properties using atomic force microscopy*. All Dissertations, Clemson University. USA. Paper 293.
- Hirano, Y., Takahashi, H., Kumeta, M., Hizume, K., Hirai, Y., Otsuka, S., Yoshimura, S. H., and Takeyasu, K., 2008. Nuclear architecture and chromatin dynamics revealed by atomic force microscopy in combination with biochemistry and cell biology. *Pflugers Arch.*, 456(1), 139-153.
- Hiratsuka, S., Mizutani, Y., Tsuchiya, M., Kawahara, K., Tokumoto, H., and Okajima, T., 2009. The number distribution of complex shear modulus of single cells measured by atomic force microscopy. *Ultramicroscopy*, 109(8), 937-941.
- Hoey, D. A., Tormey, S., Ramcharan, S., O'Brien, F. J., and Jacobs, C. R., 2012. Primary cilia-mediated mechanotransduction in human mesenchymal stem cells. *Stem Cells*, 30, 2561-70.
- Hoffman, B. D., and Crocker, J. C., 2009. Cell mechanics: dissecting the physical responses of cells to force. *Ann Rev Biomed Eng*, 11, 259-88.
- Hoffman, B. D., Grashoff, C., and Schwartz, M.A., 2011. Dynamic molecular processes mediate cellular mechanotransduction. *Nature (London)*, 475, 316.
- Hoffman, B. D., Massiera, G., Van Citters, K. M., and Crocker, J. C., 2006. The consensus mechanics of cultured mammalian cells. *Proc Natl Acad Sci U S A*, 103, 10259-64.
- Hu, S., Chen, J., Fabry, B., Numaguchi, Y., Gouldstone, A., Ingber, D. E., Fredberg, J. J., Butler, J. P., and Wang, N., 2003. Intracellular stress tomography reveals stress focusing and structural anisotropy in cytoskeleton of living cells. *Am J Physiol Cell Physiol*, 285 , C1082–90.

- Huang, H., Kamm, R., and Lee, R., 2004. Cell mechanics and mechanotransduction: pathways, probes, and physiology. *Am J Physiol-Cell Ph*, 287(1), C1-11.
- Ingber D., 2003. Tensegrity I. cell structure and hierarchical systems biology. *J Cell Sci.*, 116(7), 1157-1173.
- Ingber, D. E., Heidemann, S. R., Lamoureaux, P., and Buxbaum, R. E., 2000. Opposing views on tensegrity as a structural framework for understanding cell mechanics. *J App physiology*, 89, 1670-1678.
- Ingber, D., 1993. Cellular tensegrity: defining new rules of biological design that govern the cytoskeleton. *J Cell Sci*, 104, 613-27.
- Intension Designs Ltd. Canada. Available at: [www.intensiondesigns.com](http://www.intensiondesigns.com)
- Janmey, P. A., 1998. The cytoskeleton and cell signaling: component localization and mechanical coupling. *Physiol Rev*, 78, 763-81.
- Janmey, P. A., and Weitz, D. A., 2004. Dealing with mechanics: mechanisms of force transduction in cells. *Trends Biochem Sci*, 29, 364-70.
- Janmey, P., Euteneuer, U., Traub, P., and Schliwa, M., 1991. Viscoelastic properties of vimentin compared with other filamentous biopolymer networks. *J Cell Biol*, 113(1), 155-160.
- Jean, R. P., Chen, C. S., and Spector, A. A., 2005. Finite-element analysis of the adhesion-cytoskeleton-nucleus mechanotransduction pathway during endothelial cell rounding: axisymmetric model. *Journal of Biomechanical Engineering*, 127(4), 594-600.
- Jungbauer, S., Gao, H., Spatz, J., and Kemkemer, R., 2008. Two characteristic regimes in frequencydependent dynamic reorientation of fibroblasts on cyclically stretched substrates. *Biophysical Journal*, 95, 3470-3478.
- Kardas, D., Nackenhorst, U., and Balzani, D., 2013. Computational model for the cell-mechanical response of the osteocyte cytoskeleton based on self stabilizing tensegrity structures. *Biomec Model Mechanobio*, 12, 167-83.
- Kasas, S., Wang, X., Hirling, H., Marsault, R., Huni, B., Yersin, A., Regazzi, R., Grenningloh, G., Riederer, B., Forro, L., Dietler, G., and Catsicas, S., 2005. Superficial and deep changes of cellular mechanical properties following cytoskeleton disassembly. *Cell Motil Cytoskeleton*, 62, 124-32.

- Kaunas, R., and Hsu, H. J., 2009. A kinematic model of stretch-induced stress fiber turnover and reorientation. *J Theor Biol*, 257, 320-30.
- Kaunas, R., Hsu, H. J., and Deguchi, S., 2011. Sarcomeric model of stretch induced stress fiber reorganization. *Cell Health CSK*, 3, 13–22.
- Kaunas, R., Usami, S., and Chien, S., 2006. Regulation of stretch-induced JNK activation by stress fiber orientation. *Cell Signal*, 18, 1924–31.
- Kaverina, I., Rottner, K., and Small, J., 1998. Targeting, capture, and stabilization of microtubules at early focal adhesions. *J Cell Biol*, 142, 181-190.
- Kiyomarsioskouei, A., Saidi, M. S., and Firoozabadi, B., 2012. An endothelial cell model containing cytoskeletal components: Suspension and adherent states. *Journal of Biomedical Science and Engineering*, 5(12), 737.
- Kojima, H., Ishijima, A., and Yanagida, T., 1994. Direct measurement of stiffness of single actin filaments with and without tropomyosin by in vitro nanomanipulation. *Proceedings of the National Academy of Sciences*, 91(26), 12962-6.
- Kumar, S., Maxwell, I. Z., Heisterkamp, A., Polte, T. R., Lele, T. P., Salanga, M., Mazur, E., and Ingber, D. E., 2006. Viscoelastic retraction of single living stress fibers and its impact on cell shape, cytoskeletal organization, and extracellular matrix mechanics. *Biophys J*, 90, 3762-73.
- Lebiš R., 2007. *Computational Modeling of Mechanical Behavior of the Cell*. PhD thesis, Brno University of Technology, Czech Republic.
- Leipzig, N. D., and Athanasiou, K. A., 2008. Static compression of single chondrocytes catabolically modifies single-cell gene expression. *Biophysical Journal*, 94, 2412-2422.
- Li, W., Jiang, Y., and Tuan R., 2006. Chondrocyte phenotype in engineered fibrous matrix is regulated by fiber size. *Tissue Eng*, 12(7), 1775-85.
- Lim, C. T., Zhou, E. H., and Quek, S. T., 2006. Mechanical models for living cells - A review. *Journal Biomech*, 39(2), 195-216.
- Liu, J., Sun, N., Bruce, M. A., Wu, J. C., and Butte, M. J., 2012. Atomic Force Mechanobiology of Pluripotent Stem Cell-Derived Cardiomyocytes. *PLoS One*, 7(5), e37559.

- Maloney, J. M., Nikova, D., Lautenschlager, F., Clarke, E., Langer, R., Guck, J., and Van Vliet, K. J., 2010. Mesenchymal stem cell mechanics from the attached to the suspended state. *Biophys. J.*, 99(8), 2479-2487.
- Maniotis, A., Chen, C., and Ingber, D., 1997. Demonstration of mechanical connections between integrins, cytoskeletal filaments, and nucleoplasm that stabilize nuclear structure. *Cell Biology*, 94, 849-852.
- Matsumoto, T., and Nagayama, K., 2012. Tensile properties of vascular smooth muscle cells: bridging vascular and cellular biomechanics. *Journal of Biomechanics*, 45(5), 745-55.
- Maurin, B., Cañadas, P., Baudriller, H., Montcourrier, P., and Bettache, N., 2008. Mechanical model of cytoskeleton structuration during cell adhesion and spreading. *J Biomech*, 41(9), 2036-41.
- Mayr, M., Li, C., Zou, Y., Huemer, U., Hu, Y., and Xu, Q., 2000. Biomechanical stress-induced apoptosis in vein grafts involves p38 mitogen-activated protein kinases. *FASEB J*, 14(2), 261-70.
- McGarry, J. G., Klein-Nulend, J., Mullender, M. G., and Prendergast, P. J., 2005a. A comparison of strain and fluid shear stress in stimulating bone cell responses—a computational and experimental study. *FASEB J*, 19, 482-4.
- McGarry, J. G., and Prendergast, P. J., 2004. A three-dimensional finite element model of an adherent eukaryotic cell. *Eur Cell Mater*, 7, 27–33.
- Mehrbod, M., and Mofrad, R. K., 2011. On the significance of microtubule flexural behavior in cytoskeletal mechanics. *PloS one*, 6(10), e25627.
- Miyazaki, H., Hasegawa, Y., and Hayashi, K. 2002. Tensile properties of contractile and synthetic vascular smooth muscle cells. *JSME Int J C-Mech Sy*, 45(4), 870-9.
- Miyazaki, H., Hasegawa, Y., and Hayashi, K., 2000. A newly designed tensile tester for cells and its application to fibroblasts. *Journal of Biomechanics*, 33, 97-104.
- Mofrad, M. R., 2009. Rheology of the cytoskeleton. *Annu. Rev. Fluid Mech.*, 41, 433-453.
- Mofrad, M. R., and Kamm, R., 2006. *Cytoskeletal mechanics*. Cambridge University Press, 1st ed., USA (New York.)
- Mogilner, A., and Keren, K., 2009. The shape of motile cells. *Curr. Biol.*, 19, 762-771.

- Nagayama, K., and Matsumoto, T., 2008. Contribution of actin filaments and microtubules to quasi-in situ tensile properties and internal force balance of cultured smooth muscle cells on a substrate. *Am J Physiol-Cell Ph*, 295(6), C1569-1578.
- Nagayama, K., Nagano, Y., Sato, M., and Matsumoto, T., 2006. Effect of actin filament distribution on tensile properties of smooth muscle cells obtained from rat thoracic aortas. *J Biomech*, 39(2), 293-301.
- Nguyen, B. V., Wang, Q. G., Kuiper, N. J., El Haj, A. J., Thomas, C. R., and Zhang, Z., 2010. Biomechanical properties of single chondrocytes and chondrons determined by micromanipulation and finite-element modelling. *Journal of The Royal Society Interface*, 7(53), 1723-33.
- Nguyen, B. V., Wang, Q., Kuiper, N. J., El Haj, A. J., Thomas, C. R., and Zhang, Z., 2009. Strain-dependent viscoelastic behaviour and rupture force of single chondrocytes and chondrons under compression. *Biotechnology letters*, 31(6), 803-9.
- Ofek, G., Dowling, E., Raphael, R., McGarry, J., and Athanasiou, K., 2010. Biomechanics of single chondrocytes under direct shear. *Biomech Model Mechan*, 9(2), 153-162.
- Ofek, G., Natoli, R. M., and Athanasiou, K. A., 2009. In situ mechanical properties of the chondrocyte cytoplasm and nucleus. *J Biomech*, 42, 873-7.
- Ohara, Y., H. Miyazaki, and K. Hayashi. 2000. Atomic force microscopy measurement of the mechanical properties of vascular smooth muscle cell. *Proc. of 12th JSME Bioengineering Conference Japan*, 55-56.
- Ohashi, T., Ishii, Y., Ishikawa, Y., Matsumoto, T., and Sato, M., 2002. Experimental and numerical analyses of local mechanical properties measured by atomic force microscopy for sheared endothelial cells. *Bio-Med Mater Eng*, 12(3), 319-327.
- Pelling, A. E., and Horton, M. A., 2008. An historical perspective on cell mechanics. *Pflugers Arch.*, 456(1), 3-12.
- Pesen, D., and Hoh, J. H., 2005. Micromechanical architecture of the endothelial cell Cortex. *Biophys. J.*, 88(1), 670-679.
- Pillariseti, A., Desai, J., Ladjal, H., Schiffmacher, A., Ferreira, A., and Keefer, C., 2011. Mechanical phenotyping of mouse embryonic stem cells: increase in stiffness with differentiation. *Cell Reprogram*, 13(4), 371-80.

- Prendergast, P., 2007 Computational modelling of cell and tissue mechanoresponsiveness. *Gravit Space Res*, 20(2).
- Puech, P. H., Poole, K., Knebel, D., and Muller, D. J., 2006. A new technical approach to quantify cell–cell adhesion forces by AFM. *Ultramicroscopy*, 106(8–9), 637-644.
- Pullarkat, P. A., Fernandez, P. A., and Ott, A., 2007. Rheological properties of the eukaryotic cell cytoskeleton. *Phys. Rep.*, 449, 29-53.
- Rand, R., 1964. Mechanical properties of the red cell membrane: II. Viscoelastic breakdown of the membrane. *Biophys J*, 4(4), 303.
- Reinhart-King, C. A., Dembo, M., and Hammer, D. A., 2005. The dynamics and mechanics of endothelial cell spreading. *Biophysical journal*, 89(1), 676-89.
- Reynolds, N. H., Ronan, W., Dowling, E. P., Owens, P., McMeeking, R. M., and McGarry, J. P., 2014. On the role of the actin cytoskeleton and nucleus in the biomechanical response of spread cells. *Biomaterials*, 35(13), 4015-25.
- Rodriguez, M. L., McGarry, P. J., and Sniadecki, N. J., 2013. Review on cell mechanics: experimental and modeling approaches. *Applied Mechanics Reviews*, 65(6), 060801.
- Ronan, W., Deshpande, V. S., McMeeking, R. M., and McGarry, J. P., 2014. Cellular contractility and substrate elasticity: a numerical investigation of the actin cytoskeleton and cell adhesion. *Biomechanics and Modeling in Mechanobiology*. 13(2), 417-35.
- Roy, S., Thacher, T., Silacci, P., and Stergiopoulos, N., 2009. Arterial biomechanics after destruction of cytoskeleton by Cytochalasin D. *Journal of Biomechanics*, 42(15), 2562-8.
- Safran, S. A., and De, R., 2009. Nonlinear dynamics of cell orientation. *Physical Review E, Statistical, Nonlinear, and Soft Matter Physics*, 80(6.1), 060901.
- Sato, M., Levesque, M. J., and Nerem, R. M., 1987. Micropipette aspiration of cultured bovine aortic endothelial cells exposed to shear stress. *Arteriosclerosis, Thrombosis, and Vascular Biology*, 7(3), 276-86.
- Sato, M., Nagayama, K., Kataoka, N., Sasaki, M., and Hane, K., 2000. Local mechanical properties measured by atomic force microscopy for cultured bovine endothelial cells exposed to shear stress. *Journal of Biomechanics*, 33(1), 127-35.
- Schwarz, U., and Safran, S. S., 2013. Physics of adherent cells. *Rev. Mod. Phys.*, 85, 1327.
- Sen, S., and Kumar, S., 2009. Cell–Matrix de-adhesion dynamics reflect contractile



- mechanics. *Cell Mol. Bioeng.*, 2(2), 218-230.
- Shieh, A. C., and Athanasiou, K. A., 2007. Dynamic compression of single cells. *Osteoarthritis and Cartilage*, 15(3), 328-34.
- Slomka, N., and Gefen, A., 2010. Confocal microscopy-based three-dimensional cell-specific modeling for large deformation analyses in cellular mechanics. *J Biomech*, 43, 1806–16.
- Stamenović, D., and Coughlin, M., 1999. The role of prestress and architecture of the cytoskeleton and deformability of cytoskeletal filaments in mechanics of adherent cells: a quantitative analysis. *J Theor Biol*, 201(1), 63-74.
- Stamenović, D., and Ingber, D. E., 2009. Tensegrity-guided self-assembly: from molecules to living cells. *Soft Matter*, 5, 1137.
- Stamenović, D., Fredberg, J., Wang, N., Butler, J., and Ingber, D., 1996. A microstructural approach to cytoskeletal mechanics based on tensegrity. *J Theor Biol*, 181(2), 125-36.
- Stamenović, D., Mijailovich, S. M., Tolić-Nørrelykke, I. M., Chen, J., and Wang, N., 2002. Cell prestress. II. Contribution of microtubules. *American Journal of Physiology-Cell Physiology*, 282(3), C617-C624
- Stricker, J., Falzone, T., and Gardel., M., 2010. Mechanics of the F-actin cytoskeleton. *J Biomech*, 43, 9–14.
- Sunyer, R., 2008. *Contribution of active processes to the cytoskeleton dynamics of living cells*. Ph.D. Thesis, Facultat de Medicina, Universitat de Barcelona.
- Takai, E., Costa, K. D., Shaheen, A., Hung, C. T., and Guo, X. E., 2005. Osteoblast elastic modulus measured by atomic force microscopy is substrate dependent. *Ann Biomed Eng*, 33, 963–971.
- Tapley, E. C., and Starr, D. A., 2013. Connecting the nucleus to the cytoskeleton by SUN-KASH bridges across the nuclear envelope. *Curr Opin Cell Biol.*, 25, 57–62.
- Thoumine, O., Ott, A., Cardoso, O., and Meister, J. J., 1999. Microplates: a new tool for manipulation and mechanical perturbation of individual cells. *Journal of biochemical and biophysical methods*. 39(1), 47-62.
- Ujihara, Y., Nakamura, M., Miyazaki, H., and Wada, S., 2010. Proposed spring network cell model based on a minimum energy concept. *Ann Biomed Eng*, 38(4), 1530-8.

- Ujihara, Y., Nakamura, M., Miyazaki, H., and Wada, S., 2012. Contribution of actin filaments to the global compressive properties of fibroblasts. *Journal of the Mechanical Behavior of Biomedical Materials*, 14, 192-8.
- Unnikrishnan, G., Unnikrishnan, U., and Reddy, J., 2007. Constitutive material modeling of cell: a micromechanics approach. *J Biomech Eng*, 129(3), 315–23.
- Vaziri, A., and Gopinath, A., 2008. Cell and biomolecular mechanics in silico. *Nature Mater*, 7, 15–23.
- Wakatsuki, T., Schwab, B., Thompson, N. C., and Elson. E. L., 2001. Effects of cytochalasin D and latrunculin B on mechanical properties of cells. *J. Cell Sci.*, 114, 1025–1036.
- Wang, N., 1998. Mechanical interactions among cytoskeletal filaments. *Hypertension*, 32, 162–165.
- Wang, N., and Ingber, D., 1994. Control of cytoskeletal mechanics by extracellular matrix, cell-shape, and mechanical tension. *Biophysical Journal*, 66, 2181-2189.
- Wang, N., and Stamenović, D., 2000. Contribution of intermediate filaments to cell stiffness, stiffening, and growth. *Am J Physiol Cell Physiol*, 279, C188-94.
- Wang, N., and Suo, Z., 2005. Long-distance propagation of forces in a cell. *Biochem Bioph Res Co*, 328(4), 1133-8.
- Wang, N., Naruse, K., Stamenović, D., Fredberg, J., Mijailovich, S., Tolić-Nørrelykke, I., Polte, T., Mannix, R., and Ingber, D., 2001b. Mechanical behavior in living cells consistent with the tensegrity model. *P Natl Acad Sci USA*, 98(14), 7765-7770.
- Wang, N., Toli'c-Nø rrelykke, I. M., Chen, J., Mijailovich, S. M., Butler, J. P., Fredberg, J. J., and Stamenović, D., 2002. Cell prestress. I. Stiffness and prestress are closely associated in adherent contractile cells. *Am J physiol Cell Physiol*, 282, C606-16.
- Wang, N., Tytell, J. D., and Ingber, D. E., 2009. Mechanotransduction at a distance: mechanically coupling the extracellular matrix with the nucleus. *Nat Rev Mol Cell Biol*, 10, 75-82.
- Wyss Institute at Harvard University. Boston, USA. Available at: <https://wyss.harvard.edu/>
- Xue, F., Lennon, A., McKayed, K., Campbell, V., and Prendergast, P., 2015. Effect of

membrane stiffness and cytoskeletal element density on mechanical stimuli within cells: an analysis of the consequences of ageing in cells. *Comput Method Biomec*, 18(5), 468-76.

Yao, Y., Lacroix, D., and Mak, A. F., 2016. Effects of oxidative stress-induced changes in the actin cytoskeletal structure on myoblast damage under compressive stress: confocal-based cell-specific finite element analysis. *Biomechanics and Modeling in Mechanobiology*, 19, 1-4.

Zhu, C., Bao, G., and Wang, N., 2000. Mechanical response, cell adhesion, and molecular deformation. *Annu. Rev. Biomed. Eng*, 189-226.

---

## AUTHOR'S PUBLICATIONS

---

### Appendix A.

Original research article submitted to ASME Journal of Biomechanical Engineering

# A Finite Element Bendo-Tensegrity Model of Eukaryotic Cell

**Yogesh D. Bansod<sup>1</sup>**

Brno University of Technology

Institute of Solid Mechanics, Mechatronics and Biomechanics (ISMMB), Faculty of Mechanical Engineering (FME), Brno University of Technology (BUT), Technicka 2896/2, 61669 Brno, Czech Republic

[yogeshbansod@gmail.com](mailto:yogeshbansod@gmail.com)

**Takeo Matsumoto**

Nagoya Institute of Technology

Biomechanics Laboratory, Department of Mechanical Engineering, Nagoya Institute of Technology, Gokiso-cho, Showa-ku, Nagoya 466-8555, Japan

[takeo@nagoya-u.jp](mailto:takeo@nagoya-u.jp)

**Kazuaki Nagayama**

Nagoya Institute of Technology

Biomechanics Laboratory, Department of Mechanical Engineering, Nagoya Institute of Technology, Gokiso-cho, Showa-ku, Nagoya 466-8555, Japan

[kazuaki.nagayama.bio@vc.ibaraki.ac.jp](mailto:kazuaki.nagayama.bio@vc.ibaraki.ac.jp)

**Jiri Bursa**

Brno University of Technology

Institute of Solid Mechanics, Mechatronics and Biomechanics (ISMMB), Faculty of Mechanical Engineering (FME), Brno University of Technology (BUT), Technicka 2896/2, 61669 Brno, Czech Republic

[bursa@fme.vutbr.cz](mailto:bursa@fme.vutbr.cz)

---

<sup>1</sup> Corresponding author at: Institute of Solid Mechanics, Mechatronics and Biomechanics (ISMMB), Faculty of Mechanical Engineering (FME), Brno University of Technology (BUT), Technicka 2896/2, 61669 Brno, Czech Republic. E-mail: [yogeshbansod@gmail.com](mailto:yogeshbansod@gmail.com); tel.: +420608678342; fax: +420 541142876

**ABSTRACT**

*Although several computational models proposed on the basis of tensegrity concept explicate the cytoskeletal mechanics, they disregard the flexural behavior of microtubules (MTs). Incorporating this behavior, two finite element (FE) bendo-tensegrity models of cell in different states are proposed: a suspended cell model elucidating the global response during tensile test simulation and an adherent cell model explicating the local response during atomic force microscopy (AFM) indentation simulation. The force-elongation curve obtained from tensile test simulation lies within the range of experimentally obtained characteristics of smooth muscle cells (SMCs) and illustrates a non-linear increase in reaction force with cell stretching. The force-indentation curves obtained from indentation simulations lie within the range of experimentally obtained curves of embryonic stem cells (ESCs) and exhibit the influence of indentation site on the overall reaction force of cell. Simulation results have demonstrated that actin filaments (AFs) and MTs play a crucial role in the cell stiffness during stretching, whereas actin cortex (AC) and MTs are essential for the cell rigidity during indentation. The proposed models quantify the mechanical contribution of individual cytoskeletal components to cell mechanics, which in turn aids in better understanding of structure-function relationship of living cells.*

*Keywords: Cytoskeleton, computational modeling, cell biomechanics, mechanotransduction*

## 1. INTRODUCTION

The eukaryotic cells are continuously subjected to myriad of extracellular and intracellular mechanical stimuli. It has been well established that cell's mechanical interactions with its environment influence cell morphology, cell fate, and gene expression [1]. The cytoskeleton transmits mechanical stimuli to intracellular region and facilitates changes in cell morphology through cytoskeletal remodeling. The cytoskeletal architecture modulates cell stiffness and its individual components may have distinct mechanical roles in the cell [2]. During mechanotransduction, the extent of the changes evoked in cell behavior due to applied mechanical loads partially depends on the distribution of forces within the cell components. Although pioneering studies have provided the basic framework for understanding mechanotransduction [3], the fundamental mechanical processes for sensation and transduction of mechanical stimuli into biochemical signals are still ambiguous. Moreover, the specific contribution of cytoskeletal components to single-cell mechanics is currently not well understood. Thus, more sophisticated computational modeling is needed for better understanding of the mechanotransduction mechanism and in quest of determining the mechanical contribution of individual cytoskeletal components to the overall structural responses of cell.

Computational modeling provides better control over the form and organization of individual cytoskeletal components, thus it can be used to unravel the potential mechanism of cell responses to distinct mechanical stimuli [4-10]. In last few decades, several different approaches have been proposed to elucidate the cell mechanics. The continuum approaches describe whole cell as a homogenous isotropic continuum media assuming that the smallest length scale of interest is much larger than the dimensions of the microstructure. Although these approaches have successfully demonstrated several cellular behaviors, they are not able to interpret the contribution of discrete components such as cytoskeleton to cell mechanics.

The microstructural approaches describe cytoskeleton as a system of discrete elements critical for cell mechanics. One of the most frequently used models in this class is the cellular tensegrity model that envisioned cytoskeleton as an interconnected network of cables and struts [11], where cables in tension represent *AFs* and struts in compression represent *MTs* [2]. The tensegrity model revealed that prestress in *AFs* and interplay of the cytoskeletal components affect the cell stiffness [12]. This model has successfully predicted viscosity modules of the cytoskeleton [13], as well as many experimentally observed features of cell mechanical behavior such as prestress-induced stiffening [14] and strain hardening [12]. For more reliable formulation of mechanical behavior of cells using *FE* analysis, the hybrid approach was put forward that combines the continuum modeling with discrete approach [4]. This concept has also been employed to investigate the mechanisms for force generation and propagation by taking into account a variety of cellular processes at distinct time-scales [15, 16].

In the present study, implementing the hybrid modeling approach *FE* bendo-tensegrity models of cell in different states are proposed with the aim to characterize the nucleus deformation during distinct mechanical tests, which could be significant for mechanotransduction. Analogous to tensegrity approach, the proposed models also include the preexisting tensile stress and interaction among cytoskeletal components. Further, this structural concept is modified by incorporating the flexural behavior of *MTs* and no restriction on the spatial distribution of cytoskeletal components. Simulation of tensile test is performed with the proposed suspended cell model to investigate the cell response to global deformation and the results obtained are compared with the tensile test measurements of aortic SMCs [17]. Simulation of indentation test is carried out with the proposed adherent cell model to examine the cell response to local deformation and the simulation results are compared with the AFM indentation measurements of ESCs [18]. For both models, parametric analyses are performed to determine the contribution of individual cytoskeletal components to cell mechanics and to evaluate the effect of variations in their material properties on the overall responses of cell.

## 2. MATERIALS AND METHODS

### 2.1. *FE* Model Formulation

In this study, simulations of two mechanical tests are performed and compared with corresponding experimental results. Tensile test of suspended cell with micropipettes and indentation test of adherent cell using AFM are simulated by means of two *FE* models created in ANSYS (ANSYS Inc. PA, US).

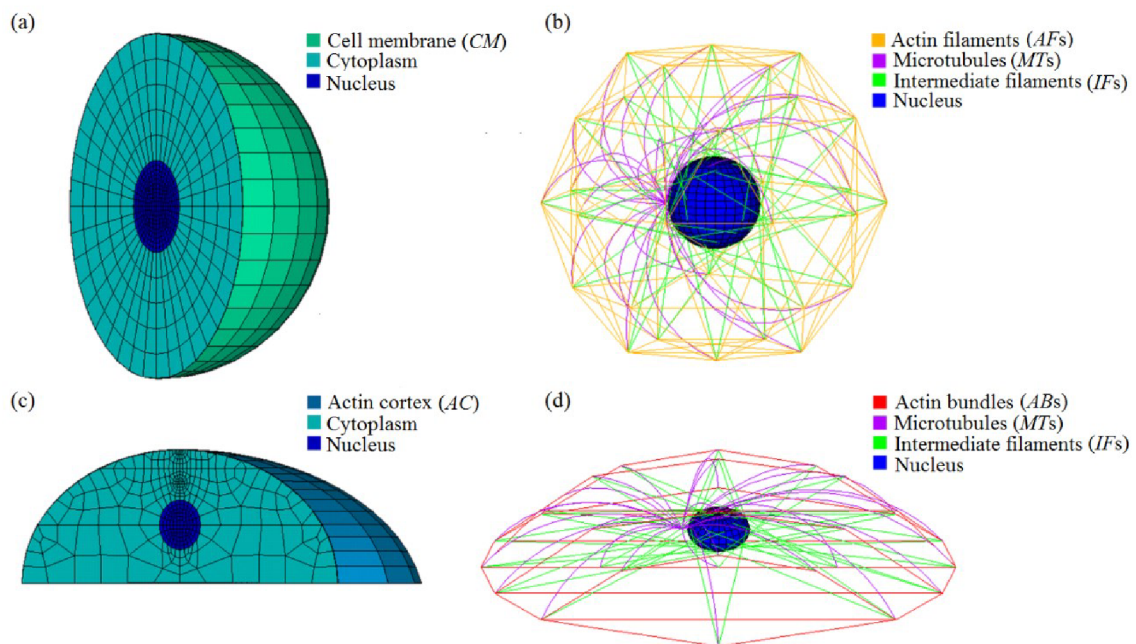


Fig 1: Sections of continuous elements and structural arrangement of cytoskeletal components with respect to the nucleus: (a) and (b) for suspended cell model and (c) and (d) for adherent cell model

The suspended cell model encompasses the nucleus and cytoplasm surrounded by the cell membrane (CM) (Fig. 1a) and cytoskeletal components like AFs, MTs, and intermediate filaments (IFs) (Fig. 1b). The adherent cell model is slightly different, the nucleus and cytoplasm are enclosed by the AC (with CM being not considered) (Fig. 1c) and cytoskeletal components like actin bundles (ABs), MTs, and IFs (Fig. 1d). For both cell models implementing the hybrid modeling approach, the continuum parts (nucleus, cytoplasm) are modeled using continuous



(volume) elements circumscribed by a thin layer of shell elements (representing *CM* and/or *AC*) and the cytoskeletal components are modeled using discrete (beam or truss) elements.

The shape of the suspended cell model is defined as spherical with diameter ( $D$ ) of 32.264  $\mu\text{m}$ , taken from one of the experimental measurements by Nagayama et al. [17]. The nucleus is also modeled as spherical and positioned at the center of the cell. Both cytoplasm and nucleus are modeled with eight-node hexahedral isoparametric elements. A thin flexible layer circumscribing the cytoplasm referred to as the *CM* is modeled with four-node quadrilateral shell elements on the outer surface of the cytoplasm, with thickness of 0.01  $\mu\text{m}$  [19] and no bending stiffness.

In a real cell, *MTs* of unequal lengths originate from the centrosome located near the nucleus and emanate outward through the cytoplasm till the cell cortex where they interact with other cytoskeletal filaments at focal adhesions (*FAs*). It is now evident that *MTs* do not have compression-only behavior but they appear highly curved (buckled) in living cells under no external load. This indicates that compressive forces in *MTs* induce substantial bending solely by the action of prestressed *AFs*; this is referred to as the “bendo-tensegrity” concept [20]. Implementing this concept, the *MTs* of varying curvature are modeled using beam elements, originating from a single node near the nucleus, representing the centrosome and further extending till the *FAs* to form a star-like shape. Thus, the *MTs* are able to resist tensional as well as compressive forces with taking their flexural (buckling) behavior into consideration. Every *FA* is connected to the centrosome with only one *MT* and it is ensured that they do not penetrate the nucleus.

*IFs* are scattered throughout the intracellular space, connecting the *FAs* to the nucleus and creating a dense network in perinuclear region that stabilizes the nucleus at the center of cell. On stretching these filaments become straight and behave stiffer, thus contributing to the cell mechanics only at large strains (above 20%) [1, 21]. To incorporate their waviness, the *IFs* are modeled as truss elements resisting only tensile loads under elongations higher than 20%. For

better transmission of mechanical stimuli to the nucleus and its stabilization at the center of the cell, each *FA* is connected to the nucleus via at least two *IFs*. To mimic their real structural arrangement, they are modeled tangentially to the nucleus thus creating a dense network in perinuclear region.

For cell in suspended state, a dense network of thin *AFs* localized beneath the *CM* [17] plays a vital role in maintaining the cell shape. This framework of thin *AFs* is created by employing the geometrical shape of icosidodecahedron with its vertices representing *FAs*. These filaments are modeled as truss elements that resist only tensile loads. To achieve the synergistic effect of cytoskeletal components, the elements representing *AFs*, *MTs*, and *IFs* are connected by sharing the same end nodes at the *CM* representing *FAs*.

For the adherent cell model, the size and approximate geometry are based on the rules described by McGarry et al. [4]. The model geometry is semi-ellipsoidal with the radius of 19  $\mu\text{m}$  (semi-major axis in both front and top views), height of 8  $\mu\text{m}$  (semi-minor axis in front view), and half-width of 12.66  $\mu\text{m}$  (semi-minor axis in top view). Based on the experimental observations [22], nucleus is also modeled ellipsoidal. It is positioned at the center of the top view at the height of 2  $\mu\text{m}$  from the substrate with radius of 2.5  $\mu\text{m}$  (semi-major axis) and height of 3  $\mu\text{m}$  (semi-minor axis of 1.5  $\mu\text{m}$ ). Due to the geometric complexity of cell configuration, both cytoplasm and nucleus are meshed with four-node tetrahedral solid elements. Using analogous approach as presented by Barreto et al. [7], a thin layer of actin-gel at the cell surface referred to as *AC* is modeled with four-node quadrilateral shell elements of 0.2  $\mu\text{m}$  thickness [23] and no bending stiffness. Here, the *CM* is not explicitly considered as it is thinner than the adjacent *AC* and therefore its minor contribution to resisting local deformation is included in the shell stiffness dominated by *AC*.

For the adherent cell model, the morphological representation and spatial distribution of both *MTs* and *IFs* are retained analogous to that of the suspended cell model. In contrast, however, in a cell adhered to the substrate thick *ABs* are observed localized at the cell periphery

running almost uniformly in the longitudinal direction [7, 24]. These bundles are modeled using truss elements that resist only tensile loads and are arranged along the *AC* with both ends anchored to it at *FAs* together with elements representing *MTs* and *IFs* to achieve their synergistic effect.

*AFs* in a suspended cell and *ABs* in an adherent cell are internally prestressed (i.e. stressed even without application of an external load); to achieve this in the proposed models, 24% prestrain [24] is assigned to them generating the initial force (prestress) essential for cell shape stability.

## 2.2. Material Properties

In both models, homogenous, isotropic, and linear elastic material properties are considered for all the cytoskeletal components; their elastic parameters taken from the literature are summarized in Table 1. For the elasticity of cell components modeled using continuous elements, however, a Neo-Hookean hyperelastic incompressible description is used with shear modulus being the only material parameter (Table 2). Due to the difficulty of measuring the mechanical properties of cellular components from single cell type, those employed in current study are acquired from literature for distinct cell types measured using various experimental techniques.

Table 1: Elastic and geometric properties of discrete cellular components

Cell components	Elastic modulus (Pa)	Poisson's ratio	Diameter (nm)
Microtubules ( <i>MTs</i> ) [25]	$1.2 \times 10^9$	0.3	(outer/inner) 25/17
Actin filaments ( <i>AFs</i> ) [25]	$2.6 \times 10^9$	0.3	7
Actin bundles ( <i>ABs</i> ) [24]	$0.34 \times 10^6$	0.3	250
Intermediate filaments ( <i>IFs</i> ) [8, 26]	$7.6 \times 10^6$	0.3	10

Table 2: Hyperelastic properties of continuous cellular components

Cell components	Elastic modulus (Pa)	Calculated shear modulus (Pa)
Cytoplasm [22]	$0.5 \times 10^3$	$0.17 \times 10^3$
Nucleus [22]	$5 \times 10^3$	$1.7 \times 10^3$
Actin cortex (AC) [27]	$2 \times 10^3$	$0.67 \times 10^3$
Cell membrane (CM) [19]	$1 \times 10^6$	$0.33 \times 10^6$

### 2.3. Boundary Conditions

The tensile test of a suspended cell with rigid micropipettes (Fig. 2) is simulated to investigate the cell response to global deformation.

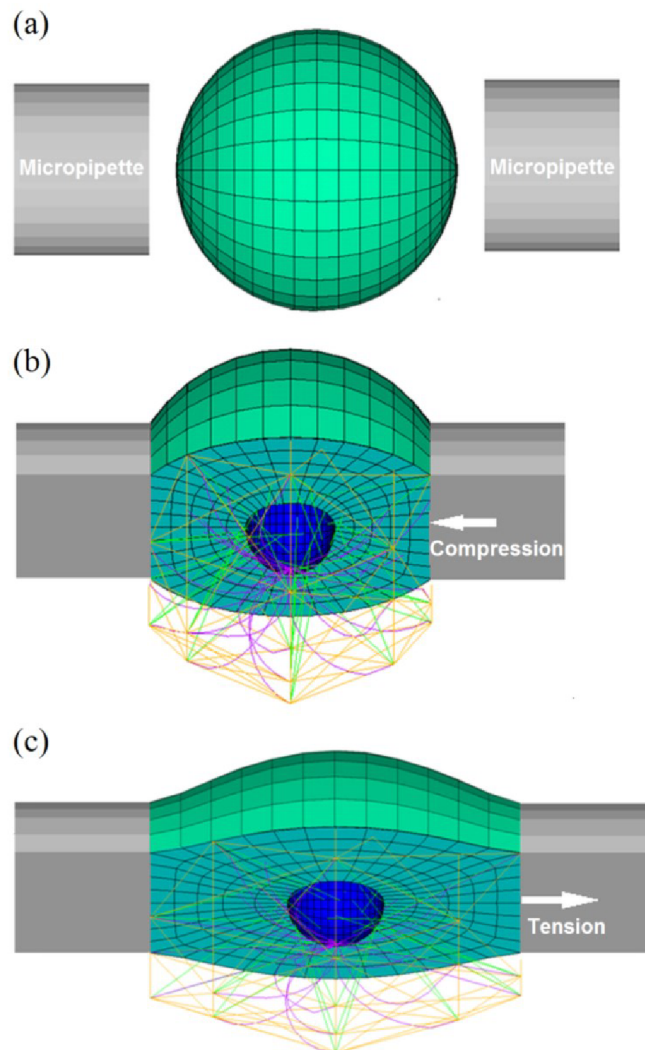


Fig 2: Sectional views of the suspended cell model during consecutive steps in simulation of tensile test with micropipettes: (a) spherical cell and micropipettes, (b) compressing the cell against fixed micropipette, and (c) stretching the cell with movable micropipette

The simulation is performed in several steps, mimicking the experiment [17]. In the first step, contact between the spherical cell and both micropipettes is established by compressing the cell (with the left micropipette being fixed). The contact is set as bonded in the program to enable transmission of tensile forces in the following steps of the simulation. In the next step, the cell is elongated to achieve zero reaction forces in the micropipettes; this shape serves then as the initial (unloaded) state of the cell. In the final step, the displacement that corresponds to cell stretching in the tensile test is applied to the nodes of the movable micropipette. The reaction force is assessed as the sum of forces at the nodes of the contact surface between the cell and the movable micropipette.

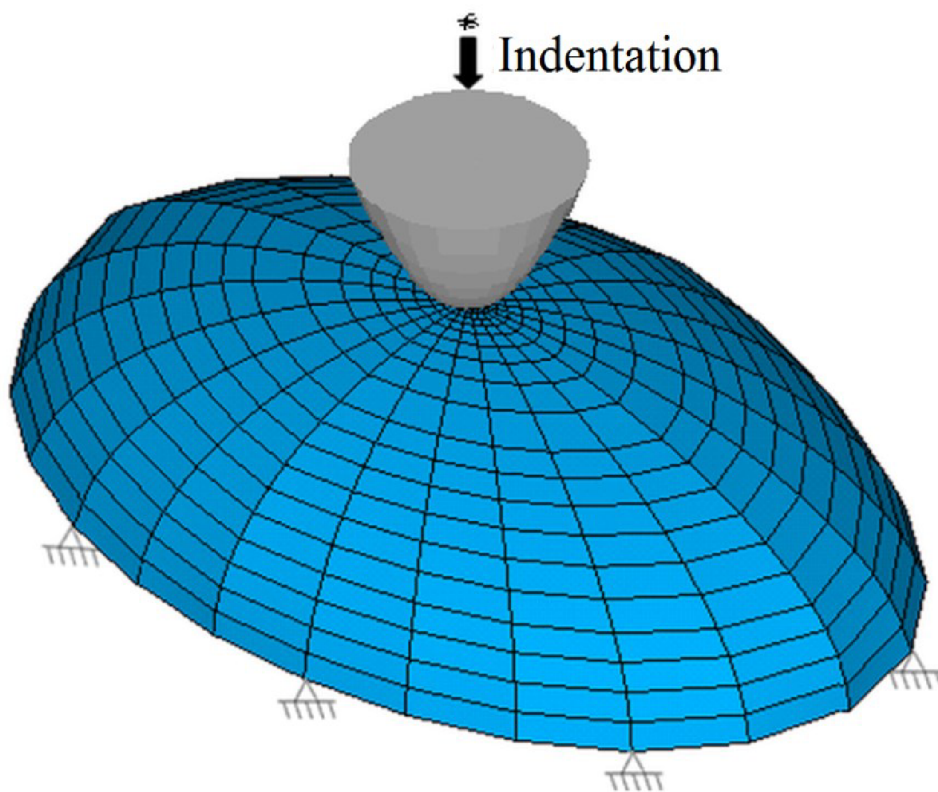


Fig 3: *FE* model of an adherent cell in the indentation test, with constraints and displacement load applied at the tip acting on the top of the cell

In the simulation of the second mechanical test, indentation of a rigid AFM tip into a cell adhered to a rigid substrate (Fig. 3) is simulated to investigate the cell response to local deformation. A rigid paraboloid indenter with the tip curvature radius of 200 nm is modeled above the cell in line with nucleus, to exert a stimulus and obtain the reaction force in the

assigned pilot node. By prescribing a vertical shift to the pilot node, the tip is advanced towards the cell to penetrate it after having come into contact. Corresponding to indentation depth in AFM experiments, the vertical displacement of  $2.5\ \mu\text{m}$  is applied to the tip. For a non-linear contact problem of tip-cell interaction the augmented Lagrangean algorithm is considered. For all nodes at the bottom of the cell a constrained boundary condition is prescribed, simulating the cell adhered to a rigid substrate.

#### **2.4. Parametric Analyses**

For both proposed models, a parametric analysis is performed considering the material properties of different cell components as parameters. The cell models incorporating all discrete and continuous elements with the material properties specified in [Tables 1](#) and [2](#) are referred to as the control models. To illustrate the influence of the material parameters on cell mechanical response their values are increased and decreased by 50% of the values used for the control model. In addition, different cell models are created by totally removing one, two, or more of the cytoskeletal components to examine their mechanical contribution. In simulation of tensile test, the reaction force of altered suspended cell models is compared with that from the control model for  $6.3\ \mu\text{m}$  elongation and in simulation of indentation test similarly, the reaction force of the altered adherent cell models is compared with that from the control model under  $1\ \mu\text{m}$  indentation. Also, mesh sensitivity studies are performed and increase in mesh densities for continuum parts shows negligible change in the results.

### **3. RESULTS**

#### **3.1. Results of Simulated Tensile Test**

The force-elongation curve calculated from tensile test simulation is in good agreement with the non-linear responses of the experimental curves obtained from the tensile test of cultured aortic SMCs [\[17\]](#), as depicted in [Fig. 4](#) and thus validates the proposed bendo-tensegrity model of a suspended cell.

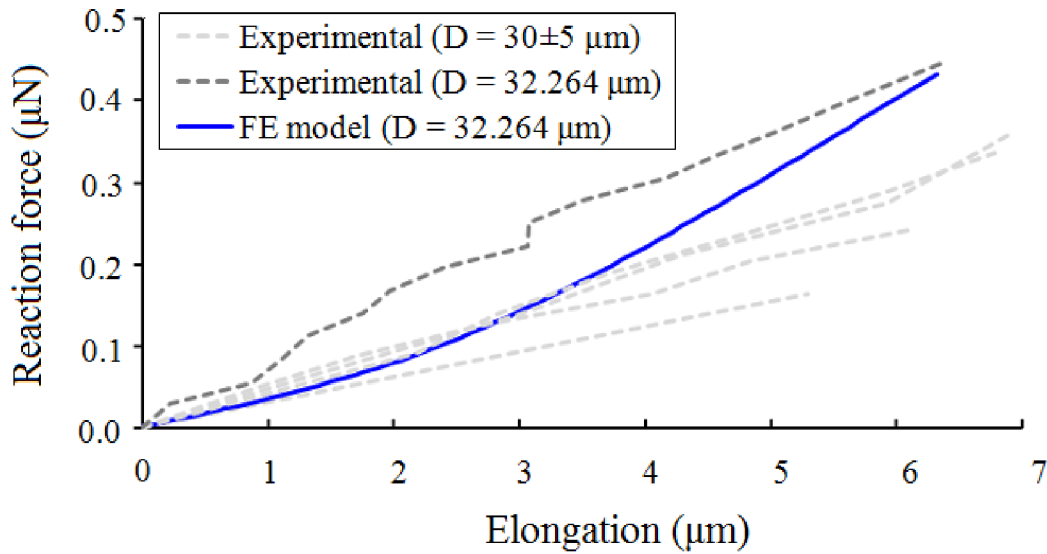


Fig 4: Comparison of simulated force-elongation curve with the experimental curves taken from a study by Nagayama et al. [17] measuring the tensile properties of cultured aortic SMCs of diameter ( $D$ ) using a cell tensile tester

The stiffness of the control model of suspended cell is evaluated as the ratio of conventional stress ( $\sigma$ ) to conventional strain ( $\varepsilon$ ) being proportional to the slope of the resulting force-elongation curve. The conventional stress is given as:

$$\sigma = \frac{f}{a} \quad (5)$$

where,  $f = 0.433 \mu\text{N}$  is the reaction force of cell at the stretched edge and  $a = 817.15 \mu\text{m}^2$  is the (maximal undeformed) cross-sectional area of cell. The conventional strain is expressed as:

$$\varepsilon = \frac{l - l_0}{l_0} \quad (6)$$

where,  $l = 33.264 \mu\text{m}$  is the elongated length of cell and  $l_0 = 26.942 \mu\text{m}$  is the length of cell at zero reaction force after having created bonded contact with the micropipettes. With reference to Fig. 4, the stiffness of 2.3 kPa calculated for the FE model ( $D=32.264 \mu\text{m}$ ) using Eqs. (5) and (6) is in good accordance with the stiffness of 2.5 kPa calculated for the experimental ( $D=32.264 \mu\text{m}$ ) cell sample.

This model enables visualization of the mechanics of individual cytoskeletal components

during tensile test. Figure 5a exhibits the deformed shape of cytoskeletal components and nucleus during simulation of tensile test where the nucleus appears elongated in the direction of stretch concomitant of cell elongation, analogous to that observed in experiments [9, 17].

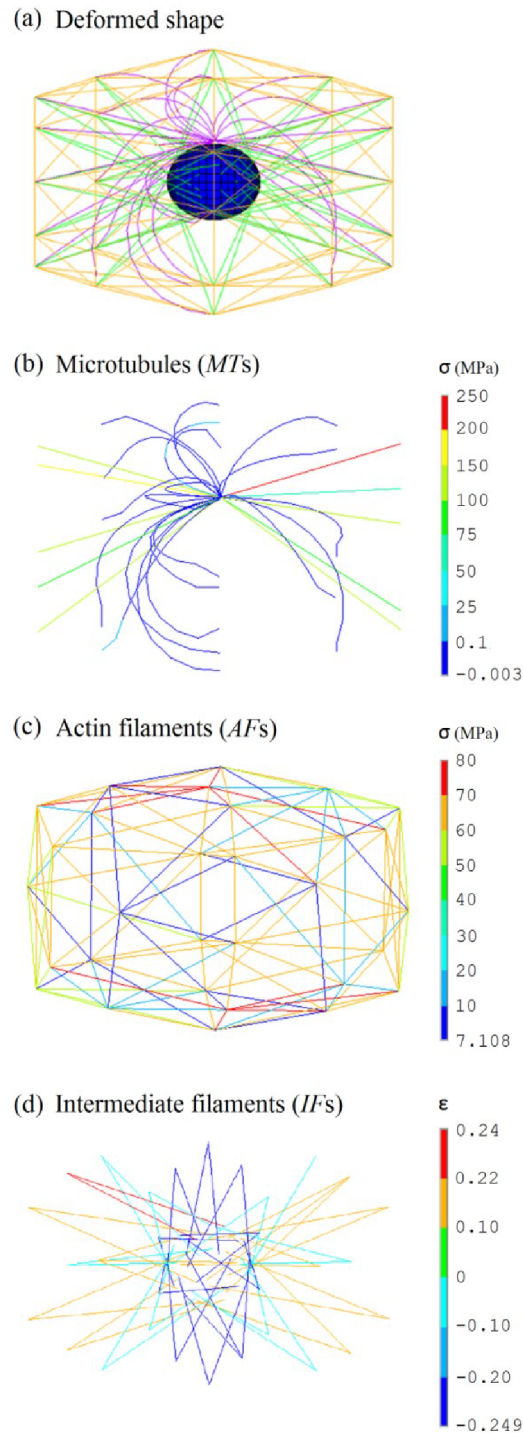


Fig 5: Simulation results of the tensile test: (a) deformed shape of the cytoskeletal components and nucleus, distribution of axial stress in the discrete elements representing (b) MTs and (c) AFs, and distribution of axial strain in the discrete elements representing (d) IFs



During cell stretching, the randomly oriented *AFs* are likely to be aligned in the direction of stretch. This passive realignment gradually increases the overall reaction force of the cell, causing the force-elongation curve to be non-linear [9, 28]. During cell stretching some of the *MTs* are straightened out while others remain bended (Fig. 5b), similar to that observed in experiments [29].

The proposed models can predict correlation of cellular mechanical properties and stress distribution within the specific cytoskeletal components. *MTs* that are straightened and aligned in the direction of stretch resist tensile forces and generate high stresses, while the ones that are bended due to compressive forces generate low negative stresses (Fig. 5b); this effect highlights the influence of the shape of this component on cell deformation. High stresses in straightened *MTs* can be attributed to the large difference between their flexural and tensional stiffness, which may significantly contribute to the non-linearity of cell responses. High stresses are observed also for the *AFs* (Fig. 5c) that are aligned in the direction of stretch and resist tensile forces. *IFs* aligned in the direction of stretch are linearized from their assumed initial waviness and exhibit high strains, while low strains are observed in those ones localized in the central region indicating that they remain wavy (Fig. 5d).

### 3.2. Results of Simulated Indentation Test

The force-indentation curves calculated from simulations of AFM tip indenting the adherent cell model at the apex (Fig. 6a) and at a receptor distant from apex (Fig. 6b) are depicted in Fig. 6c. Both results lie within the variation range of the experimental curves obtained with AFM indentation of ESCs [18], which thus validates the proposed bendo-tensegrity model of an adherent cell. The indentation test is simulated at two distinct locations on the cell, to explore the significance of its structural inhomogeneity that could be one of the reasons for scattering of experimental curves [30].

For indentation depth of 2.5  $\mu\text{m}$ , the reaction force predicted by the model at the apex is

4.05 nN and at a receptor is 5.72 nN, thus illustrating approximately 40% stiffer response when indenting at a receptor compared to the apex. This can be explained by the direct transmission of indenting force to cytoskeleton that is much stiffer than the surrounding cytoplasm. Therefore, these results exhibit that the indentation site dominates the force-indentation curve which corresponds to the experimental observations [30, 31].

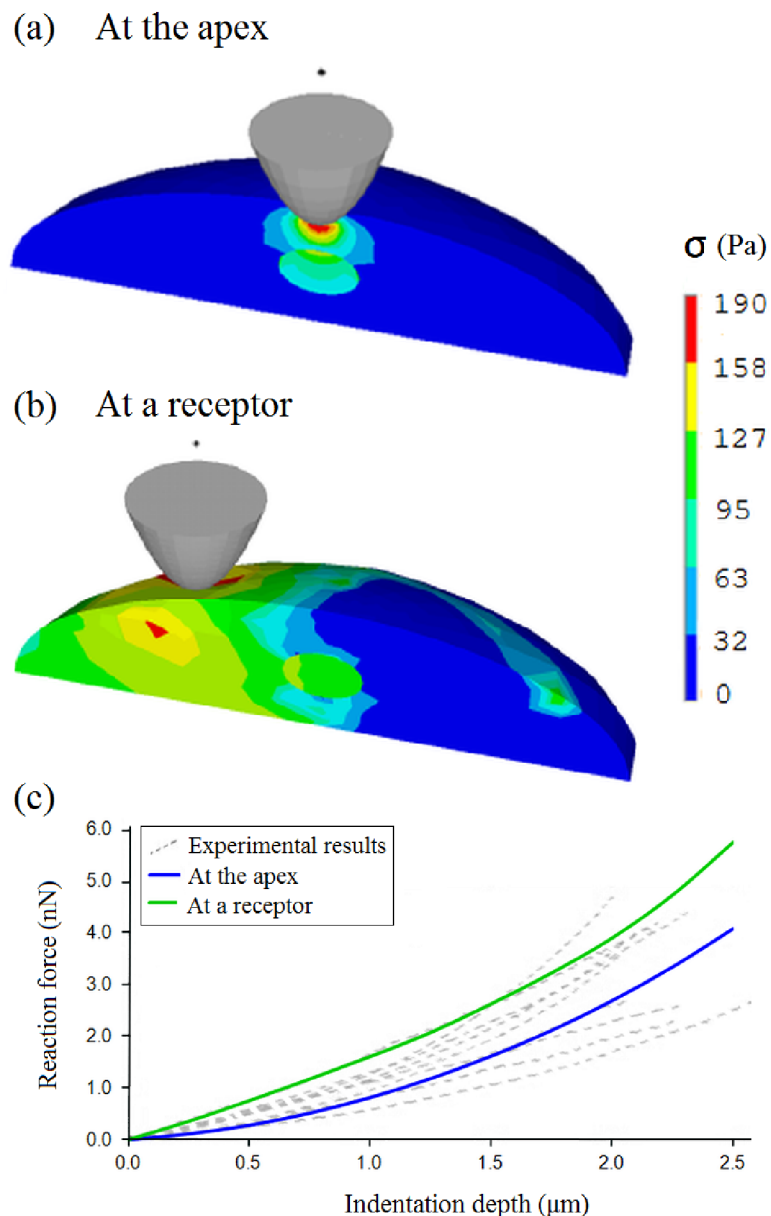


Fig 6: Sectional views comparing the contour plots of von Mises stress inside the cell during AFM simulation for indentation depth of  $1 \mu\text{m}$  at (a) the apex and (b) a receptor; (c) comparison of simulated force-indentation curves with the experimental curves taken from a study by Pillarisetti et al. [18] measuring the stiffness of ESCs using AFM indentation

A remarkable difference in stress distribution pattern within the cell is observed when indenting at the apex compared to a receptor, underlining the synergistic effect of cytoskeletal components on localized load transmission to the distant parts of the cell known as action-at-a-distance effect [32].

### 3.3. Results of Parametric Analyses

#### 3.3.1 Role of the Cytoskeletal Components

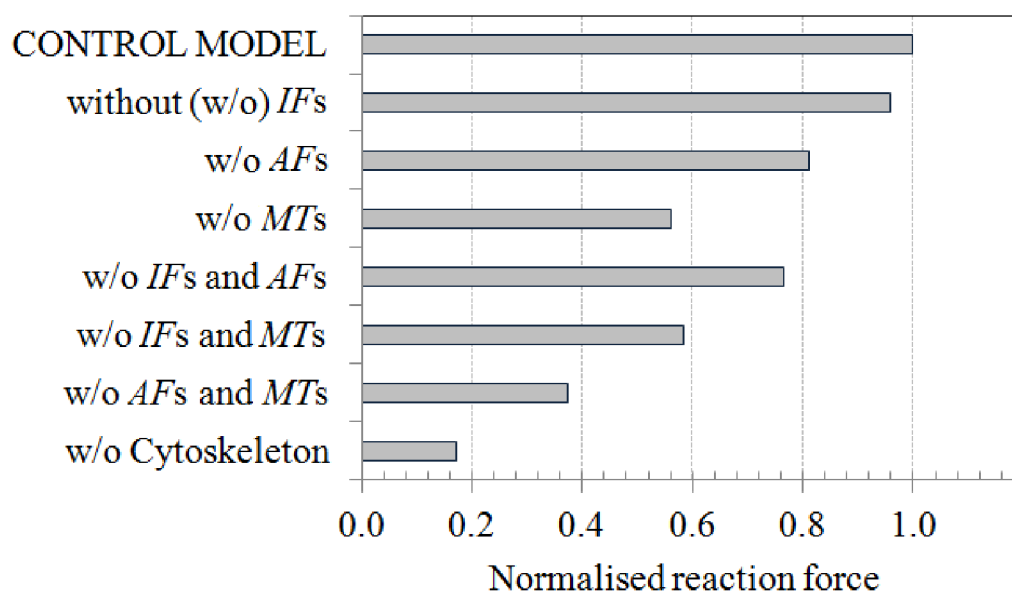
Figure 7 illustrates the results of parametric studies investigating the mechanical contribution of individual cytoskeletal components to the overall reaction force of cell models to distinct mechanical stimuli. The role of each cytoskeletal component in resisting global deformation is investigated via removal of each cytoskeletal component from the proposed suspended cell model.

The maximum reaction force of the cell model (under elongation of  $6.3 \mu\text{m}$ ) without cytoskeletal components is 5.82 times lower than the control model (Fig. 7a), emphasizing their pivotal role in characterizing the tensile properties of cell during global deformation. The reaction force of the cell model without *IFs* is slightly less than the reaction force of the control model indicating their minimal contribution to cell stiffness at low strains (below 20%). Comparing to the reaction force of the control model, removal of *AFs* reduces the reaction force of cell model by one fifth, whereas removal of *MTs* reduces it to approximately half, suggesting that *MTs* resist intracellular tension generated by *AFs*. Moreover, removal of both *AFs* and *MTs* reduces the reaction force of cell model significantly making it more compliant, indicating their synergistic effect. Therefore, *AFs* and *MTs* play crucial roles in maintaining cell stiffness during stretching, similar to that observed in experiment [29].

The role of each cytoskeletal component in resisting local deformation is investigated similarly via the proposed adherent cell model. The maximum reaction force of the cell model without cytoskeletal components is 1.52 times lower than the control model (Fig. 7b), pointing

out their contribution in resisting the mechanical perturbations from exterior.

(a) Response of the suspended cell model to stretching



(b) Response of the adherent cell model to indentation

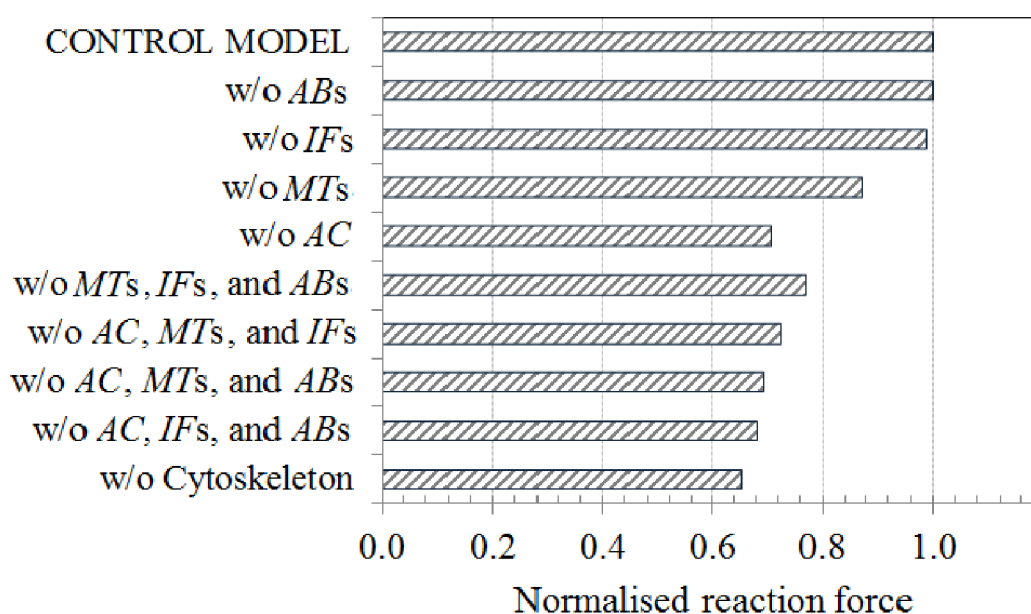


Fig 7: Contribution of the cytoskeletal components individually and in mutual combination to the response of cell models during (a) tensile test and (b) indentation test, highlighting their synergistic effect. The reaction force of different models is normalized with respect to that from the corresponding control model.

For model without *ABs* and model without *IFs*, the reaction force is comparable to that of the control model, indicating their minimal effect on cell rigidity during indentation. When *AC* is removed the model shows approximately twofold decrease in the reaction force compared to the model with *MTs* being removed. Thus, *AC* and *MTs* play critical role in maintaining cell rigidity during indentation, analogous to that observed in experiment [7]. Furthermore, the cell models created without two or more cytoskeletal components are also incompetent to withstand cell forces, emphasizing their mutual interdependence during indentation test.

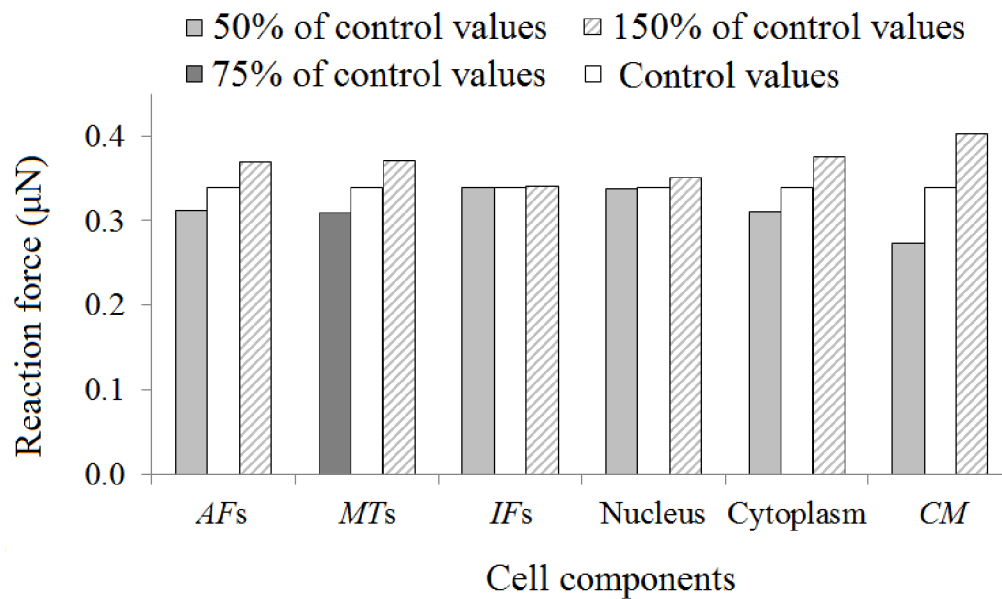
### 3.3.2 Parametric Variations of Material Properties

Figure 8 depicts the results of parametric studies investigating the effect of varying Young's modulus of individual cell components on the overall reaction force of cell models. During these studies, the prestress in *AFs* and *ABs* is retained constant. It is observed that the reaction force of both models is highly sensitive to the variation of Young's modulus of certain cell components. In tensile test simulation, the variation of Young's modulus of both *AFs* and *MTs* substantially affect the reaction force of suspended cell model (Fig. 8a). A 50% decrease in Young's modulus of *MTs* was not realized due to problems with convergence and thus only 25% decrease in the same is considered. Among continuum elements, regardless of small thickness the change in Young's modulus of *CM* has significant influence on the reaction force followed by cytoplasm. The parametric study revealed that the reaction force of suspended cell model is relatively insensitive to the changes in Young's modulus of *IFs* and nucleus.

In indentation test simulation, the variation of Young's modulus of *AC* considerably affects the reaction force of adherent cell model (Fig. 8b), probably due to constraining the volume of cytoplasm. Parametric analysis revealed that the adherent cell model is highly sensitive to the variations in rigidity of cytoplasm, whereas its sensitivity to changes in rigidity of nucleus is very limited that can be associated to their different volumes. On the contrary, changing the Young's modulus of *ABs*, *MTs*, and *IFs* to 50% or 150% of their control values did not affect the

reaction force.

(a) For suspended cell model



(b) For adherent cell model

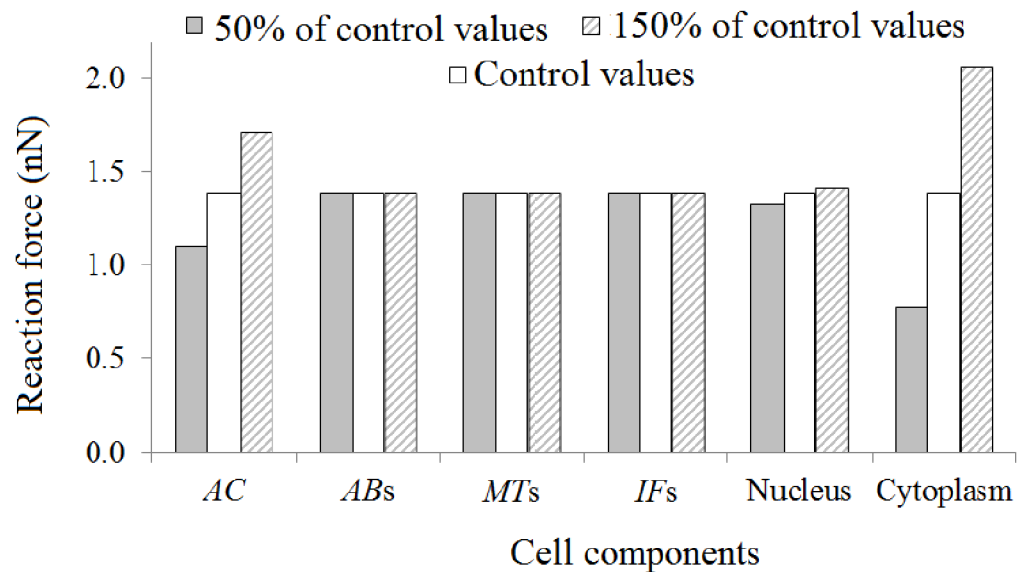


Fig 8: The effect of varying Young's modulus of individual cell components from the control values (Table 1 and Table 2) on the overall reaction force of (a) suspended cell model in tensile test simulation and (b) adherent cell model in indentation test simulation

Although not presented in Fig. 8, simulation results have demonstrated that inclusion of cytoplasm compressibility did not affect the overall reaction force of both cell models.

#### 4. DISCUSSION

The presented models aim at realistic simulation of the deformation of cell, primarily focusing on its nucleus deformation. It is well established that cells respond to mechanical stimuli in a variety of ways that range from changes in cell morphology to activation of biochemical responses, which affect the cell's phenotype. The nucleus plays a central role in defining cell responses thus the current study provides an insight into its deformation by means of *FE* modeling of distinct mechanical tests of eukaryotic cells. In tensile test simulation, the deformation of the nucleus reached a maximum of about 8% (first principal strain) for cell stretching of 6.3  $\mu\text{m}$  (global deformation), whereas in the simulation of indentation test it is approximately 4% under indentation of 2.5  $\mu\text{m}$  (local deformation), suggesting that nucleus deformation depends on the nature of the biophysical stimulus [16]. For both simulations, a symmetrical strain distribution pattern was noticed in the nucleus that was almost uniform during cell stretching and non-uniform being concentrated at the top center region during cell indentation at apex. Furthermore, it is observed that cell indentation of 2.5  $\mu\text{m}$  induces nucleus deformation that corresponds to cell stretching of 2.081  $\mu\text{m}$ . This quantitative characterization of nucleus deformation could be hypothetically decisive for transducing mechanical signals into changes in gene expression.

Although it was intended to simulate various mechanical tests using the same model, the distinctness in the form and organization of actin protein for cell in suspended and adherent states served as a motivation for creating two distinct models of cell. In numerous experimental studies, for cell in suspended state a dense network of thin *AFs* is observed at cell periphery localized beneath the *CM* [17, 33-35], whereas for cell in adherent state a thin layer of actin-gel referred as *AC* is observed at the cell periphery along with thick *ABs* running almost uniformly in the longitudinal direction [7, 17, 24, 35, 36].

In tensile test simulation, the bended *MTs* are highly compliant with stresses below 1 MPa, whereas the straight ones (being in tension only) show much higher stresses highlighting

the significant contribution of *MTs* arranged in loading direction to the cell stiffness. The suspended cell model stretched by approximately 100 % gives the reaction force of 1.8  $\mu\text{N}$  that evaluates the cell stiffness of 2.4 kPa, which is in good agreement with normalized stiffness of  $2.6 \pm 0.5$  kPa measured for cultured SMC [17]. Although the simulation response shows higher non-linearity (strain stiffening) than the experiments (Fig. 4), this tendency is in accordance with other experimental results [28]. However, removal of *AFs* in the proposed model reduces the cell stiffness by approximately 20 % (Fig. 7a) which is less than the value observed experimentally [17].

The cellular tensegrity models envision *AFs* as tension supporting cables and *MTs* as compression supporting struts [2]. Although, these models successfully explain several observations in cell mechanics, the excessive compression stiffness of the struts introduces non-realistic artifacts in tension test simulations as shown by Bursa et al. [5]. The previous tensegrity models neither take into account the influence of flexural behavior of *MTs* nor predict the mechanics of individual cytoskeletal components during cytoskeleton disruption studies. The proposed bendo-tensegrity models modify this structural concept by taking into account both flexural (buckling) as well as tensional behavior of *MTs* and having no restriction on the spatial distribution of fibers.

Implementing the hybrid modeling approach, the interaction of discrete and continuous elements is ensured at the nodes representing *FAs* and thus, the external forces transmitted through *FAs* are sensed by the entire discrete structure as well as all the continuum parts. These models defined the structural adaptability for cytoskeleton, which allows complete removal of the cytoskeletal components individually or in combination of two or more, without collapsing the shape of cell. In both models, the suggested form and organization of individual cytoskeletal components allow exploration of the force transmission pathways for mechanical stimuli acting on the cell surface to propagate to the nucleus, ultimately resulting in mechanotransduction. The quantitative information on forces transmitted by individual cytoskeletal components in distinct



cell types can be obtained by varying the mechanical properties of individual cytoskeletal components in the proposed models. The simulation results show capability of the proposed models in describing the response of not only the cell as a whole but also of nucleus and individual cytoskeletal components to distinct mechanical stimuli.

Nevertheless, there are certain limitations of the proposed models. The structural arrangement of cytoskeletal components does not capture their true complexity and dynamic (i.e. time-dependent) behavior as observed in living cells. These models do not take into consideration the viscoelastic nature of cell. Due to their passive nature, they also do not capture active responses of the cell such as remodeling of *AFs* and *MTs* exhibited under mechanical loading.

In future work, the models proposed in this study should be considered with viscoelastic material properties. Additionally, to study cell deformation under distinct mechanical loading, multiple single-cell mechanical tests could be simulated with these models by applying appropriate boundary conditions.

## **5. SUMMARY**

In summary, three-dimensional *FE* bendo-tensegrity models of a single cell in different states are proposed to simulate the mechanical behavior of cell during distinct mechanical stimuli. The tensile test simulations demonstrate that *AFs* and *MTs* play a crucial role in cell stiffness including its increase with stretching, whereas the indentation test simulations exhibit that indentation site dominates the cell behavior where *AC* and *MTs* are essential for cell rigidity. Thus, the current study provides new insight into interdependence of cell mechanical properties, mechanical role of individual cytoskeletal components, and quantitative information of nucleus deformation hypothetically decisive for mechanotransduction.

## **ACKNOWLEDGMENT**

The authors are thankful to Prof. Kozaburo Hayashi for valuable discussions concerning experimental results.

## **FUNDING**

This study was supported through NETME CENTRE PLUS (LO1202) by financial means from the Ministry of Education, Youth and Sports under the “National Sustainability Program I” and by Czech Science Foundation, project number 13-16304S.

**NOMENCLATURE**

$a$	cross-sectional area of cell, $\mu\text{m}^2$
$AB$	actin bundle
$AC$	actin cortex
$AF$	actin filament
$AFM$	atomic force microscopy
$CM$	cell membrane
$D$	suspended cell diameter, $\mu\text{m}$
$ESC$	embryonic stem cell
$f$	reaction force at the stretched edge, $\mu\text{N}$
$FA$	focal adhesion
$FE$	finite element
$IF$	intermediate filament
$l$	elongated length of cell, $\mu\text{m}$
$l_0$	length of cell at zero reaction force, $\mu\text{m}$
$MT$	microtubule
$SMC$	smooth muscle cell
$\varepsilon$	conventional strain
$\sigma$	conventional stress, $\text{N}/\text{m}^2$

## REFERENCES

- [1] Janmey, P., Euteneuer, U., Traub, P., and Schliwa, M., 1991, "Viscoelastic properties of vimentin compared with other filamentous biopolymer networks," *J Cell Biol*, **113**(1), pp. 155-160. DOI: 10.1083/jcb.113.1.155
- [2] Ingber, D., 1993, "Cellular tensegrity: defining new rules of biological design that govern the cytoskeleton," *J Cell Sci*, **104**, pp. 613–27.
- [3] Huang, H., Kamm, R., and Lee, R., 2004, "Cell mechanics and mechanotransduction: pathways, probes, and physiology," *Am J Physiol-Cell Ph*, **287**(1), pp. C1-11. DOI: 10.1152/ajpcell.00559.2003
- [4] McGarry, J., and Prendergast, P., 2004, "A three-dimensional finite element model of an adherent eukaryotic cell," *Eur Cells Mater*, **7**, pp. 27–33.
- [5] Bursa, J., Holata, J., and Lebis, R., 2012, "Tensegrity finite element models of mechanical tests of individual cells," *Technol Health Care*, **20**(2), pp. 135-150. DOI: 10.3233/THC-2011-0663
- [6] Bursa, J., Lebis, R., and Janicek, P., 2006, "FE models of stress-strain states in vascular smooth muscle cell," *Technol Health Care*, **14**(4,5), pp. 311-20.
- [7] Barreto, S., Clausen, C., Perrault, C., Fletcher, D., and Lacroix, D., 2013, "A multi-structural single cell model of force-induced interactions of cytoskeletal components," *Biomaterials*, **34**(26), pp. 6119-26. DOI: 10.1016/j.biomaterials.2013.04.022
- [8] Xue, F., Lennon, A., McKay, K., Campbell, V., and Prendergast, P., 2015, "Effect of membrane stiffness and cytoskeletal element density on mechanical stimuli within cells: an analysis of the consequences of ageing in cells," *Comput Method Biomec*, **18**(5), pp. 468-76. DOI: 10.1080/10255842.2013.811234
- [9] Ujihara, Y., Nakamura, M., Miyazaki, H., and Wada, S., 2010, "Proposed spring network cell model based on a minimum energy concept," *Ann Biomed Eng*, **38**(4), pp. 1530-8. DOI: 10.1007/s10439-010-9930-8
- [10] Maurin, B., Cañadas, P., Baudriller, H., Montcourrier, P., and Bettache, N., 2008, "Mechanical model of cytoskeleton structuration during cell adhesion and spreading," *J Biomech*, **41**(9), pp. 2036-41. DOI: 10.1016/j.jbiomech.2008.03.011
- [11] Stamenović, D., and Coughlin, M., 1999, "The role of prestress and architecture of the cytoskeleton and deformability of cytoskeletal filaments in mechanics of adherent cells: a quantitative analysis," *J Theor Biol*, **201**(1), pp. 63-74. DOI: 10.1006/jtbi.1999.1014
- [12] Stamenović, D., Fredberg, J., Wang, N., Butler, J., and Ingber, D., 1996, "A microstructural approach to cytoskeletal mechanics based on tensegrity," *J Theor Biol*, **181**(2), pp. 125-36. DOI: 10.1006/jtbi.1996.0120
- [13] Cañadas, P., Laurent, V., Chabrand, P., Isabey, D., and Wendling-Mansuy, S., 2003, "Mechanisms governing the visco-elastic responses of living cells assessed by foam and tensegrity models," *Med Biol Eng Comput*, **41**(6), pp. 733-9. DOI: 10.1007/BF02349982
- [14] Wang, N., Naruse, K., Stamenović, D., Fredberg, J., Mijailovich, S., Tolić-Nørrelykke, I., Polte, T., Mannix, R., and Ingber, D., 2001, "Mechanical behavior in living cells consistent with the

tensegrity model," Proceedings of the National Academy of Sciences, **98**(14), pp. 7765-7770. DOI: 10.1073/pnas.141199598

[15] McGarry, J., Klein-Nulend, J., Mullender, M., and Prendergast, P., 2005, "A comparison of strain and fluid shear stress in stimulating bone cell responses - a computational and experimental study," FASEB J, **19**(3), pp. 482-4. DOI: 10.1096/fj.04-2210fje

[16] Prendergast, P., 2007, "Computational modelling of cell and tissue mechanoresponsiveness," Gravit Space Res, **20**(2), pp. 43-50.

[17] Nagayama, K., Nagano, Y., Sato, M., and Matsumoto, T., 2006, "Effect of actin filament distribution on tensile properties of smooth muscle cells obtained from rat thoracic aortas," J Biomech, **39**(2), pp. 293-301. DOI: 10.1016/j.jbiomech.2004.11.019

[18] Pillarisetti, A., Desai, J., Ladjal, H., Schiffmacher, A., Ferreira, A., and Keefer, C., 2011, "Mechanical phenotyping of mouse embryonic stem cells: increase in stiffness with differentiation," Cell Reprogram, **13**(4), pp. 371-380. DOI: 10.1089/cell.2011.0028

[19] Rand, R., 1964, "Mechanical properties of the red cell membrane: II. Viscoelastic breakdown of the membrane," Biophys J, **4**(4), pp. 303-316.

[20] Mehrbod, M., and Mofrad, R., 2011, "On the significance of microtubule flexural behavior in cytoskeletal mechanics," PloS One, **6**(10), pp. e25627. DOI: 10.1371/journal.pone.0025627

[21] Wang, N., and Stamenović, D., 2000, "Contribution of intermediate filaments to cell stiffness, stiffening, and growth," Am J Physiol-Cell Ph, **279**(1), pp. C188-194.

[22] Caille, N., Thoumine, O., Tardy, Y., and Meister, J., 2002, "Contribution of the nucleus to the mechanical properties of endothelial cells," J Biomech, **35**, pp. 177-87. DOI: 10.1016/S0021-9290(01)00201-9

[23] Unnikrishnan, G., Unnikrishnan, U., and Reddy, J., 2007, "Constitutive material modeling of cell: a micromechanics approach," J Biomech Eng, **129**(3), pp. 315-23. DOI: 10.1115/1.2720908

[24] Deguchi, S., Ohashi, T., and Sato, M., 2005, "Evaluation of tension in actin bundle of endothelial cells based on preexisting strain and tensile properties measurements," Mol Cell Biomech, **2**(3), pp. 125-133. DOI: 10.3970/mcb.2005.002.125

[25] Gittes, F., Mickey, B., Nettleton, J., and Howard, J., 1993, "Flexural rigidity of microtubules and actin filaments measured from thermal fluctuations in shape," J Cell Biol, **120**(4), pp. 923-934. DOI: 10.1083/jcb.120.4.923

[26] Bertaud, J., Qin, Z., and Buehler, M., 2010, "Intermediate filament-deficient cells are mechanically softer at large deformation: a multi-scale simulation study," Acta Biomater, **6**(7), pp. 2457-2466. DOI: 10.1016/j.actbio.2010.01.028

[27] Stricker, J., Falzone, T., and Gardel, M., 2010, "Mechanics of the F-actin cytoskeleton," J Biomech, **43**(1), pp. 9-14. DOI: 10.1016/j.jbiomech.2009.09.003

[28] Miyazaki, H., Hasegawa, Y., and Hayashi, K., 2002, "Tensile Properties of Contractile and Synthetic Vascular Smooth Muscle Cells," JSME Int J C-Mech Sy, **45**(4), pp. 870-879. DOI: 10.1299/jsmec.45.870

- [29] Nagayama, K., and Matsumoto, T., 2008, "Contribution of actin filaments and microtubules to quasi-in situ tensile properties and internal force balance of cultured smooth muscle cells on a substrate," *Am J Physiol-Cell Ph*, **295**(6), pp. C1569-1578. DOI: 10.1152/ajpcell.00098.2008
- [30] Ohara, Y., Miyazaki, H., and Hayashi, K., 2000, "Atomic force microscopy measurement of the mechanical properties of vascular smooth muscle cell," *Proc. of 12th JSME Bioengineering Conference, Kanazawa, Japan*, pp. 55-56.
- [31] Ohashi, T., Ishii, Y., Ishikawa, Y., Matsumoto, T., and Sato, M., 2002, "Experimental and numerical analyses of local mechanical properties measured by atomic force microscopy for sheared endothelial cells," *Bio-Med Mater Eng*, **12**(3), pp. 319-327.
- [32] Wang, N., and Suo, Z., 2005, "Long-distance propagation of forces in a cell," *Biochem Bioph Res Co*, **328**(4), pp.1133-8. DOI:10.1016/j.bbrc.2005.01.070
- [33] Guck, J., Schinkinger, S., Lincoln, B., Wottawah, F., Ebert, S., Romeyke, M., Lenz, D., Erickson, H., Ananthakrishnan, R., Mitchell, D., Kas, J., Ulvick, S., and Bilby, C., 2005, "Optical deformability as an inherent cell marker for testing malignant transformation and metastatic competence," *Biophys J*, **88**(5), pp. 3689–3698. DOI: 10.1529/biophysj.104.045476
- [34] Ofek, G., Dowling, E., Raphael, R., McGarry, J., and Athanasiou, K., 2010, "Biomechanics of single chondrocytes under direct shear," *Biomech Model Mechan*, **9**(2), pp. 153-162. DOI: 10.1007/s10237-009-0166-1
- [35] Li, W., Jiang, Y., and Tuan, R., 2006, "Chondrocyte phenotype in engineered fibrous matrix is regulated by fiber size," *Tissue Eng*, **12**(7), pp. 1775-85. DOI: 10.1089/ten.2006.12.1775
- [36] Darling, E., Zauscher, S., Block, J., and Guilak, F., 2007, "A thin-layer model for viscoelastic, stress-relaxation testing of cells using atomic force microscopy: do cell properties reflect metastatic potential?," *Biophys J*, **92**(5), pp. 1784-91. DOI: 10.1529/biophysj.106.083097

## Appendix B.

Review article published in Journal of Biological, Biomolecular, Agricultural, Food and Biotechnological Engineering

Citation Reference: Bansod Y.D., and Bursa J. (2015). Continuum-based modelling approaches for cell mechanics. *World Academy of Science, Engineering and Technology, International Journal of Biological, Biomolecular, Agricultural, Food and Biotechnological Engineering*. 9(9):921-32.

# Continuum-Based Modeling Approaches to Cell Mechanics

Yogesh D. Bansod, Jiri Bursa

*Abstract*—The quantitative study of cell mechanics is of paramount interest, since it regulates the behavior of the living cells in response to the myriad of extracellular and intracellular mechanical stimuli. The novel experimental techniques together with robust computational approaches have given rise to new theories and models, which describe cell mechanics as combination of biomechanical and biochemical processes. This review paper encapsulates the existing continuum-based computational approaches that have been developed for interpreting the mechanical responses of living cells under different loading and boundary conditions. The salient features and drawbacks of each model are discussed from both structural and biological points of view. This discussion can contribute to the development of even more precise and realistic computational models of cell mechanics based on continuum approaches or on their combination with microstructural approaches,

which in turn may provide a better understanding of mechanotransduction in living cells.

*Keywords*— Cell mechanics, computational models, continuum approach, mechanical models

## I. INTRODUCTION

Living cells in human body are continuously subjected to the myriad of extracellular and intracellular mechanical stimuli and in response they generate stresses and strains. It has been observed in different experiments, that the cell deformation can affect both their physiological functions as well as biological processes. The novel experimental techniques provide substantial information regarding the mechanical properties of the cell along with their responses to diverse chemical and mechanical stimuli. This leads to the development of new theories and mechanical models of living cells that can characterize cell responses when subjected to distinct loading types.

There are innumerable computational models at distinct temporal and spatial scales that have been developed to capture and simulate the cell responses corresponding to the experimental observations. The existing computational modeling approaches for cell mechanics are broadly classified into two categories namely the continuum approaches and the microstructural approaches, which are outlined in Fig 1[30]. The microstructural approaches consider the cytoskeleton (CSK) as the critical component in cell mechanics, whereas the continuum approaches ignore the contribution of distinct molecular

---

Y.D. Bansod is with the Brno University of Technology, Antoninska 548/1, 601 90, Brno, Czech Republic (corresponding author: phone: 00420-608-678-342; e-mail: yogeshbansod@gmail.com).

J. Bursa is with the Brno University of Technology, Antoninska 548/1, 601 90, Brno, Czech Republic (email: bursa@fme.vutbr.cz).

structures to cell mechanics and are employed when the smallest length scale of interest is much larger than the space over which the structures and properties of the cell vary significantly [30].

The continuum mechanics uses coarse-graining approach to localize the microscopic stress-strain relationships, which then yields a constitutive relationship and deformation description of the material that can be applied at macroscopic scale. The models under continuum paradigm are validated and the associated material constants are evaluated by comparing the results obtained from canonical experimental techniques with computational predictions [31]. The finite element method is the frequently used technique in computational simulations to study a variety of cellular processes, whereas the boundary element method has also been employed as an alternative technique wherever necessary [30].

The majority of the mechanical models under continuum paradigm assume that cell is passive in nature. Recent studies have successfully overcome this drawback by incorporating the inherent active nature of the cell in computational modeling [6]. This review article outlines the existing mechanical models of cell mechanics that are premised on the continuum mechanics.

## II. LIQUID DROP MODELS

The suspended cell types (like neutrophils, leukocytes, and erythrocytes) often adopt spherical shape and behave like a liquid droplet. In micropipette aspiration at certain threshold of pressure difference, these cells can be aspirated into a micropipette with a smaller diameter and then, upon release they regain their initial spherical shape. The liquid drop models also known as cortical shell-liquid core models were invented to elucidate this rheological behavior of suspended cells. These models view the suspended cell or its parts as a deformable material with certain continuous material properties. This class of models incorporates the Newtonian liquid drop model, the compound Newtonian liquid drop model, the shear-thinning liquid drop model, and the Maxwell liquid drop model [1].

### A. Newtonian Liquid Drop Model

The Newtonian liquid drop model has been invented to simulate the continuous deformation of leukocytes when flowing into the micropipette [1]. The cell is modeled as Newtonian liquid droplet as depicted in Fig 2 (a). The outer cortex was assumed to be viscous fluid with constant surface tension and no bending resistance circumscribing its endogenous part, which was assumed to be

homogenous Newtonian viscous liquid [1]. The state of stress is considered to be independent of any displacement and the constitutive relations for the cortex are described by two equilibrium equations as

$$\begin{aligned} (T_1 + T_2)/2 &= T_0 + k(V_a/2), \\ (T_1 - T_2)/2 &= \eta V_s, \quad k = 3\eta \end{aligned} \quad (1)$$

where  $T_1$  and  $T_2$  are the in plane principal stress resultants,  $T_0$  is the static in-plane isotropic tension corresponding to zero shearing and dilatatory rates,  $k$  and  $\eta$  are the coefficients of viscosity for surface area dilation and shear respectively, and  $V_a$  and  $V_s$  are the rates of dilation and shear, respectively [31].

The micropipette aspiration of neutrophil indicates that the cytoplasm behaves as a Newtonian fluid. The relationship between the rate of the change of the projection length of the cell inside the pipette  $\dot{L}$  and the radius of the cell outside the pipette  $R_c$  [32] is described as follows

$$\frac{(\Delta P - P_{cr})}{\mu (L/R_p)} = m \left(1 - \frac{R_p}{R_c}\right) \text{ for } 0.5 \leq R_p/R_c \leq 1.0 \quad (2)$$

Where

$$P_{cr} = 2T_0 (1/R_p - 1/R_c) \quad (3)$$

where  $\Delta P$  is the total suction pressure,  $P_{cr}$  is the critical excess suction pressure,  $\mu$  is the shear viscosity,  $R_p$  is the radius of the pipette, and  $m$  is a coefficient that is dependent on the ratio of the cortical dissipation to the core dissipation  $\tilde{\eta}$ . Here,  $m \approx 6$  corresponds to  $\tilde{\eta} \approx 0.01$  [33].

This model was devised to study the recovery behavior of neutrophil after going through large deformation in micropipette aspiration test. The theoretical recovery process was obtained as a function of non-dimensional time and the initial deformation ratio. Some of the experimental observations of this model are in accordance with the theoretical predictions indicating that the Newtonian liquid drop model can predict the overall deformation of the cell and its ability to recover its original shape [34]. However, it neither illustrates the initial rapid entry of the cell into the pipette [31], [32], [34], [35] nor its resistance to mechanical stresses [30]. Apart from this, due to several discrepancies between this model's predictions and experimental findings [3], [33], [34], [36]; this leads to the development of the compound Newtonian liquid drop model [3].

### B. Compound Newtonian Liquid Drop Model

It has been observed in different experiments that nucleus is stiffer and more viscous than its circumscribing cytoplasm [2], [37], [38], [39].



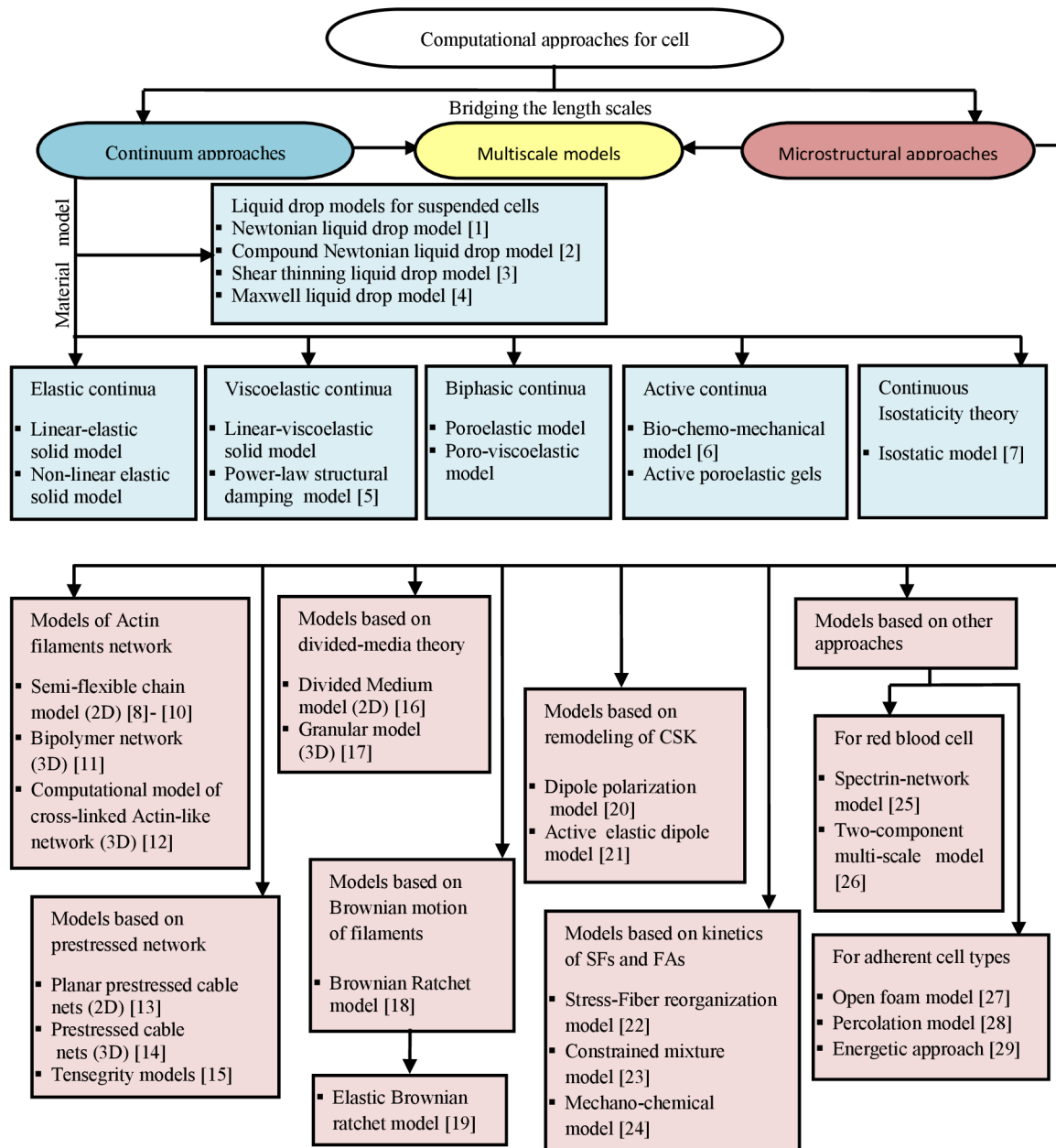


Fig 1: The schematic representation of computational approaches (continuum and microstructural) for cell mechanics (modified from [30]).

The compound Newtonian liquid drop model, which is a refinement of the earlier model, views cell as a heterogeneous structure composed of three layers as illustrated in Fig 2 (b) [2]. The outer layer describing the plasma membrane is modeled as a thin cortical shell with constant isotropic surface tension. The middle thick layer representing the cytoplasm is modeled as the Newtonian fluid with relatively small viscosity. The inner layer characterizing the segmented nucleus surrounded by CSK is also modeled as Newtonian liquid, but with relatively large viscosity [35]. This layer is under constant cortical tension due to nuclear envelope [40].

This model predicts a smaller viscosity in larger pipet for small deformation analysis [35]. Further, it can exhibit Newtonian behavior [34] by tuning the time scale ratios of the nucleus and the cytoplasm [41], [42]. This model can grasp the initial fast recoil phase of the recovery process, which indicates that it can describe the non-Newtonian behavior of the cells as well [41], [42]. It has been evident that the nucleus plays a vital role in defining the leukocyte rheological behavior, which depends on the ratio of the surface tension, the ratio of the viscosity between layers, and the extent of deformation of the nucleus [40], [41]. The set of mechanical parameters of this model cannot

be deduced by recovery experiment alone [31].

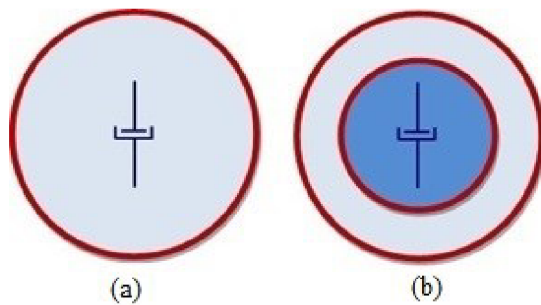


Fig 2: (a) The Newtonian liquid drop model: An intracellular region is modeled as Newtonian liquid (light blue) surrounded by cortex (red) modeled as fluid layer with constant tension. (b) The Compound Newtonian liquid drop model: An intracellular region is comprised of heterogeneous parts where the nucleus is modeled with more viscous Newtonian fluid (dark blue) than the circumscribing cytoplasm (light blue) and is enclosed by the nucleus cortex layer of static surface tension (red). The plasma membrane is modeled as prestressed cortical shell (red) (modified from [31])

### C. Shear Thinning Liquid Drop Model

The study of non-Newtonian behavior of the cell served as a motivation to develop the Shear thinning liquid drop model. As demonstrated in Fig 3 (a), the cytoplasm is modeled as a homogenous non-Newtonian fluid bounded by a layer with constant surface tension representing the cortex of the cell. It evaluates the changes in apparent cytoplasmic viscosity of the cell corresponding to an applied shear rate at a large deformation [3].

It has been observed in the experiments that increase in the mean shear rate causes decrease in the apparent cytoplasmic viscosity  $\eta$  conforming to power-law relationship as follows

$$\eta = \eta_c (\dot{\gamma}_m / \dot{\gamma}_c)^{-b} \quad (4)$$

here  $\eta_c$  is the characteristic viscosity at characteristic shear rate  $\dot{\gamma}_c$ ,  $b$  is the power, and  $\dot{\gamma}_m$  is the mean shear rate averaged over the whole process and domain [3], [31]. The constitutive relationship for the Newtonian liquid drop model at constant shear rate  $\dot{\gamma}$  gives

$$\tau = \eta_c (\dot{\gamma}_m)^{-b} \dot{\gamma} \quad (5)$$

The Shear thinning liquid drop model can explain well the non-linear deformation of the cell at its entrance into the micropipette compared to the Newtonian liquid drop model. The finite element analysis of the model not only elucidates the basic relationship between the aspiration rate and the micropipette diameter, [43] but also

demonstrates the ejection behavior of the cell [44]. Nonetheless, this model is not able to forecast the initial phase of rapid entry of the cell into the micropipette [3]. Also, a number of cell types did not reveal the shear-thinning behavior when subjected to small strain deformations [45].

### D. Maxwell Liquid Drop Model

The Maxwell's liquid drop model has been proposed to explicate the rapid initial entry of the cell into the micropipette at the beginning of the aspiration test. It premises the cell as pre-stressed static-tension cortical shell containing incompressible Maxwell viscoelastic fluid [4] as depicted in Fig 3 (b). This model encompasses an elastic element, which makes it different from the Newtonian liquid drop model [1]. The constitutive relationship is given by

$$\tau + \frac{\mu}{k} \dot{\tau} = \mu \dot{\gamma} \quad (6)$$

where  $\tau$  is the shear stress,  $\mu$  is a viscous constant of a dashpot arranged in series,  $k$  is an elastic constant of a spring,  $\dot{\tau}$  is the shear stress rate, and  $\dot{\gamma}$  is the shear strain rate[4], [31].

For a small strain aspiration test, results obtained using series solutions and the finite element method demonstrated that; this model can interpret the initial rapid entry and the recovery behavior of the cell [4]. It has been observed, that in the initial phase of the micropipette aspiration test when the deformation is rapid but small, the cytoplasm behaves like the Maxwell fluid for a very short duration, whereas in later phase when the deformation is large but slow, it behaves more like the Newtonian fluid of high viscosity [46]. In the large deformation finite element simulations of aspiration test, the model was not able to produce valid results unless both the viscous and elastic coefficients of the Maxwell fluid were increased steadily as the cell was sucked into the micropipette. This infers that the Maxwell liquid drop model is not able to explain the rheological properties of the cell [2], [46], [47].

All liquid drop models analyzed under similar boundary conditions may exhibit a linear dependence of stiffness on prestress [48]. Even though the results provided by liquid drop models are in accordance with the experimental findings under specific experimental conditions, in general they are not able to predict (from the mechanistic principles) how these properties can influence the cell functions. In addition, they are also not able to predict the resistance of living cells to mechanical

stress [30].

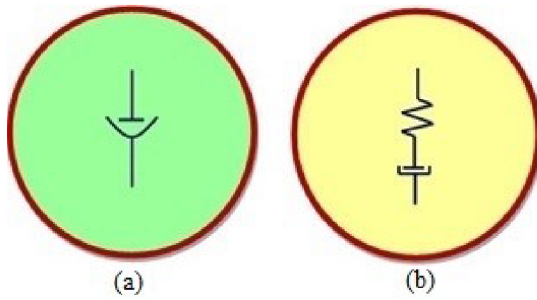


Fig 3: (a) The shear thinning liquid drop model: An intracellular region is modeled as a homogenous non-Newtonian fluid (green). (b) The Maxwell liquid drop model: An intracellular region is modeled as a homogenous Maxwell fluid (yellow). In both models, an intracellular region is surrounded by prestressed cortical shell (red) (modified from [31])

### III. ELASTIC CONTINUA

The elastic or viscoelastic solid models were invented to capture the solid-like behavior of the cell into micropipette aspiration. They consider the cell as an elastic or viscoelastic incompressible and homogenous half-space [49], [50], [51]. This class of models are different from the preceding ones in the sense that the cell is considered either as homogenous or heterogeneous solid (nucleus is defined discretely embedded in the cytoplasm) without accommodating the distinct cortical layer [31]. The material models belonging to this class are the linear elastic models, non-linear elastic models (hyperelastic), and linear-viscoelastic models.

#### A. Linear and Non-linear Elastic Solid Models

In both linear and non-linear elastic (hyperelastic) solid models, the cell is represented as homogenous solid and the time factor is disregarded [31]. The elastic behavior of the linear model follows the Hooke's law, whereas the non-linear model does not [44], [52]. Both, the linear and non-linear elastic model could be useful for finding the material properties of the cell subjected to small and large deformations, respectively. The linear elastic solid model coupled with the tensegrity model is simulated to determine the mechanical behavior of the smooth muscle cell subjected to compression and indentation test [53]. As these models are highly oversimplified compared to the intricate living cells they are not able to explain some of the natural cellular characteristics such as motility [54].

## IV. VISCOELASTIC CONTINUA

### A. Linear Viscoelastic Solid Models

The linear viscoelastic solid models have been proposed to study both solid and fluid like material properties of the cell.

In this approach, the cell is illustrated as either homogenous or heterogeneous solid where the stress is linearly dependent on strains and their time derivatives [44], [55]. These models are deduced to unravel the obscure behavior of cell under transient loading conditions, that is creep or stress relaxation. They are able to characterize the nucleus and the cytoplasm separately [56], [57]. In conjunction with other models, these models are employed to investigate the changes in cell mechanics during cell migration [58] and deformation [51]. Recently, a finite element viscoelastic model has been developed to forecast the osteoblast behavior subjected to cyclic isotropic radial strain [59].

In the computational simulation of single cell experiments to evaluate the cell deformation the neo-Hookean hyperelastic [56], [57] and the standard linear solid (Klevin) models are the widely used non-linear elastic and linear viscoelastic type of solid models, respectively [31], [60].

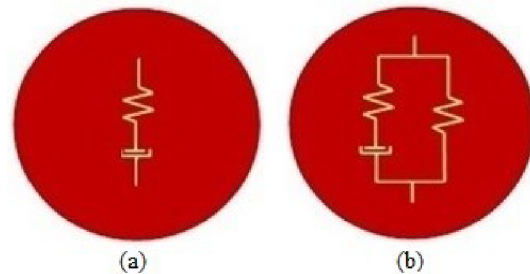


Fig 4: The whole cell is modeled as (a) linear elastic solid and (b) linear viscoelastic solid (modified from [31])

Both the linear elastic solid model depicted in Fig 4 (a) and the linear viscoelastic solid model depicted in Fig 4(b), were developed to mimic different observations of the single cell experiments. They have been enormously used in computational simulations of distinct cell types undergoing different mechanical tests and are summarized in TABLE. 1. The major drawback of both solid models is that a unique set of material properties cannot be employed to simulate the mechanical behavior of both the suspended and adherent cell types [44].

### B. The Power-law Structural Damping Model

In the last decade, the power-law structural damping model also known as Soft Glassy Rheological (SGR) model has gained great acclaim in the field of cell biology due to its unique ability to predict the power-law as well as other time-dependent types of behavior observed in living cells. A phenomenological model based on SGR theory has been proposed to evaluate the dynamic behaviors of cells subjected to the time-varying forces. This model describes the cell as soft glassy material existing close to the glass transition, and suggests that the CSK proteins may govern the mechanical properties of cells mainly by modulating the effective noise temperature of the matrix [5].

The class of soft glassy materials comprises of a diverse group of substances that include foams, pastes, colloids, emulsions, and slurries etc. The materials under this paradigm are composed of elements that are discrete, numerous, and aggregated with one another via weak interactions. In addition, they are not in thermodynamic equilibrium below glass transition (similar to glass thus, sometimes called as soft-glassy materials) and their geometrical arrangement is structurally disordered and metastable [75].

TABLE 1: THE SOLID MODELS WERE DEVELOPED ON THE BASIS OF OBSERVATIONS OF THE CORRESPONDING EXPERIMENTAL METHODS AND THEIR IMPLEMENTATION IN THE COMPUTATIONAL SIMULATION TO EVALUATE THE DEFORMATION OF VARIOUS CELL TYPES

Material model	Experimental method	Cell types
Linear and non-linear elastic	Micropipette aspiration [49]	Stem cells [65], [66], Osteosarcoma cells [67],
	Atomic force microscopy [61]	Vascular endothelial cells [68],
	Cytointender [62]	Bovine endothelial cells [69], [70],
	Magnetic twisting cytometry [63]	Endothelial cells and their nuclei [38], [49].
Linear viscoelastic		Myoblasts [57],
	Micropipette aspiration [50]	Chondrocytes and their nuclei [37], [71] Endothelial cells [72],
	Flat punch indentation [64]	Leukocytes [73], Osteocytes [74].

The SGR theory considers that each individual element of the cytoskeletal matrix exists within an energy landscape containing many wells of varying depths as depicted in Fig 5.

In case of living cells, these wells are thought to be formed due to the binding energies between the neighboring cytoskeletal elements. Due to lack of thermal energy in the system, it is not able to undergo structural rearrangement, and as a consequence of this, the elements are unlikely to escape from the energy wells [76]. Over the time, the element escapes from the energy barriers of neighboring elements and hops out of that well to fall into another, reaching a more stable state with very slow relaxation rates [77].

In such systems, the non-thermal energy source provides agitation (represented by an effective temperatures, or noise level,  $x$ ) to the elements so that they can hop out from the energy well in which they are trapped. As a result of this, the system undergoes structural rearrangement causing the material to flow [76].

The structural damping model that follows the power-law trend has been proposed in [5] to describe the frequency-dependent rheological behavior of adherent cell types. The complex modulus  $G^*(\omega)$  of this model is expressed as

$$G^*(\omega) = G'(\omega) + iG''(\omega) \\ = G_0 \left(\frac{\omega}{\Phi_0}\right)^{x-1} (1 + i\bar{\eta}) \Gamma(2-x) \cos\frac{\pi}{2}(x-1) + i\omega\mu \quad (7)$$

where  $x-1$  is the power-law exponent,  $\bar{\eta}$  is the structural damping coefficient given by  $\bar{\eta} = G''(\omega)/G'(\omega) = \tan((x-1)\pi/2)$ ,  $\omega$  is the radian frequency  $2\pi f$ ,  $G_0$  and  $\Phi_0$  are scaling factors for the stiffness and frequency, respectively,  $\Gamma$  denotes the Gamma function,  $i^2 = -1$ , and both  $G_0$  and  $\mu$  (viscosity material parameter [Pa.s]) depend on bead-cell geometry [55]. T

he elastic modulus also known as storage modulus  $G'(\omega)$  corresponds to the real part of (7), which increases for all values of  $\omega$  according to the power-law exponent, whereas the loss modulus  $G''(\omega)$  corresponds to an imaginary part of (7), and includes a component that also increases as a power-law with same exponent.

The loss modulus is a frequency-independent fraction  $\bar{\eta}$  of the elastic modulus; such direct coupling of the loss modulus to the elastic modulus is a characteristic feature of structural damping behavior. The loss modulus also includes a Newtonian viscous term  $i\omega\mu$ , which comes into play only at higher frequencies. The changes in exponent of the power-law (7) describes the transition from solid state ( $x=1$ ) to liquid state ( $x=2$ ) [5].

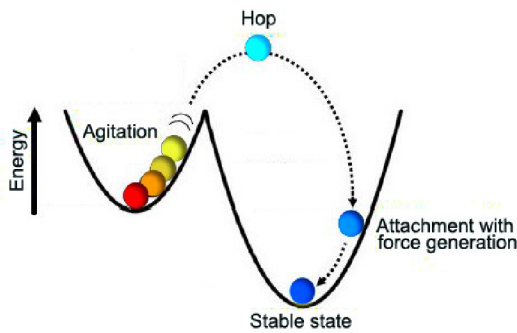


Fig 5: The schematic illustration of trap dynamics in SGR model of CSK, the natural reorganization and dynamics of intracellular biopolymers can be modeled as an array of transitions between a fluid and solid state. This is illustrated by hopping of elements between the energy wells of varying depths, reaching a more stable state [78]

It has been experimentally observed that under controlled conditions the dynamic moduli increases with increasing frequency following the weak power-law [45]. The frequency-dependent response of a single cell can be given by two regions of diverse rheology; at actin cortex the power-law is lower and the region is more elastic, on the contrary an intracellular region has a higher power and is more liquid-like [79]. The prestress that regulates the transition between the solid-like and fluid-like behavior in cells has a unique inverse relationship with the power-law exponent. The dynamic moduli ( $G'$  and  $G''$ ) increase linearly with increase in the cytoskeletal prestress [59].

It has been evident in various experiments, that the cells can demonstrate some of the key characteristics of soft glassy materials like dynamical heterogeneity, physical aging, and shear-induced rejuvenation, which are in favor with SGR model [45],[52],[79]. A material law related to Power-Law Rheology (PLR) model has been developed and incorporated in the biomechanical model of the cell in microbead twisting experiments, which deduces the material constants related to PLR using the finite element method [80], [81].

Recently, a similar model has been developed and implemented in computational simulation of cell in micropipette aspiration [82]. This model has an advantage over the solid viscoelastic models due to its ability to manifest dynamic behavior of the cells following power-law trend [31]. It has been employed to simulate the dynamic response of a cell in various experimental techniques for instance magnetic twisting cytometry [45], [80], [81],

atomic force microscopy [83], and micropipette aspiration [82].

Nevertheless, an unidentified non-thermal origin of the effective temperature has been used in this model and there are difficulties in interpreting the depth of the energy wells [84]. As assumed by this model the biological responses of the living cells are not timescale-invariant under relevant biological conditions [85]. There is a discrepancy between the loss behavior measured for CSK experimentally and the one predicted by SGR model. In addition, this model was not able to differentiate between the above and below glass transition states [86]. It neither takes into account the molecular details nor does it consider the active contraction of the cells [87]. It also fails to explain the strain stiffening or the cell rheological behavior at high frequencies [88], [89], [90].

## V. BIPHASIC CONTINUA

All the continuum models discussed earlier considered the cytoplasm as a single phase material, either solid or liquid, whereas the biphasic model views it as a two-phase material, a combination of both solid and liquid phase [91] as depicted in Fig 6.

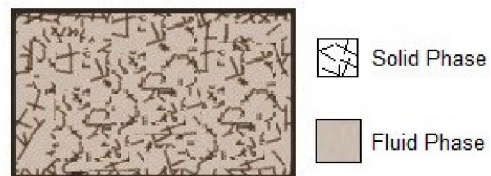


Fig 6: The schematic representation of the bi-phasic model of the cytoplasm illustrating the solid phase (consisting of CSK, organelles, and macromolecules) and the fluid phase (consisting of cytosol)

### A. Biphasic Poroelastic Models

In this continuum mixture theory approach, the solid phase of the cytoplasm is treated as linear elastic solid and the fluid phase is treated as a non-viscous fluid [92] and described as

$$\begin{aligned}\sigma^s &= -\phi^s p I + \lambda_s \text{tr}(\varepsilon) I + 2\mu_s \varepsilon \\ \sigma^f &= -\phi^f p I\end{aligned}\quad (8)$$

where the superscripts  $s$  and  $f$  denote the solid and fluid phases, respectively,  $\sigma$  is the Cauchy stress tensor,  $\varepsilon$  is the Cauchy's infinitesimal strain tensor,  $I$  is the identity tensor,  $p$  is the fluid pressure,  $\phi^s$  and  $\phi^f$  denote the solid and fluid volumetric fractions, respectively (where  $\phi^s + \phi^f = 1$ ), and  $\lambda_s$  and  $\mu_s$  are the Lamé constants for the solid phase [91]. For this model, the liquid phase can emanate through the solid phase and the momentum

exchange between these two phases is in the form of friction, which could be the reason for the viscoelastic behavior of cells and tissues [31].

The chondrocytes are usually modeled as biphasic when their response to the deformation (mechanical loading) is simulated using the multiscale modeling approach [93], [94], [95], [96], [97], [98], [99]. The pressure that actuates the blebbing process is not equally distributed across the cell, but generated and used locally. This is in accordance with the hypothesis of a poroelastic cytoplasm [100]. It has been demonstrated that the passive aspiration of the neutrophil inside a micropipette can be described by the biphasic poroelastic model [101]. Recently, it has been experimentally evident that this model can define the cell rheological properties at short time scales [102]. This model has also been implemented in 3-D computational simulation of pericellular matrix [103], [104]. In conjunction with other standard models it can define the biphasic responses of cartilage [105].

In addition to the complexity of the governing equations of continuum mixture theory, the irregularity of the cell shapes make the analytical solution along with the computational modeling of this model very complicated [54]. It neither predicts the complete creep response of the chondrocytes to a step aspiration [106] nor their initial deformation behavior under compression [107]. Also, it disregards the plasma membrane [92].

### B. Biphasic Poro-viscoelastic Models

The biphasic poro-viscoelastic model was introduced to capture the time-dependent responses of the chondrocytes both in full and partial micropipette aspiration experiments [106], [108]. This model can be further extended to triphasic model by entailing the ionic phase. This can be achieved by precise coupling of mechanical, chemical, and electrical events [91].

## VI. ACTIVE CONTINUA

This class of models has an ability to incorporate the inherent active nature of the living cells and measure their material characteristics.

### A. Bio-chemo-mechanical Model

This biochemical and mechanical model has been proposed to simulate the force dependent assembly and disassembly of Stress Fibers (SFs) and Focal Adhesions (FAs) by incorporating the dynamic reorganization of the CSK [6]. This model elucidates the biochemistry of SF remodeling along with a biomechanical description of SF

contractility. The biochemistry of SF formation is based on two key experimental observations; SFs assemble due to activation of signaling molecules and they dissociate on reduction in tension in CSK [109]. The mechanical response of the single SF remodeling consists of three coupled phenomena and these are employed in this model using simple phenomenological relations as follows

(a) An activation signal that triggers the formation of SFs

For this model, generally an exponentially decaying signal is presumed on the basis of experimental observation. The activation signal can be expressed by dimensionless signal intensity  $C$

$$C = \exp(-t_i/\theta) \quad (9)$$

here  $t_i$  is the time measured from the onset of the  $i^{\text{th}}$  activation signal and  $\theta$  is the decay constant of the signal [6].

(b) The SF formation rate dependent on the activation signal, coupled with their dissociation rate affected by the tension in the CSK

The first-order kinetic equation describing the rate of SF assembly and disassembly is given by

$$\frac{dn}{dt} = \left[ (1 - \eta) \frac{c\bar{k}_f}{\theta} \right] - \left[ \left( 1 - \frac{T}{T_0} \right) \eta \bar{k}_b \right] \quad (10)$$

where  $\eta$  is a non-dimensional activation level that measures the extent to which the actin and myosin are incorporated into SF and  $\left(\frac{dn}{dt}\right)$  denotes differentiation with respect to time  $t$  measured from the instant of application of the first signal. The term  $T$  is the tension in SF and  $T_0$  is the isometric tension considered to be directly proportional to the activation level  $\eta$  and expressed as  $T_0 = \eta T_{max}$ , where  $T_{max}$  is the isometric tension in SF at maximum activation level ( $\eta = 1$ ). The non-dimensional constants  $\bar{k}_f$  and  $\bar{k}_b$  govern the rate of formation and dissociation of the SF, respectively [110].

The first term on the right hand side in (10) delineates the rate of the SF formation; it decreases with increase in activation level  $\eta$  and increases with the activation signal  $C$ . The second term on the same side defines the rate of the SF dissociation; it decreases with increase in tension  $T$  in the SF and increases with the activation level  $\eta$  [110]. The SFs are stable at the isometric stress level, but as the stress falls below this level they disassemble [111]. The SF assembly rate is indirectly and disassembly rate is directly dependent on stress [112].

(c) The cross-bridge mechanics between the actin and the myosin filaments generates the tension in the SFs.

Considering the analogy of the force generation mechanism between the SFs and muscle cells, the influence of this generated tension on the SF contraction/extension rate is embedded in a version of Hill's equation as follows:

$$\frac{T}{T_0} = 1 + \frac{\bar{k}_v}{\eta} \left( \frac{\dot{\epsilon}}{\dot{\epsilon}_0} \right) \quad (11)$$

where  $\dot{\epsilon}$  is the strain rate,  $\dot{\epsilon}_0$  is the maximum strain rate, and the dimensionless Hill type constant  $\bar{k}_v$  describes the reduction in tension due to the strain rate [110]. The fast shortening rate provides the maximum rate of SF disassembly resulting in the reduction in tension and finally, the cell reaches a steady-state level of contraction [44]. This constitutive description of the cell includes both the active contribution from the actin SFs and the passive elastic contribution from the intermediate filaments (IFs) and the microtubules (MTs) [6]. The results of parallel-microplates technique for myoblast subjected to compression were found to be in good accordance with this stress-strain relationship [116].

The rigidity of the sites where the cell is attached to the substrate governs the concentration of SFs through orientation distribution of isometric stress. This model predicts that for stiffer attachments to the substrate the orientation of isometric stress is more anisotropic and subsequently, the concentration of SFs is higher [6] as illustrated in Fig 7 (a) and (b).

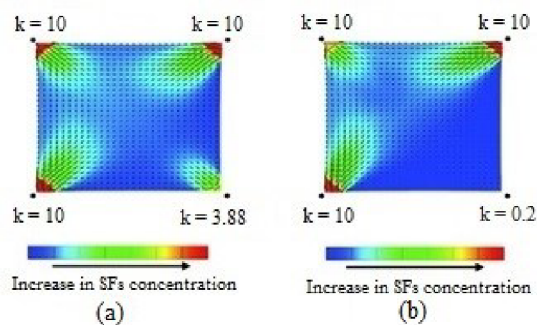


Fig 7: Results of computational simulations predicting the effect of reduction in the stiffness of support. Here, all the supports have equal stiffness  $k = 10$ , except the bottom right support in (a)  $k = 3.88$  and (b)  $k = 0.2$ . The contours of SFs concentration have been plotted along with the line segments representing the direction of maximum principal stress (modified from [6])

This model is able to capture the coupling mechanism arising from cell-substrate interaction and intracellular machinery. It predicts the influence of substrate compliance on the cellular

traction forces in 2-D simulation of cell on micro-needles [114]. In addition, this model is able to describe the influence of variegated stiffness and architecture of the substrates on the cell behavior. It has been demonstrated that cells adherent to stiffer substrates exert higher traction forces and simultaneously form more prominent FAs and SFs [130].

In conjunction with mixed-mode implementation of the FA assembly model, this model predicts the cell response to the substrate stiffness in 3-D application and the results obtained are in line with the experimental observations [116]. This model is not only able to predict the spatial distribution of traction forces but also the decrease in the force generated by the cell with increasing substrate compliance; this is in accordance with the experimental observations [110].

The kinetic model of the SF formation and disassociation (10) has been incorporated with force-dependent model for the assembly of FA. The new coupled model has been employed to elucidate the experimental observations of dispositions of SFs and FAs at the periphery of convex ligand patterns. It also predicts the high concentration of FAs along the edges of cells on the V-shaped ligand pattern as depicted in Fig 8 (a) and the enhanced formation of highly aligned SFs along the non-adherent edges as illustrated in Fig 8(b) [117]. The same model has been implemented to investigate the relationship between the cytoskeletal contractile forces and FA dynamics [111].

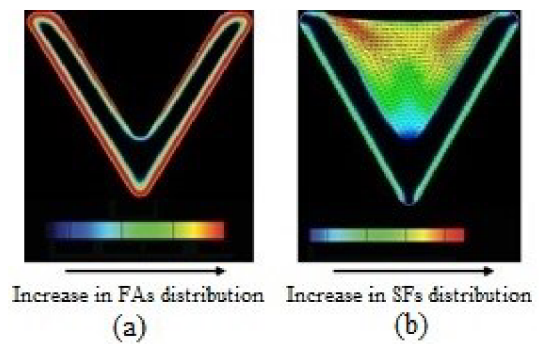


Fig 8: The predictions of (a) FAs concentration and (b) SFs distribution in computational simulation for a cell on the V-shaped ligand pattern (modified from [117])

This model is able to predict the changes in SF orientation and assembly for the 2-D cells subjected to the cyclic uniaxial stretch. It has been demonstrated in the simulation that the stress generated perpendicular to the direction of stretch is greater than the stress generated in parallel and is consistent with the higher actin polymerization levels in the same direction [118]. This model has

also been employed in simulations of 1-D and 2-D cell migration to evaluate the spatial distribution of traction forces [119].

The bio-chemo-mechanical model has been refined to include a signaling model based on the messenger molecules used in signal transduction [120]. The implementation of active formulation in 3-D simulations has demonstrated remarkable difference in the stress distribution in cytoplasm and nucleus compared to the simulation with the conventional passive material models [116], [121].

Overall, this model is able to simulate the responses of cells to a wide range of loading scenarios. On the other hand, this model neither includes the FAs explicitly nor the biomechanical behavior of MTs and IFs. This model has assumed space independent activation of the signal for 2-D and 3-D applications [52].

## VII. ISOSTATIC MODEL

An isostatic model has been proposed because the classical theory of elasticity was not able to explain the channeled long-distance force propagation phenomenon [7]. This model has proposed a framework for the CSK network based on the continuous isostaticity theory that has been developed in [122], [123], [124]. This model is based on the concept that the focused propagation of force stimuli in the framework over large-distances and the “action at a distance” effect is feasible only when the considerable parts of the CSK network are isostatic [7].

Isostatic structures belong to the class of statistically determinate systems (for a given external loading and boundary conditions) [125]. Due to the peculiar structure of an isostatic network, the force in an individual structural member of the network can be deduced from equations of equilibrium and geometrical properties of the network without considering the constitutive equations of structural members [123]. It is noteworthy, that such partial differential equation of stress field is hyperbolic in nature and can predict the long-distance stress propagation over specified directions [7], [125].

Several conditions are described for the isostaticity of CSK network. In scenario A, all nodes of the CSK network can support torques, which is in accordance with the assumption of open-foam cell model that has been proposed in [27], [126]. This situation may occur when the forces applied to the cell are not sufficient to buckle the filaments. In scenario B, only some of the nodes of the CSK network can support torques. This situation appears when all filaments that are converging at a node carry tensile forces

(representing microfilaments (MFs) and IFs) except a single filament, that may carry compressive forces (representing MT). Lastly, in scenario C, in the limit where none of the nodes of the CSK network support torques the structure behaves like tensegrity [15], [127]. Through the cytoskeletal remodeling process the cell can propagate the mechanical signals to some regions of the cytoplasm, while blocking them in other regions. Thus the CSK network could be viewed as partially isostatic [7], [125].

This model is able to predict the relationship between the long-distance force transfer and the cytoskeletal prestress. The prestress in the network can be regulated via tightening or loosening of filaments that causes three effects on the isostatic CSK network as explained in the following cases. In the first case, no filament is tightened or slackened and as a result of this, the CSK network will remain isostatic and there will be either negligible or no effect on the force transmission. In the second case, loose filaments are tightened. This adds a number of force-bearing elements in the CSK network thus making the CSK to lose its isostaticity by becoming statically undetermined. As a consequence of this force transmission within the network will get scattered and weakened over short distances. In the third case, tight filaments are slackened this reduces the number of force-bearing elements in the CSK network making the system unstable and lose its isostatic properties. As a repercussion, force-transmission via these loose filaments will not be possible and they will disperse [7]. This observation is in line with the experimental findings of disrupted long-distance force transmission in airway smooth muscle cells [128].

The novel framework proposed by this model is independent of the structurally defined pathways (like SFs) to describe the force transmission in cells, thus they can describe how cells transmit forces in 3-D extracellular matrix (ECM) and in cells adhering to 2-D soft substrates. On the contrary, the concept of isostaticity is strongly dependent on the distribution of the tensed filaments (representing MFs and IFs) and compressive filaments (representing MTs) in the CSK network, but so far, there is no experimental evidence for such force distribution in living cells. The hyperbolic field equation proposed by this model is true only when the network achieves its marginal stability, this may not be the case for the CSK network in living cells, which constantly changes and reorganizes its structure [7].

## VIII. LIMITATIONS AND FUTURE SCOPE

The continuum approach ignores the



contribution of molecular structures that form CSK by considering them too small compared to the size of cell. Thus, this approach does not provide an explanation for how to modulate the cell functions via mechanical forces [54]. The multiscale model, [129] which would bridge the gap between the continuum approaches and the microstructural approaches could be one of the solutions to overcome this limitation. These models could be devised by precise coupling of simulation results from individual length scales [30], [31].

The structural model of single cell mechanics should be universal, such that it accurately predicts the responses of all cell types for all loading scenarios. The model should entail not only the physical structure and organization of distinct cell types, but also the changes in them during any cell cycle. In addition, it should also account for all cellular processes and timescales [130]. For computational simulations of a wide variety of single cell experiments, the constitutive formulation involving molecular processes should be implemented [52].

#### ACKNOWLEDGMENT

This work was supported by Czech Science Foundation project No. 13-16304S.

#### REFERENCES

- [1] Yeung, E. Evans, "Cortical shell-liquid core model for passive flow of liquid-like spherical cells into micropipets," *Biophys J.*, vol. 56, no. 1, pp. 139–149, 1989.
- [2] C. Dong, R. Skalak, and K. L. Sung, "Cytoplasmic rheology of passive neutrophils," *Biorheology*, vol. 28, no. 6, pp. 557–567, 1991.
- [3] M. A. Tsai, R. S. Frank, and R. E. Waugh, "Passive mechanical behaviour of human neutrophils: power-law fluid," *Biophysical Journal*, vol. 65, no. 5, pp. 2078–2088, 1993.
- [4] C. Dong, R. Skalak, K. L. Sung, G. W. Schmid-Schonbein, and S. Chien, "Passive deformation analysis of human leukocytes," *Journal of Biomechanical Engineering*, vol. 110, no. 1, pp. 27–36, 1988.
- [5] B. Fabry, G. Maksym, J. Butler, M. Glogauer, D. Navajas, and J. Fredberg, "Scaling the microrheology of living cells," *The American Physical Society*, vol. 87, no. 14, pp. 148102, 2001.
- [6] V. S. Deshpande, R. M. McMeeking, and A. G. Evans, "A bio-chemo-mechanical model for cell contractility," *Proc. Natl. Acad. Sci. U.S.A.*, vol. 103, no. 38, pp. 14015–14020, 2006.
- [7] R. Blumenfeld, "Isostaticity and controlled force transmission in the cytoskeleton: A model awaiting experimental evidence," *Biophys Journal*, vol. 91, pp. 1970–1983, 2006.
- [8] F. C. MacKintosh, J. Kas, and P. A. Janmey, "Elasticity of semiflexible Biopolymer Networks," *Phys. Rev. Lett.*, vol. 75, no. 24, pp. 4425–4428, 1995.
- [9] P. Onck, T. Koeman, T. van Dillen, and E. van der Giessen, "Alternative explanation of stiffening in cross-linked semiflexible networks," *Phys. Rev. Lett.*, vol. 95, pp. 178102, 2005.
- [10] D. Head, A. Levine, and F. MacKintosh, "Distinct regimes of elastic response and deformation modes of cross-linked cytoskeletal and semiflexible polymer networks," *Phys. Rev. E*, vol. 68, pp. 061907, 2003.
- [11] H. Isambert, A. Maggs, "Dynamics and rheology of actin solutions," *Macromolecules*, vol. 29, no. 3, pp. 1036–1040, 1996.
- [12] T. Kim, W. Hwang, and R. Kamm, "Computational analysis of a cross-linked actin-like network," *Experimental Mechanics*, vol. 49, no. 1, pp. 91–104, 2009.
- [13] M. Coughlin, D. Stamenovic, "A prestressed cable network model of the adherent cell cytoskeleton," *Biophysical Journal*, vol. 84, no. (2 Pt 1), pp. 1328–1336, 2003.
- [14] D. Stamenovic, M. Coughlin, "The role of prestress and architecture of the cytoskeleton and deformability of cytoskeletal filaments in mechanics of adherent cells: a quantitative analysis," *Journal of Theoretical Biology*, vol. 201, no. 1, pp. 63–74, 1999.
- [15] D. E. Ingber, "Cellular tensegrity—defining new rules of biological design that govern the cytoskeleton," *J. Cell Sci.*, vol. 104, pp. 613–627, 1993.
- [16] J. Milan, S. Wendling-Mansuy, M. Jean, and P. Chabrand, "Divided medium-based model for analyzing the dynamic reorganization of the cytoskeleton during cell deformation," *Biomech Model Mechanobiol*, vol. 6, no. 6, pp. 373–390, 2007.
- [17] B. Maurin, P. Canadas, H. Baudriller, P. Montcourrier, and N. Bettache, "Mechanical model of cytoskeleton structuration during cell adhesion and spreading," *Journal of Biomechanics*, vol. 41, no. 9, pp. 2036–2041, 2008.
- [18] C. S. Peskin, G. M. Odell, and G. F. Oster, "Cellular motions and thermal fluctuations: The Brownian ratchet," *Biophysical Journal*, vol. 65, pp. 316–324, 1993.
- [19] Mogilner, G. Oster, "Cell motility driven by actin polymerization," *Biophysical Journal*, vol. 71 no. 6, pp. 3030–3045, 1996.
- [20] Zemel, I. Bischofs, and S. Safran, "Active elasticity of gels with contractile cells," *Physical Review Letters*, vol. 97, no. 12, pp. 128103, 2006.
- [21] R. De, A. Zemel, and S. A. Safran, "Dynamics of cell orientation," *Nature Physics*, vol. 3, pp. 655, 2007.
- [22] R. Kaunas, H. J. Hsu, "A kinematic model of stretch-induced stress fiber turnover and reorientation," *Journal of Theoretical Biology*, vol. 257, no. 2, pp. 320–330, 2009.
- [23] F. J. Vernerey, M. Farsad, "A constrained mixture approach to mechano-sensing and force Generation in contractile cells," *J. Mech. Behav. Biomed. Mater.*, vol. 4, no. 8, pp. 1683–1699, 2011.
- [24] M. Maraldi, K. Garikipati, "The mechanochemistry of cytoskeletal force generation," *Biomechanics and Modeling in Mechanobiology*, vol. 14, pp. 59–72, 2015.
- [25] J. Li, M. Dao, C. T. Lim, and S. Suresh, "Spectrin-level modeling of the cytoskeleton and optical tweezer stretching of the erythrocyte," *Biophysical Journal*, vol. 88, pp. 3707–3719, 2005.
- [26] X. Li, Z. Peng, H. Lei, M. Dao, and G. E. Karniadakis, "Probing red blood cell mechanics, rheology and dynamics with a two-component multi-scale model," *Phil. Trans. R. Soc. A*, vol. 372, pp. 20130389, 2014.
- [27] J. Satcher, C. Dewey, "Theoretical estimates of mechanical properties of the endothelial cell cytoskeleton," *Biophysical Journal*, vol. 71, no. 1, pp. 109–118, 1996.
- [28] G. Forgacs, "Commentary on the possible role of cytoskeletal filamentous network in intracellular signalling: an approach based on percolation," *Journal of Cell Science*, vol. 108, pp. 2131–2143, 1995.
- [29] D. Stamenovic, S. Mijailovich, I. Norrrellykke, J. Chen, and N. Wang, "Cell prestress. II. contribution of microtubules," *The American Physiological Society*, vol. 282, pp. C617–C624, 2002b.

- [30] Vaziri, A. Gopinath, "Cell and biomolecular mechanics in silico," *Nature Materials*, vol 7, pp. 15 – 23, 2008.
- [31] T. Lim, E. H. Zhou, and S. T. Quek, "Mechanical models for living cells - A review," *J. Biomech*, vol. 39, no. 2, pp. 195–216, 2006.
- [32] Needham, R. M. Hochmuth, "Rapid flow of passive neutrophils into a 4 microns pipet and measurement of cytoplasmic viscosity," *ASME J. Biomech. Eng.*, vol. 112, no. 3, pp. 269–276, 1990.
- [33] Evans, A. Yeung, "Apparent viscosity and cortical tension of blood granulocytes determined by micropipet aspiration," *Biophys J.*, vol. 56, no. 1, pp. 151–160, 1989.
- [34] R. Tran-Son-Tay, D. Needham, A. Yeung, and R. M. Hochmuth, "Time-dependent recovery of passive neutrophils after large deformation," *Biophys J.*, vol. 60, no. 4, pp. 856–866, 1991.
- [35] R. M. Hochmuth, H. P. Ting-Beall, B. B. Beaty, D. Needham, and R. Tran- Son-Tay. "Viscosity of passive human neutrophils undergoing small deformations," *Biophysical Journal*, vol. 64, no. 5, pp. 1596–1601, 1993b.
- [36] D. Needham, R. Hochmuth, "A sensitive measure of surface stress in the resting neutrophil," *Biophys J.*, vol. 61, no. 6, pp. 1664–1670, 1992.
- [37] Guilak, J. R. Tedrow, and R. Burgkart, "Viscoelastic properties of the cell nucleus," *Biochemical and Biophysical Research Communications*, vol. 269, no. 3, pp. 781–786, 2000.
- [38] N.Caille, O. Thoumine, Y. Tardy, and J. J. Meister, "Contribution of the nucleus to the mechanical properties of endothelial cells," *Journal of Biomechanics*, vol. 35, no. 2, pp. 177–187, 2002.
- [39] J. Maniotis, C. S. Chen, and D. E. Ingber, "Demonstration of mechanical connections between integrins, cytoskeletal filaments, and nucleoplasm that stabilize nuclear structure," *Proceeding of the national academy of sciences of the United States of America*, vol. 94, pp. 849–854, 1997a.
- [40] H. C. Kan, H. S. Udaykumar, W. Shyy, and R. Tran-Son-Tay, "Hydrodynamics of a compound drop with application to leukocyte modelling," *Physics of Fluids*, vol. 10, no. 4, pp. 760–774, 1998.
- [41] R. Tran-Son-Tay, H. C. Kan, H. S. Udaykumar, E. Damay, and W. Shyy, "Rheological modelling of leukocytes," *Medical & Biological Engineering & Computing*, vol. 36, no. 2, pp. 246–250, 1998.
- [42] H. C. Kan, W. Shyy, H. S. Udaykumar, P. Vigneron, and R. Tran-Son-Tay, "Effects of nucleus on leukocyte recovery," *Annals of Biomedical Engineering*, vol. 27, no. 5, pp. 648–655, 1999.
- [43] J. L. Drury, M. Dembo, "Aspiration of human neutrophils: effects of shear thinning and cortical dissipation," *Biophysical Journal*, vol. 81, no. 6, pp. 3166–3177, 2001.
- [44] M. Rodriguez, N. J. Sniadecki, *In computational modelling of biomechanics in the musculoskeletal system: tissues, replacements and regeneration*. 1st ed. Woodhead Publishing; 2014.
- [45] Fabry, G. N. Maksym, J. P. Butler, M. Glogauer, Navajas D, N. A. Taback, E. J. Millet, J. J. Fredberg, "Time scale and other invariants of integrative mechanical behaviour in living cells," *Physical Review E*, vol. 68, no 4, pp. 041914, 2003.
- [46] Dong, R. Skalak, "Leukocyte deformability: finite element modeling of large viscoelastic deformation," *Journal of Theoretical Biology*, vol. 158, no. 2, pp. 173–193, 1992.
- [47] R. M. Hochmuth, "Measuring the mechanical properties of individual human blood cells," *ASME J. Biomech. Eng.*, vol. 115, no. 4B, pp. 515–519, 1993.
- [48] M. Mofrad, H. Karcher, and R. Kamm, "Continuum elastic or viscoelastic models of the cell," *In Cytoskeletal Mechanics models and measurements*, 1st edition, M. Mofrad, R. Kamm, Editors. USA: Cambridge University Press, 2006; pp. 71-83.
- [49] Theret, M. Levesque, M. Sato, R. Nerem, and L. Wheeler, "The application of a homogeneous half-space model in the analysis of endothelial-cell micropipette measurements," *ASME J Biomech Eng.* vol. 110, pp. 190–199, 1988.
- [50] M. Sato, D. P. Theret, L. T. Wheeler, N. Ohshima, and R. M. Nerem, "Application of the micropipette technique to the measurement of cultured porcine aortic endothelial cell viscoelastic properties," *Journal of Biomechanical Engineering*, vol. 112, no. 3, pp. 263–268, 1990.
- [51] M. A. Haider, F. Guilak, "An axisymmetric boundary integral model for incompressible linear viscoelasticity: application to the micropipette aspiration contact problem," *ASME J. Biomech. Eng.* vol. 122, no. 3, pp. 236–244, 2000.
- [52] M. Rodriguez, N. Sniadecki, "Review on cell mechanics: Experimental and modelling approaches," *Applied Mechanics Review*, vol. 65, pp. 060801, 2013.
- [53] J. Bursa, R. Lebis, and J. Holata, "Tensegrity finite element models of mechanical tests of individual cells," *Technology and Health Care*, vol. 20, no. 2, pp. 135-150, 2012.
- [54] M. M. Nava, M. T. Raimondi, R. Pietrabissa, "Bio-chemo-mechanical models for nuclear deformation in adherent eukaryotic cells," *Biomechanics and Modeling in Mechanobiology*, vol. 13, no. 5, pp. 929-943, 2014.
- [55] S. Moreno-Flores, R. Benitez, and J. L. Toca-Herrera, "Stress relaxation and creep on living cells with the atomic force microscope: a means to calculate elastic moduli and viscosities of cell components," *Nanotechnology*, vol. 21, pp. 445101, 2010.
- [56] J. McGarry, P. McHugh, "Modelling of in vitro chondrocyte detachment," *J. Mech Phys Solids*, vol. 56, no. 4, pp. 1554–1565, 2008.
- [57] J. McGarry, "Characterization of cell mechanical properties by computational modeling of parallel plate compression," *Ann Biomed Eng.* vol. 37, no. 11, pp. 2317–2325, 2009.
- [58] P. A. Dimilla, K. Barbee, and D. A. Lauffenburger, "Mathematical model for the effects of adhesion and mechanics on cell migration speed," *Biophys. J.* vol. 60, no. 1, pp. 15–37, 1991.
- [59] J. Milner, M. Grol, K. Beaucage, S. Dixon, and D. W. Holdsworth, "Finite- element modeling of viscoelastic cells during high- frequency cyclic strain," *Journal of Funct Biomater*, vol. 3, no. 1, pp. 209–224, 2012.
- [60] J. Chen, "Nanobiomechanics of living cells: a review," *Interface Focus*, vol. 4, no. 2, pp. 20130055, 2014.
- [61] G. Bilodeau, "Regular pyramid punch problem," *Journal of Applied Mechanics*, vol. 59, no. 3, pp. 519–523, 1992.
- [62] Shin, K. Athanasiou, "Cytoindentation for obtaining cell biomechanical properties," *Journal of Orthopaedic Research*, vol. 17, no. 6, pp. 880–890, 1999.
- [63] S. M. Mijailovich, M. Kojic, M. Zivkovic, B. Fabry, and J. J. Fredberg, "A finite element model of cell deformation during magnetic bead twisting," *Journal of Applied Physiology*, vol. 93, no. 4, pp. 1429–1436, 2002.
- [64] J. Koay, A. C. Shieh, and K. A. Athanasiou, "Creep indentation of single cells," *Journal of Biomechanical Engineering*, vol. 125, no. 3, pp. 334–341, 2003.
- [65] X. Zeng, S. Li, "Modelling and simulation of substrate elasticity sensing in stem cells," *Comput Methods Biomech Biomed Eng.* vol. 14, no. 5, pp. 447–458, 2011a.
- [66] X. Zeng, S. Li, "Multiscale modeling and simulation of soft adhesion and contact of stem cells," *J Mech Behav Biomed Mater*, vol. 4, no. 2, pp. 180–189, 2011b.
- [67] Y. Cao, R. Bly, W. Moore, Z. Gao, A. Cuitino, and W. Soboyejo, "On the measurement of human osteosarcoma cell elastic modulus using shear assay experiment," *J Mater Sci*, vol. 18, no. 1, pp. 103–109, 2007.
- [68] M. Ferko, A. Bhatnagar, M. Garcia, and P. Butler, "Finite-element stress analysis of a multicomponent model of sheared and focally-adhered endothelial cells," *Ann Biomed Eng.* vol. 35, no. 2, pp. 858–859, 2007.

- [69] Nelson, R. Jean, J. Tan, W. Liu, N. Sniadecki, A. Spector, and C. Chen, "Emergent patterns of growth controlled by multicellular form and mechanics," *Proc Natl Acad Sci USA*, vol. 102, no. 33, pp. 11594–11599, 2005.
- [70] T. Ohashi, Y. Ishii, Y. Ishikawa, T. Matsumoto, and M. Sato, "Experimental and numerical analyses of local mechanical properties measured by atomic force microscopy for sheared endothelial cells," *Biomed Mater Eng*, vol. 12, no. 3, pp. 319–327, 2002.
- [71] F. Guilak, G. Erickson, and H. Ting-Beall, "The effects of osmotic stress on the viscoelastic and physical properties of S. M. Mijailovich, M. Kojic, M. Zivkovic, B. Fabry, and J. J. Fredberg, "A finite element model of cell deformation during magnetic bead twisting," *Journal of Applied Physiology*, vol. 93, no. 4, pp. 1429–1436, 2002.
- [72] M. Sato, N. Ohshima, and R. M. Nerem, "Viscoelastic properties of cultured porcine aortic endothelial cells exposed to shear stress," *Journal of Biomechanics*, vol. 29, no. 4, pp. 461–467, 1996.
- [73] W. Schmid-Schonbein, K. L. Sung, H. Tozeren, R. Skalak, and S. Chien, "Passive mechanical properties of human leukocytes," *Biophysical Journal*, vol. 36, no. 1, pp. 243–256, 1981.
- [74] Qiu, A. Baik, X. Lu, E. Hillman, Z. Zhuang, C. Dong, and E. Guo, "A non-invasive approach to determine viscoelastic properties of an individual adherent cell under fluid flow," *Journal of Biomechanics*, vol. 47, no. 6, pp. 1537–1541, 2014.
- [75] P. Sollich, F. Lequeux, P. Hébraud, and M. Cates, "Rheology of soft glassy materials," *Physical Review Letters*, vol. 78, no. 10, pp. 2020–2023, 1997.
- [76] P. Sollich, "Rheological constitutive equation for a model of soft glassy materials," *Physical Review Letters*, vol. 8, pp. 738–759, 1998.
- [77] P. Bursac, G. Lenormand, B. Fabry, M. Oliver, D. A. Weitz, V. Viasnoff, J. P. Butler, and J. J. Fredberg, "Cytoskeletal remodelling and slow dynamics in the living cell," *Nat Mater*, vol. 4, no. 7, pp. 557–61, 2005.
- [78] P. Kollmannsberger, B. Fabry, "Active soft glassy rheology of adherent cells," *Soft Matter*, vol. 5, no. 9, pp. 1771–1774, 2009.
- [79] B. Hoffman, J. Crocker, "Cell mechanics: Dissecting the physical responses of cells to force," *Annual Review of Biomedical Engineering*, vol. 11, pp. 259–288, 2009.
- [80] Stamenovic, B. Suki, B. Fabry, N. Wang, and J. Fredberg, "Rheology of airway smooth muscle cells is associated with cytoskeletal contractile stress," *Journal of Appl. Physiol*, vol. 96, no. 5, pp. 1600–1605, 2004.
- [81] Vaziri, Z. Xue, R. D. Kamm, M. R. Mofrad, "A computational study on power-law rheology of soft glassy materials with application to cell mechanics," *Computer Methods in Applied Mechanics and Engineering*, vol. 196, no. 31–32, pp. 2965–2971, 2007.
- [82] H. Zhou, F. Xu, S. T. Quek, and C. T. Lim, "A power-law rheology-based finite element model for single cell deformation," *Biomech Model Mechanobiol*, vol. 11, no. 7, pp. 1075–84, 2012.
- [83] Alcaraz, L. Buscemi, M. Grabulosa, X. Trepast, B. Fabry, R. Farre, and D. Navajas, "Microrheology of human lung epithelial cells measured by atomic force microscopy," *Biophys. J*, vol. 84, no. 3, pp. 2071–2079, 2003.
- [84] M. R. Mofrad, "Rheology of the cytoskeleton," *Annu. Rev. Fluid Mech*, vol. 41, pp. 433–453, 2009.
- [85] D. Stamenovic, N. Rosenblatt, M. Montoya-Zavala, B. Matthews, S. Hu, B. Suki, N. Wang, and D. Ingber, "Rheological behaviour of living cells is timescale-dependent," *Biophysical Journal*, vol. 93, no. 8, pp. 39–41, 2007.
- [86] Mandadapu, S. Govindjee, and M. Mofrad, "On the cytoskeleton and soft glassy rheology," *Journal of Biomechanics*, vol. 41, no. 7, pp. 1467–1478, 2008.
- [87] P. Kollmannsberger, B. Fabry, "Linear and nonlinear rheology of Living Cells," *Annual Review of Materials Research*, vol. 41, pp. 75–97, 2011.
- [88] D. Wirtz, "Particle-tracking microrheology of living cells: principles and applications," *Annual Review of Biophysics*, vol. 38, pp. 301–326, 2009.
- [89] R. Pritchard, Y. Huang, and E. Terentjev, "Mechanics of biological networks: from the cell cytoskeleton to connective tissue," *Soft Matter*, vol. 10, pp. 1864–1884, 2014.
- [90] Moeendarbary, A. R. Harris, "Cell mechanics: principles, practices, and prospects," *WIREs Syst Biol Med*, vol. 6, pp. 371–388, 2014.
- [91] Guilak, M. Haider, L. Setton, T. Laursen, and F. Baaijens, "Multiphasic models of the cell mechanics," in *Cytoskeletal Mechanics models and measurements*, M. Mofrad, R. Kamm, editors. USA: Cambridge University Press. 2006, pp. 84–102.
- [92] Guilak, V. C. Mow, "The mechanical environment of the chondrocyte: a biphasic finite element model of cell–matrix interactions in articular cartilage," *Journal of Biomechanics*, vol. 33, no. 12, pp. 1663–1673, 2000.
- [93] G. Alexopoulos, G. M. Williams, M. L. Upton, L. A. Setton, and F. Guilak, "Osteoarthritic changes in the biphasic mechanical properties of the chondrocyte pericellular matrix in articular cartilage," *J. Biomech*, vol. 38, no. 3, pp. 509–517, 2005.
- [94] O. Chahine, C. T. Hung, and G. A. Ateshian, "In-situ measurements of chondrocyte deformation under transient loading," *Eur. Cell Mater*, vol. 13, pp. 100–111, 2007.
- [95] R. K. Korhonen, P. Julkunen, W. Wilson, and W. Herzog, "Importance of collagen orientation and depth-dependent fixed charge densities of cartilage on mechanical behavior of chondrocytes," *ASME Journal Biomech. Eng*, vol. 130, no. 2, pp. 021003, 2008.
- [96] E. Kim, F. Guilak, and M. A. Haider. "An axisymmetric boundary element model for determination of articular cartilage pericellular matrix properties in situ via inverse analysis of chondron deformation," *ASME J. Biomech. Eng*, vol. 132, no. 3, pp. 031011, 2010.
- [97] S. K. Han, S. Federico, and W. Herzog, "A depth-dependent model of the pericellular microenvironment of chondrocytes in articular cartilage," *Comput Methods Biomech Biomed Eng*, vol. 14, pp. 657–64, 2011.
- [98] E. Moo, W. Herzog, S. Han, N. Abu Osman, B. Pinguan-Murphy, and S. Federico, "Mechanical behaviour of in-situ chondrocytes subjected to different loading rates: a finite element study," *Biomech Model Mechanobiol*, vol. 11, pp. 983–93, 2012.
- [99] Guo, S. A. Maher, and P. A. Torzilli, "A biphasic multiscale study of the mechanical microenvironment of chondrocytes within articular cartilage under unconfined compression," *J Biomech*, vol. 47, no. 11, pp. 2721–2729, 2014.
- [100] T. Charras, J. C. Yarrow, M. A. Horton, L. Mahadevan, T. J. Mitchison, "Non-equilibration of hydrostatic pressure in blebbing cells," *Nature*, vol. 435, pp. 365–369, 2005.
- [101] Herant, W. A. Marganski, and M. Dembo, "The mechanics of neutrophils: Synthetic modeling of three experiments" *Biophys Journal*, .vol. 84, pp. 3389–3413, 2003.
- [102] E. Moeendarbary, L. Valon, M. Fritzsche, A. R. Harris, D. A. Moulding, A. J. Thrasher, E. Stride, L. Mahadevan, and G. T. Charras, "The cytoplasm of living cells behaves as a poroelastic material," *Nature Materials*, vol. 12, pp. 253–261, 2013.
- [103] L. Cao, F. Guilak, and L. A. Setton, "Pericellular matrix mechanics in the annulus fibrosus predicted by a three-dimensional finite element model and in situ morphology," *Cell. Mol. Bioeng*, .vol. 2, no. 3, .pp 306–319, 2009.
- [104] Julkunen, W. Wilson, J. S. Jurvelin, and R. K. Korhonen, "Composition of the pericellular matrix modulates the deformation behaviour of chondrocytes in articular cartilage under static loading," *Med. Biol. Eng. Comput*, vol. 47, no. 12, pp. 1281–1290, 2009.

- [105] Y. Huang, M. A. Soltz, M. Kopacz, V. C. Mow, and G. A. Ateshian, "Experimental verification of the roles of intrinsic matrix viscoelasticity and tension-compression nonlinearity in the biphasic response of cartilage," *ASME J. Biomech. Eng.*, vol. 125, no. 1, pp. 84–93, 2003.
- [106] F. P. Baaijens, W. R. Trickey, T. A. Laursen, and F. Guilak, "Large deformation finite element analysis of micropipette aspiration to determine the mechanical properties of the chondrocyte," *Ann Biomed Eng.*, vol. 33, pp. 494–501, 2005.
- [107] N. D. Leipzig, K. A. Athanasiou, "Unconfined creep compression of chondrocytes," *Journal of Biomechanics*, vol. 38, no. 1, pp. 77–85, 2005.
- [108] W. R. Trickey, F.P. Baaijens, T. A. Laursen, L. G. Alexopoulos, and F. Guilak, "Determination of the Poisson's ratio of the cell: recovery properties of chondrocytes after release from complete micropipette Aspiration," *Journal of Biomechanics*, vol. 39, no. 1, pp. 78–87, 2006.
- [109] N. Wang, J. D. Tytell, and D. E. Ingber, "Mechanotransduction at a distance: mechanically coupling the extracellular matrix with the nucleus," *Nature Reviews Molecular Cell Biology*, vol. 10, pp. 75–82, 2009.
- [110] V. S. Deshpande, R. M. McMeeking, A. G. Evans, "A model for the contractility of the cytoskeleton including the effects of stress-fibre formation and dissociation," *Proceedings of the Royal Society of London A: Mathematical, Physical and Engineering Sciences*, vol. 463, no. 2079, pp. 787–815, 2007.
- [111] V. S. Deshpande, M. Mrksich, R. M. McMeeking, and A. G. Evans, "A bio-mechanical model for coupling cell contractility with focal adhesion formation," *Journal of the Mechanics and Physics of Solids*, vol. 56, pp. 1484–1510, 2008.
- [112] E. L. Elson, G. M. Genin, "The role of mechanics in actin stress fiber kinetics," *Experimental Cell Research*, vol. 319, no. 16, pp. 2490–2500, 2013.
- [113] D. Mitrossilis, J. Fouchard, A. Guirouy, N. Desprat, N. Rodriguez, B. Fabry, A. Asnacios, "Single-cell response to stiffness exhibits muscle-like behaviour," *Proc. Natl. Acad. Sci. U.S.A.*, vol. 106, no. 43, pp. 18243–18248, 2009.
- [114] J. P. McGarry, J. Fu, M. T. Yang, C. S. Chen, R. M. McMeeking, A. G. Evans, and V. S. Deshpande, "Simulation of the contractile response of cells on an array of micro-posts," *Philos. Trans. R. Soc. London, Ser. A*, vol. 367, no. 1902, pp. 3477–3497, 2009.
- [115] A. Pathak, V. S. Deshpande, A. Evans, and R. McMeeking, "Simulations of cell behaviour on substrates of variegated stiffness and architecture," in *Computer Models in Biomechanics From Nano to Macro*, G. A. Holzapfel, E. Kuhl, Dordrecht: Springer Science + Business Media Dordrecht, 2013; 25–41.
- [116] W. Ronan, V. S. Deshpande, R. M. McMeeking, and J. P. McGarry, "Cellular contractility and substrate elasticity: A numerical investigation of the actin cytoskeleton and cell adhesion," *Biomechanics and Modeling in Mechanobiology*, vol. 13, no. 2, 417–435, 2014.
- [117] Pathak, V. S. Deshpande, R. M. McMeeking, and A. G. Evans, "The simulation of stress fibre and focal adhesion development in cells on patterned substrates," *J. R. Soc. Interface*, vol. 5, no. 22, pp. 507–524, 2008.
- [118] Z. Wei, V. S. Deshpande, R. M. McMeeking, A. G. Evans, "Analysis and interpretation of stress fiber organization in cells subject to cyclic stretch," *ASME J. Biomech. Eng.*, vol. 130, no. 3, pp. 031009, 2008.
- [119] S. J. Han, N. J. Sniadecki, "Simulations of the contractile cycle in cell migration using a bio-chemical-mechanical model," *Comput Methods Biomech Biomed Engin.*, vol. 14, no. 5, pp. 459–68, 2011.
- [120] Pathak, R. M. McMeeking, A. G. Evans, and V. S. Deshpande, "An analysis of the co-operative mechano-sensitive feedback between intracellular signalling, focal adhesion development, and stress fiber Contractility," *J. Appl. Mech.*, vol. 78, no. 4, pp. 041001, 2011.
- [121] E. P. Dowling, W. Ronan, and J. P. McGarry, "Computational investigation of in situ chondrocyte deformation and actin cytoskeleton remodelling under physiological loading," *Acta Biomater.*, vol. 9, no. 4, pp. 5943–5955, 2013.
- [122] R. Blumenfeld, "Stresses in granular systems and emergence of force chains," *Phys. Rev. Lett.*, vol. 93, pp. 108301–108304, 2004.
- [123] R. Blumenfeld, "Stress transmission in planar disordered solid foams," *J Phys A: Math Gen*, vol. 36, pp. 2399–2411, 2003.
- [124] R. C. Ball, R. Blumenfeld, "The stress field in granular systems: loop forces and potential formulation," *Phys. Rev. Lett.*, vol. 88 pp. 115505–115508, 2002.
- [125] Stamenović, N. Wang, "Stress transmission within the cell," *Comprehensive Physiology*, vol. 1, pp. 499–524, 2011.
- [126] R. Satcher, Jr. C. Dewey, and J. Hartwig, "Mechanical remodelling of the endothelial surface and actin cytoskeleton induced by fluid flow," *Microcirculation*, vol. 4, no. 4, pp. 8–453, 1998.
- [127] D. Ingber, N. Wang, and D. Stamenovi, "Tensegrity, cellular biophysics, and the mechanics of living systems," *Progress in Physics*, vol. 77, no. 4, pp. 046603, 2014.
- [128] S. Hu, J. Chen, B. Fabry, Y. Numaguchi, A. Gouldstone, D. E. Ingber, J. J. Fredberg, J. P. Butler, and N. Wang, "Intracellular stress tomography reveals stress focusing and structural anisotropy in cytoskeleton of living cells," *Am J Physiol Cell Physiol*, vol. 285, pp. C1082–1090, 2003.
- [129] Kardas, U. Nackenhorst, and D. Balzani, "Computational model for the cell-mechanical response of the osteocyte cytoskeleton based on self-stabilizing tensegrity structures," *Biomech Model Mechanobiol*, vol. 12, pp. 167–183, 2013.
- [130] Robert, "Cellular and molecular structure as a unifying framework for whole-cell modeling," *Curr. Opin. Struct. Biol.*, vol. 25, pp. 86–91, 2014.

## Appendix C.

Review article published in Engineering Mechanics

Citation Reference: Bansod Y. D., Burša J. (2014). Overview of tensegrity – II: High frequency spheres. *Engineering Mechanics*. 21(6):437 - 449.

# Overview of Tensegrity-II: High frequency spheres

Yogesh D. Bansod<sup>2</sup>, Deepesh Nandanwar<sup>3</sup>, Jiří Burša<sup>4a</sup>

*The paper continues the overview of tensegrity, part I of which deals with the fundamental classification of tensegrities based on their topologies. This part II focuses on special features, classification and construction of high frequency tensegrity spheres. They have a wide range of applications in the construction of tough large scale domes, in the field of cellular mechanics, etc. The design approach of double layer high frequency tensegrities using T-tripods as compression members for interconnecting the inner and outer layers of tendons is outlined. The construction of complicated single and double bonding spherical tensegrities using a repetitive pattern of three-strut octahedron tensegrity in its flattened form is reviewed. Form-finding procedure to design a new tensegrity structure or improve the existing one by achieving the desired topology and level of prestress is discussed at the end. The types of tensegrities, their configurations and topologies studied in both parts of this overview paper can be helpful for their recognition in different technical fields and, consequently, can bring their broader applications.*

Keywords: *Tensegrity, Frequency, T-tripod, Double layer, Form-finding*

---

<sup>2</sup> Yogesh Deepak Bansod, email: [yogeshbansod@gmail.com](mailto:yogeshbansod@gmail.com)

Institute of Solid Mechanics, Mechatronics and Biomechanics, Faculty of Mechanical Engineering, Technická 2896/2, 616 69 Brno, Czech Republic

<sup>3</sup> Deepesh Nandanwar, email: [deepeshnandanwar@gmail.com](mailto:deepeshnandanwar@gmail.com)

Indian Institute of Technology, Hauz khas, 110016, New Delhi, India

<sup>4a</sup> Corresponding author. <sup>4</sup> Prof. Ing. Jiří Burša Ph.D., e-mail: [bursa@fme.vutbr.cz](mailto:bursa@fme.vutbr.cz)

## 1. Introduction

Sphere-like tensegrity structures are needed in a number of applications. High-frequency spheres represent geodesic shapes created on the basis of principal polyhedrons (see Fig 9) but composed of a greater number of members. Many methods have been developed for disintegrating the basic polyhedral form into a larger number of components. Knowledge of geometrical constraints of high frequency spheres and resulting polyhedrons, is important to design tensegrity structure while maintaining its structural and fabrication limits. For applications where the stiffness of basic tensegrities is not sufficient, double-layer tensegrities may be applied. Methods for organizing tensegrity trusses into spheres are based on geodesic subdivision of an octahedron [1].

## 2. Formation of geodesic polyhedrons

Most of the geodesic polyhedrons are derived from five principal polyhedrons as depicted in Fig 9.



*Fig 9: Principal (Platonic) polyhedrons (from [2]).*

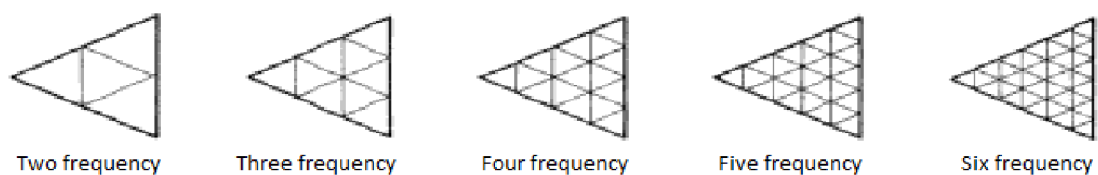


*Fig 10: Division of triangular faces of polyhedron into various frequencies (from [2]).*

A triangular grid is constructed by dividing the edges of each triangle of the principal polyhedron into equal number of parts and then joining them by drawing lines between them as depicted in Fig 10. The number of subdivisions for an edge is called the frequency of a particular subdivision and denoted by 'v'. When the average length of the members remains constant, more members imply that linear dimensions of the whole structure increase proportionally to the frequency [3]. The subdivisions with even frequencies only are used in tensegrity designing [2].

## 2.1 Diamond structures

As in the model for a T-tetrahedron, the tensegrities are considered to be a collection of tendon triangles interconnected via struts and tendons with their vertices lying on a sphere. The lengths of the struts as well as the lengths of the tendons forming tendon triangles are fixed. In addition to different number of tendons, another difference between 2 v diamond T-tetrahedron (see Fig 11(a)) and Zig-zag T-tetrahedron (see Fig 11 (b)) is in the position of tendon triangles. The T-icosahedron with diamond pattern is actually a special case of the two frequency diamond T-tetrahedron with all tendons having the same length.

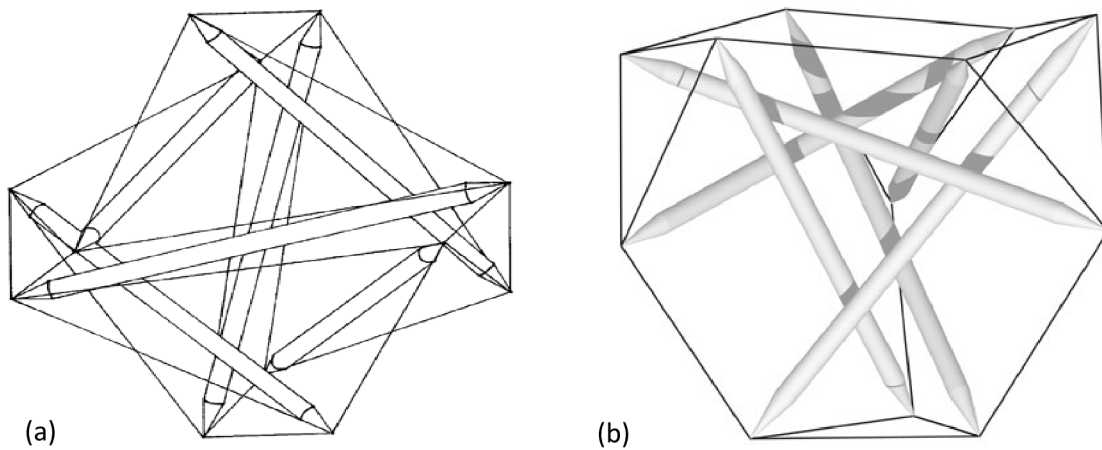


*Fig 11:(a) 2 v diamond T-tetrahedron and (b) Zig-zag T-Tetrahedron (from [4]).*

In Fig 12, label  $a$  represents equilateral, whereas  $b$  represents isosceles triangles. The bold lines represent the geodesic breakdown lines used in the tensegrity design. It is called a 4v structure because its geometry derives from the 4v geodesic subdivision of the tetrahedron [4]. An example of 4v diamond T-tetrahedron is illustrated in Fig 13.

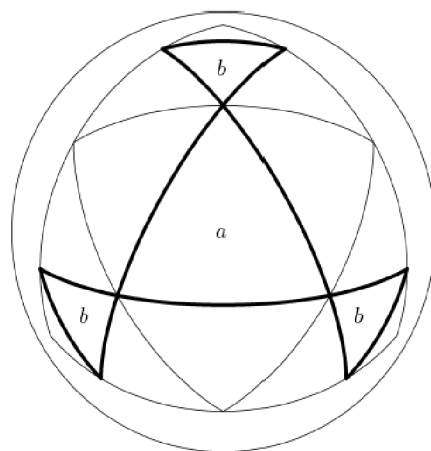


*Fig 12: Face triangle of a four frequency tetrahedron projected onto a sphere (from [4]).*

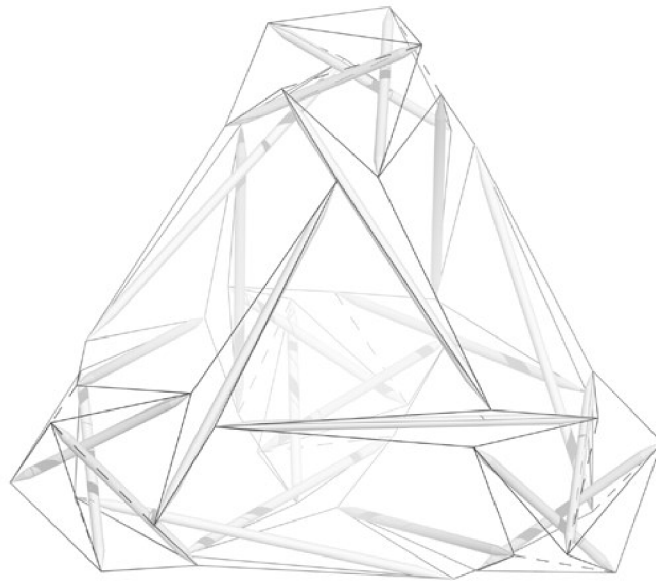


Fig 13: 4v diamond T-tetrahedron (from [4]).

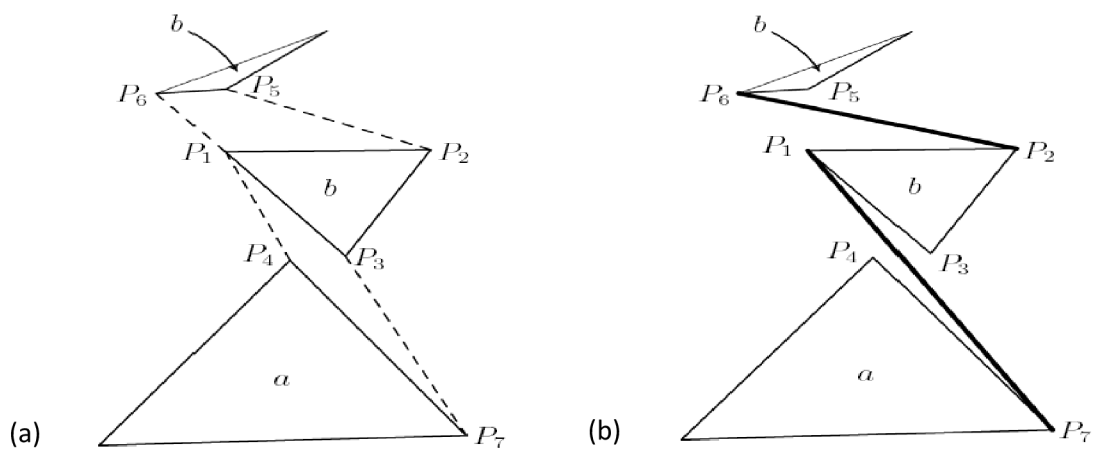


Fig 14 : (a) Tendons arrangement (dotted lines) and (b) Struts arrangement (bold lines) of 4v diamond T-tetrahedron (from [4]).

Arrangement of struts and tendons connecting two types of tendon triangles, a (equilateral) and b (isosceles), is shown in Fig 14. Adjacent tendon triangles are always connected by a pair of tendons (see Fig 14(a)) and a strut (see Fig 14(b)) [4].

## 2.2 Zig-zag structures

A zig-zag structure has a similar arrangement of struts and tendons as the corresponding diamond structure. In a diamond tensegrity structure two adjacent triangles are interconnected by two tendons (in addition to a strut), whereas in a zig-zag tensegrity they are connected by only one strut and one tendon (see Fig 15). From the structural point of view each strut is traversed by a



"zig-zag" of three tendons [4]. An example of 4v zig-zag T-tetrahedron tensegrity is presented in Fig 16.

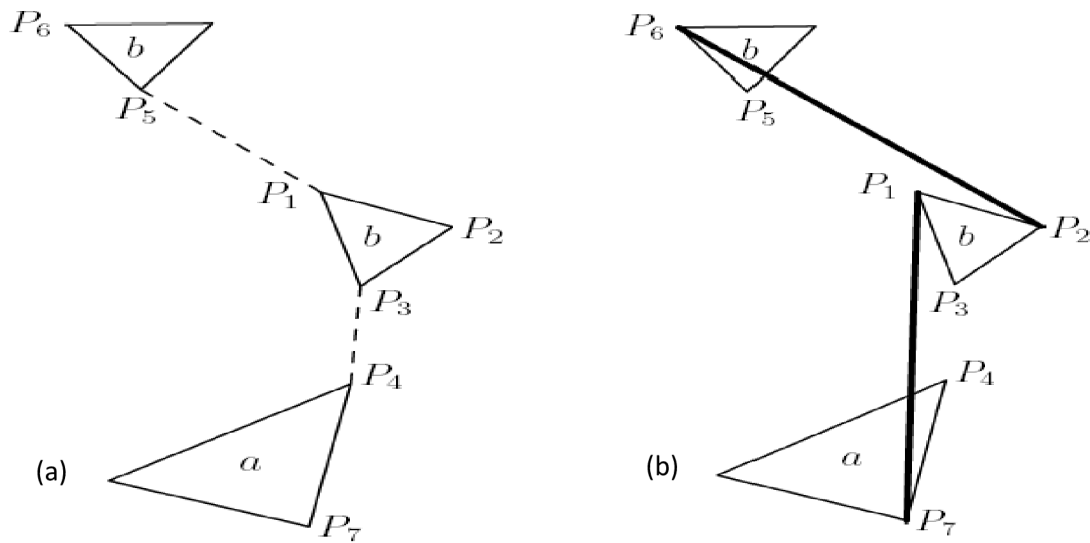


Fig 15:(a) Tendons arrangement and  
(b) Struts arrangement of 4v Zig-zag T-Tetrahedron (from [4]).

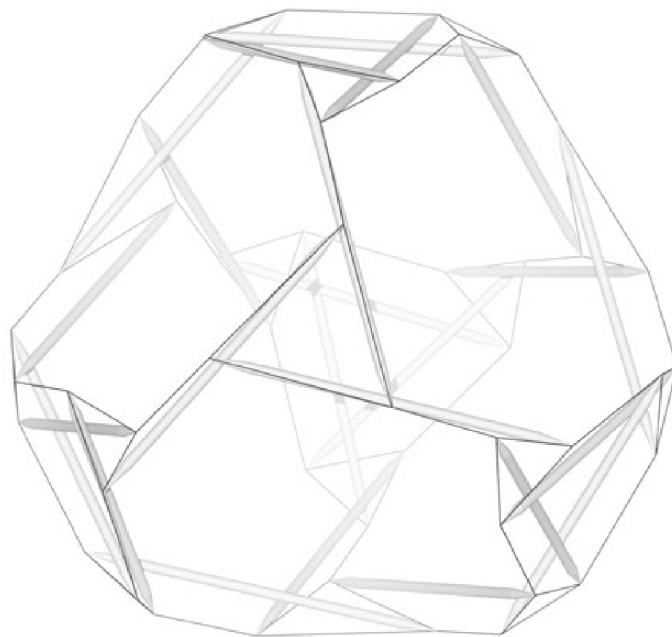


Fig 16: 4v Zig-zag T-tetrahedron (from [4]).

### 3. Trusses or Double-Layer Tensegrities

For most of the tensegrities discussed so far, the tensile members create a single continuous spherical layer, thus they are rather compliant and tend to vibrate significantly

in many practical applications. Even the high frequency spherical tensegrities have little resistance to concentrated load. These drawbacks are overcome by developing space truss configuration for tensegrity structures which would be analogous to the space truss arrangements developed for the geodesic dome. Tensegrity space trusses are characterized by outer and inner layers of tendons interconnected by a collection of struts and tendons. Consequently, the structure becomes more rigid and has more resistance to concentrated loads [4, 8].

### 3.1 Tensegrity tripod

In tensegrity prism, removing the triangle of tendons corresponding to one of the ends and pressing the struts at the free end close to each other, resist and stay apart. The structure obtained is called tensegrity tripod or T-tripod as illustrated in Fig 17. When attached to other tensegrity structures, this composite compression member can keep them apart and enable creation of multilayer tensegrities [4].

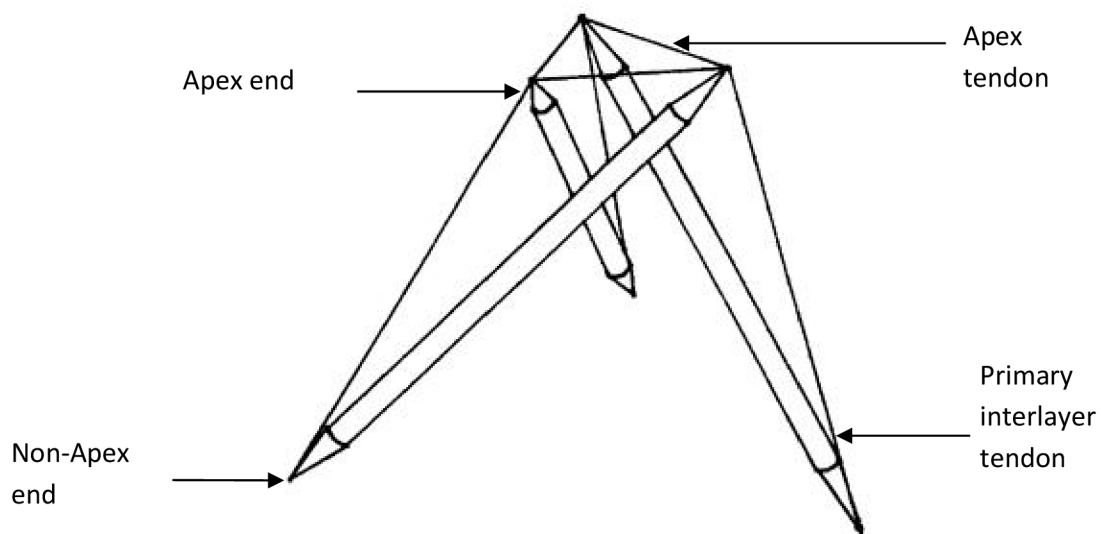


*Fig 17: Tensegrity Tripod (T-tripod) (from [4]).*

T-tripod has 6 tendons, three of them called as apex or outer convergence tendons binding the three struts together at one end to form a triangle representing the apex of tripod and the remaining three tendons are called as primary interlayer tendons which join the apex end of one strut to the non-apex end of an adjacent strut in the T-tripod (see Fig 17) [3]. Alternatively, another compression member called 'T-polypod' is designed from any polyilateral prism by eliminating its tendons on one end and can be used instead of T-tripods [4].

When T-tripods are used as compression members to support a spherical single-layer tendon

network, the T-tripods struts lie outside the layer of tendons (see Fig 18). This eliminates the intractable interference problems occurring in larger structures when supported by simple two-hubbed struts as they lie in the same layer which they support [5].

### 3.2 Construction of double tensegrity sphere using T-tripod

#### 3.2.1. Outer convergence and corresponding binding

Consider a sphere made of single-layer network supported by T-tripods as described in the previous section. This network consists of vertex-connected rings of tendons called as polylaterals (non-planar equivalent of a polygon) which are connected pairwise in vertexes (hubs). The condition is not more than one vertex is shared between adjacent polylaterals, and every vertex is shared by exactly two polylaterals (here, triangles created by edges of neighbouring polylaterals are not considered as polylaterals).

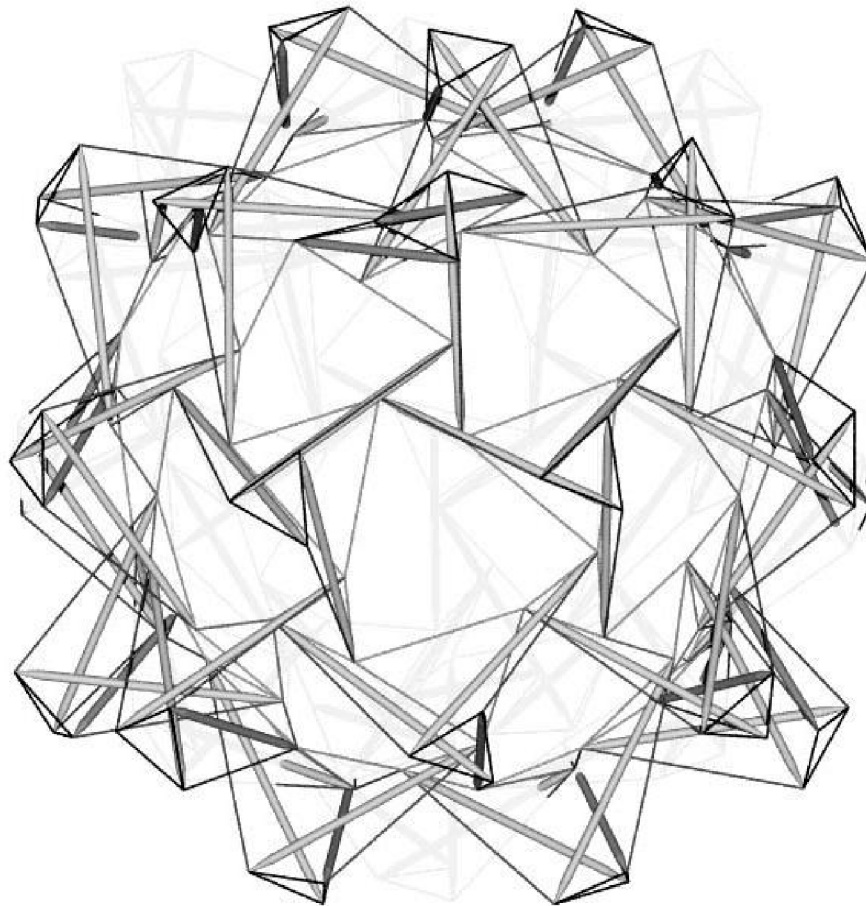


*Fig 18: Spherical assembly of tripods embedded in the tensegrity network (from [4]).*

The smallest polylateral is a triangle of three hubs connected by three tendons [3, 7]. The apex tendons of the T-tripods lie on the outer surface called as outer convergence. Apart from continuous inner single-layer spherical network there is a discontinuous outer network formed by

the tendon triangles of the apexes of the T-tripods which serve as compression members. These apex tendons (triangles) are called as outer convergence tendons [4]. To achieve more structural stability, the outer network is completed by binding together the T- tripod apexes using another set of tendons called outer binding tendons (see Fig 19). In this way the outer convergence (layer of tendons) is created.

Although the lengths of outer network tendons are different, the outer and inner networks should be bound in such a way that both networks have the same topology. The distance between the three non-apex ends of struts of the t-tripod increases on untwisting the T-tripod (i.e. they move further apart from each other by elongating the primary interlayer tendons). Thus, the outer convergence tendons should be bound together in such a way that tension in the outer binding tendons untwists the T-tripods. Consequently, the outer network of tendons is pushed farther from the inner network by the virtue of expanding compression members i.e. untwisting of T-tripods [4].

### **3.2.2. Inner convergence and corresponding binding**

Struts from several different T-tripods converge at inner network where they are connected together by tendons called as inner convergence tendons forming a polylateral and having a similar topology as outer binding tendons. The remaining tendons of the inner network creating triangles are called inner binding tendons. When the appropriate tendons are added to connect the convergence polylateral to the opposite ends of the struts they are called secondary interlayer tendons and complete the truss network as illustrated in Fig 19. The tensegrity truss generated using this method has two groups of geometrical shapes in each layer, triangles and polylaterals.

In the final design, a triangle or polylateral from one group will be completely surrounded by polylaterals from another group [4]. The combination of triangles and polylaterals yield a more rigid structure than general polylaterals only [6]. In this configuration each strut is secured by 12 tendons, which is the minimum number of tendons required to rigidly fix one system in its surrounding system [7]. In planar view, the truss section looks same viewed either from inside or outside the tensegrity sphere. This technique can be applied to any tensegrity network on the condition that it can be divided into alternating polylaterals [5].

In this way maximum stiffness can be achieved with minimum strut density, as all T-tripods act as compression members (between outer and inner convergence) and convergences (layers) consist of tendons only. The geodesic networks on the basis of this approach belong to the class of double layer tensegrities [4]. Most of the structures

discussed till now have spherical symmetry. The drawback of this technique is that it does not result into a perfect spherical shape network as triangles eliminate the polyhedrons which have much more faceted appearance [5]. The final outcome is a rigid tensegrity space frame aimed at extremely large-scale applications for instance, for covering superstructure of a space station [4].

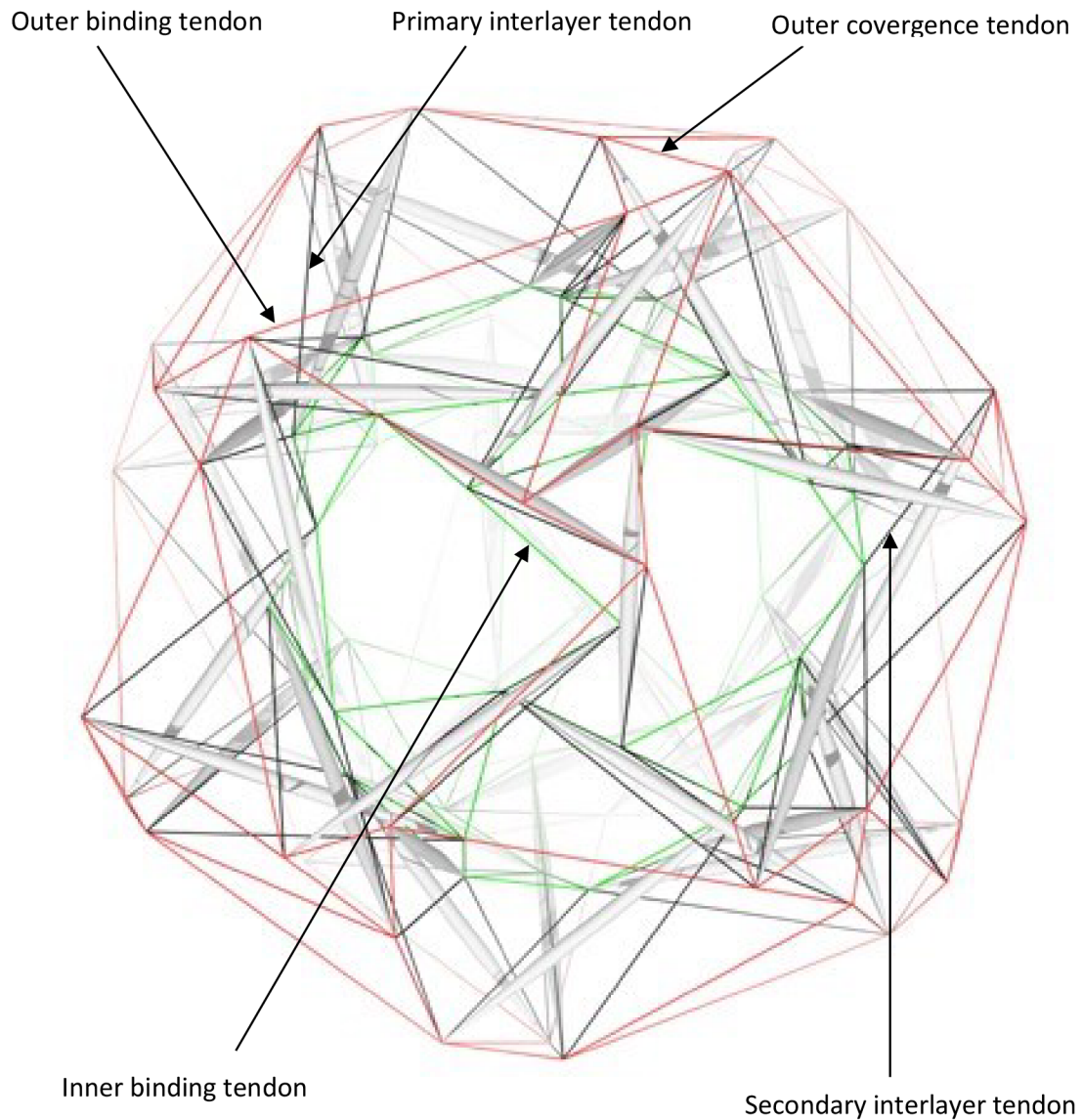


*Fig 19: 4v T-Octahedron double-layer tensegrity (from [4]).*

#### 4. Spherical Tensegrity

The spherical tensegrities have a wide scope of applications, especially in the field of architecture, cellular mechanics, etc. Further, a dome can be induced by truncating the tensegrity

sphere. The simplest form of tensegrity is an octahedron consisting of three compression members i.e. the struts cross and do not touch each other as they pass at the centre. They are held together only at their terminals by the triangular tension net (tendons) as depicted in Fig 20 (a).

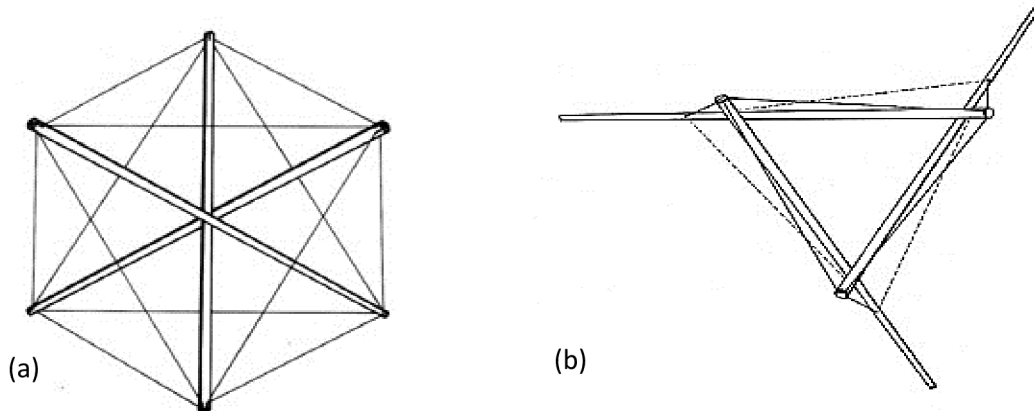


Fig 20: (a) Three-strut tensegrity octahedron (b) Corresponding flattened form (from [7]).

The same three islanded struts of the tensegrity octahedron may be mildly reorganized or asymmetrically transformed into flattened form by removing three tendons and lengthening or shortening the others (see Fig 20 (b)). The struts may be of the same or different lengths and the vertexes can be shifted along the struts from their original positions at their ends. Even in flattened form the compression members still do not touch each other. This fundamental unit used repeatedly to construct the spherical tensegrity structures [7].

Formation of a tensegrity structure can be done in two ways. The first way is called single-bonding in which a single strut of basic three strut structure in flattened form is directly connected to the strut of another basic three strut structure in flattened form accomodating the tensegrity sub-unit hexagonal ring of tendons as depicted by dotted lines in Fig 21 (b).

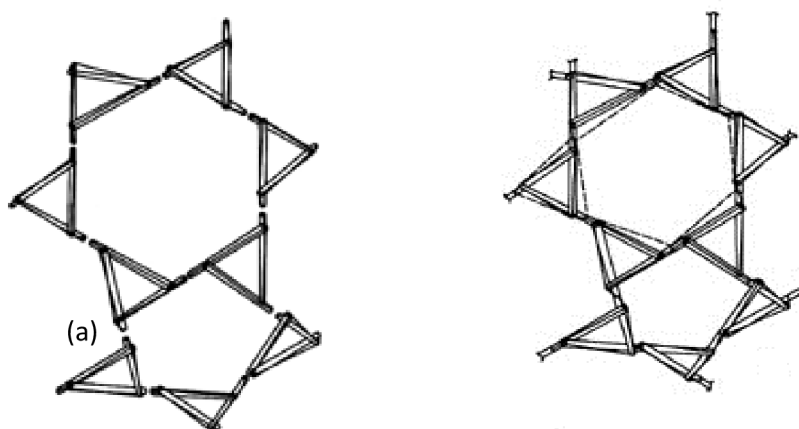


Fig 21: Complex of basic three-strut tensegrities, with axial alignment whose exterior terminals (a) before and (b) after joining in single bond as 90-strut tensegrity (from [7]).

Another way known as double bonding, the basic structures in flattened form has direct connection between struts on a straight line (as that of single bonding) and also, are joined by two parallel struts with the help of tendons. Thus, basic three-strut tensegrities in flattened form may be joined to form a complex, 270-struts, isotropic triacontrahedron tensegrity geodesic spheres either in single-bonding with positive rotating triangles (see Fig 22 (a)) or double-bonding with negative rotating triangles (see (b)).

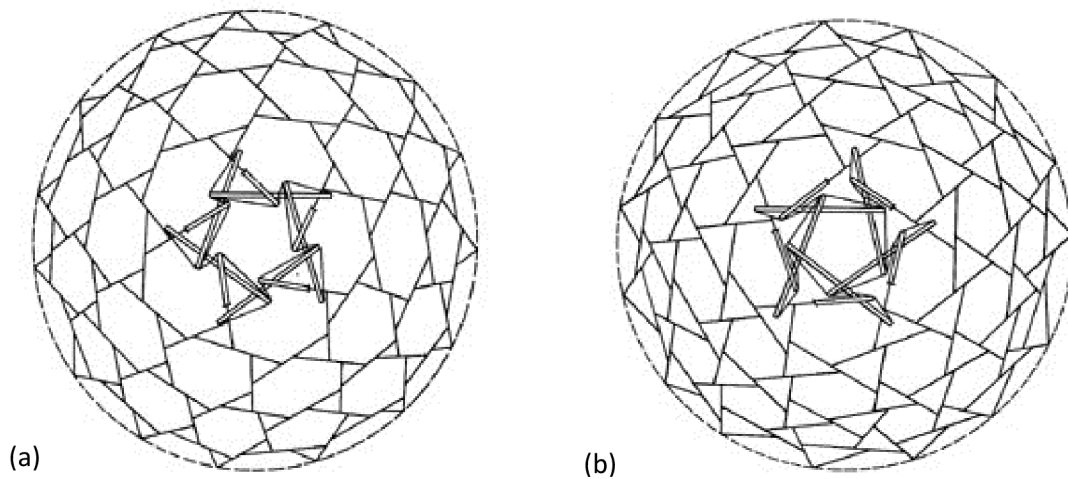


Fig 22: A 270-strut isotropic tensegrity geodesic sphere forming a complex six-frequency triacontrahedron tensegrity (a) Single bonded clockwise rotating tendon triangles and (b) double bonded anticlockwise rotating tendon triangles (from [7]).

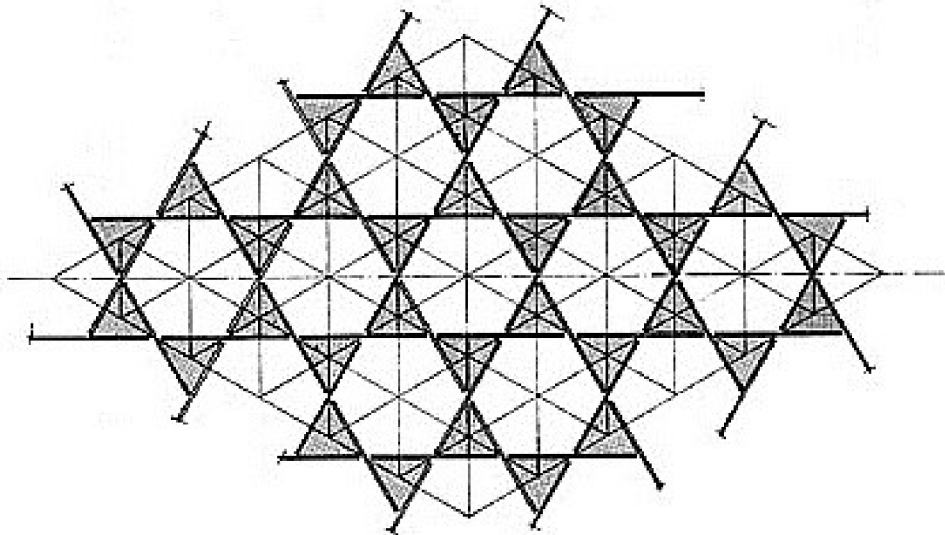


Fig 23: The basic 12 frequency matrix (from [7]).

Within the tensegrity sphere compression generated in discontinuous struts is balanced by the tension applied by omni integrated tendons network. The spherical tensegrity consist of

continuous tension network of single or double tendons between the ends of discontinuous compression network of islanded struts. The load distribution and uniform stress flow within the system can be better achieved with double tendon tension network. These tendons always yield in obtuse or acute ‘V’ shape at their point of contact with islanded struts [7].

In a spherical tensegrity system, the tension tendons are positioned closely to the struts and they do not yield away. The basic 12-frequency tensegrity matrix (see Fig 23) employs collections of the basic three-strut units joined at dead centre between single-bonded and double-bonded discontinuities and the shaded triangles represent the sites for each of the three- strut units [7].

## 5. Form-finding Technology

Any tensegrity structure is designed by keeping its parameters in mind mainly, certain amount of pre-stress, length of its constituents and basic morphology. A new topologic and geometric design aims at achieving a certain higher level of prestress and to keep it under the externally applied forces while maintaining its geometrical constraints [9]. As tensegrities belong to the class of statically indeterminate structures, their static analysis requires an initial form-finding procedure [10, 11]. Form-finding is technique based on mathematical programming view of tensegrity for finding a certain geometrical configuration which makes the system stable on its own (an intrinsic property of statically indeterminate structures with members bearing tension or compression, only). It involves computing of the shape of a tensegrity structure when being pre-stressed and sets in self-equilibrium.

Form-finding procedure is very useful for civil engineers, architects and the people dealing with mechanisms and structures. Although designed to achieve the same goal, it has been defined in contradictory ways by many authors [12, 13, 14]. Therefore, based on a comprehensive literature study, the authors have proposed the following definition: Form-finding is a method to design and generate the stable geometrical configuration of a tensegrity structure (using mathematical modelling) inspired by other geometrical forms and structures, under a given condition of pre-stress such that it will remain stable and maintain its shape under a certain range of external forces and impacts.

The truncated tetrahedron was analysed for its form-finding tensegrity structure with the same length for all cables and another length for all struts [9]. In Fig 24, first image represents truncated icosahedron in polyhedron form and the second one represents its corresponding tensegrity structure created using form-finding procedure. The truncated icosahedron is combination of hexagonal and pentagonal polylaterals, whereas the corresponding form-finding tensegrity has structure of pentagons surrounded by triangles. In addition, the tensegrity structure consists of 30 compression elements (thick bars) and 120 tension elements (thin black bars) that do not provide smooth edges as that of the corresponding polyhedron. Thus it is evident, that the form-finding



tensegrity structures may or may not be similar to the polyhedron from which it originates [10,11,14].

The form-finding methods in tensegrity architectures are broadly divided into kinematical methods and statical methods. In statical method, a relationship is set between equilibrium configurations of a structure with a given topology and the forces in members, which are then analysed using various methods, for instance force-density method, energy method, etc. In other words, it will search for equilibrium configurations that permit the existence of a state of prestress in the structure with certain required characteristics. On the other hand, kinematical method is characterised by increasing (decreasing) the length of the struts (tendons) and keeping the length of tendons (struts) constant until a maximum (minimum) of length of strut (tendon) is achieved to stabilise the system. This is a practical approach to build the tensegrity structure without requiring the tendons to be in pre-tension [10].

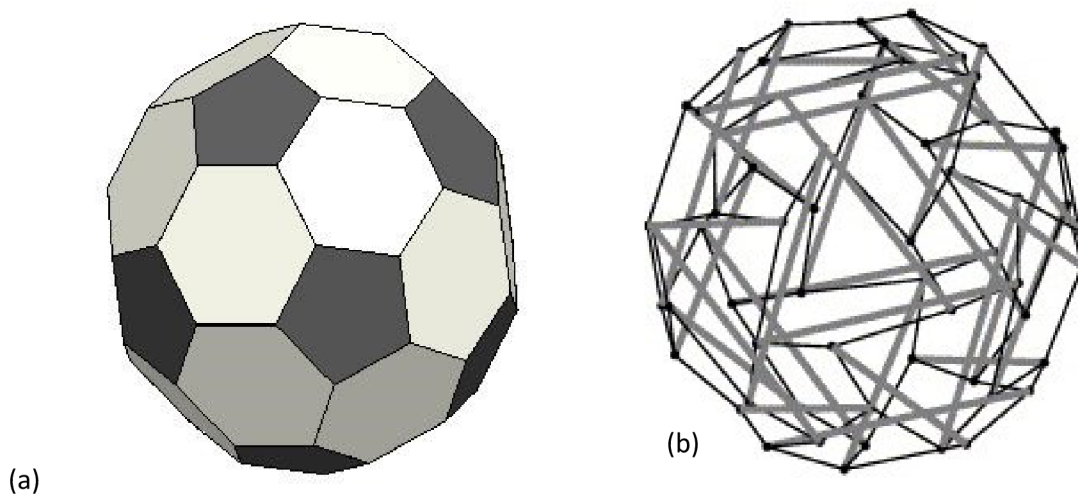


*Fig 24: (a) Truncated Icosahedron in polyhedron form and (b) The corresponding tensegrity structure having rhombic configuration designed using form-finding technology (from [14]).*

Further, the kinematical methods are classified into analytical approach, non-linear optimization and pseudo-dynamic iteration, whereas statical methods include analytical methods, based on formulation of linear equations of equilibrium in terms of force densities, energy minimization and a search for equilibrium configurations of the struts of the structure connected by tendons whose lengths are to be determined using a reduced set of equilibrium equations. A lot of new methods were also introduced in recent years. These methods do not require the members to be in state of pre-stress [10]. All the form-finding methods presented so far (based on different approaches) have been summarised and tabulated by Jaun & Tur [13]. In most of the existing form-finding procedures; however, assumptions on the tension coefficients (force divided by length as a variable for each element), the element lengths or the symmetry of the whole structure

must be imposed a priori [11]. Therefore, the evaluation of complex tensegrity structures with these procedures remains difficult. A form-finding procedure typically gives the value of critical parameters such as (i) a twisting angle (ii) a cable-to-strut ratio (iii) a force-to-length ratio also known as the tension coefficient or the force density coefficient [14]. The advanced tensegrity principle based computational model of smooth muscle cell cytoskeleton (see Fig 25) is developed at Brno University of Technology with its nucleus and centrosome tensegrities designed using form-finding technology.

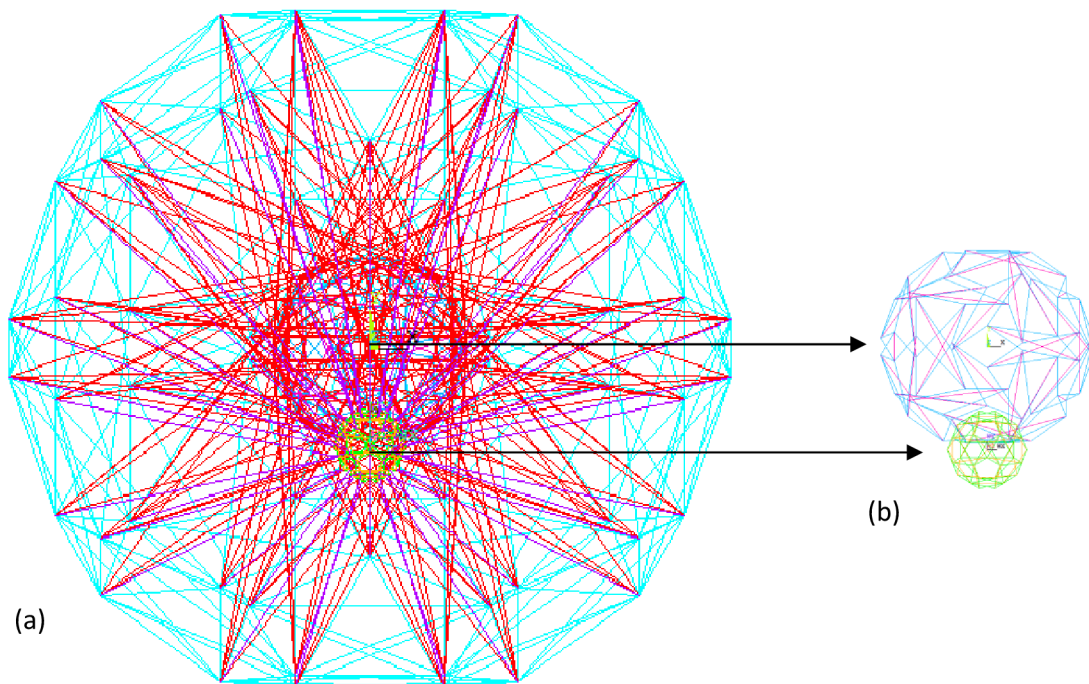


*Fig 25: (a) Tensegrity principle based computational model of smooth muscle cell cytoskeleton (b) Nucleus and centrosome designed using form-finding technique.*

Following are the four methods to evolve new tensegrity structures [2]:

- a) To postulate a new concept of tensegrity or to modify an existing one.
- b) Solution for different relationships between struts and tendons which can be achieved in any of the following ways. First, interpreting the existing relationship between them in a different way. Second, manipulate the number of struts and tendons until a new pattern is achieved. Third, discover the relation from an entirely new figure. And finally, consider various ways in which the struts and tendons can be related to each other.
- c) Discover or develop new polyhedral figures which serve as bases for tensegrity systems based on already established relationships between the struts and tendons.

- d) Extend an existing idea of figures; for instance, develop tensegrity structure from two layer figure to three layer diamond structures, geodesic domes [4].

## 6. Conclusion

In part I, we have introduced the principal tensegrities and their classification based on topologies and weaving configurations, whereas in this part of the paper we have overviewed the fabrication of complex high frequency spheres and double layered tensegrity structures using form-finding technology. Several methods to create higher order tensegrity structures have been presented and illustrated with relevant examples applicable to various fields. The objective of this two-part overview paper is to introduce amazing tensegrity structures and their extraordinary features to the researchers and students from various fields, to encourage them to contribute in this area by creating their new applications.

## Acknowledgement

The results of this project NETME CENTRE PLUS (LO1202) were co-funded by the Ministry of Education, Youth and Sports within the support programme "National Sustainability Programme I".

## References

- [1] Kenner H. (1976): Geodesic Math and How to Use It, 1st edition, Berkeley, California.
- [2] Pugh A. (1976) : An Introduction to Tensegrity, University of California Press, Berkeley, California.
- [3] Burkhardt R. (2007): A Technology for designing tensegrity domes and spheres. Last edition, Tensegrity solutions, Cambridge.
- [4] Burkhardt R. (2004): A Practical Guide to Tensegrity Design, 2nd edition, Tensegrity Solutions, Cambridge, Massachusetts.
- [5] Snelson K. (2012): The Art of Tensegrity, International Journal of Space Structures, 27 (2-3), pp. 71-80.
- [6] Hanaor A. (1987): Preliminary Investigation of Double-Layer Tensegrities, In.: H. Topping (ed.), Proceedings of International Conference on the Design and Construction of Non-conventional Structures, Vol. 2, Edinburgh, Scotland: Civil-Comp press, p. 35.

- [7] Fuller B. (1975): *Synergetics: Explorations in the Geometry of thinking*, in collaboration with E. J. Applewhite, First Published by Macmillan Publishing Co. Inc., New York.
- [8] Jáuregui V. (2004): *Tensegrity Structures and their Application to Architecture*, Submitted to the School of Architecture, Queen's University, Belfast, pp. 1-12.
- [9] Juan S., Tur J. (2009): *Tensegrity frameworks: Dynamics analysis review and open problems*, *Mech. & Mach. Theory*, 44 (1), pp. 1-18.
- [10] Tibert A., Pellengrino, S. (2009): *Review of Form-Finding Methods for Tensegrity Structures*, *International Journal of Space structures*, 18 (4), pp. 209-223.
- [11] Motro R. (2003): *Tensegrity: Structural Systems for the Future*, Hermes Penton Science, London.
- [12] Motro R. (2009): *Structural Morphology of Tensegrity Systems*, *Asian Journal of Civil Engineering (Building and Housing)*, 10 (1), pp. 1-19.
- [13] Juan S., Tur J. (2008): *Tensegrity frameworks: static analysis review*, *Mech. & Mach. Theory*, 43 (7), pp. 859–881.
- [14] Estrada G., Bungartz H., Mohrdieck C. (2006): *Numerical form-finding of tensegrity structures*, *International Journal of Solids and Structures*, 43 (22-23), pp. 6855–6868.
- [15] Kardas D., Nackenhorst U., Balzani D. (2013): *Computational model for the cell-mechanical response of the osteocyte cytoskeleton based on self-stabilizing tensegrity structure*, *Biomech Model Mechanobiol*, Vol. 12, pp. 167-183.

## Appendix D.

Review article published in Engineering Mechanics

Citation Reference: Bansod Y. D., Nandanwar D., Burša J. (2014) Overview of tensegrity – I: Basic structures. *Engineering Mechanics*. 21(5):355 - 367.

# Overview of Tensegrity-I: Basic structures

Yogesh D. Bansod<sup>5</sup>, Deepesh Nandanwar<sup>6</sup>, Jiří Burša<sup>7a</sup>

*The tensegrity framework consists of both compression members (struts) and tensile members (cables) in a specific topology stabilized by induced prestress. Tensegrity plays a vital role in technological advancement of mankind in many fields ranging from architecture to biology. In Part I of this two-part article, we have reviewed topological classification of elementary cells of tensegrity structures including rhombic, circuit and Z type configuration. Further, different types of tensegrities created on the basis of these configurations are studied and analysed, for instance Tensegrity prism, Diamond tensegrity, and Zig-zag tensegrity. The Part II focuses on the applications of tensegrity principle in construction of high frequency spheres & domes.*

Keywords: *Tensegrity, Struts, Cables, Prestress, Configuration*

## 1. Introduction

The technique used in constructions by architects around the world is based on holding the structure with the help of its weight and continuity of stresses induced basically in compression. For example, each component of a stone dome or bridge is pulled by tension downward through

---

<sup>5</sup> Yogesh Deepak Bansod, email: [yogeshbansod@gmail.com](mailto:yogeshbansod@gmail.com)

<sup>5,3</sup> Institute of Solid Mechanics, Mechatronics and Biomechanics, Faculty of Mechanical Engineering, Technická 2896/2, 616 69 Brno, Czech Republic

<sup>6</sup> Deepesh Nandanwar, email: [deepeshnandanwar@gmail.com](mailto:deepeshnandanwar@gmail.com)

Indian Institute of Technology, Hauz khas, 110016, New Delhi, India

<sup>a</sup> Corresponding author. <sup>7</sup> Prof. Ing. Jiří Burša Ph.D., e-mail: [bursa@fme.vutbr.cz](mailto:bursa@fme.vutbr.cz)

the structure, but the compressive continuity is still in charge of sustaining most of the load. On the other hand, tensegrity architecture represents a totally different principle, it does not rely on the gravity for its stability (as gravity creates tension in other structures). Tensegrities represent a system of “equilibrated omnidirectional stresses” [1]. They don’t need any support and are self-equilibrated as well as pre-stressed structures. The theory of tensegrity structures is well known in statutory or civil engineering while in other engineering branches the potential of these structures is not yet fully explored. This paper summarizes the up to date knowledge on tensegrity structures and presents some of their non-conventional applications in computational modelling in various technical fields.

## 2. Features of Tensegrity

Fuller [2] coined the term “tensegrity” by combining two words “Tensional + Integrity”; it means that integrity of a structure consisting of tension and compression components relies on the tension members. His definition of tensegrity structures was ‘A tensegrity system is established when a set of discontinuous compressive components interacts with a set of continuous tensile components to define a stable volume in space’. If we apply this definition in broader sense, then the entire universe can be viewed as a tensegrity structure. Such as planetary systems at a space level and atomic systems at a microstructural level, all of them consist of discontinuous compressed members (spheres) connected by gravitational (tensional) forces that symbolize tensile members. It is evident, that this definition is too broad, and a more precise one is needed.

K. Snelson [3] describes tensegrity as a closed structural system composed of a set of three or more elongated compression struts within a network of tensioned tendons, the combined parts mutually supportive in a way, that the struts do not touch one another, but press outwardly against nodal points (vertices) in the tension network to form a firm, triangulated, prestressed, tension and compression unit. In short, he defined tensegrity as discontinuous compression, continuous tension structures [4]. Probably the most complete definition of tensegrity structures is presented in [5] as “Tensegrity is a structural principle based on the use of isolated components in compression inside a net of continuous tension, in a way that the compressed members (usually known as bars/struts) do not touch each other and the prestressed tensioned members (usually known as cables/tendons/strings) delineate the system spatially”. In living nature, tensegrity structures can be found as a governing principle in many biological systems ranging from cells [6] to tissues [7]. For instance, musculo-skeletal system can be understood as a tensegrity structure [8] some of the recent studies show that DNA molecules [9] and cell cytoskeleton can also be viewed as tensegrity based stable structures [6]. In technology, tensegrity principle is used widely in building new structures, shelters (see Fig 1) bridges, etc.



*Fig 1: A tensigrity shelter built at Brno University of Technology, Brno*

Apart from above, it is used for the development of advanced materials, smart materials [10, 11] and deployable devices for aerospace technology [12]. On the other hand, some natural (spider web) and man made structures (such as bicycle wheels or multi cable domes – Olympics stadium in Seoul (1986), etc.) can not be truly considered as tensigrity structures because their compressive members are in mutual contact; in Snelson words, they don't have floating compression system [3].

## **2.1 Characteristics of tensigrities**

Characteristics of tensigrities can be summarized as follows:

- a) They have a *higher load-bearing capacity with similar weight*.
- b) They are *light weight* in comparison to other structures with similar resistance.
- c) They don't need to be anchored or don't have to lean on any surface as they don't *depend on their weight or gravity*. They are stabilized in any position by equilibrium of compressive forces in struts with tensional forces in prestressed cables. Prestrain in the cables can be transformed into prestress only if the structure is statically indeterminate.
- d) They are *enantiomorphic* i.e. exist as right and left-handed mirror pairs [13].
- e) Elementary *tensigrity modules* can be used (such as masts, grids, ropes, rings etc.) to make more complex tensigrity structures.

- f) Higher the pre-stress, stiffer the structure would be, i.e. its *load bearing capacity increases with the increasing pre-stress* [14]. The degree of tension of the pre-stressed components is directly proportional to the amount of space they occupy [15].
- g) In a tensegrity structure the compressive members are *short and discontinuous*, hence they *do not undergo buckling* easily and *no torque* is generated in them [16].
- h) The *resilience* depends on the structure assembly and material used.
- i) They *work synergically* i.e. their behaviour cannot be predicted by considering the behaviour of any of their components separately.
- j) They are *sensitive to vibrations* under dynamic loading. Slight change in load causes the stress to redistribute in the whole structure within no time and thus, they have the *ability to respond as a whole*.
- k) Kenner [16] introduced a term “*Elastic Multiplication*” for the tensegrity structures. It is a property of tensegrity structure which depends on the distance between two struts. If two struts are separated by a certain distance the elongation of tendons (tensile members) attached to them is much less compared to this distance.
- l) The *deformation response of entire tensegrity structure to load is non-linear* as its stiffness increases rapidly with increasing load, like at a suspension bridge [16].
- m) The tensegrities are commonly modelled *with frictionless joints, and the self-weight of cables and struts is neglected*.

## 2.2 Advantages of tensegrity over conventional (continuous) structures

- a) As the load is distributed in whole structure there are *no critical points of weakness* [16].
- b) They *don't suffer any kind of torsion and buckling* due to space arrangement and short length of compression members [1].
- c) *Forces are transferred naturally* and consequently, the members position themselves precisely by aligning with the lines of forces transmitted in the shortest path to withstand the induced stress.
- d) They are *able to vibrate and transfer loads very rapidly* and hence, absorb shocks and seismic vibrations which make them *applicable as sensors or actuators* [10, 11].
- e) They can be *extended endlessly through adding elementary structures*.
- f) Construction of structures using tensegrity principle *makes it highly resilient* and, at the same time, *very economical*.



### 2.3 Disadvantages of tensegrity over conventional (continuous) structures

- a) If the structure becomes too large it faces a *problem of bar congestion* (i.e. the struts start running into each other) [17].
- b) They show relatively *high deflections and low material efficiency* as compared to conventional continuous structures [17].
- c) *Fabrication complexity* is a major barrier in developing floating compression structures [5].
- d) *Adequate design tools are not available* for their design, software “Tensegrite 2000” (developed by R. Motro et al.) is the most advanced tool available to design tensegrity structures.
- e) At *large constructions* the structure cannot withstand loads higher than critical, related to its dimensions and prestress [17].

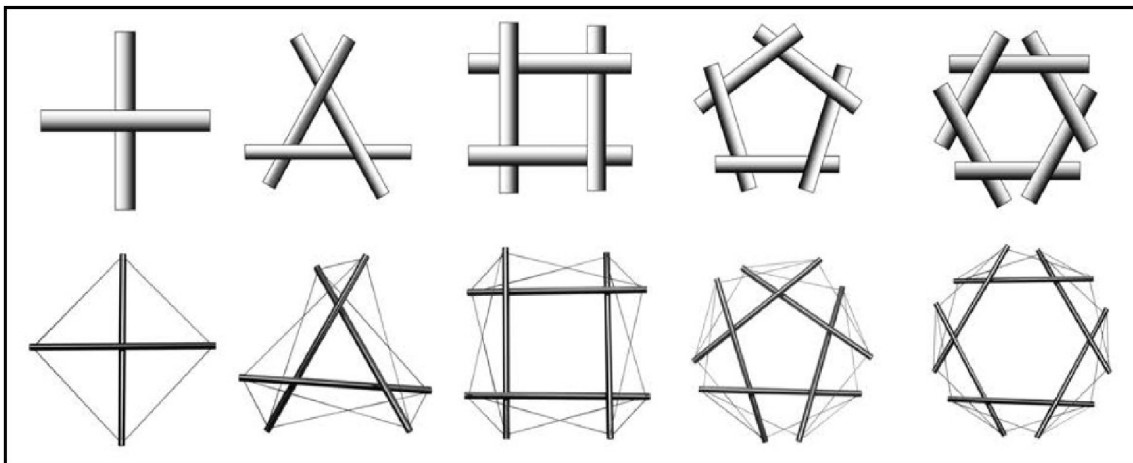


Fig 2: Primary weaves cells & equivalent basic tensegrity modules (from [4]).

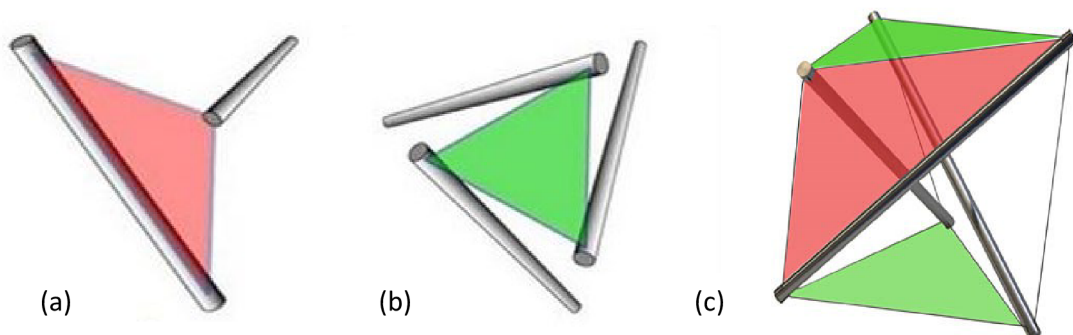


Fig 3:(a) Tension/compression triangle (b) Tension only triangle (c) 3 strut prism (from [3]).

### 3. Tensegrity weaving & triangulated tension network

Snelson [4] has defined 5 basic weave cells as depicted in Fig 2 which can be translated into basic tensegrity structures. Among these the first two geometries on the left hand side (two and three-way cross units) have total triangulation making the tensegrity structures firm. The remaining geometries are flaccid because they have less tendons than required for total triangulation (as compared to the number of struts in the weave unit). On the basis of the relative position of tendons and complexity of arrangement of struts Pugh [14] classified the basic patterns to configure tensegrity structures which were further refined by Motro [18] as a spherical system, star system, irregular system and cylindrical system. In this overview article, we have focused only on spherical systems due to their large scale application in designing tensegrity structures. Spherical systems can be further divided into rhombic, circuit and zig-zag configurations.

The triangles formed by tendons in a tensegrity network can be classified in two different ways. First, the tension/compression triangle is formed with two struts and two tendons where two cables from the end of one strut join the two ends of a second strut as depicted in Fig 3 (a). Second, a tensegrity only triangle can be formed with three different cables attached to three different struts as shown in Fig 3 (b). The tension/compression triangles always occur in pairs like butterfly wings, whereas tension only triangles do not (see Fig 3 (c)) [3].

## 4. Topological classification of elementary cells of tensegrity structures

### 4.1 Rhombic configuration

The name of tensegrity patterns is based on the way they are constructed (tendon patterns). In Fig 4, each strut (blue/black colour) of a system represents the longest diagonal of a rhombus formed by four corresponding tendons or cables (red/orange colour) and can be folded following these diagonal. Generally, this configuration corresponds to the diamond tensegrity. T-prism (section 4.1) and T-icosahedron (section 4.2) tensegrities are well known examples of the rhombic configuration where rhombus represents a non-planar quadrilateral formed by tendons [14].

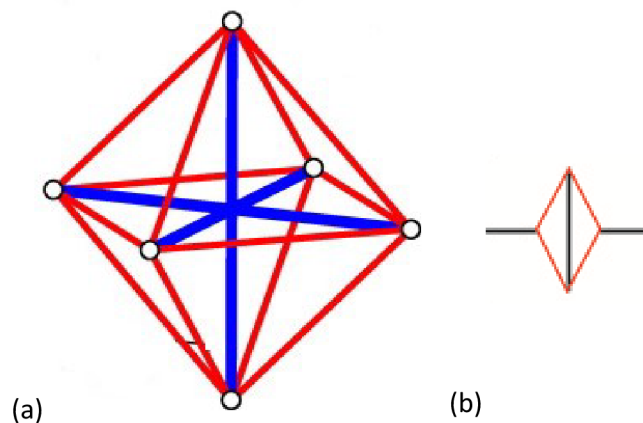
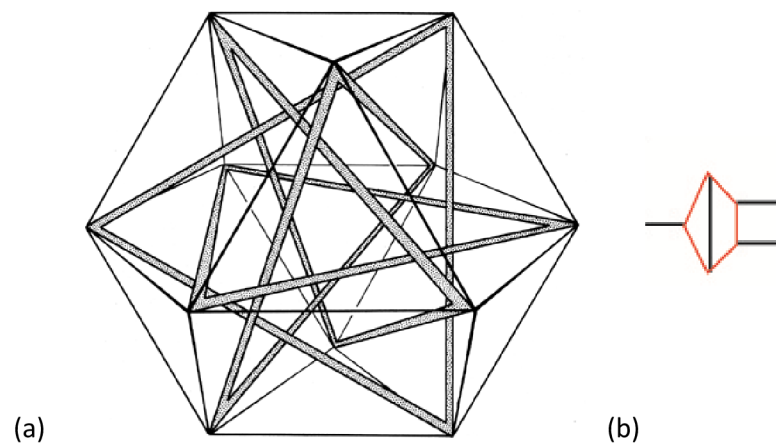


Fig 4: (a) Assembly of rhombic configuration and (b) its pattern (from [19]).

## 4.2 Circuit Configuration

In this system, the compressed members are formed by close circuits (see Fig 5) which do not comply with standard definition of tensegrity [17]. This can be constructed by closing the rhombus generated by struts and cables of the diamond pattern tensegrity such as T-icosahedron (see Fig 11).



*Fig 5: (a) Circuit configuration of cuboctahedron tensegrity having 4 non-touching triangular circuits and (b) its pattern (from [20]).*

A new tendons-struts relationship is established by joining the struts to form the circuit pattern which gets compact in size and able to withstand greater external load compared to the tensegrity structure built using diamond pattern for the same number of struts. It was Pugh's discovery that a circuit system is more rigid than a rhombic one with the same number of struts. Several regular and semiregular polyhedra can be built using this configuration, for instance icosidodecahedron, cuboctahedron, snub cube and snub icosahedron, etc. [14]. If opposite pair of squares are forced toward one another in a three-layer twelve struts structure, then the whole system twists and contracts.

As shown in Fig 5, the cuboctahedron is composed of four circuits of three struts each (triangles) and the cables defining the edges of the polyhedron. These triangles are intertwined and their equilibrium is ensured by a hexagon of cables and the effect of the other three triangles for three of the apices of each hexagon. It may be claimed it is not a true tensegrity structure since the struts here are connected to each other but now the triangles of struts act as a single compression unit, and hence these structures can be regarded as tensegrity structures.

A rhombicuboctahedron has 8 triangular and 18 square faces. It has 24 vertices, each shared by one triangle and three squares. The tensegrity structure has 24 struts making 6 square circuits (see Fig 6 (a)) arranged in three pairs perpendicular to each other and 48 tendons. Icosidodecahedron consists of twenty triangular faces and twelve pentagonal faces. It has 60 edges of the same length

and 30 vertices, each of them shared by two triangles and two pentagons. The corresponding tensegrity structure based on circuit configuration has 30 struts of equal length arranged into 6 non-touching circuits of pentagons (see Fig 6 (b)); it contains 60 tendons [21].

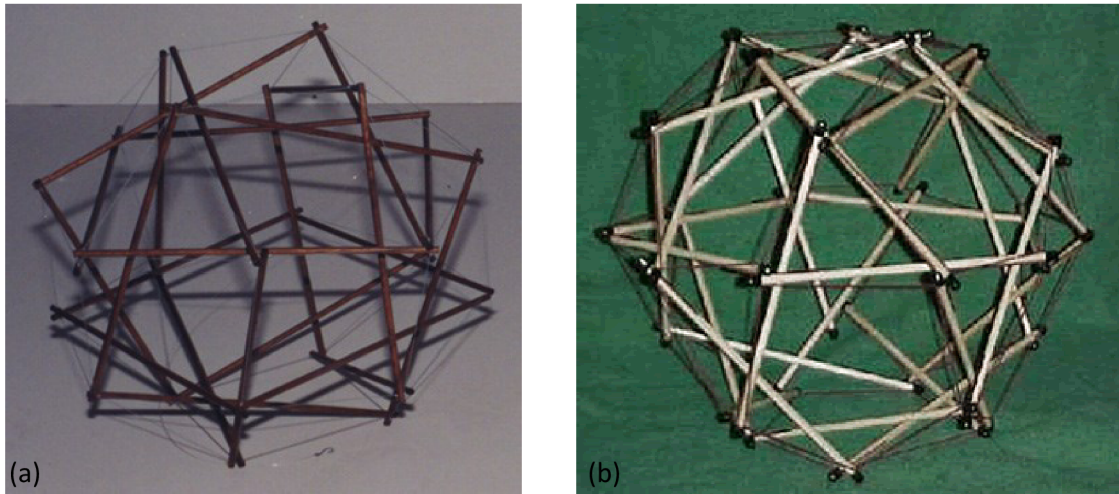


Fig 6: (a) Rhombicuboctahedron tensegrity using 6 non-touching square circuits. (b) Icosidodecahedron tensegrity from 6 non-touching pentagonal circuits (from [21]).

#### 4.3 ‘Z type’ configuration

A “zig-zag” configuration (also being an enantiomorphic) is obtained from the rhombic configuration as the basic structure. Both ends of any strut should be connected by three non-aligned tendons arranged to form a ‘Z’ shape. Truncated tetrahedron (see Fig 7) is a classic example of Z type configuration obtained from truncated icosahedron which belongs to the class of rhombic configurations (refer section 4.1 and 5.2).

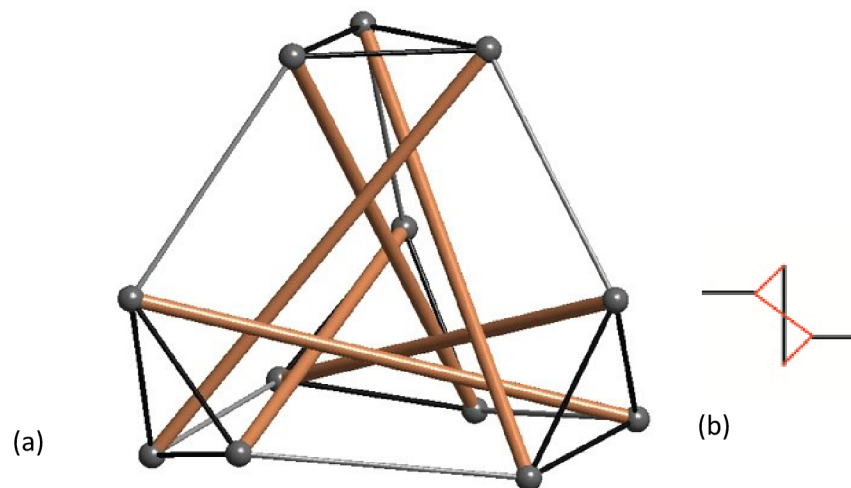
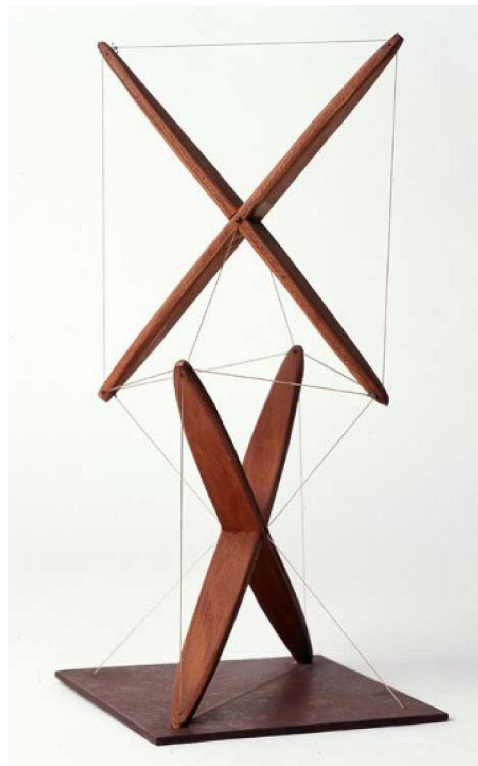


Fig 7: (a) Truncated tetrahedron (T-tetrahedron) using Z type configuration and (b) its pattern (from [22]).

This type of configuration can be obtained by removing two tendons of the opposite sides of a non-planar rhombus of truncated icosahedron. In this way, the number of cables is reduced and their arrangement can be changed in such a way that three nonaligned tendons connecting both ends of a strut form a 'Z' shape [5]. The distortion of regular polygon may rise due to the orientation of struts that converge in each face. To obtain the perfect geometry, additional cables can be inserted into the original system [18].

## 5. Types of tensegrities

The tensegrity structures are widely classified as prestressed and geodesic structures. They are divided into three main categories: Tensegrity prism, Diamond tensegrity and Zig-zag tensegrity. The X-module (see Fig 8) built by Snelson had given birth to tensegrity. This simple tensegrity structure consists of two X-shaped wooden struts suspended in air by stretched nylon cables [4]. The simple kite frame is the basic prestressed tension-compression cell of X-module tensegrity structure. It consists of two crossed struts firmly held together by a girth of four tension members, because the (vector) sum of compression forces pushing out equals the sum of tension forces pulling in. As shown in Fig 9, the change in length of both struts and tendons i.e. change in proportion of frame is related to the variation in distribution of forces, both tension and compression.



*Fig 8: Wood X-module (from [4]).*

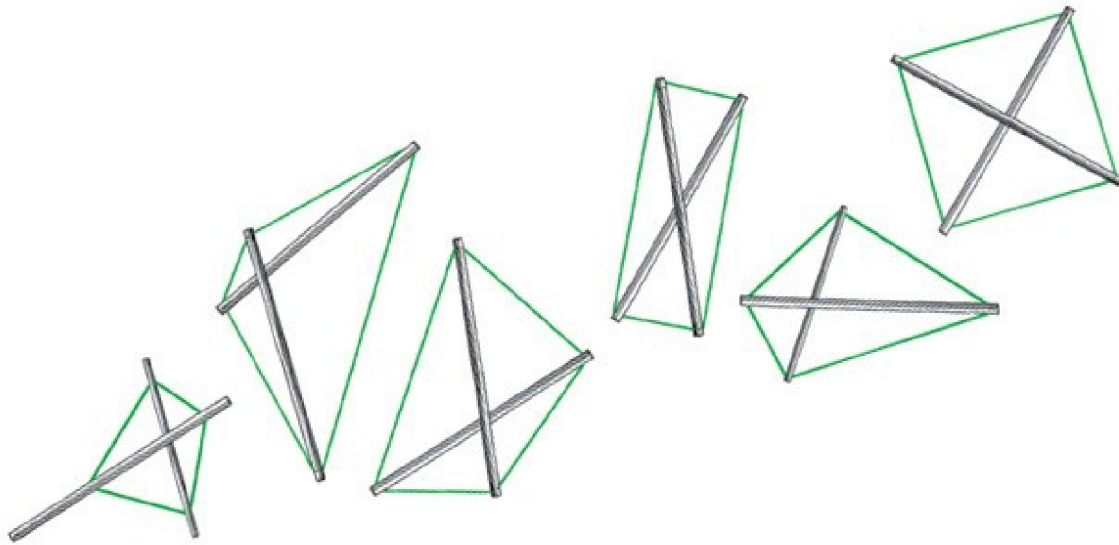


*Fig 9: Kite frame shape in various proportions (from [3]).*

It is a quasi-tensegrity structure because it is planar (2D), and the struts touch each other. If any one of the tendons is removed, then the blank side will work as a compressed component; this is called as “strut effect”. This basic principle is required to design various elementary components of two layer and three layer tensegrity systems. The lengths of the four tendons and the lengths of the two struts determine the shape of the kite frame (see Fig 9) [13].

### 5.1 Tensegrity Prism (T-Prism)

Also known as 'Three struts T-prism'; it was invented by Karl Ioganson in Moscow in 1921 [23]. It is the simplest and therefore one of the most instructive members of the tensegrity family. The T-prism has 9 tendons and 3 struts (see Fig 10) and belongs to a subclass of prismaticoids.

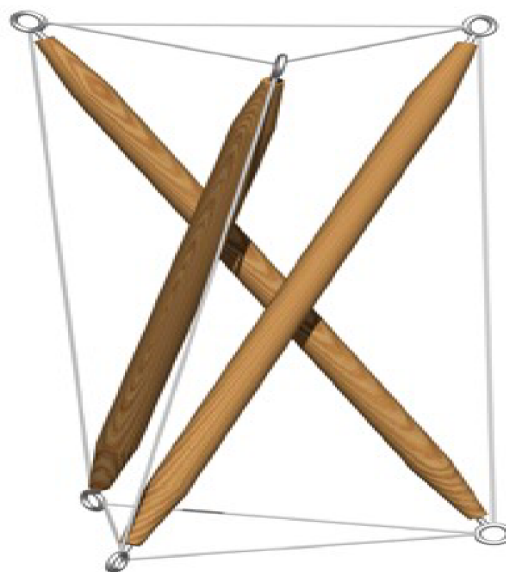


*Fig 10: Diamond Configuration of T-prism (from [1]).*

It has been called tensegrity prism or T-prism as it can be considered as a twisted prism consisting of two triangular faces twisted with respect to each other. Generally, these tensegrity structures are designed by keeping the lengths of one set of tendons and struts constant and determining the lengths of another set of tendons. When one end of the prism is twisted relative to the other, the rectangular sides of the prism become non-planar quadrilaterals. Thus, two opposite angles of each quadrilateral become obtuse and acute. For structure to be stable and prestressed, the prism is twisted in such a way that the distance between the obtuse angles is least (an intermediate stage of twisting) and hence, a completely stable T-prism is formed [17].

## 5.2 Diamond Tensegrity

The tensegrity icosahedron also known as T-icosahedron is depicted in Fig 11 as a classic example of diamond tensegrity. These tensegrities are characterized by the fact that each triangle of tendons is connected to the adjacent one via a strut and two interconnecting tendons [17]. It was first exhibited by Buckminster Fuller [23] in 1949 and is one of a few tensegrities which exhibit mirror symmetry. This tensegrity is classified as a "diamond" type because each of its struts is surrounded by a diamond form of four tendons which are supported by two adjacent struts making them distinct from a Zig-zag tensegrity. It has 6 struts and 24 tendons with tendon to strut lengths ratio of 0.612 [14].

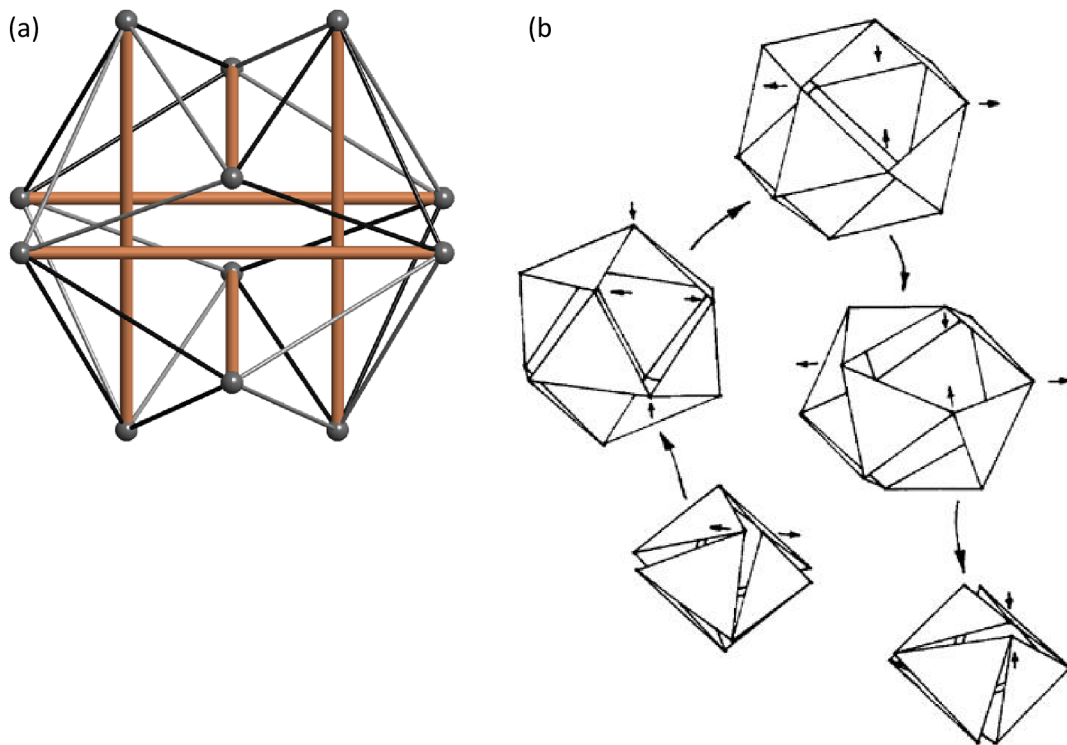


Fig 11: (a) T-icosahedron and (b) its corresponding transformation from and back to doubled-up octahedron (from [17]).

If the quadrilaterals nested with struts are changed to squares then the tendons form a cuboctahedron network. Fig 11 illustrates the change in system of tendons from an octahedral arrangement (with each strut doubled-up by presence of two struts in the identical position) to cuboctahedron and back. Small arrows indicate the direction of movement of the struts and of the corresponding pair of opposite points of the quadrilateral as the tendon system goes through transformations [17].

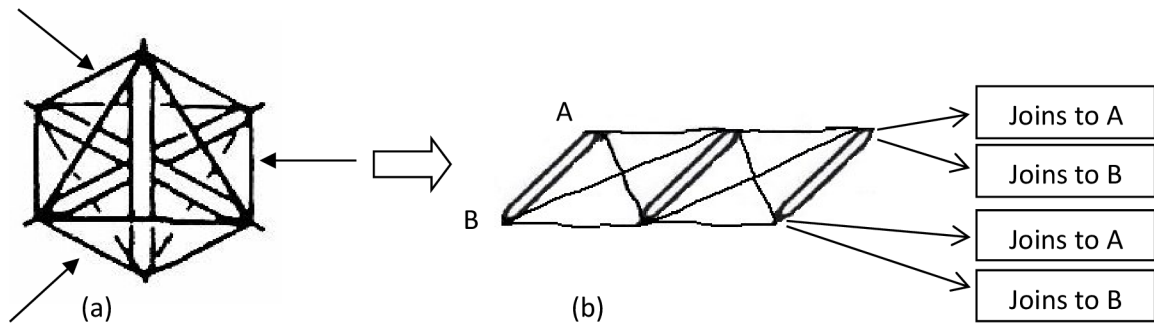


Fig 12: (a) Octahedral structure (b) corresponding 3-struts single layer tensegrity system (modified from [14]).

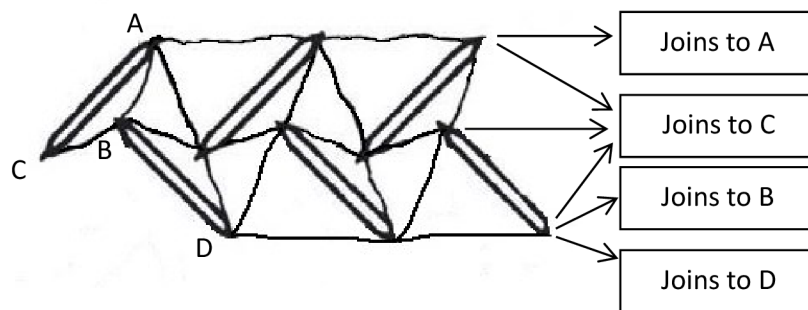


Fig 13: Planar view of 6-struts two layer tensegrity system (modified from [14]).

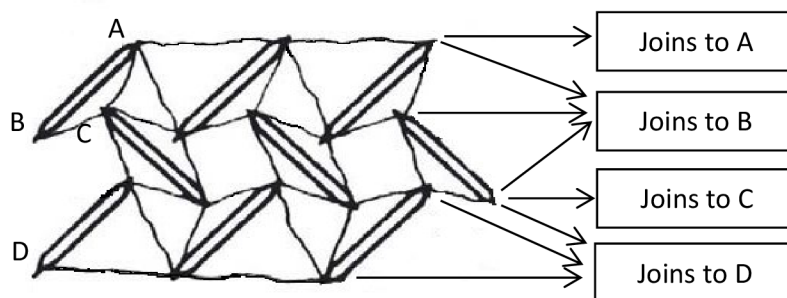


Fig 14: Planar view of 9-struts three-layer tensegrity system (modified from [14]).



Opening the octahedral structure carefully from one end gives a single layer diamond structure as depicted in Fig 12. New tensegrity structures with spherical symmetry can be generated by a layer by layer addition of struts and tendons and joining both ends of each layer. Planar views of tensegrity systems based on this approach are depicted in Fig 13 and Fig 14.

### 5.3 Zig-zag tensegrity

The tensegrity tetrahedron also known as (T-tetrahedron) depicted in Fig 15 is a classic example of diamond tensegrity developed by Francesco della Sala in 1952 [23]. The T-tetrahedron is the zig-zag counterpart of the diamond T-icosahedron (see Fig 11). Although both structures have 6 struts, the major difference is that T-tetrahedron has four tendon triangles, whereas the T-icosahedron has eight of them.

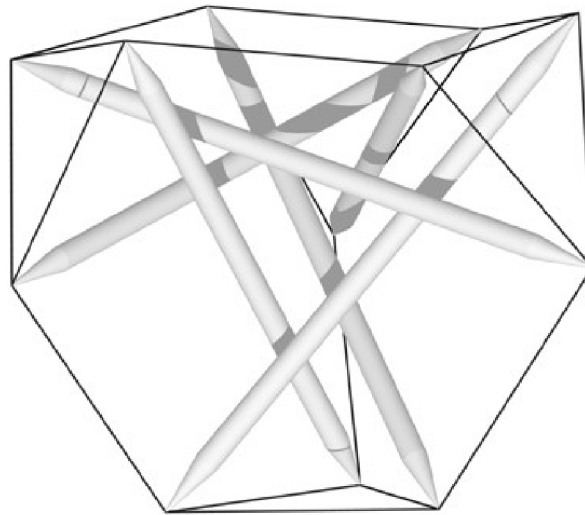


*Fig 15: T-Tetrahedron (Z type configuration) (from [17]).*

In general, zig-zag structures with Z type configuration are simpler and less rigid due to their lower number of tendons than their diamond counterparts with rhombic configuration [17].

## 6. Conclusion

In this part-I of the overview article, the authors have introduced the tensegrity principle and its unique features over conventional solid structures. Further, the topological classification of elementary cells (tendon patterns) and tensegrities based on these types of cells were presented here. The tensegrity structures have a wide range of applications specifically in structural engineering such as domes, bridges, and towers, as well as in biological sciences for computational modelling of human anatomy, eukaryotic cells, etc as depicted by an example in Fig 16. The tensegrity principle based computational model of smooth muscle cell cytoskeleton has been developed at Brno University of Technology [24] as a part of simulation study of different

mechanical tests of eukaryotic cells. In Fig 16 the lines in purple colour symbolise the cables (microfilaments) being in tension, the green ones are struts (microtubules) loaded in compression and the red ones are bars (intermediate filaments) acting as springs. In Part II of this article high frequency double layer spherical tensegrity structures will be discussed.

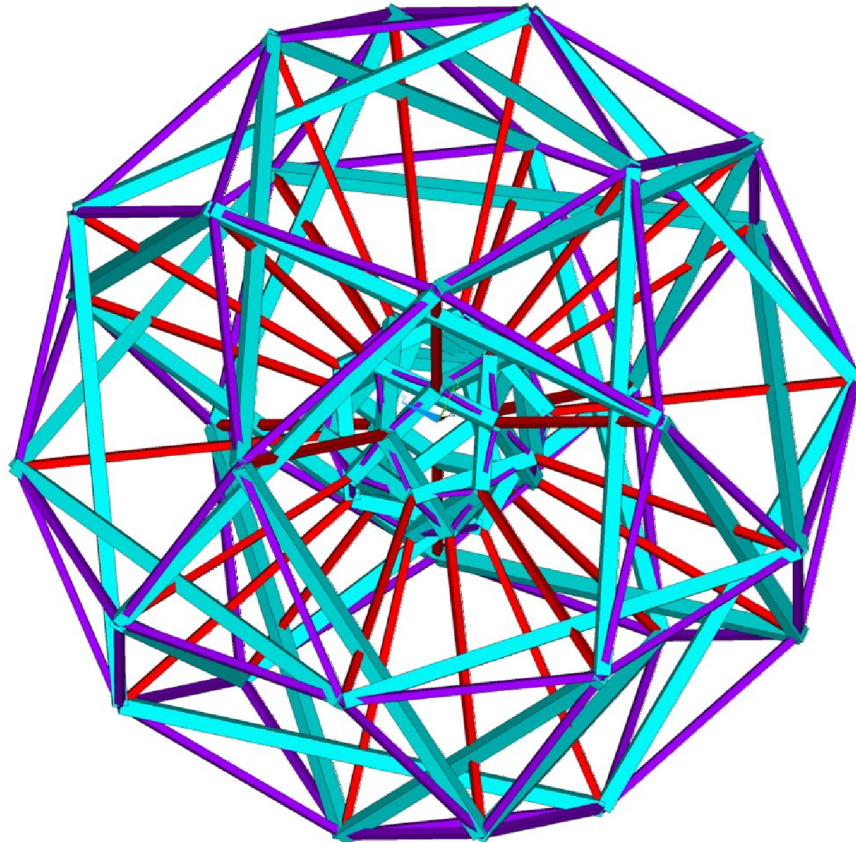


*Fig 16: Tensegrity computational model of smooth muscle cell cytoskeleton based on icosidodecahedron (from [24]).*

## **Acknowledgement**

The results of this project NETME CENTRE PLUS (LO1202) were co-funded by the Ministry of Education, Youth and Sports within the support programme "National Sustainability Programme I". This work is also supported by Czech Science Foundation project number 13-16304S and by faculty project No. FSI-S-14-2344. The First author is supported by JCCM project number.

## References

- [1] Fuller B. (1975-1979): Synergetics: Explorations in the geometry of thinking, in collaboration with E. J. Applewhite, Macmillan Publishing Co. Inc., New York.
- [2] Fuller R. (1961): Tensegrity, Portfolio and Art News Annual, 144 (4), pp. 112-127.
- [3] Snelson K. (2004): Tensegrity, E-Book, New York. Also available on <http://www.kennethsnelson.net/tensegrity/>
- [4] Snelson K. (2012): The art of tensegrity, International Journal of Space Structures, 27, pp. 71-80.
- [5] Jauregui V. (2004): Tensegrity Structures and Their Application to Architecture, submitted to school of architecture, Queen's University, Belfast, pp.1-12.
- [6] Ingber D. (1998): The Architecture of Life, Scientific American Magazine, 278 (1), pp.48-57.
- [7] Maina J. (2007): Spectacularly robust! Tensegrity principle explains the mechanical strength of the avian lung, Respir. Physiol. Neuro., 155 (1), pp.1-10.
- [8] Levin S. (1982): Continuous tension, discontinuous compression, a model for biomechanical support of the body, Bulletin of Structural Integration, pp.31-33.
- [9] Liu D., Wang S., Deng Z., Walulu R., Mao C. (2004): Tensegrity: Construction of rigid DNA triangles with flexible four-arm DNA junctions, Journal of the American Chemical Society, 126 (8), pp. 2324-2325.
- [10] Tibert G. (2002): Deployable Structures for Space Applications. Doctoral thesis. Royal Institute of Technology, Stockholm (Sweden). Available on [www.mech.kth.se/thesis](http://www.mech.kth.se/thesis)
- [11] Skelton R, Sultan C. (1997): Controllable tensegrity: A new class of smart structures, In. Proceedings of SPIE: Smart Structures and Materials, Varadan V., Jagdish C. (ed.), Vol. 3039, pp.166-177.
- [12] Sultan C.: Tensegrity (2009): 60 years of art, science, and engineering, Advances in Applied Mechanics, Vol. 46, pp.69-145.
- [13] Snelson K. (2004): Arts & Ideas, E-Book, New York.
- [14] Pugh A. (1976): An introduction to tensegrity, University of California Press, Berkeley, California.
- [15] Tibert A., Pellengino S. (1996): Review of finding methods for tensegrity structures, International Journal of Space Structures, 18 (4), pp.209-223.
- [16] Kenner H. (1976): Geodesic Math and How to Use It, 1st edition, Berkeley,

California.

- [17] Hanaor A. (1987): Preliminary Investigation of Double-Layer Tensegrities, In.: H. Topping (ed.), Proceedings of International Conference on the Design and Construction of Non-conventional Structures, Vol.2, Edinburgh, Scotland: Civil-Comp press, p.35.
- [18] Motro R. (2003): Tensegrity: Structural Systems for the Future, Hermes Penton Science, London.
- [19] Zhang L., Yue L., Cao Y., Feng X. ( 2012): A unified solution for self-equilibrium and super-stability of rhombic truncated regular polyhedral tensegrities, International Journal of Solids and Structures, 50 (1), pp. 234-245.
- [20] Yasushi K.: Tensegrity Precesion, Research blog. Also avaiable on <http://synergetics.jp/tensegrityblog>.
- [21] Ingber D., Tensegrity.wikispaces.com. Avariable on <http://tensegrity.wikispaces.com/>
- [22] Estrada G., Bungartz H., Mohrdieck C. (2006): Numerical form-finding of tensegrity structures, International Journal of Solids and Structures, 43 (22-23), pp. 6855-6868.
- [23] Fuller B., Buckminster R., Marks R. (1973): The Dymaxion World of Buckminster Fuller, Garden City, New York.
- [24] Bursa J., Lebis R., Holata J. (2012): Tensegrity finite element models of mechanical tests of individual cells, Technology and Health Care, 20 (2), pp.135-150.

## Appendix E.

Review article published in Engineering Mechanics

Citation Reference: Bansod Y. D., Burša J. (2014) A concise review of soft glassy rheological model of cytoskeleton. *Engineering Mechanics*. 21(4):279 - 285.

# A concise review of soft glassy rheological model of cytoskeleton

Yogesh D. Bansod<sup>8</sup>, Jiří Burša<sup>9</sup>

*A cytoskeletal network contributes significantly to intracellular regulation of mechanical stresses, cell motility and cellular mechanics. Thus, it plays a vital role in defining the mechanical behaviour of the cell. Among the wide range of models proposed for dynamic behaviour of cytoskeleton, the soft glassy rheology model has gained special attention due to the resemblance of its predictions with the mechanical data measured from experiments. The soft glassy material, theory of soft glassy rheology and experiment on cytoskeleton has been discussed, which leads to a discussion of the unique features and flaws of the model. The soft glassy rheological model provides a unique explanation of the cytoskeleton ability to deform, flow and remodel.*

Keywords: *Cytoskeleton, Model, Soft glassy rheology, Magnetic Twisting Cytometry*

### 1. Introduction

The cytoskeleton (CSK) is an interconnected structure of various cross-linked and interlinked filamentous biopolymers that extends from the nucleus to the cell surface.

---

<sup>8</sup> Yogesh Deepak Bansod, email: [yogeshbansod@gmail.com](mailto:yogeshbansod@gmail.com)

Institute of Solid Mechanics, Mechatronics and Biomechanics, Faculty of Mechanical Engineering, Technická 2896/2, 616 69 Brno, Czech Republic

<sup>9</sup> Corresponding author. Prof. Ing. Jiří Burša Ph.D., e-mail: [bursa@fme.vutbr.cz](mailto:bursa@fme.vutbr.cz)

The mechanical forces of the cytoskeleton are associated with many biological functions of cells such as its growth, differentiation, and apoptosis, (programmed cell death) which cause the changes in cell shape [1]. Numerous evidences have shown that CSK plays a vital role in transmitting mechanical stresses from the cell surface to the nucleus across the cytoplasm [2, 3, 4, 5].

The cytoskeletal network is composed of three types of filaments: actin filaments, microtubules and intermediate filaments [6] as shown in Fig 1. The actin filaments (diameter of 6-8 nm) are woven into network with little extensible cross-linked filaments [7]. These filaments are in tension due to the cell contractile apparatus and also passively by the cell distension through its adhesive substrate or by the swelling pressure of liquid cytoplasm [2]. Microtubules are tubular biopolymers (outer and inner diameter of 24 and 12 nm, respectively) [7] and are in compression to resist the contraction from interconnected actin network [8]. Intermediate filaments (diameter of 10 nm) that are believed to be in tension contribute significantly to cell stiffness only at large strains (>20%) [9]. These three filamentous networks are physically interlinked [10] which enable a force transmission among them

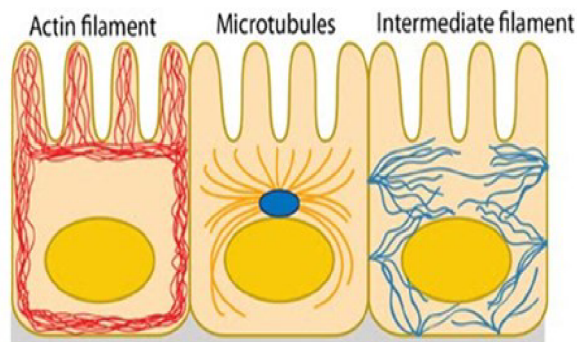


*Fig 1: (a) Actin filaments are mainly concentrated on the cell cortex. (b) Microtubules are developed from the centrosome near the nucleus. (c) Intermediate filaments are distributed in the central regions of the cell and across to neighbouring cells.*

During their spreading process, most of the cells are anchored to the extracellular matrix (ECM) to balance the forces induced by the CSK filaments to achieve equilibrium. The transmembrane integrin receptors concentrated in focal adhesion plaques transfer a portion of the mechanical forces within the CSK to the ECM [11]; as a consequence traction forces rise at the cell-ECM interface. These traction forces are in equilibrium with forces within the CSK [2]. Thus, understanding of CSK stabilization leads to recognition how living cells can sense and respond to the mechanical stresses. The mechanical models of living cells have been generally described either by microstructural or continuum

approaches [12][13].

A soft glassy rheological model is based on the measurement of cell mechanics. Cytoskeletal mechanics plays a vital role in the cellular mechanotransduction and motility that involves in contraction, spreading, and crawling. It also plays a key role in other mechanical functions such as cell division and apoptosis. In this context, rheological properties of the cytoskeleton are of uttermost importance [14].

## 2. Experiments on cytoskeleton

### 2.1 Soft glassy material (SGM)

Soft glassy materials comprise a diverse group of substances that include foams, pastes, colloids, emulsions and slurries [14][15][16]. The empirical criteria that define this class of materials are as follows: they are very soft, both elastic modulus,  $G'(\omega)$  and loss modulus,  $G''(\omega)$  increase with the same weak power-law dependencies upon frequency, hysteresivity,  $\eta$  (ratio of loss to elastic modulus) is frequency insensitive and of the order 0.1 and under certain conditions they display physical aging behaviour [15][17][18]. At a given frequency, both  $G'(\omega)$  and  $G''(\omega)$  moduli increase linearly with an increasing prestress [19]. The generic feature shared by all soft glassy materials is each one of them is composed of elements that are discrete, numerous, and aggregate with one another via weak interactions [18].

### 2.2 Magnetic Twisting Cytometry (MTC)

Considering a parallelism between the living cells and SGM, it was hypothesized in [14] that the CSK can be added to the list of SGM and may be modelled using a soft glassy rheology theory (SGR) proposed by Sollich [17]. Magnetic twisting cytometry (MTC) has been performed to obtain the mechanical response of variety of cells; in this method the cell is sheared between a plate at the cell base and a magnetic microsphere partially embedded into the cell surface, as shown in Fig 2 (a) and (b).

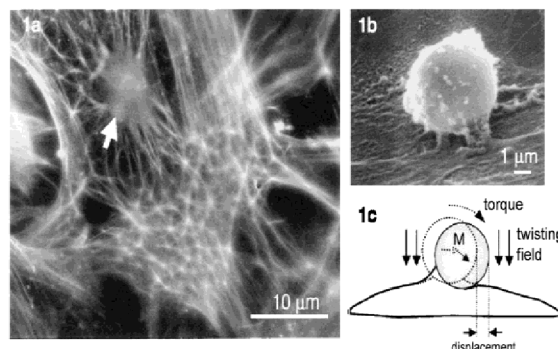


Fig 2: (a) & (b) Beads attached to the cytoskeleton of human airway smooth muscle (HASM) cells via cell adhesion molecules (integrins) (c) The application of magnetic field and the displacement of the bead [16].

The magnetic twisting field introduces a torque and thus causes the bead to rotate and displace as shown in Fig 2 (c), which is detected by a CCD camera mounted on an inverted microscope.

The frequency dependence of both  $G'$  and  $G''$  has been then extracted from the structural response at the point of bead attachment [14]. Results are shown in

Fig 3,  $G'$  increases with increasing frequency,  $\omega$  according to power law  $\sim \omega^{x-1}$  with effective temperature or noise level,  $x$  equals to 1.20 under control conditions. Similarly,  $G''$  also increases with increasing frequency and follows the same power law in the range of 0.01–10 Hz [14, 16]. On the contrary, within the same frequency range the loss tangent was relatively frequency insensitive [15].

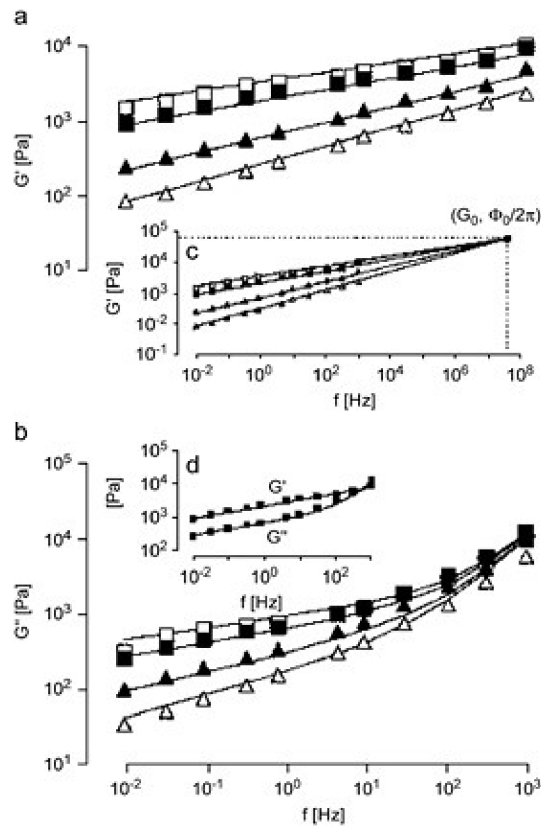


Fig 3: (a) and (b) represent the elastic modulus,  $G'(\omega)$  and loss modulus,  $G''(\omega)$  as functions of frequency,  $\omega$  for different drug treatments. Filled squares represent response under control conditions, unfilled squares are for treatment with histamine, filled triangles depict treatment with DBcAMP and unfilled triangles indicate treatment with cytochalasin D. The solid lines satisfy the structural damping equation with the values of scale factor for stiffness,  $G_0 = 53.6$  kPa and frequency,  $\Phi_0 = 25 \times 10^7$  rad/sec, and viscosity constant  $\mu = 1.41$  Pa s. (c) Extrapolation of Eq.(2) to higher frequencies yields crossover at coordinate  $(G_0, \Phi_0)$  (d) Dynamic moduli under control conditions [16].



### 2.3 The structural damping equation

In time domain, the mechanical stress response  $G(t)$  to a unit step change in strain imposed at  $t = 0$  is given by

$$G(t) = \mu \delta(t) + G_0 (t/t_0)^{(1-x)} \quad (1)$$

Here,  $G_0$  is the ratio of stress to the unit strain measured at an arbitrary chosen time  $t_0$ ,  $\mu$  is a Newtonian viscous term and  $\delta(t)$  is the Dirac delta function. The complex modulus for the same can be given as

$$G(\omega) = G_0 \left( \frac{\omega}{\Phi_0} \right)^{(1-x)} (1 - i\eta) \Gamma(2 - x) \times \cos \frac{\Pi}{2} (x - 1) + i\omega\mu \quad (2)$$

Where,  $\eta$  is called as structural damping coefficient and  $\omega$  is the radian frequency  $2\pi f$ ,  $G_0$  &  $\Phi_0$  are scale factors for stiffness and frequency, respectively,  $\Gamma$  denotes the Gamma function and  $i^2 = -1$ ,  $G_0$  and  $\mu$  depend on bead-cell geometry.

In the above equation, the elastic modulus,  $G'(\omega)$  corresponds to the real part which increases for all values of  $\omega$  according to the power law exponent,  $x-1$  [14]. On the other hand, the loss modulus  $G''(\omega)$  corresponds to an imaginary part and is a frequency-independent fraction  $\eta$  of the elastic modulus; such a direct coupling of the loss modulus to the elastic modulus is the characteristic feature of structural damping behaviour [20]. Loss modulus also includes a Newtonian viscous term,  $i\omega\mu$  which comes into play only at higher frequencies. The key characteristic of glassy materials is that, they are not in thermodynamic equilibrium below their glass transition temperature,  $T_g$ . In addition, these materials are arrayed in a microstructural geometry that is structurally disordered and metastable [14]. The structural damping coefficient is not an independent parameter but depends on  $x$  only [15].

## 3. Soft glassy rheology (SGR)

### 3.1 Theory of soft glassy rheology

Sollich [18] extended the earlier work of Bouchaud's glass model [21] to develop the unified theory of SGR. This theory considers that each individual element of the matrix exists within an energy landscape containing many wells of differing depth Fig 4. These traps are formed by interactions of an element with neighbouring ones. Each of the energy well is regarded as being so deep that the elements are unlikely to escape the well by

thermal fluctuations alone. Instead, elements are imagined to be agitated and rearranged by mutual interactions with neighbouring elements within the matrix. This agitation can be represented by an effective temperature or noise level,  $x$  [17, 18].

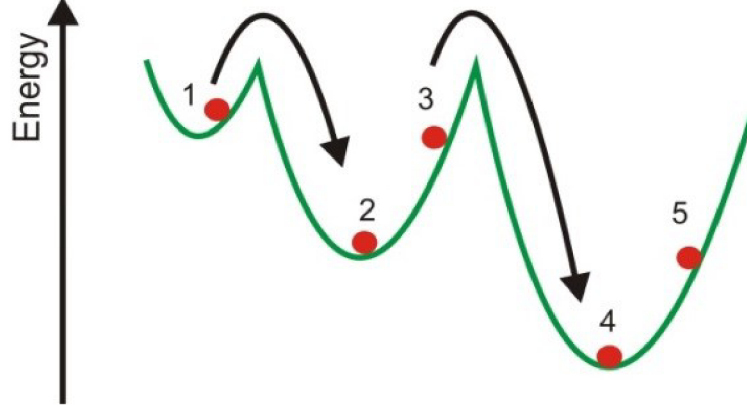


*Fig 4: Schematic illustration of the soft glassy rheology model of the cytoskeleton in which the natural reorganization and dynamics for intracellular biopolymers can be modelled as a series of transitions (red positions 1-5) between a fluid and solid state [22].*

In Eq. (2) when  $x > 1$ , there is sufficient agitation in the matrix for an element to hop randomly between the wells. Consequently, the system becomes disordered and as a whole it can flow. It thus behaves like a glassy material. However, when  $x$  approaches 1, the element is trapped in such a deep well that the agitation in the matrix (under a given temperature and noise level) is not high enough to hop off. Consequently, the system becomes stabilized and thus behaves like an elastic material. The higher the effective temperature,  $x$  the more frequently an element trapped in the energy well manages to hop from this well into another [17]. Thus the hop can be viewed as the fundamental molecular remodelling event [23].

### 3.2 Sollich's evolutionary probability equation

The SGR theory follows a conservation law for probability  $P(E, l, t)$  of an element being trapped in an energy well of depth  $E$  & local displacement  $l$ , at time  $t$ :

$$\left( \frac{\partial P(E, l, t)}{\partial t} \right) - \gamma \frac{\partial P}{\partial l} = -g(E, l)P(E, l, t) + f(E)\varphi(t)\delta(l) \quad (3)$$

Where,  $\varphi(t) = \int dE dl g(E, l) P(E, l, t)$  (required for conservation of probability),  $\delta(l)$  is the Dirac delta function and  $f(E)$  is the distribution of energy well depths. The above equation is known as structural or hysteretic damping; the second term on the left hand side represents the change in probability because of the motion of the energy trap itself,  $E$ ,

while the first term on the right hand side is depletion, equal to the probability of resident elements to be hopping out, given by the product of the probability of occupancy  $P$  and a transition rate  $g(E, l)$ . The second term on the same side is an accumulation rate, equal to the product of the total number of available transitions  $\phi(t)$  and the delta function constraint forcing elements to hop into the wells at zero local strain. The  $\delta(l)$  function is due to the assumption that the local strain becomes zero immediately after the relaxation [16, 17, 23].

Sollich has taken  $f(E) = \exp(-E)$  and  $g(E, l) = \Phi_0 \exp\left(-\frac{\left(E + \frac{kl^2}{2}\right)}{x}\right)$ . The transition  $g(E, l)$  rate for hopping out of wells is distributed over  $E$ , which is a non-linear regime and function of strain. It must be noted that the selection of energy well is not correlated with the previous position [15]. In structural damping Eq. (2), when  $x > l$ , there is sufficient agitation in the matrix that the element can hop randomly between wells as a result, the system as a whole can flow and become disordered which are the fundamental features of glassy materials [17].

#### 4. Discussion

Fabry et al. [14] used the magnetic twisting cytometry with optical detection of bead motion for measurement of human airway smooth muscle cell and suggested that the CSK proteins might regulate cell mechanical properties mainly by modulating the effective noise temperature,  $x$  of the cytoskeletal network. In other words, the effective noise temperature,  $x$  measures the CSK ability to deform, flow and reorganize. Further, the weak power-law dependence of both elastic and frictional moduli on the frequency over a wide frequency range characterized the dynamic behaviour of adherent cells. The cells as a soft glassy material lie close to the glass transition [14, 15, 16]. It has been noted that the prestress of CSK and effective noise temperature have a unique inverse relationship [24]. Both dynamic elastic moduli and frictional moduli increase linearly with the increasing CSK prestress [19]. The unique features of soft glassy rheology theory make it well-suited to describe the rheological behaviour of cytoskeleton.

However, nothing has been mentioned about the regulation of effective temperature or noise level in the cells (either by drugs or mechanical stimuli, etc.) An unidentified but non-thermal origin has been used by Sollich as a jostling of elements to interpret the

effective noise temperature,  $x$ . The parameters that determine the scale factor for frequency,  $\Phi_0$  in the Sollich's evolution equation are yet unexplained. There are difficulties with the interpretation of depth of the energy well,  $E$  [14]. Prestress, which plays a significant role in defining the steady-state behaviour of the cell, is not taken into consideration by soft glassy rheology theory [6].

## 5. Conclusion

This review showed that the soft glassy behaviour and the underlying notion of the noise temperature might provide a unique explanation of the cytoskeleton ability to deform, flow and remodel. It can also be stated that the structural disorder and metastability are the essential features that may comprise the basis of cytoskeleton mechanical functions.

## Acknowledgment

This work is an output of research and scientific activities of NETME Centre, regional R&D centre built with the financial support from the Operational Programme Research and Development for Innovations within the project NETME Centre (New Technologies for Mechanical Engineering), Reg. No. CZ.1.05/2.1.00/01.0002 and, in the follow-up sustainability stage, supported through NETME CENTRE PLUS (LO1202) by financial means from the Ministry of Education, Youth and Sports within the support programme "National Sustainability Programme I".

## References

- [1] Ingber D., Dike L., Hansen L., Karp S., Liley H., Maniotis A. et al.: Cellular tensegrity: exploring how mechanical changes in the cytoskeleton regulate cell growth, migration and tissue pattern during morphogenesis, *International Review of Cytology*, vol. 150, (1994), pp. 173.
- [2] Ingber D.: Cellular tensegrity: defining new rules of biological design that govern the cytoskeleton, *Journal of Cell Science*, vol. 104, (1993), pp. 613-627.
- [3] Wang N., Butler J. & Ingber D.: Mechanotransduction across the cell surface and through the cytoskeleton, *Science*, vol. 260, (1993), pp. 1124-1127.
- [4] Ingber D.: Cellular tensegrity revisited: I. Cell structure and hierarchical system biology, *Journal of Cell Science*, vol. 116, (2003), pp.1157-1163.

- [5] Ingber D.: Tensegrity: The architectural basis of cellular mechanotransduction, *Annu. Rev. Physiol*, vol. 59, (1997), pp. 575-599.
- [6] Amos L. & Amos W.: *Molecules of the Cytoskeleton*, Guilford Press 1991, New York.
- [7] Gittes F., Mickey B., Nettleton J. & Howard J.: Flexural rigidity of microtubules and actin filaments measured from thermal fluctuations shape, *J. Cell Biol*, vol. 120, (1993), pp. 923-934.
- [8] Stamenovic D., Mijailovich S., Norrelkykke I., Chen J. & Wang N.: Cell Prestress. II. Contribution of microtubules, *The American Physiological Society*, vol. 282, (2002), pp. C617-C624.
- [9] Stamenovic D. & Wang N.: Engineering approaches to cytoskeletal mechanics, *J Appl Physiol*, vol. 89, (2000), pp. 2085-2090.
- [10] Paul R., Heil P., Spatz J. & Schwarz U.: Propagation of Mechanical stress through Actin cytoskeleton toward Focal Adhesions: Model and Experiment, *Biophysical Journal*, vol. 94, (2008), pp.1470-1482.
- [11] Wang N., Nauseef K., Stamenovic D., Fredberg J., Mijailovich S., Norrelkykke I., Polte T., Mannix R. & Ingber D.: Mechanical behaviour in living cells consistent with the tensegrity model, *Proceedings of the National Academy of Sciences of the United States of America*, vol. 98, no.14, (2001), pp. 7765-7770.
- [12] Lim C., Zhou E. & Quek S.: Mechanical models for living cells – a review, *Journal of Biomechanics*, vol. 39, (2006), pp. 195-216.
- [13] Vaziri A., Gopinath A. and Deshpande V.: Continuum-based computational models for cell and nuclear mechanics, *Journal Mechanics of Materials and Structures*, vol. 2, no.6, (2007),pp. 1169-1191.
- [14] Fabry B., Maksym G., Butler J., Glogauer M., Navajas D. & Fredberg J.: Scaling the Microrheology of living cells, *The American Physical Society*, vol. 87, no.14, (2001), 148102.
- [15] Mandadapu K., Govindjee S. & Mofrad M.: On the cytoskeleton and soft glassy rheology, *Journal of Biomechanics*, vol. 41, (2008), pp. 1467-1478.
- [16] Fabry B., Maksym G., Butler J., Glogauer M., Navajas D., Taback N., Millet E., Fredberg J.: Time scale and other invariants of integrative mechanical behavior in living cells, *Physical Review E* 68, (2003), 041914

- [17] Sollich P.: Rheological constitutive equation for a model of soft glassy materials, *Physical Review Letters*, Vol. 8, (1998), pp. 738-759.
- [18] Sollich P., Lequeux F. et al.: Rheology of soft glassy materials, *Physical Review Letters*, Vol. 78, (1997), pp. 2020-2023.
- [19] Stamenovic D., Liang Z., Chen J., Wang N.: Effect of the cytoskeletal prestress on the mechanical impedance of cultured airway smooth muscle cells, *Journal of Applied Physiology*, vol. 92, (2002a), pp. 1443–1450.
- [20] Fredberg J. and Stamenovic D.: On the imperfect elasticity of lung tissue, *Journal of Applied Physiology*, vol. 67, (1989), pp. 2408–2419.
- [21] Bouchaud, J.: Weak ergodicity breaking and aging in disordered systems, *Journal de Physique I, France 2*, (1992), pp. 1705-1713.
- [22] Holecek M., Kochova P. & Tonar Z.: Mechanical properties of living cells and tissues related to thermodynamics, experiments and quantitative morphology-A review, *Theoretical Biomechanics*, University of West Bohemia, Czech Republic, pp.1-20.
- [23] Mofrad M. & Kamm R.: *Cytoskeletal Mechanics*, Cambridge University Press 2006, USA.
- [24] Stamenovic D., Suki B., Fabry B., Wang N. & Fredberg J.: Rheology of airway smooth muscle cells is associated with cytoskeletal contractile stress, *Journal of Appl. Physiol*, vol. 96, (2004), pp. 1600-1605.

## LIST OF AUTHOR'S PUBLICATIONS

### IF Journal

- [1] Bansod Y.D., Matsumoto T., Nagayama K., and Burša J. A finite element bendotensegrity model of eukaryotic cell.

**Submitted to:** ASME - Journal of Biomechanical Engineering with IF of 1.745

### Peer-review journals

- [1] Bansod Y.D. and Burša J. Continuum-based modelling approaches for cell mechanics. *World Academy of Science, Engineering and Technology, International Journal of Biological, Biomolecular, Agricultural, Food and Biotechnological Engineering*. 2015, 9(9): 921-32.
- [2] Bansod Y.D. and Burša J. Overview of tensegrity - II: High frequency spheres. *Engineering Mechanics*. 2014, 21(6): 437-449.
- [3] Bansod Y.D., Nandanwar D., and Burša J. Overview of tensegrity - I: Basic structures. *Engineering Mechanics*. 2014, 21(5): 355-367.
- [4] Bansod Y.D. and Burša J. A concise review of soft glassy rheological model of cytoskeleton. *Engineering Mechanics*. 2014, 21(4): 279-285.
- [5] Burša J. and Bansod Y.D. Design and applications of prestressed tensegrity structures. *Engineering Mechanics 2014, Book of full texts*. Svratka: Czech Society for Mechanics, 2014, p. 30-33.

### Conference papers

- [1] Bansod Y.D. and Burša J. Tensegrity principle based computational model of cytoskeleton. *6<sup>th</sup> World Conference on Structural Control and Monitoring (6WCSCM)*, Barcelona, Spain. 2014. p. 3317-3326.
- [2] Burša J. and Bansod Y.D. Models of living cells on the basis of tensegrity structures. *6<sup>th</sup> World Conference on Structural Control and Monitoring (6WCSCM)*, Barcelona, Spain. 2014. p. 140-146.

## Conference abstracts

- [1] Bansod Y.D. and Burša J. *Finite element simulation of mechanical tests with bendotensegrity models of smooth muscle cell*. XXIVs Cytoskeleton club 2016 conference, Vranovská Ves - Czechia, 20-22 May, 2016.
- [2] Bansod Y.D. and Burša J. *Computational model of vascular smooth muscle cell*. XXII Cytoskeleton club 2015 conference, Vranovská Ves - Czechia, 20-22 May, 2015.
- [3] Bansod Y.D. and Burša J. *Computational model of intracellular structure for simulation of mechanical tests of cells*. 11th World Congress on Computational Mechanics (WCCM XI), 5<sup>th</sup> European Conference on Computational Mechanics (ECCM V), 6<sup>th</sup> European Conference on Computational Fluid Dynamics (ECFD VI), Barcelona - Spain, 20-25 July, 2014.
- [4] Bansod Y.D. and Burša J. *Application of tensegrity principle to cytoskeleton*. 6th World Conference on Structural Control and Monitoring (6WCSCM), Barcelona - Spain, 15-17 July, 2014.
- [5] Bansod Y.D. and Burša J. *Computational modeling of cell based on tensegrity principle*. XXII Cytoskeleton club 2014 conference, Vranovská Ves - Czechia, 21-23 May, 2014.
- [6] Bansod Y.D. and Burša J. *Tensegrity models of mechanical behaviour of living cell*. Computational Mechanics 2013 conference, Spicak - Czechia, 4-6 November, 2013.

## Internship

Completed one month internship at Laboratory of Biology of Cytoskeleton, Institute of Molecular Genetics of the ASCR, v.v.i., Prague, work focused on the study of intracellular structure of different cell types and single-cell experimental techniques.



# CURRICULUM VITAE

## Yogesh Deepak Bansod

Email address: [yogeshbansod@gmail.com](mailto:yogeshbansod@gmail.com)

Mobile: +420-608678342

### Education

- 2012 - Present: Brno University of Technology, Brno, Czechia  
Pursuing PhD studies in Biomechanics
- 2007 - 2008: The University of Manchester, Manchester, United Kingdom  
MSc, Mechanical Engineering Design, GPA- 6/10, 2:1 Degree

### Work Experience

- 2009 - 2012: Rheinmetall Automotive AG, Pune, India  
Research Engineer
- 2008 - 2009: The University of Manchester, Manchester, United Kingdom  
Research Assistant
- 2004 - 2007: Varsha Forgings Ltd., Aurangabad, India  
Design Engineer

### Scholarships

- 2012 - Present: South Moravian Centre of International Mobility (JCMM) scholarship
- 2012 - 2016: Doctoral scholarship at Brno University of Technology
- 2007 - 2008: The Don Hanson Foundation scholarship for international students

### Awards

Thesis of the year award for final year Bachelor's project undertaken at National Environmental Engineering Research Institute, Nagpur, India